5-2022

Advances in Process Understanding and Methods to Support River Temperature Modeling in Large Regulated Systems

Bryce A. Mihalevich
Utah State University

ADVANCES IN PROCESS UNDERSTANDING AND METHODS TO SUPPORT RIVER TEMPERATURE MODELING IN LARGE REGULATED SYSTEMS

by

Bryce A. Mihalevich

A dissertation submitted in partial fulfillment
of the requirements for the degree

of

DOCTOR OF PHILOSOPHY

in

Civil and Environmental Engineering

Approved:

_____	_____
Bethany T. Neilson, Ph.D. Major Professor	Charles B. Yackulic, Ph.D. Committee Member
_____	_____
Caleb A. Buahin, Ph.D. Committee Member	David G. Tarboton, Ph.D. Committee Member
_____	_____
John C. Schmidt, Ph.D. Committee Member	D. Richard Cutler, Ph.D. Interim Vice Provost of Graduate Studies

UTAH STATE UNIVERSITY
Logan, Utah

2022

ABSTRACT

Advances in Process Understanding and Methods to Support

River Temperature Modeling in Large Regulated Systems

by

Bryce A. Mihalevich, Doctor of Philosophy

Utah State University, 2022

Major Professor: Dr. Bethany T. Neilson
Department: Civil and Environmental Engineering

River temperatures influence ecosystem characteristics by controlling chemical reactions, physiological responses, and trophic interactions. While many factors influence temperatures, water development has transformed flow and thermal regimes in many rivers, reshaping aquatic ecosystems. As water managers make decisions to address climate induced changes in runoff, aquatic ecosystems may be further altered. To understand how water supply decisions and future climate will impact aquatic ecosystems, robust river and reservoir temperature predictions associated with future management decisions are needed. Process-based models are advantageous in these settings because they identify mechanisms controlling thermal regimes. Yet, to fully realize ecosystem responses to water management decisions, spatial and temporal differences among water management and temperature modeling frameworks must be overcome. Predicting temperatures over large river networks is also challenged by the lack of process understanding in topographically complex areas subject to limited data. This dissertation addresses these limitations by adapting mechanistic river temperature

modeling approaches that incorporate topographic shading and remotely sensed, spatially varying weather data while describing model coupling and data assimilation methods linking temperature responses to water management model predictions. When applied to different portions of the Colorado River basin, shading in deep canyon areas was found to increase the importance of typically small atmospheric heat fluxes. In Grand Canyon, temperatures are primarily controlled by discharge and release temperature from Lake Powell reservoir in the upstream 167 km, while predictions further downstream and during lower flows highlighted the need for spatially varying weather information to better estimate atmospheric heat fluxes. Using the ERA5-Land Climate Reanalysis Dataset, combined with elevation corrections, spatially varying weather was tested in the Grand Canyon and Green River. ERA5-Land information significantly improved temperature predictions when compared to models using ground-based weather stations. With these river temperature modeling advances, a water management model was linked to temperature models to evaluate future management impacts on ecosystem indicators. River temperatures were forecasted over a large portion of the Colorado River using flows from the Colorado River Simulation System and strategically resampled weather and water temperature information. This modeling framework allows future climate and water management impacts on aquatic ecosystems to be evaluated.

(305 pages)

PUBLIC ABSTRACT

Advances in Process Understanding and Methods to Support River Temperature Modeling in Large Regulated Systems

Bryce A. Mihalevich

River temperatures play a key role in determining the suitability of habitat for aquatic ecosystems. While thermal regimes are influenced by many factors, flow and temperature patterns in large rivers are often shaped by water development. As such, water management associated with large reservoirs and diversions have also altered aquatic ecosystems. As climate change introduces new climate and hydrologic patterns, the decisions water managers make to address changes in runoff may further impact aquatic ecosystems. This calls for robust modeling tools that can predict river and reservoir temperature responses to water management decisions over large regions. However, highly variable topography and data limitations that are inherent over large spatial scales complicate our understanding of river temperature controls. Further, differences among modeling frameworks need to be overcome in order to holistically understand ecosystem responses to water management decisions. This dissertation addresses these limitations by adapting mechanistic river temperature models to account for topographic shading and spatially varying weather information and describing methods for linking temperature responses to water management decisions. The Colorado River basin was used to evaluate these methods because it experiences significant flow regulation, remote river sections, and highly variable terrain. The findings here show that discharge and release temperatures from large reservoirs, particularly Lake Powell and

Flaming Gorge, influence river temperatures over significant distances, while topographic shading increases the relative importance of heat fluxes, other than solar radiation, that require representative weather data for estimation. Spatially varying weather information from a climate reanalysis dataset, combined with elevation corrections, was tested in different modeling domains and found to significantly improve temperature predictions when compared to models using sparsely distributed ground-based weather stations. With the advances in modeling over topographically complex regions, water management models were linked to river temperature responses so that ecosystem indicators could be evaluated. Using an existing water management model for flow information and strategic resampling of weather and water temperature information, river temperatures were forecasted over more than 1000 km of river. The work presented here provides the foundational tools for evaluating climate and water management impacts on aquatic ecosystems in large managed basins.

ACKNOWLEDGMENTS

I am indebted to numerous individuals who helped me reach my goals. First and foremost, I would like to express my gratitude for my advisor, Dr. Bethany Neilson. Beth, thank you for your patience with me and never letting up over the past four years. From modeling and critical thinking to life's highs and lows, you have taught me a tremendous amount and shared invaluable wisdom that will help me succeed in many aspects of my future. Your mentorship went above and beyond what I could ask for, and I am truly grateful. I will miss working with you, but hope to collaborate on projects in the future.

I am also immensely thankful for my committee members; Dr. Caleb Buahin, Dr. Charles Yackulic, Dr. David Tarboton, and Dr. Jack Schmidt. Caleb, thank you for taking the time to teach me about modeling. Without your help setting up models, debugging errors, and guidance on model adaptations I would not have been able to achieve the accomplishments presented here. Charles, you have provided a perspective into aquatic ecosystems that opened my eyes to thinking about river systems more holistically. I am tremendously excited to continue working with you in the future. David, thank you for always being available to help me understand various processes, from the importance of diffuse radiation to correcting climate reanalysis datasets. Further, your continuous thinking about river processes with Jack while driving across the Wyoming prairie helped uncover key mechanisms that significantly improved our modeling abilities. And Jack, without your drive to provide a voice for Colorado River ecosystems I would not have had this opportunity. You are a wealth of knowledge and I will miss learning from the thoughts and perspectives you have developed over your decorated and admirable career.

To Tyler King, Hyrum Tennant, Eileen Lukens, and Dane Brophy of the Neilson Lab, thank you for being readily available to bounce ideas off of and always providing an appropriate amount of distraction, even when work needed to be done. I will miss the conversions we had in the office.

This work could not have been completed without the help from many other individuals. Thanks to the Grand Canyon Monitoring and Research Center staff for assistance in data collection (Maria Dzul), insights, and discussions on data and modeling results (Kimberly Dibble, Theodore Kennedy, Nick Voichick, and Bridget Deemer) and help with the shading model (Mike Yard and Glenn Bennett). Additional thanks to Joshua Walston at the DRI for help in acquiring shortwave radiation data. Thanks to the U.S. Fish and Wildlife Service (Jana Mohrman, Tom Chart, Don Anderson, and Jim Renne) and Utah Division of Wildlife Resources (Katie Creighton and Christopher Michaud) for providing crucial river temperature data. Special thanks to Jian Wang and Kevin Wheeler for helping me understand the Colorado River Simulation System and providing me with model outputs. To Brad Udall, thank you for helping incorporate climate projects in model forecasts. Further thanks to the U.S. Bureau of Reclamation (Robert Radtke and Jeremiah Drewel) for help with the Lake Powell model.

To my friends and family, without your support I would not have had the strength to persevere over these four years. From biking and skiing trips to dinner nights in Logan, you have provided many smiles and much needed joy. To my parents, Rick and Connie, your never-ending support and encouragement to purse my goals cannot be matched, and for that I thank you.

Bryce A. Mihalevich

CONTENTS

Page

Abstract iii

Public Abstract v

Acknowledgments vii

List of Tables xiii

List of Figures xv

Chapter

1. Introduction 1

References 7

2. Water Tempeature Controls for Regulated Canyon-Bound Rivers 13

Abstract 13
1. Introduction 14
2. Methods 18

2.1. Model formulation 18
2.2. Model adaptations 20

2.2.1. Radiation balance 20
2.2.2. Internal fluid shear friction 26

2.3. Model application 27

2.3.1. Study Site: The Colorado River in the Grand Canyon 27
2.3.2. Model domain, simulation period and forcing data 29
2.3.4. Sediment conduction 34
2.3.5. Radiation balance in Grand Canyon 34
2.3.6. Model scenarios 36

3. Results 39

3.1. Radiation balance 39
3.2. Long-term model results 41
3.3. High flow and low flow period model results 43
3.4. Dominant heat fluxes 45

3.4.1. All modeled external heat fluxes over time and space 45

3.4.2. Fluxes during high and low flows 49

3.5. Sensitivity analysis 49

4. Discussion 53

4.1. Radiation balance 53
4.2. Long term model results 55
4.3. High flow and low flow periods 57
4.4. Estimated heat fluxes 58
4.5. Sensitivity analysis 59

5. Conclusions 62
Acknowledgements 64
References 65

3. Evaluation of the ERA5-Land Reanalysis Dataset for Process-Based River Temeprature Modeling over Data Sparse and Topographically Complex Regions 76

Abstract 76
1. Introduction 77
2. Methods 81

2.1. Study Area 81
2.2. River Temperature Model 85
2.3. Input Meteorological Data 88

2.3.1. Ground-based weather data 88
2.3.2. Climate reanalysis data 90

2.4. Elevation corrections 91
2.5. Model Simulation period 94
2.6. Analyses 94

2.6.1. Testing of elevation corrections in Grand Canyon 94
2.6.2. Differences in elevation corrected weather data 95
2.6.3. Model performance using different weather data products 95

3. Results 96

3.1. Grand Canyon 96

3.1.1. Testing of elevation corrections in Grand Canyon 96
3.1.2. Differences in input weather data 100
3.1.3. Model accuracy using tested weather inputs 101
3.1.4. Differences between model predictions 103

3.2. Green River 105

3.2.1. Differences in input weather data 105
3.2.2. Model accuracy using tested weather inputs 107
3.2.3. Differences between model predictions 110

4. Discussion 111

4.1. Comparison of ERA5-010 dataset to ground-based weather data. 111
4.2. Differences in input weather data 113
4.3. Model accuracy using tested weather inputs 114
4.4. Differences between model predictions 115
4.5. Future considerations 116
4.6. Broader Impacts 116

5. Conclusion 119
Acknowledgements 121
References 122

4. Data Intregration and Coupled Modeling to Evaluate River Temperature Responses to Water Management Decisions 129

Abstract 129
1. Introduction 130
2. Modeling Approach 134

2.1. Process-based models 135

2.1.1. River Temperature Model 135
2.1.2. Reservoir Temperature model 136

2.2. Linking Water Management Models to Process-Based Models ... 137
2.3. Linking Forcing Data to Process-Based Models 138

3. Case Study: Colorado River Basin 139

3.1. Study Area 139
3.2. Models 141

3.2.1. Colorado River Simulation System (CRSS) 143
3.2.2. HydroCouple 146
3.2.3. CE-QUAL-W2 151

3.5. Results and Discussion 153

4. Conclusion 162
Acknowledgments 164
References 165

5. Conclusion 172

6. Engineering Significance 176

7. Reccomendations for Future Work 180

References 183

Appendices 184

A. Supporting Information for Chapter 2 185

References 214

B. Supporting Information for Chapter 3 217

References 246

C. Supporting Information for Chapter 4 249

References 271

D. License Agreement 272

Vita 278

LIST OF TABLES

Page

Table 2-1. Statistics for modeled external heat fluxes (W/m^2) and percent of total external heat fluxes for the Colorado River in Grand Canyon between Jan 1, 2000 and Jan 1, 2018. Statistics for the relative contribution (%) were calculated from the absolute values for each heat flux over space and time divided by the sum of absolute values for all heat fluxes over space and time. 47

Table 3-2. Sites along the mainstem branches used for boundary conditions, inflows, and evaluating model predictions in the Colorado and Green River models. Stream flow and temperature locations are indicated with a "S" and weather stations are indicated with a "W" and correspond to the locations mapped in Figure 3-1. The river kilometer indicates the approximate location of flow and river temperature sites and for weather stations they represent the range over which data were applied in the model domain. 85

Table 3-3. Mean error (ME) between GCMRC-WS data and input weather data used in the river temperature models before (Pre) and after (Post) elevation corrections were applied. Errors are calculated as the input weather data (i.e., CR-WS, ERA5-010, or ERA5-100) minus GCMRC-WS, where positive errors are overestimates of ground-based observations. Post elevation correction values that were the same or greater than pre elevation corrections values, based on the absolute ME, are shaded in light gray. The bottom two rows represent the mean error and standard deviation (σ) of all GCMRC-WS sites combined. 99

Table 4-1. Subset of CRSS nodes used to model river temperatures in the Colorado River basin. CRSS Objects have been combined and renamed for readability. A complete list of CRSS nodes used in this study is shown in Table C-2. The river kilometer indicates the approximate location of where CRSS point inflows were assigned or the range over which distributed flows were assigned in the process-based models. 145

Table A-1. Current and historical Colorado River monitoring stations within Grand Canyon in order of river kilometer. Bold font indicates stations that were used in this model 209

Table A-2. Calibrated roughness values for each segment of the Colorado River in Grand Canyon. 210

Table A-3. Comparison of air temperature data from weather stations within Grand Canyon and at Page, AZ. The mean air temperature from within

Grand Canyon (excluding Page, AZ and Regressed Air Temperature) is 19.95 °C..... 211

Table A-4. Remote automated weather station (RAWS) network sites used to aggregate measured shortwave radiation into a hourly median time series ($J_{sn,meas}$). 212

Table B-1. Monthly estimates of air temperature lapse rates and dew point temperature lapse rates for the Northern Hemisphere (Kunkel 1989). 227

Table B-2. Mean error (ME) between remote automated weather stations (RAWS) and input weather data used in the river temperature models. CR-WS solar radiation is a median time series of all RAWS data. Error is calculated as the CR-WS or ERA-010 input weather dataset minus the RAWS data, resulting in positive errors equating to overestimates. The bottom two rows represent the mean error and standard deviation (σ) of all RAWS sites combined. 228

Table B-3. Nash-Sutcliffe Efficiency (NSE) between GCMRC-WS data and input weather data used in the river temperature models before (Pre) and after (Post) elevation corrections were applied. 229

Table B-4. Root Mean Square Error (RMSE) between GCMRC-WS data and input weather data used in the river temperature models before (Pre) and after (Post) elevation corrections were applied. 230

Table C-1. Example of two resampling methods used to generate plausible future hydrologic traces. For both examples historical flow information occurring between 2000 and 2018 (19 years) is resampled to produce traces that are used simulate flow between 2022 and 2040 in a water management model. The left Table illustrates a random resampling method that can generate N number of traces. The Table on the right illustrates the index-sequential method (ISM) for resampling that creates as many traces as there are years of information (i.e., 19 in this example)..... 261

Table C-2. Subset of CRSS nodes used to model river temperatures in the Colorado River basin. 262

Table C-3 USGS gage sites used for boundary conditions and tributary inflow water temperature information. The temporal resolution column indicates how these data were resampled before being applied in the river temperature model. 265

LIST OF FIGURES

Page

Figure 2-1. Schematic illustrating the radiation balance used in this model for a cross-section of the river at a given model cell (c). LB = left bank, RB = right bank, C = river center, d = distance in meters away from the river bank, θ = the solar zenith angle, $\Psi_{E,0}$ = is the elevation angle from river center at 0° azimuth (Φ), $\Psi_{E,180}$ = is the elevation angle from river center at Φ=180°, $\Psi_{L,0}$ = is the land re-emittance angle from river center at Φ = 0°, $\Psi_{L,180}$ = is the land re-emittance angle from river center at Φ =180°. For the radiation balance Φ is calculated from 0° to 359°, but only 0° and 180° are shown here for illustration. Shortwave radiation received at the water surface within the canyon consists of 1) direct shortwave radiation ($J_{sn,dir,c}$) originating from the sun and scaled by topographic shading factors (S_f), 2) diffuse shortwave radiation ($J_{sn,diff,c}$) originating from any sky direction as the result of scattering by atmospheric gases and particles and scaled by the sky view factor (SV_f), and 3) land-reflected longwave radiation ($J_{sn,refl,c}$) from nearby terrain. Longwave radiation components considered in this model include 4) rock longwave radiation ($J_{rock,c}$) within a specified distance (d) of the edge of water 5) water longwave radiation ($J_{br,c}$), and 6) atmospheric longwave radiation ($J_{an,c}$) scaled by the sky view factor ($SV_{f,c,d}$) calculated from the river center and including the area at a specified distance (d) from the edge of water. 21

Figure 2-2. Map of the study area depicting model extent (RM0-RM225), major river segments (Melis, 2011), and the location of discharge and temperature monitoring sites used in the river temperature model. Only tributaries with measured discharge and temperature are shown. Note that not all remote automated weather station (RAWS) network sites used in our model are shown on this map. 29

Figure 2-3. Comparison of shortwave radiation measurements from the LCR ($J_{sn,LCR}$) to estimated components of shortwave radiation (i.e., $J_{sn,net}$, $J_{sn,dir}$, $J_{sn,diff}$, $J_{sn,refl}$) derived from the median value of measured shortwave radiation at RAWS network sites ($J_{sn,meas}$) near the study area. Daily RMSE values are provided above each day to illustrate the influence of the diffuse radiation correlation model and correspond to the fit of $J_{sn,meas}$ to $J_{sn,LCR}$ before and after radiation scaling. 41

Figure 2-4. Plot of long-term river temperature model residuals (observed minus modeled) for the simple and detailed radiation schemes at 5 gaging stations within Grand Canyon (RM30, RM61, RM88, RM167, and RM225). The right panels show the distribution of residuals between observed and modeled temperatures in °C. 44

Figure 2-5. Comparison of model results during low flow and high flow summer periods. The left and right columns show model results for July and August of 2000 and 2011, respectively. The top row shows observed discharge at Lees Ferry. Subsequent rows from top to bottom show modeled temperature predictions and observed data at RM61, RM88, and RM167..... 45

Figure 2-6. Boxplot of relative contribution of heat fluxes averaged over each model segment (shown in Figure 2-1) and each season of the year (Winter = Dec.-Feb., Spring = Mar.-May, Summer = Jun.-Aug., and Fall = Sep.-Nov.) for the entire simulation period. Mean values are included as horizontal dots. Shortwave and longwave radiative heat fluxes and lateral sources have been combined for readability. Variables being compared are net shortwave radiation ($J_{sn,net}$), net longwave radiation ($J_{lw,net}$), latent heat (J_e), sensible heat (J_c), friction (J_f), bed conduction (J_{sed}), and the apparent sensible heat from lateral sources (J_{lat}). 48

Figure 2-7. Sensitivity analysis of river temperature to input data perturbations at three locations during Winter and Summer averaged over the entire simulation time (Winter = Dec.-Feb., Summer = Jun.-Aug.). The residual is calculated as the detailed model minus scenario. Variables being compared are net shortwave radiation ($J_{sn,net}$), air temperature (T_{air}), rock temperature (T_{rock}), upstream boundary flow (Q_{BC}), upstream boundary condition temperature (T_{BC}), relative humidity (RH), wind speed (WS), distributed flows (Q_{dist}), distributed flow temperatures (T_{dist}). Box plot order follows that of the legend. Figure A-10 depicts sensitivity analysis results for Spring and Fall. 52

Figure 3-1. Map of the study area depicting the location of monitoring sites used in analyses and river temperature models for the Green River and Colorado River in Grand Canyon. Stream flow and temperature locations are indicated with a “S” and weather stations used in the modeling are indicated with a “W” and correspond to the information presented in Table 3-2. Yellow circles with X’s are the location of the solar radiation stations aggregated in the Grand Canyon model described by Mihalevich et al. (2020). Colored circles along the river show the location of GCMRC weather stations (GCMRC-WS) and correspond to the colors used in Figure B-2. Only tributaries with active monitoring stations are shown. 84

Figure 3-2. Spatial and temporal differences between weather input data for each variable. Values in plots A, C, E, and G are calculated as CR-WS minus ERA5-010. Values in plots B, D, F, and H are calculated as ERA5-100 minus ERA5-010. Black and white bars to the left of each plot show the spatial resolution of weather inputs from CR-WS (X1), ERA5-010 (X2) and ERA5-100 (X3), with each shade indicating a

different weather station or ERA5-Land grid. Data were averaged from hourly to daily resolution for illustration. 101

Figure 3-3. Figure showing boundary condition flow and temperature for the Colorado River (A) with river temperature predictions at downstream monitoring locations (B, C, and D) shown in Figure 3-1. Boxplots on the right-hand side show model residuals calculated as modeled minus observed. Time series data were aggregated into daily average values for illustration purposes. 103

Figure 3-4. Spatial and temporal differences between river temperature model predictions in the Colorado River. Values in plot A are calculated as CR-WS minus ERA5-010, and values in plot B are calculated as ERA5-100 minus ERA5-010. Black and white bars to the left of each plot show the spatial variability of weather inputs from CR-WS (X1), ERA5-010 (X2) and ERA5-100 (X3), with each shade indicating a different weather station or ERA5-Land grid. Labels on the right denote tributary locations. 105

Figure 3-5. Spatial and temporal differences between weather input data for each variable. Values in plots A, C, E, and G are calculated as GR-WS minus ERA5-010. Values in plots B, D, F, and H are calculated as ERA5-100 minus ERA5-010. Black and white bars to the left of each plot show the spatial variability of weather inputs from GR-WS (X1), ERA5-010 (X2) and ERA5-100 (X3), with each shade indicating a different weather station or ERA5-Land grid. 107

Figure 3-6. Figure showing boundary condition flow and temperature for the Yampa and Green Rivers (A) with river temperature predictions at downstream monitoring locations (B, C, and D) shown in Figure 3-1. Boxplots on the right-hand side show model residuals calculated as modeled minus observed. Time series data were aggregated into daily averaged values for illustration purposes. 109

Figure 3-7. Spatial and temporal differences between river temperature model predictions where (A) represents GR-WS minus ERA5-010, and (B) represents ERA5-100 minus ERA5-010. Black and white bars to the left of each plot show the spatial variability of weather inputs from GR-WS (X1), ERA5-010 (X2) and ERA5-100 (X3), with each shade indicating a different weather station or ERA5-Land grid. Labels on the right denote tributary locations. 111

Figure 4-1. (A) Example stream network representation in a water resources management model (RiverWare). Each icon represents a “node” which can be a specific location (i.e., stream gage, inflow, or reservoir) or a non-descript delineation of abstractions and redistributions within a river segment (i.e., regional uses). (B) Conceptual schematic of how

the water management model in Figure 4-1A is linked to a process-based river temperature model. Each trapezoidal prism is considered a model element (or cell) and can be many meters to many kilometers long. The dark blue directional arrow represents a point inflow while light blue bidirectional arrows represent distributed flow (either in or out of the model). Distributed flows can be calculated as the aggregate of all regional uses, shown above in Figure 4-1A. Red directional arrows represent the temperature associated with the point or distributed inflow (distributed outflows are given the instream temperature). Yellow directional arrows indicate weather information inputs which are applied to each model cell and can come from multiple sources. 132

Figure 4-2. Map of the study area depicting the sections Colorado River basin modeled using process-based river and reservoir models..... 142

Figure 4-3. Model coupling sequence (green arrows) used to conduct river routing and water temperature predictions throughout the Colorado River basin. RiverWare icons are used to illustrate how point inflow (dark blue directional arrows) and distributed flow (light blue bidirectional arrows) from the water management model are assigned to process-based model cells. Note that the process-based models are comprised of 100's of model cells, but have been reduced here for illustrative purposes. 143

Figure 4-4. Variability in Lake Powell water elevation for the 50 traces (grey lines) selected from the Millennium Drought hydrology (Salehabadi et al., 2020). The "Minimum Power Pool Elevation" is the elevation needed to generate hydropower. The "River Outlets Elevation" refers to the elevation at which water is drawn from for the bypass tubes, which are used when elevations drop below minimum power pool. 146

Figure 4-5. Modeled river and reservoir temperatures in the Green River, Lake Powell, and Grand Canyon river sections for the forecast year 2030. Temperatures are the mean of all 50 traces simulated. Surface water (epilimnion) temperatures are shown for Lake Powell (approximately 800 km to 1000 km). 156

Figure 4-6. Plot showing the cumulative percent probability that temperature differences between the Yampa River and Green River near their confluence are within certain temperature thresholds during summer months (A). Change in temperature differences between the Green and Yampa river temperatures at their confluence for summer months (June, July, and August) (B). The relative increase in river temperatures since 2022 for summer months in the Green and Yampa rivers immediately upstream of their confluence (C) 157

Figure 4-7. Thermally suitable days for humpback chub at three locations within Grand Canyon. Vertical lines on each series indicates the 25th and 75th percentiles and markers indicate the median for all 50 traces simulated..... 158

Figure 4-8. Longitudinal plot of temperature predictions for all 50 hydrologic traces on July 15, 2030, 6:00 pm. The date was arbitrarily chosen for illustration purposes. Our model was not setup to report temperatures of reservoir model cells that go dry due to reservoir drawdown, resulting in a gap between approximately 725 km and 825 km. Epilimnion lines (red) represent the variability in surface water temperatures. Hypolimnion lines (blue) represent the variability of temperatures deep in the reservoir, which was assumed to be at the bypass elevation. Release temperatures from Lake Powell become the upstream boundary condition in the Grand Canyon model, which are slightly different than the penstock elevation temperatures (gray) shown here because release temperatures are calculated from multiple layers near the penstocks. 161

Figure A-1. Simple schematic of external heat fluxes and lateral inflows accounted for in the river temperature model. Included terms are net shortwave radiation (Jsn,net), atmospheric longwave radiation (Jan), water longwave radiation (Jbr), bedrock longwave radiation (Jrock), sensible heat (conduction and convection; Jc), latent heat (evaporation and condensation; Je), internal fluid shear friction (Jf), sediment conduction (Jsed), tributary flows (Jtrib) and distributed flows (Jdist). Radiative terms are shown in red (Jsn,net, Jan, Jbr, and Jrock) and are described and illustrated in greater detail in the manuscript. Ysed is the depth of the shallow sediment layer, and Ygr is the depth to the ground boundary layer. Tsed is the temperature of the shallow sediment layer and Tgr is the temperature of the ground boundary layer..... 196

Figure A-2. Flow gained per water year in Grand Canyon between Lees Ferry (RM0) and RM225. The mean annual intervening flow is 30.4 m^3/s. The contribution from gaged tributaries is roughly half, with a mean annual flow of 14.6 m^3/s. 197

Figure A-3. Comparison between monthly average air temperature at Page, AZ municipal airport and Phantom Ranch within Grand Canyon to illustrate the general difference between the two locations (A). Relationship between sub-hourly air temperature measured at Phantom Ranch and air temperature regressed to Phantom Ranch using measured air temperature at Page, AZ (B). Histogram of residuals between measured and regressed air temperature data (C). The residuals have a mean of 0.0 and a standard deviation of 3.02 °C. The 99% confidence interval of the residuals are ± 0.012 °C..... 198

Figure A-4. Comparison of all shortwave radiation measurements from remote automated weather station network sites (grey lines) within the Grand Canyon region over a 5-day period. The Page, AZ municipal airport weather station characterizes the first two days as being overcast with light to moderate rain. The third day was mostly clear with periods of cloud cover. The last two days were clear conditions. 199

Figure A-5. Plot of long-term observations and model predictions of discharge at five gaging stations within Grand Canyon (RM30, RM61, RM88, RM167, and RM225). The right panels show the distribution of residuals between observed and modeled discharge in cubic meters per second. 200

Figure A-6. Plot of long-term observations and model predictions of temperature at five gaging stations within Grand Canyon (RM30, RM61, RM88, RM167, and RM225). The right panels show the distribution of residuals between observed and modeled temperature. 201

Figure A-7. Boxplot of temperature model residuals for simple and detailed radiation schemes by month for five gaging stations within Grand Canyon. Residuals were calculated as observed minus modeled temperatures. Colors correspond to the median value of a box where blue color/positive values represent model underestimated temperatures and red color/negative values represent over estimated temperatures. 202

Figure A-8. Illustration of calculated elevation angles (Ψ_E) from Glen Canyon Dam (24.1 km upstream of Lees Ferry) to Spencer Creek (395.9 km downstream of Lees Ferry) that were used to calculate spatiotemporal topographic shading (see Text A-2) (A). Shading factors (S_f) for each model cell at hourly resolution over a 1-year period used to scale incoming shortwave radiation (Jsn, dir) using Eqn. 2-8 (B). A shade factor of zero indicates no direct shortwave radiation. Note that 15-minute resolution S_f was used in the temperature model (i.e., Text A-2). 203

Figure A-9. Pie charts comparing the relative contribution of external heat fluxes from the detailed model during the entire simulation period (A), the summer of 2000 low flow period (B) and the summer of 2011 high flow period during (C). Variables being compared are net shortwave radiation ($J_{sn,net}$), net longwave radiation ($J_{lw,net}$), latent heat (J_e), sensible heat (J_c), friction (J_f), bed conduction (J_{sed}), and heat from lateral sources (J_{lat}). Percent contributions are calculated from the absolute value of the average for each flux over space and time. Each pie represents the fraction of the total heat exchanged, with $J_{lw,net}$ and J_e having negative average fluxes for each period shown. 204

Figure A-10. Sensitivity analysis of river temperature to input data perturbations at three locations during Fall and Spring averaged over the entire simulation time (Spring = Mar.-May, Fall = Sep.-Nov.). The residual is calculated as the detailed model minus scenario. Variables being compared are net shortwave radiation ($J_{sn,net}$), air temperature (T_{air}), bedrock temperature (T_{rock}), upstream boundary flow (Q_{BC}), upstream boundary condition temperature (T_{BC}), relative humidity (RH), wind speed (WS), distributed flows (Q_{dist}), distributed flow temperatures (T_{dist}). Box plot order follows that of the legend..... 205

Figure A-11. Sensitivity analysis of river temperature to input data perturbations at three locations during low flow (July 1, 2000 – Sept. 1, 2000) and high flow (July 1, 2011 – Sept. 1, 2011) periods. The residual is calculated as the detailed model minus scenario. Variables being compared are net shortwave radiation ($J_{sn,net}$), air temperature (T_{air}), rock temperature (T_{rock}), upstream boundary flow (Q_{BC}), upstream boundary condition temperature (T_{BC}), relative humidity (RH), wind speed (WS), distributed flows (Q_{dist}), distributed flow temperatures (T_{dist}). Box plot order follows that of the legend..... 206

Figure A-12. Comparison of predicted illumination angles 8.1 km upstream from Lees Ferry (i.e., RM -5) using the model presented by Yard et al. (2005) (red line) and the algorithm used here (i.e., Text A-2) (blue line). Root mean square error between the two models is 0.884 degrees of illumination angle. 207

Figure A-13. Historical daily water temperature at Lees Ferry (blue line) and daily elevation at Lake Powell (black line). Start of initial storage is approximately April 13, 1963 and completion of initial filling is approximately June 6, 1980. 208

Figure B-1. Weather stations within 20 miles of the Colorado River in Grand Canyon available on the MesoWest database. The bar chart on top shows the temporal availability of data for each site. Sites are color coded by the number of variables available for river temperature modeling (i.e., air temperature, wind speed, solar radiation, and relative humidity or dew point temperature). 231

Figure B-2. Data availability for weather stations within Grand Canyon. Sites are listed top to bottom in order of distance downstream of Glen Canyon Dam. River mile zero is located at Lees Ferry (Table 2-2) and downstream river distances are positive and upstream river distances are negative. Spatial trends of each variable are shown in subsequent plots in the left column. Temporal trends of each variable are shown in subsequent plots in the right column. The color used for each location corresponds to the colors shown in Figure 1 of the manuscript. 232

Figure B-3. Weather stations within 10 miles of the Green River available on the MesoWest database. The bar chart on right shows the temporal availability of data for each site. Sites are color coded by the number of variables available for river temperature modeling (i.e., air temperature, wind speed, solar radiation, and relative humidity or dew point temperature). 233

Figure B-4. Spatial and temporal tendencies of weather parameters for the stations shown in Figure B-3. Sites with limited information (n=16) were excluded. 234

Figure B-5. Simple schematic of external heat fluxes and lateral inflows accounted for in the river temperature model. Included terms are net shortwave radiation ($J_{sn,net}$), atmospheric longwave radiation (J_{an}), water longwave radiation (J_{br}), bedrock longwave radiation (J_{rock}), sensible heat (conduction and convection; J_c), latent heat (evaporation and condensation; J_e), internal fluid shear friction (J_f), sediment conduction (J_{sed}), tributary flows (J_{trib}) and distributed flows (J_{dist}). Radiative terms are shown in red ($J_{sn,net}$, J_{an}, J_{br}, and J_{rock}) and are described and illustrated in greater detail in the manuscript. Y_{sed} is the depth of the shallow sediment layer, and Y_{gr} is the depth to the ground boundary layer. T_{sed} is the temperature of the shallow sediment layer and T_{gr} is the temperature of the ground boundary layer. 235

Figure B-6. Example ERA5-Land grid resampling technique. The areal fraction (AF) is the fraction of original grid overlapped by the resample grid. The weight fraction (WF) is calculated as the AF of a single grid divided by the sum of AF and sums to 1. Resampling is done after values have been elevation corrected. 236

Figure B-7. Density ridgeline plots showing the distribution of residuals, calculated as Page, AZ or ERA5-Land data minus GCMRC-WS datasets, for each variable before and after elevation corrections were applied. Only a subset of GCMRC-WS is shown here, but before and after distributions were similar among all sites. Dashed ridgelines represent raw, uncorrected data, and solid ridgelines represent data after elevation corrections. Negative residuals represent underestimates and positive residuals represent overestimates. 237

Figure B-8. Spatial coverage of ERA5-010 and ERA5-100 grids in the Colorado River Grand Canyon temperature model. 238

Figure B-9. Tukey's Honest Significant Difference test for each of the three input weather datasets at the three locations evaluated in the Colorado River in Grand Canyon. Vertical overlaps represent statistically similar means. 239

Figure B-10. Seasonal differences in water temperature predictions between the CR-WS model and different sensitivity runs that apply one spatially varying weather variable from ERA5-Land (elevation corrected) and the remaining three weather variables are from the CR-WS dataset. Each of the four weather inputs were tested independently. Comparison between CR-WS model and ERA5-010 model (which includes all four ERA5-Land variables) is also included for reference. 240

Figure B-11. Spatial coverage of ERA5-010 and ERA5-100 grids in the Green River temperature model..... 241

Figure B12. Tukey's Honest Significant Difference test for each of the three input weather datasets at the three locations evaluated in the Green River. Vertical overlaps represent statistically similar means. 242

Figure B-13. Seasonal differences in water temperature predictions between the GR-WS model and different sensitivity runs that apply one spatially varying weather variable from ERA5-Land (elevation corrected) and the remaining three weather variables are from the GR-WS dataset. Each of the four weather inputs were tested independently. Comparison between GR-WS model and ERA5-010 model (which includes all four ERA5-Land variables) is also included for reference. 243

Figure B-14. Boundary condition flow for the Green River (A) with discharge predictions at downstream monitoring locations (B, C, and D) shown in Figure 1 and Table 2. Histograms on the right hand side show model residuals calculated as observed minus modeled. Time series data shown are hourly. Root mean square error (RMSE) values are for the data available over the two-year simulation period. 244

Figure B-15. Boundary condition flow for the Colorado River (A) with discharge predictions at downstream monitoring locations (B, C, and D) shown in Figure 1 and Table 2. Histograms on the right hand side show model residuals calculated as observed minus modeled. Time series data shown are hourly. Root mean square error (RMSE) values are for the data available over the two-year simulation period. 245

Figure C-1. Simple schematic of external heat fluxes and lateral inflows accounted for in the river temperature model. Included terms are net shortwave radiation (Jsn,net), atmospheric longwave radiation (Jan), water longwave radiation (Jbr), bedrock longwave radiation (Jrock), sensible heat (conduction and convection; Jc), latent heat (evaporation and condensation; Je), internal fluid shear friction (Jf), sediment conduction (Jsed), tributary flows (Jtrib) and distributed flows (Jdist). Radiative terms are shown in red (Jsn,net, Jan, Jbr, and Jrock) and are described and illustrated in greater detail in the manuscript. Ysed is the depth of the shallow sediment layer, and Ygr is the depth to the ground

boundary layer. Tsed is the temperature of the shallow sediment layer and Tgr is the temperature of the ground boundary layer. 266

Figure C-2. Example of flow information from the water management model (black line) and flow information reformatted for the process-based river and reservoir models (blue line). 267

Figure C-3. Complete model schematic of the Colorado River Simulation System. 268

Figure C-4. Map of the Colorado River basin showing the subset of CRSS nodes (Table C-2) used to model river temperatures using process-based models. River segments highlighted in blue were simulated using HydroCouple and CE-QAUL-W2 models. Lake Powell evaporation and change in bank storage were applied as distributed flows to the main Colorado River branch in the CE-QUAL-W2 model. 269

Figure C-5. Increases in air temperature relative to 2021 for a single 1.0° x 1.0° latitude and longitude grid located in the Colorado River basin based on the ensemble mean of BOR's Bias Corrected and Spatially Disaggregated (BCSD) CMIP5 projections with a RCP 4.5 emissions pathway. 270

Figure C-6. Map of Lake Powell showing all inflow tributaries accounted for in the CE-QUAL-W2 model. Modeled branches include the main Lake Powell water body, Bullfrog Creek, Escalante River, San Juan River, Rock Creek, Last Chance Creek, Warm Creek, Navajo Creek, and Wahweap Creek. 270

CHAPTER 1

INTRODUCTION

Diversions and impoundments have significantly altered the flow regime, thermal regime, sediment supply, and floodplain connection of large rivers throughout the world (Collier et al. 1996; Graff 1999; Lowney 2000). By extension, aquatic ecosystems have significantly changed in locations inundated by large reservoirs and in river sections downstream of dams (Nilsson and Renöfält 2008; Olden and Naiman 2010; Ward and Stanford 1983). In many regions, on-going climate change is expected to alter hydrologic patterns by reducing annual snowfall totals, shifting the timing of spring snowmelt runoff to earlier in the year, and decreasing overall basin runoff (Clifton et al. 2018; Dettinger et al. 2015; McCabe et al. 2017; Udall and Overpeck 2017; Woodhouse et al. 2016). The decisions water managers make regarding storage and distribution of water resources in highly managed rivers may further alter ecosystems via significant changes in downstream flow and thermal regimes.

River temperatures are fundamentally important to aquatic ecosystems because they drive rates of chemical and physiological processes, cue biological events, and control trophic interactions in food webs. Altered aquatic thermal regimes due to changes in climate and hydrology have the potential to disrupt life-history traits of populations by causing spatial and temporal mismatches between resources and consumers within existing food chain connections (Daufresne et al., 2009; Olden & Naiman, 2010; Winder & Schindler, 2004; Woodward et al., 2010; Vinson, 2001). Among native fish communities, elevated water temperatures may lead to higher rates of parasitism (Burkhardt-Holm et al. 2005), increased competition with non-native fishes (Carmona-

Catot et al. 2013; Cucherousset and Olden 2011), and predation by non-native species (Yard et al. 2011). As such, being able to predict river temperatures associated with future climate and hydrologic conditions is important for identifying management strategies that maintain healthy aquatic ecosystems.

River temperatures are most confidently forecasted using process-based models (Arismendi et al. 2014; Leach and Moore 2019), which estimate heat fluxes that influence warming or cooling as a function of hydraulic, hydrologic, and weather conditions. These approaches enable quantification of the individual mechanisms controlling thermal regimes at high spatial and temporal resolutions (King and Neilson 2019; Meier et al. 2003; Webb and Zhang 2004). For many river systems, shortwave radiation is the dominant heat flux (Caissie 2006; Dugdale et al. 2017; Webb and Zhang 1997a). However, additional factors such as flow regimes, inflows, other weather variables, and surrounding landscape features all play a role in shaping unique aspects of river thermal regimes around the world (Cardenas et al. 2014; King et al. 2016; Leach and Moore 2010; Neilson et al. 2010a). Further, streams of different size vary in sensitivity to meteorological conditions and inflows due to differences in thermal inertia (Anderson and Wright 2007; Carron 2000; Gu et al. 1998; Webb and Walling 1993). The surface area, which influences heat transfer rates at the air-water interface (Polehn and Kinsel 1997; Risley et al. 2010; Schmadel et al. 2015), also influences the rates of heat exchange and thermal sensitivity. Therefore, as flow varies over time and space, the role of different heat fluxes will also vary.

While our general understanding of river processes is quite advanced (Caissie 2006; Dugdale et al. 2017; Webb et al. 2008), there remain uncertainties and challenges

in modeling river temperature when dominant heat fluxes, such as shortwave radiation, are reduced. Some process-based modeling of river temperatures in complex terrain has been conducted (e.g., Carron and Rajaram 2001; Rutherford et al. 1997), but less attention has been placed on the spatiotemporal shading dynamics (Zhang et al. 2018) and landscape sources (e.g., from adjacent rock and vegetation) of radiation (Moore et al. 2014) that may become important in controlling the thermal regimes in shaded settings. In the context of canyon-bound river sections, where shortwave radiation can be limited at the water surface due to topography (Yard et al. 2005), the role of other heat fluxes will differ. However, these systems are also often affected by large upstream reservoirs which further complicates our understanding of the temperature controls due to highly variable flow magnitudes. This makes it difficult to quantify how thermal regimes, and subsequently ecosystems, in canyon-bound rivers will respond to different climate and hydrologic conditions.

To predict river temperatures and controls using a process-based model, significant amounts of data are required. In particular, detailed weather information is needed for river temperature predictions across entire river networks, but the spatial resolution requirements are uncertain (Benyahya et al. 2010; Johnson 2003). Process-based models that rely on a single ground-based weather station may not capture the spatial variability of meteorology across large geographic areas (Dugdale et al. 2017). To appropriately represent large areas, many weather stations are generally needed. However, the number of long-term hydrological and meteorological networks has been highly variable over the last two decades and some regions lack observations entirely (Lins 2008; Menne et al. 2018; NASA-GISS 2019). While these data limitations reduce

our ability to develop process-based models, quantifying heat flux dynamics is still needed to resolve climate related impacts on aquatic thermal regimes (Arismendi et al. 2014; Diabat et al. 2013; Dugdale et al. 2017; Leach and Moore 2019). This highlights the need to evaluate climate reanalysis datasets (CRDs) to supply spatially and temporally consistent weather information over large modeling domains. Currently, the application of CRDs to river temperature models is limited to only a few examples (Daniels & Danner, 2020; Li et al., 2015; Van Beek et al., 2012; Van Vliet et al., 2012), which leaves many unknowns about their feasibility and the spatial resolution needed to ensure reasonable river temperature predictions for different sizes of rivers. Overcoming these challenges is expected to advance temperature model development for data sparse regions, enabling far reaching understanding of thermal regimes. Yet, the evaluation of ecosystem responses to future conditions using these models cannot be fully realized without also considering water management decisions.

Water resources decision makers often conduct future planning by employing water management models (e.g., IQQM, Simons et al., 1996; MODSIM DSS, Fredericks et al., 1998; RiverWare, Zagona et al., 2001) that codify current policies to simulate how water is distributed and allocated throughout a basin and provide forecasts of flow and water volumes at certain locations. However, to understand ecosystem responses to water management decisions, water temperature responses to water allocation decisions must also be forecasted. Integrating water management model forecasts with process-based temperature models can be challenging because water management models generally operate on coarse spatial and temporal (e.g., monthly) scales that are practical for guiding decisions regarding basin-wide water supply distribution, while temperature models are

run at finer spatial and temporal scales. Furthermore, long-term boundary condition water temperature and weather forecasts are needed to predict river temperature responses to management decisions, but are often unavailable.

While several efforts have been made to directly link water quality responses to river management decisions (Bovee et al. 2008; Campbell et al. 2001; Sapin et al. 2017), higher spatiotemporal resolution water quality predictions, in particular water temperature, are needed to understand ecosystems responses to within-day hydrologic and climate variability (Alexander et al. 2013). To provide a more holistic understanding of thermal and ecosystem responses to water management decisions over entire river basins, new tools are needed to bridge the gap between instream water management models, water quality models, and ecosystem responses. Therefore, the overarching goal of this dissertation was to better understand water temperature controls in regulated rivers to understand the consequences of water management decisions on temperature regimes and ecosystems in large basins.

With the potential decreases in water supply due to climate change in some parts of the world combined with the inherent ecosystem challenges downstream from large reservoirs, there is a clear need to develop modeling frameworks that account for key riverine attributes (e.g., high canyon walls) and water management decisions to anticipate thermal regime changes under future climate conditions. Therefore, this work starts with the application of a process-based river temperature model and detailed shading algorithm for the Colorado River in Grand Canyon to identify the dominant temperature controls in a highly regulated and topographically diverse river reach (Chapter 2).

In complex topographic river basins, there is often limited ground-based meteorological data because they are inherently difficult to obtain. This poses a challenge when trying to understand river temperature processes at large spatial scales. This led to Chapter 3 focusing on the application of climate reanalysis datasets (CRDs) in the Grand Canyon temperature model developed in Chapter 2 and a new temperature model of the Green River tributary to test predictive capabilities over large portions of the Colorado River basin (Chapter 3).

Lastly, anticipating changes in aquatic ecosystems over large spatial scales in highly regulated rivers ultimately requires overcoming the major differences in the spatial and temporal representations of river basins in water management and water temperature models. To bridge this gap, a generic coupled modeling and data assimilation approach was developed that uses water management model outputs and strategically resampled weather and river temperature information to produce process-based model river and reservoir temperature forecasts at large scales (Chapter 4). This approach was tested using the Colorado River Simulation System forecasts over a large section of the Colorado River basin and used to evaluate aquatic ecosystems indicators at key habitat locations.

References

Alexander, C., Olson, E., Carron, J., & Conservancy, P. by E. T. L. and H. C. for the C. R. P. of T. N. (2013). Integrated Water Management in the Colorado River Basin Evaluation of Decision Support Platforms and Tools Final Report. January 2013, 107.

Anderson, C. R., & Wright, S. A. (2007). Development and application of a water temperature model for the Colorado River below Glen Canyon Dam, Arizona. Proceedings of the American Institute of Hydrology, 23, 1–11.

Arismendi, I., Safeeq, M., Dunham, J. B., & Johnson, S. L. (2014). Can air temperature be used to project influences of climate change on stream temperature? Environmental Research Letters, 9(8), 084015. https://doi.org/10.1088/1748-9326/9/8/084015

Benyahya, L., Caissie, D., El-Jabi, N., & Satish, M. G. (2010). Comparison of microclimate vs. remote meteorological data and results applied to a water temperature model (Miramichi River, Canada). Journal of Hydrology, 380(3–4), 247–259. https://doi.org/10.1016/j.jhydrol.2009.10.039

Bovee, K., Waddle, T., Talbert, C., Hatten, J., & Batt, T. (2008). Development and application of a decision support system for water management investigations in the upper Yakima River, Washington. 289.

Burkhardt-Holm, P., Giger, W., GUttinger, H., Ochsenbein, U., Peter, A., Scheurer, K., Segner, H., Staub, E., & Suter, M. J.-F. (2005). Where Have All the Fish Gone? Environmental Science & Technology, 39(21), 441A-447A. https://doi.org/10.1021/es053375z

Caissie, D. (2006). The thermal regime of rivers: A review. Freshwater Biology, 51(8), 1389–1406. https://doi.org/10.1111/j.1365-2427.2006.01597.x

Campbell, S. G., Hanna, R. B., Flug, M., & Scott, J. F. (2001). Modeling Klamath River System Operations for Quantity and Quality. Journal of Water Resources Planning and Management, 127(5), 284–294. https://doi.org/10.1061/(ASCE)0733-9496(2001)127:5(284)

Cardenas, M. B., Doering, M., Rivas, D. S., Galdeano, C., Neilson, B. T., & Robinson, C. T. (2014). Analysis of the temperature dynamics of a proglacial river using time-lapse thermal imaging and energy balance modeling. Journal of Hydrology, 519(PB), 1963–1973. https://doi.org/10.1016/j.jhydrol.2014.09.079

Carmona-Catot, G., Magellan, K., & García-Berthou, E. (2013). Temperature-Specific Competition between Invasive Mosquitofish and an Endangered Cyprinodontid Fish. PLoS ONE, 8(1). https://doi.org/10.1371/journal.pone.0054734

Carron, J. C. (2000). Simulation and optimization of unsteady flow and water temperature in reservoir regulated rivers. Civil, Environmental and Architectual Engineering Ph.D. Thesis, University of Colorado, Boulder CO., 159.

Carron, J. C., & Rajaram, H. (2001). Impact of variable reservoir releases on management of downstream water temperatures. Water Resources Research, 37(6), 1733–1743. https://doi.org/10.1029/2000WR900390

Clifton, C. F., Day, K. T., Luce, C. H., Grant, G. E., Safeeq, M., Halofsky, J. E., & Staab, B. P. (2018). Effects of climate change on hydrology and water resources in the Blue Mountains, Oregon, USA. Climate Services, 10(January 2017), 9–19. https://doi.org/10.1016/j.cliser.2018.03.001

Collier, M., Webb, R. H., & Schmidt, J. C. (1996). Dams and rivers: a primer on the downstream effects of dams. US Geological Survey Circular, 1126. https://doi.org/10.3133/cir1126

Cucherousset, J., & Olden, J. D. (2011). Ecological impacts of Non-Native freshwater fishes. Fisheries, 36(5), 215–230. https://doi.org/10.1080/03632415.2011.574578

Daniels, M. E., & Danner, E. M. (2020). The Drivers of River Temperatures Below a Large Dam. Water Resources Research, 56(5), 1–15. https://doi.org/10.1029/2019wr026751

Daufresne, M., Lengfellner, K., & Sommer, U. (2009). Global warming benefits the small in aquatic ecosystems. Proceedings of the National Academy of Sciences, 106(31), 12788–12793. https://doi.org/10.1073/pnas.0902080106

Dettinger, M., Udall, B., & Georgakakos, A. (2015). Western water and climate change. Ecological Applications, 25(8), 2069–2093. https://doi.org/10.1890/15-0938.1

Diabat, M., Haggerty, R., & Wondzell, S. M. (2013). Diurnal timing of warmer air under climate change affects magnitude, timing and duration of stream temperature change. Hydrological Processes, 27(16), 2367–2378. https://doi.org/10.1002/hyp.9533

Dugdale, S. J., Hannah, D. M., & Malcolm, I. A. (2017). River temperature modelling: A review of process-based approaches and future directions. Earth-Science Reviews, 175(October), 97–113. https://doi.org/10.1016/j.earscirev.2017.10.009

Fredericks, B. J. W., Labadie, J. W., & Altenhofen, J. M. (1998). DECISION SUPPORT SYSTEM FOR CONJUNCTIVE STREAM-AQUIFER MANAGEMENT By Jeffrey W. Fredericks; Member, ASCE, John W. Labadie,2 Member, ASCE, and Jon M. Altenhofen,3 Member, ASCE. 124(2), 69–78.

Graff, W. (1999). Dam Nation: A Geographic Census of American Dams and Their Large-Scale Hydrologic Impacts. 35(4), 1305–1311.

Gu, R., Montgomery, S., & Austin, T. AL. (1998). Quantifying the effects of stream discharge on summer river temperature. Hydrological Sciences Journal, 43(6), 885–904. https://doi.org/10.1080/02626669809492185

Johnson, S. L. (2003). Stream temperature: scaling of observations and issues for modelling. Hydrological Processes, 17(2), 497–499. https://doi.org/10.1002/hyp.5091

King, T. V., & Neilson, B. T. (2019). Quantifying reach-average effects of hyporheic exchange on arctic river temperatures in an area of continuous permafrost. Water Resources Research, 1–21. https://doi.org/10.1029/2018WR023463

King, T. V., Neilson, B. T., Overbeck, L. D., & Kane, D. L. (2016). Water temperature controls in low arctic rivers. Water Resources Research, 52(6), 4358–4376. https://doi.org/10.1002/2015WR017965

Leach, J. A., & Moore, R. D. (2010). Above-stream microclimate and stream surface energy exchanges in a wildfire-disturbed riparian zone. Hydrological Processes, 24(17), 2369–2381. https://doi.org/10.1002/hyp.7639

Leach, J. A., & Moore, R. D. (2019). Empirical stream thermal sensitivities may underestimate stream temperature response to climate warming. Water Resources Research, 2018WR024236. https://doi.org/10.1029/2018WR024236

Li, H.-Y., Ruby Leung, L., Tesfa, T., Voisin, N., Hejazi, M., Liu, L., Liu, Y., Rice, J., Wu, H., & Yang, X. (2015). Modeling stream temperature in the Anthropocene: An earth system modeling approach. Journal of Advances in Modeling Earth Systems, 7(4), 1661–1679. https://doi.org/10.1002/2015MS000471

Lins, H. F. (2008). Challenges to hydrological observations. WMO Bulletin, 57(January), 55–58.

Lowney, C. L. (2000). Stream temperature variation in regulated rivers: Evidence for a spatial pattern in daily minimum and maximum magnitudes. Water Resources Research, 36(10), 2947–2955. https://doi.org/10.1029/2000WR900142

McCabe, G. J., Wolock, D. M., Pederson, G. T., Woodhouse, C. A., & McAfee, S. (2017). Evidence that recent warming is reducing upper Colorado river flows. Earth Interactions, 21(10), 1–14. https://doi.org/10.1175/EI-D-17-0007.1

Meier, W., Bonjour, C., Wüest, A., & Reichert, P. (2003). Modeling the effect of water diversion on the temperature of mountain streams. Journal of Environmental Engineering, 129(8), 755–764. https://doi.org/10.1061/(ASCE)0733-9372(2003)129:8(755)

Menne, M. J., Williams, C. N., Gleason, B. E., Jared Rennie, J., & Lawrimore, J. H. (2018). The Global Historical Climatology Network Monthly Temperature Dataset,

Version 4. Journal of Climate, 31(24), 9835–9854. https://doi.org/10.1175/JCLI-D-18-0094.1

Moore, R. D., Leach, J. A., & Knudson, J. M. (2014). Geometric calculation of view factors for stream surface radiation modelling in the presence of riparian forest. Hydrological Processes, 28(6), 2975–2986. https://doi.org/10.1002/hyp.9848

NASA-GISS. (2019). GISS Surface Temperature Analysis Station Data: GHCN v3 and SCAR. https://data.giss.nasa.gov/gistemp/stdata/

Neilson, B. T., Stevens, D. K., Chapra, S. C., & Bandaragoda, C. (2010). Two-zone transient storage modeling using temperature and solute data with multiobjective calibration: 2. Temperature and solute. Water Resources Research, 46(12), 1–14. https://doi.org/10.1029/2009WR008759

Nilsson, C., & Renöfält, B. M. (2008). Linking Flow Regime and Water Quality in Rivers: a Challenge to Adaptive Catchment Management. Ecology and Society, 13(2), art18. https://doi.org/10.5751/ES-02588-130218

Olden, J. D., & Naiman, R. J. (2010). Incorporating thermal regimes into environmental flows assessments: Modifying dam operations to restore freshwater ecosystem integrity. Freshwater Biology, 55(1), 86–107. https://doi.org/10.1111/j.1365-2427.2009.02179.x

Polehn, R. A., & Kinsel, W. C. (1997). Transient temperature solution for stream flow from a controlled temperature source. Water Resources Research, 33(1), 261–265. https://doi.org/10.1029/96WR03016

Risley, J. C., Constantz, J., Essaid, H., & Rounds, S. (2010). Effects of upstream dams versus groundwater pumping on stream temperature under varying climate conditions. Water Resources Research, 46(6). https://doi.org/10.1029/2009WR008587

Rutherford, J. C., Blackett, S., Blackett, C., Saito, L., & Davies-Colley, R. J. (1997). Predicting the effects of shade on water temperature in small streams. New Zealand Journal of Marine and Freshwater Research, 31(5), 707–721. https://doi.org/10.1080/00288330.1997.9516801

Sapin, J. R., Saito, L., Dai, A., Rajagopalan, B., Blair Hanna, R., & Kauneckis, D. (2017). Demonstration of Integrated Reservoir Operations and Extreme Hydroclimate Modeling of Water Temperatures for Fish Sustainability below Shasta Lake. Journal of Water Resources Planning and Management, 143(10), 04017062. https://doi.org/10.1061/(ASCE)WR.1943-5452.0000834

Schmadel, N. M., Neilson, B. T., & Heavilin, J. E. (2015). Spatial considerations of stream hydraulics in reach scale temperature modeling. Water Resources Research, 51(7), 5566–5581. https://doi.org/10.1002/2015WR016931

Simons, M., Podger, G., & Cooke, R. (1996). IQQM - A hydrologic modelling tool for water resource and salinity management. Environmental Software, 11(1–3), 185–192. https://doi.org/10.1016/S0266-9838(96)00019-6

Udall, B., & Overpeck, J. (2017). The twenty-first century Colorado River hot drought and implications for the future. Water Resources Research, 53(3), 2404–2418. https://doi.org/10.1002/2016WR019638

Van Beek, L. P. H., Eikelboom, T., Van Vliet, M. T. H., & Bierkens, M. F. P. (2012). A physically based model of global freshwater surface temperature. Water Resources Research, 48(9). https://doi.org/10.1029/2012WR011819

Van Vliet, M. T. H., Yearsley, J. R., Franssen, W. H. P., Ludwig, F., Haddeland, I., Lettenmaier, D. P., & Kabat, P. (2012). Coupled daily streamflow and water temperature modelling in large river basins. Hydrology and Earth System Sciences, 16(11), 4303–4321. https://doi.org/10.5194/hess-16-4303-2012

Vinson, M. R. (2001). Long- Term Dynamics of an Invertebrate Assemblage Downstream From a Large Dam. Ecological Applications, 11(3), 711–730. https://doi.org/10.1890/1051-0761%282001%29011%5B0711%3ALTDOAI%5D2.0.CO%3B2

Ward, J. V., & Stanford, J. A. (1983). The serial discontinuity concept of lotic ecosystems.

Webb, B. W., Hannah, D. M., Moore, R. D., Brown, L. E., & Nobilis, F. (2008). Recent advances in stream and river temperature research. Hydrological Processes, 22(7), 902–918. https://doi.org/10.1002/hyp.6994

Webb, B. W., & Walling, D. E. (1993). Temporal variability in the impact of river regulation on thermal regime and some biological implications. Freshwater Biology, 29(1), 167–182. https://doi.org/10.1111/j.1365-2427.1993.tb00752.x

Webb, B. W., & Zhang, Y. (1997). Spatial and seasonal variability in the components of the river heat budget. Hydrological Processes, 11(1), 79–101. https://doi.org/10.1002/(SICI)1099-1085(199701)11:1<79::AID-HYP404>3.0.CO;2-N

Webb, B. W., & Zhang, Y. (2004). Intra-annual variability in the non-advective heat energy budget of Devon streams and rivers. Hydrological Processes, 18(11), 2117–2146. https://doi.org/10.1002/hyp.1463

Winder, M., & Schindler, D. E. (2004). CLIMATE CHANGE UNCOUPLES TROPHIC INTERACTIONS IN AN AQUATIC ECOSYSTEM. Ecology, 85(8), 2100–2106. https://doi.org/10.1890/04-0151

Woodhouse, C. A., Pederson, G. T., Morino, K., McAfee, S. A., & McCabe, G. J. (2016). Increasing influence of air temperature on upper Colorado River streamflow.

Geophysical Research Letters, 43(5), 2174–2181. https://doi.org/10.1002/2015GL067613

Woodward, G., Perkins, D. M., & Brown, L. E. (2010). Climate change and freshwater ecosystems: Impacts across multiple levels of organization. Philosophical Transactions of the Royal Society B: Biological Sciences, 365(1549), 2093–2106. https://doi.org/10.1098/rstb.2010.0055

Yard, M. D., Bennett, G. E., Mietz, S. N., Coggins, L. G., Stevens, L. E., Hueftle, S., & Blinn, D. W. (2005). Influence of topographic complexity on solar insolation estimates for the Colorado River, Grand Canyon, AZ. Ecological Modelling, 183(2–3), 157–172. https://doi.org/10.1016/j.ecolmodel.2004.07.027

Yard, M. D., Coggins, L. G., Baxter, C. V., Bennett, G. E., & Korman, J. (2011). Trout piscivory in the Colorado River, Grand Canyon: Effects of turbidity, temperature, and fish prey availability. Transactions of the American Fisheries Society, 140(2), 471–486. https://doi.org/10.1080/00028487.2011.572011

Zagona, E. A., Fulp, T. J., Shane, R., Magee, T., & Goranflo, H. M. (2001). RIVERWARE: A GENERALIZED TOOL FOR COMPLEX RESERVOIR SYSTEM MODELING1. JAWRA Journal of the American Water Resources Association, 37(4), 913–929. https://doi.org/10.1111/j.1752-1688.2001.tb05522.x

Zhang, Y. L., Li, X., Cheng, G. D., Jin, H. J., Yang, D. W., Flerchinger, G. N., Chang, X. L., Wang, X., & Liang, J. (2018). Influences of topographic shadows on the thermal and hydrological processes in a cold region mountainous watershed in northwest China. Journal of Advances in Modeling Earth Systems, 10(7), 1439–1457. https://doi.org/10.1029/2017MS001264

CHAPTER 2[1]

WATER TEMPERATURE CONTROLS FOR REGULATED CANYON-BOUND RIVERS

Abstract

Many canyon-bound rivers have been dammed and downstream flow and water temperatures modified. Climate change is expected to cause lower storage in reservoirs and warmer release temperatures, which may further alter downstream flow and thermal regimes. To anticipate potential future changes, we first need to understand the dominant heat transfer mechanisms in canyon-bound river systems. Towards this end, we adapt a dynamic process-based river routing and temperature model to account for complex shading and radiation characteristics found in canyon-bound rivers. We apply the model to a 362 km segment of the Colorado River in Grand Canyon National Park, USA to simulate temperature over an 18-year period. Extensive temperature and flow datasets from within the canyon were used to assess model performance. At the most downstream gaging location, root mean square errors of hourly flow routing and temperature predictions were 11.5 m^3/s and 0.93 °C, respectively. We found that heat fluxes controlling temperatures were highly variable over space and time, primarily due to shortwave radiation dynamics and hydropeaking flow conditions. Additionally, the large differences between air and water temperature during summer periods resulted in high sensible and latent heat fluxes. Sensitivity analyses indicate that reservoir release temperatures are most influential above the RM88 gage (141 kilometers below Glen Canyon Dam), while a combination of discharge, shortwave radiation, and air

[1]Coauthored by Bryce A. Mihalevich, Bethany T. Neilson, Caleb A. Buahin, Charles B. Yackulic, and John C. Schmidt

temperature become more important farther downstream. This study illustrates the importance of understanding the spatial and temporal variability of topographic shading when predicting water temperatures in canyon-bound rivers.

1. Introduction

Temperature plays a key role in aquatic ecosystems by driving rates of chemical reactions and resulting physiological processes, synchronizing phenological processes, and modifying trophic interactions in food webs (Olden & Naiman, 2010). As such, understanding how temperature may respond to changes in climate and hydrology is important for predicting ecosystem responses. Process-based river temperature models allow for the quantification of individual heat fluxes and the identification of dominant mechanisms, allowing for robust, temperature predictions. Because these models are built on heat transfer fundamentals that are driven by instream flow conditions and local meteorological information, they also provide insights regarding the sensitivity of river temperatures to anticipated future conditions. Many types of river systems have been studied and models adapted to represent their unique aspects including radiation from adjacent rock cliffs (e.g., Cardenas et al., 2014), surface and subsurface transient storage heat contributions (e.g., King & Neilson, 2019; Neilson et al., 2010), and longwave radiation from terrain and riparian vegetation visible from the water surface (e.g., Leach & Moore, 2010). However, the mechanisms controlling water temperatures when shortwave radiation is reduced due to significant topographic shading are not as well understood.

In deep canyons, topography obstructs direct shortwave radiation from reaching the water surface during a large portion of each day. The timing of this shading is highly

dependent on the orientation of the river section, the latitude, and the day of the year (Yard et al., 2005). Many river temperature models incorporate the effects of shading from vegetation or land surfaces by scaling shortwave radiation by shading factors. These shading factors are often estimated from physical observations or land surface elevation models and can vary from constant shade factors applied over entire reaches to hourly values for specific coordinates (Chen et al., 1998a; Loinaz et al., 2013; Rutherford et al., 1997; Wawrzyniak et al., 2017). However, less attention has been given to the spatiotemporal dynamics of shading in deep canyons, which can be highly variable over relatively small scales, and therefore become important when investigating thermal regimes of canyon-bound rivers over different seasons.

When considering radiation influences in natural systems, it is common to focus on direct solar radiation and less emphasis has been given to the lower energy, diffuse component. The diffuse fraction consists of shortwave radiation that has been absorbed and scattered within the atmosphere before reaching the land or water surface (Dubayah & Rich, 1995). In the context of process-based river temperature modeling, the diffuse shortwave radiation has at times been estimated using a fixed ratio (e.g., 20% or 30%) of the total incoming shortwave radiation (Rutherford et al., 1997; Westhoff et al., 2007). Others have used more complex empirical formulations to estimate diffuse radiation from extraterrestrial radiation and atmospheric transmissivity (Cox & Bolte, 2007; Sridhar et al., 2004) or based on a clearness index (Chen et al., 1998a; Leach & Moore, 2010; Zhang et al., 2018). Despite this heat flux often being negligible, in canyon-bound rivers the diffuse component can be the only source of shortwave radiation for extended periods of time (Stanitski-Martin, 1996; Yard et al., 2005).

Also inherent in systems with complex topography is the reduction in the atmospheric longwave radiation that reaches the water surface. Longwave radiation is an important heat source to most river systems (Caissie, 2006; Webb et al., 2008), but is reduced if a large portion of the sky is obstructed by topography or riparian vegetation (Moore et al., 2014). This decrease in atmospheric longwave radiation will increase the relative importance of longwave radiation contributed by the surrounding terrain (Cardenas et al., 2014; Matzinger et al., 2003; Plüss & Ohmura, 1997) or overhanging canopy (Leach & Moore, 2010; Roth et al., 2010). The importance of radiation emitted from surrounding topography has been shown for cirque walls of mountainous areas that re-emit longwave radiation resulting in greater incoming longwave radiation and a subsequent increase in the rates of alpine snowmelt (Brazel & Marcus, 1987; Olyphant, 1986). In the Glen Canyon portion of the Colorado River, Stanitski-Martin (1996) found that surrounding walls absorbed shortwave and longwave radiation during the day and the re-emitted longwave radiation from rock walls resulted in increased energy received at the water surface. These findings, combined with the recent emphasis on the importance of incorporating longwave radiative fluxes from landscape features (Moore et al., 2014) suggests that river temperature models applied in settings with complex topography need to be adapted to account for radiation influences from a variety of sources.

In addition to the complex radiative dynamics, canyon-bound rivers may also be affected by water development (e.g., large upstream reservoirs) which changes the natural downstream hydrologic and thermal characteristics (Collier et al., 1996; Graff, 1999; Lowney, 2000), and by extension, the downstream aquatic ecosystems (Nilsson & Renöfält, 2008; Olden & Naiman, 2010; Ward & Stanford, 1983). Reservoir release

volumes can have large daily fluctuations because of power demands, resulting in higher volume releases during the daytime when demand increases and lower volume releases at night when demand decreases. This affects the thermal inertia of the river (Anderson & Wright, 2007; Carron, 2000; Webb & Walling, 1993), a property that describes the amount of energy required to alter temperatures given the volume of water in the system (Gu et al., 1998). Depending on the pattern, magnitude, and timing of releases, upstream discharge and water temperature can affect river segments that may be 100's of kilometers downstream (Carron & Rajaram, 2001; Ferencz et al., 2019). Lastly, the river surface area to volume ratio also influences downstream temperatures (Polehn & Kinsel, 1997; Risley et al., 2010). In canyon-bound rivers where the rating relation between river stage and discharge is typically steep (Wenzel & Fishel, 1942), large changes in flow may result in relatively small changes in surface area because the channel width is confined by bedrock. Therefore, the surface area available to exchange heat remains relatively constant while discharges can change significantly.

Despite the importance of canyon-bound rivers for water supply, and inherent ecosystem challenges below dammed rivers, there is limited information about which heat fluxes control temperatures in these settings or how this may change with future climate and management practices. We hypothesize that heat fluxes responsible for controlling river temperature in regulated, canyon-bound rivers during high and low flows are highly dependent on the distance downstream of the dam, nearby topographic shading, and the time of year when they occur. Specifically, river temperatures become advection dominated under high flows, but will be controlled by a wide variety of surface heat fluxes during low flows. We test this hypothesis by adapting a dynamic routing and

temperature modeling framework to capture the unique features of canyon-bound rivers and apply it to the highly regulated Colorado River in Grand Canyon. We analyze heat flux dynamics over a long simulation period (2000-2018) that includes typical daily fluctuations of flow, but also periods of both extended high and low flow experiments. While this paper does not explicitly evaluate climate change scenarios, quantifying the dominant heat transfer mechanisms provides a conceptual basis for inferring potential linkages between climate change and water temperatures in canyon-bound rivers. This modeling framework also provides the foundation for future work to investigate climate change projections and aquatic ecosystem implications.

2. Methods

2.1. Model formulation

In order to test our hypothesis about the key heat fluxes in canyon-bound rivers, we adapt a dynamic process-based routing and river temperature model to account for the influences of complex topography on river radiation balances. The foundational modeling framework, described by Buahin et al. (2019) and based on Neilson et al. (2010), includes various heat transfer and routing components that were developed and implemented within HydroCouple (Buahin & Horsburgh, 2018). The components included here are: EPA SWMM (Storm Water Management Model; Rossman, 2006) for dynamic wave hydraulic routing (solving the complete form of the St. Venant flow equations); the channel solute and heat transport (CSH) component for channel advection and dispersion, and sensible and latent heat fluxes; the radiative heat exchange (RHE) component used for shortwave and longwave radiation terms; the hyporheic transient storage (HTS) component used for sediment conduction; and the time series provider component to

apply externally calculated scaling factors to select heat flux terms (i.e., spatial and temporal shading factors).

The CSH component uses the finite volume method to numerically approximate the 1D advection and dispersion heat transport equation:

$$\rho_w c_p \frac{\partial T_w}{\partial t} = \rho_w c_p \frac{\partial (v T_w)}{\partial x} + \rho_w c_p \frac{\partial}{\partial x}\left(D \frac{\partial T_w}{\partial x}\right) + \frac{\rho_w c_p}{V}(Q_{trib} T_{trib} + Q_{dist} T_{dist}) + \frac{J_{total}}{Y} \quad (2\text{-}1)$$

where T_w is the water temperature (°C), t is the time (s), v is the velocity of the water in the channel (m/s), x is the distance along the channel (m), D is longitudinal dispersion (m^2/s), ρ_w is the water density (kg/m^3), c_p is the specific heat capacity of water (J/kg/°C), Q_{trib} is the external flow from a tributary (m^3/s), Q_{dist} is the external distributed inflow or outflow (m^3/s), T_{trib} is the tributary temperature (°C), T_{dist} is the distributed flow temperature, J_{total} is the sum of all heat fluxes into and out of the river (W/m^2), V is the volume of the channel (m^3), and Y is the depth of water in the channel (m) that is calculated within the routing component as a function of channel shape and discharge. The J_{total} is calculated using the CSH, RHE, and HTS components and includes:

$$J_{total} = J_{sn,net} + J_{lw,net} + J_c + J_e + J_f + J_{sed} \quad (2\text{-}2)$$

where all heat fluxes are in W/m^2 and include net shortwave radiation ($J_{sn,net}$), net longwave radiation ($J_{lw,net}$), sensible heat (conduction and convection; J_c), latent heat (evaporation and condensation; J_e), internal fluid shear friction (J_f), and sediment conduction (J_{sed}) (Figure A-1). Air-water interface fluxes ($J_{sn,net}$, $J_{lw,net}$, J_c, and J_e) are a function of channel width which is determined by channel shape and discharge. In order to account for heat transfer processes associated with canyon-bound rivers, components $J_{sn,net}$, $J_{lw,net}$, and J_f were adapted from the original HydroCouple formulation and are

described in detail below. Components J_e, J_c, and J_{sed} were not altered from the original formulation as described within Buahin et al. (2019).

2.2. Model adaptations

2.2.1. Radiation balance

Due to the attenuating, diffusive, and reflective effects of varying topography and river orientation on the net shortwave radiation received at the river surface ($J_{sn,net}$), it is necessary to account for the individual components of this radiation in canyon-bound systems at higher spatial and temporal resolution. Shortwave radiation was estimated as the sum of three individual terms (Figure 2-1): direct shortwave ($J_{sn,dir}$), diffuse shortwave ($J_{sn,diff}$), and land-reflected shortwave radiation ($J_{sn,refl}$; Eqn. 2-3).

$$J_{sn,net} = J_{sn,dir} + J_{sn,diff} + J_{sn,refl} \quad (2\text{-}3)$$

Process-based models commonly only consider longwave radiation coming from the atmosphere (J_{an}) and from the water (J_{br}). However, canyon-bound rivers are often adjacent to rock walls that can absorb radiation and re-emit longwave radiation. To account for this re-emitted radiation, the term J_{rock} was included in the longwave radiation balance (Figure 2-1). Therefore, the net longwave radiation balance is calculated as:

$$J_{lw,net} = J_{an} + J_{rock} - J_{br} \quad (2\text{-}4)$$

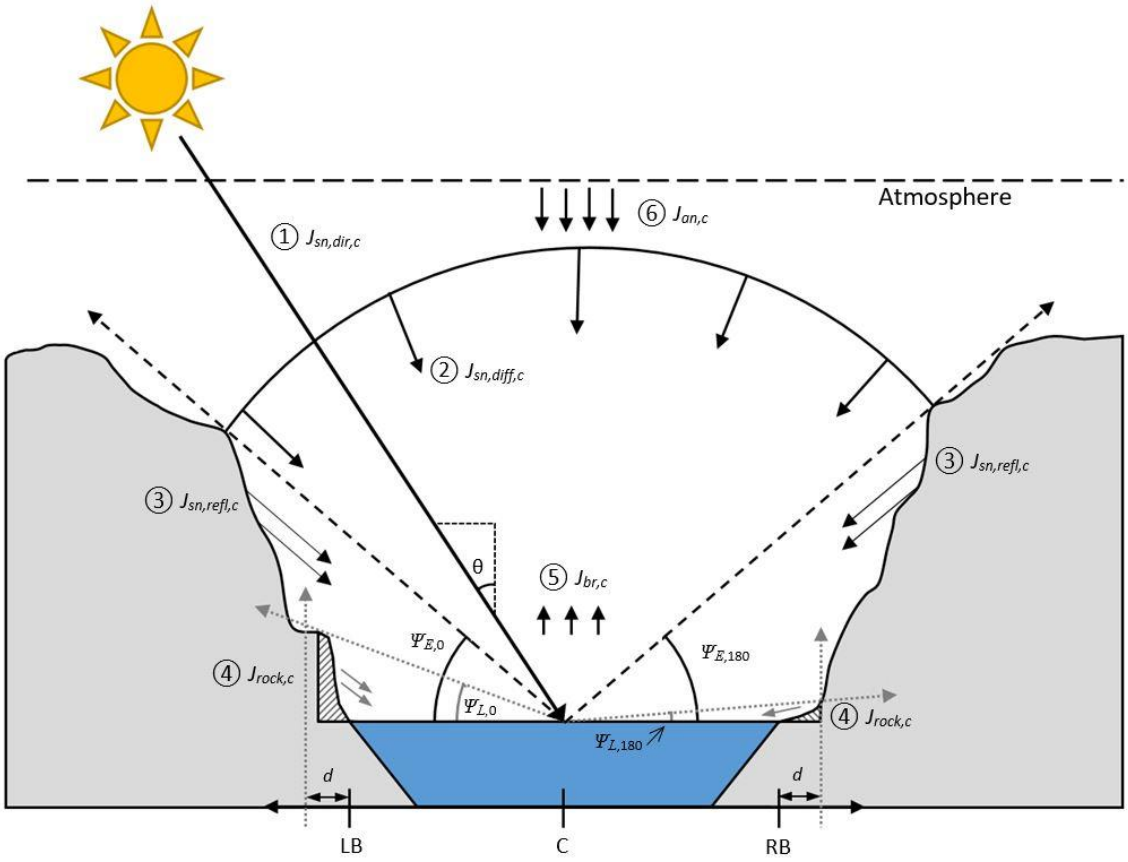

Figure 2-1. Schematic illustrating the radiation balance used in this model for a cross-section of the river at a given model cell (*c*). LB = left bank, RB = right bank, C = river center, d = distance in meters away from the river bank, θ = the solar zenith angle, $\Psi_{E,0}$ = is the elevation angle from river center at 0° azimuth (Φ), $\Psi_{E,180}$ = is the elevation angle from river center at Φ=180°, $\Psi_{L,0}$ = is the land re-emittance angle from river center at Φ = 0°, $\Psi_{L,180}$ = is the land re-emittance angle from river center at Φ =180°. For the radiation balance Φ is calculated from 0° to 359°, but only 0° and 180° are shown here for illustration. Shortwave radiation received at the water surface within the canyon consists of 1) direct shortwave radiation ($J_{sn,dir,c}$) originating from the sun and scaled by topographic shading factors (S_f), 2) diffuse shortwave radiation ($J_{sn,diff,c}$) originating from any sky direction as the result of scattering by atmospheric gases and particles and scaled by the sky view factor (SV_f), and 3) land-reflected longwave radiation ($J_{sn,refl,c}$) from nearby terrain. Longwave radiation components considered in this model include 4) rock longwave radiation ($J_{rock,c}$) within a specified distance (*d*) of the edge of water 5) water longwave radiation ($J_{br,c}$), and 6) atmospheric longwave radiation ($J_{an,c}$) scaled by the sky view factor ($SV_{f,c,d}$) calculated from the river center and including the area at a specified distance (*d*) from the edge of water.

2.2.1.1. Shortwave radiation

Measurements of shortwave radiation within canyon-bound rivers are uncommon because these locations are often remote and difficult to access. Furthermore, the complex topography near any monitoring locations within canyons results in observations that are highly site-specific due to local shading dynamics. This makes it unrealistic to apply observations to river segments outside of the location where the observations were made. Therefore, in order to have realistic estimates of shortwave radiation reaching canyon-bound river surfaces, individual shortwave radiation terms ($J_{sn,dir}$, $J_{sn,diff}$, $J_{sn,refl}$) were estimated for specific river locations by scaling measured shortwave radiation ($J_{sn,meas}$) outside of the canyon. We do this by assuming that shortwave radiation measurements taken outside of the canyon are free from significant obstructions that would shade or influence observations via reflection from nearby features (e.g., canyon walls). Therefore, $J_{sn,meas}$ values represent:

$$J_{sn,meas} = \hat{J}_{sn,dir} + \hat{J}_{sn,diff} \quad (2\text{-}5)$$

where $\hat{J}$ denotes estimates of shortwave radiation on a horizontal surface (e.g., above the canyon). Note that since we assumed that $\hat{J}_{sn,refl} = 0$ for measurements outside of the canyon, this term was omitted from Eqn. 2-5.

Direct and diffuse components of $J_{sn,meas}$ can be separated out through the application of empirical correlation equations (Dervishi & Mahdavi, 2012). Because the relationship between these shortwave radiation components varies globally as a function of atmospheric characteristics, several models have been developed to fit site-specific observations (e.g., Erbs et al., 1982; Lam & Li, 1996; Orgill & Hollands, 1977). Each of these models result in a correlation equation (Text A-1) that predicts the fraction of

diffuse radiation (k_d) as a function of the ratio between $J_{sn,meas}$ and modeled extraterrestrial radiation ($J_{sn,mod}$), known as the clearness index or clear sky index (k_t; Eqn. 2-6):

$$k_t = J_{sn,meas}/J_{sn,mod} \times \cos\theta \quad (2\text{-}6)$$

where θ is the solar zenith angle and values of k_t range between 0 and 1 with a value of 1 indicating clear sky. In this paper, $J_{sn,mod}$ was estimated using the Modular Distributed Watershed Educational Toolbox (MOD-WET; Huning & Margulis, 2015) functions in MATLAB. These functions calculate solar coordinates and top-of-atmosphere shortwave radiation as a function of geographical latitude and time. Applying k_t to the correlation equations results in an estimate of k_d above the canyon, such that

$$\hat{J}_{sn,diff} = J_{sn,meas}(k_d) \quad (2\text{-}7)$$

The $\hat{J}_{sn,dir}$ component is then calculated from Eqn. 2-5 via subtraction.

Direct shortwave radiation within a canyon. When trying to understand temperature dynamics in deep canyon settings over large spatial and temporal model domains, spatiotemporal shading information is needed to account for the variability in direct shortwave radiation reaching the water surface during different times of the year. A model for predicting shade in a canyon-bound setting, specifically Glen and Grand Canyon, was previously developed (Yard et al., 2005). However, this model predicts the photosynthetic photon flux density at the water surface, which is the visible light in the shortwave radiation spectrum (i.e., 400 nm – 700 nm). In order to get the complete estimate of shortwave radiation (~285 nm – 3000 nm), we developed an algorithm to compute topographic shade factors (S_f) over space and time following the methods of Yard et al. (2005; Text A-2). These factors were calculated at regularly spaced

increments along the river centerline and averaged over each respective model cell (c) to get $S_{f,c}$. $S_{f,c}$ is applied to the time variable direct shortwave radiation outside of the canyon ($\hat{J}_{sn,dir}$) to estimate the direct shortwave radiation reaching the water surface at each c:

$$J_{sn,dir,c} = (S_{f,c})\hat{J}_{sn,dir} \quad (2\text{-}8)$$

Diffuse shortwave radiation within a canyon. Diffuse radiation incident at the water surface is reduced by the fraction of the overlying visible hemisphere, referred to as the sky view factor (SV_f). SV_f can be calculated at specific coordinates along the river following the formulation from Dozier and Frew (1990). For these calculations only, we assume that the slope of the river could be approximated as zero to simplify the equation to:

$$SV_f = \frac{1}{2}\sum_{\Phi_j=1}^{360} sin^2\,(90 - \Psi_{E,\Phi}) \quad (2\text{-}9)$$

where Φ is the azimuth angle and $\Psi_{E,\Phi}$ is the elevation angle in the Φ direction (Figure 2-1). In this application, SV_f was calculated at regularly spaced increments along the river centerline and averaged over each respective c to get $SV_{f,c}$. The diffuse shortwave radiation reaching the water surface of each model cell over time is then calculated as:

$$J_{sn,diff,c} = (SV_{f,c})\hat{J}_{sn,diff} \quad (2\text{-}10)$$

Land-reflected shortwave radiation within a canyon. Land-reflected radiation is the combination of both direct radiation and diffuse radiation incident on the water surface which has been reflected off the surrounding terrain. This source of shortwave radiation can become important in deep valleys when considering an entire year, but is generally small compared to the direct and diffuse components (Chen et al., 2006). While it is often neglected in river temperature modeling, for land surface energy budgets in deep mountain valleys, measured reflected shortwave radiation has been shown to be 14

to 21% of the incoming shortwave radiation (Matzinger et al., 2003; Whiteman et al., 1989). Due to rock walls being adjacent to many canyon-bound rivers, it is presumed that a portion of the reflected shortwave radiation makes it to the water surface. We included reflected shortwave radiation, calculating it following Gates (1980) as:

$$J_{sn,refl,c} = \alpha_{land}(1 - SV_{f,c}) \times (\hat{J}_{sn,dir} + \hat{J}_{sn,diff}) \quad (2\text{-}11)$$

where α_{land} is the albedo of the surrounding terrain. This approach does not account for conditions where only a fraction of the terrain is illuminated by $\hat{J}_{sn,dir}$, but instead assumes that $J_{sn,refl}$ is isotropic. Because $J_{sn,refl}$ is reportedly small (Chen et al., 2006), the complex process of modeling the anisotropic nature of $J_{sn,refl}$ that involves computing multiple reflections from all viewable terrain cells was not considered.

2.2.1.2. Longwave radiation

Rock longwave radiation. Heat emitted from rock as longwave radiation was estimated following the Stefan-Boltzmann Law (Chapra, 1997). However, because the intensity of longwave radiation quickly attenuates as you move away from its source, only rock features adjacent to the river are expected to contribute significant amounts of heat to the river. In order to account for this effect, we recomputed the SV_f only considering terrain within 5 m from the river's edge ($SV_{f,5}$). Following Eqn. 2-9, $SV_{f,5}$ were calculated at specific coordinates by replacing elevation angles (Ψ_E) with land re-emittance angles (Ψ_L), where Ψ_L is defined as the largest angle between river center and the adjacent terrain within a distance of 5 m from the river banks (Figure 2-1). The $SV_{f,5}$ were averaged over space for each c to get $SV_{f,c,5}$. J_{rock} was then computed as:

$$J_{rock,c} = (1 - SV_{f,c,5})(\varepsilon_{lc}\, \sigma\, T_{rock}^4) \quad (2\text{-}12)$$

where σ is the Stefan-Boltzmann constant ($W/m^2/K^4$) and $\mathcal{E}_{lc}$ is the emissivity of the land. T_{rock} is the rock temperature (K) and was assumed to be the same as the air temperature (T_{air}). This assumption was consistent with other studies that estimated longwave radiation from both terrain and vegetation (Benyahya et al., 2012; Caissie, 2016; MacDonald et al., 2014). It is considered to be an underestimate of temperature for terrain sources because direct shortwave radiation can elevate rock surface temperatures approximately 10-25 °C higher than the ambient air temperature, while shaded surfaces will be equal to or slightly cooler than the ambient air temperature due to convective or evaporative fluxes (Gates, 1980; Larson et al., 2000).

Atmospheric longwave radiation. Heat emitted from the atmosphere as longwave radiation is obstructed by surrounding topography, reducing the amount that is received at the water surface. To account for this, atmospheric longwave radiation was scaled by the sky view factor that considered terrain greater than 5 m from the shoreline. Therefore, the formulation of J_{an} is:

$$J_{an,c} = SV_{f,c,5}(\varepsilon_{atm}\ \sigma\ T_{air}^4)(1 - R_L) \quad (2\text{-}13)$$

where $\mathcal{E}_{atm}$ is the emissivity of the atmosphere and R_L is the reflection coefficient.

2.2.2. Internal fluid shear friction

Heat generated by friction is typically small in rivers, but can be a significant source of heat in steep streams (Meier et al., 2003; Theurer et al., 1984) or streams with relatively high discharge, both of which can be present in canyon-bound rivers or streams. Heat generated in this process is related to the potential energy lost from the change in elevation, resulting in friction and turbulent energy dissipation. Following the

formulation by Theurer et al. (1984), internal fluid shear friction was added to the CSH component and is a function of flow, bed slope, and channel width (Text A-3).

2.3. Model application

2.3.1. Study Site: The Colorado River in the Grand Canyon

The Colorado River flows for approximately 800 km through the uplifted landscape of the southern Colorado Plateau, including 450 km of the Grand Canyon. Within Grand Canyon, the most downstream 65 km of the river is inundated by Lake Mead. Immediately upstream from Grand Canyon, the river is impounded by Glen Canyon Dam forming Lake Powell (Figure 2-2). The river in Grand Canyon is organized in a series of steps, with steep, turbulent rapids, and flat intervening sections (Magirl et al., 2005). Surrounding the river, the terrain is topographically complex with an average canyon depth of 1,200 m and average width of 1,600 m which limits the amount of direct shortwave radiation received at the water surface (Yard et al., 2005). As the Colorado River flows through this region, it often changes orientation, resulting in dynamic shade patterns that are highly variable over time from one river kilometer to the next. In many sections of the canyon, the river adjoins bedrock features which complicate the radiation balance by re-emitting longwave radiation to the water surface (Stanitski-Martin, 1996). The geology is comprised of nearly 40 major sedimentary rock layers including limestone, sandstone, shale, and metamorphic schist and granite intrusions (Karlstrom et al., 2012). Many seeps and springs emerge from the limestone layers that are karst (Fitzgerald, 1996; Goings, 1985; Zukosky, 1995), feeding several perennial tributaries that combined, contribute an average discharge of approximately 30.4 m^3/s to the Grand Canyon on an annual basis (Figure A-2).

Comprehensive information about the management of Glen Canyon Dam and the effects it has had on flow regimes, water quality, and aquatic ecology in the downstream Colorado River can be found in Gloss et al. (2005) and U.S. Bureau of Reclamation (2012). An exhaustive review of this material is outside the scope of this paper, however, a brief summary of river temperature characteristics, data collection programs, and modeling efforts is provided in Text A-4. While these studies are major contributions to our understanding of hydrology and river temperature within Grand Canyon, the actual mechanisms controlling temperatures in the Colorado River have yet to be identified and quantified. The work presented here seeks to build on the considerable body of literature that already exists for the Colorado River while also building our understanding of river temperature controls in flow regulated canyon-bound rivers.

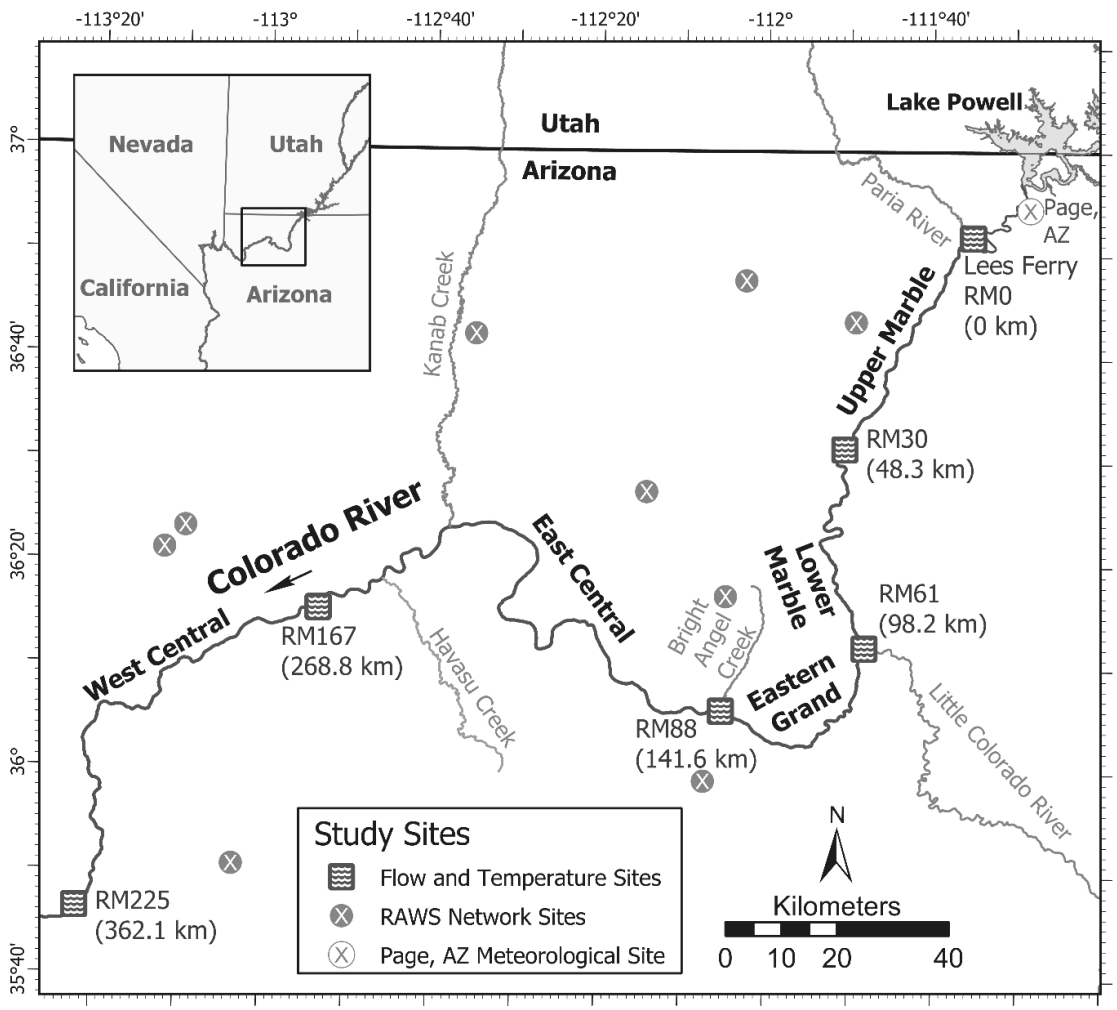

Figure 2-2. Map of the study area depicting model extent (RM0-RM225), major river segments (Melis, 2011), and the location of discharge and temperature monitoring sites used in the river temperature model. Only tributaries with measured discharge and temperature are shown. Note that not all remote automated weather station (RAWS) network sites used in our model are shown on this map.

2.3.2. Model domain, simulation period and forcing data

To understand the dominant processes controlling water temperatures in Grand Canyon, we modeled flow and temperature for a 362 km section and 18-year period (Jan. 1, 2000 to Jan. 1, 2018) at approximately a 1 km spatial and hourly temporal resolution. This simulation period was largely dictated by the availability of sub-daily (15-20 minute) temperature data at the USGS gage at Lees Ferry (*USGS 09380000 Colorado*

River at Lees Ferry, AZ) that was used as the upstream boundary condition in the model (Table A-1). This gaging station is the oldest main channel gage that has measurements of both discharge (Q_{BC}) and temperature (T_{BC}) downstream from Glen Canyon Dam (Figure 2-2). The most downstream gage that measures discharge and temperature became the downstream modeling domain boundary and is located above Diamond Creek (Table A-1), approximately 362 km downstream of Lees Ferry. Four additional main channel discharge and temperature measurement sites (RM30, RM61, RM88, RM167) located between Lees Ferry and Diamond Creek, at the transition of geomorphically distinct river segments (labeled segments in Figure 2-2) were used for model development, hydraulic routing calibration, and evaluation of the river temperature model. The nomenclature for defining river segments between these gages was adopted from Melis (2011). When reporting locations within our results, we use the river mile (RM) convention that is well established for the Grand Canyon where RM zero is located at Lees Ferry and downstream river distances are positive while upstream river distances are negative.

For hydraulic routing (using the SWMM component), channel geometry data between Lees Ferry (RM0) and Diamond Creek (RM225) were obtained from a subset of 2,680 cross-sections delineated from LiDAR by Magirl et al. (2008) and aggregated to the selected 1 km model cell size. Model cells representing locations of tributary inflows or main channel gaging stations were shortened to approximately 200 m and centered around the tributary inflow or gage in order to better represent local conditions. All other components used for the river temperature modeling (i.e., CSH, RHE, and HTS) use identical discretization as the SWMM component.

Channel roughness was calibrated for 2013 and 2014 on a segment-by-segment basis (Figure 2-2) by sequentially incrementing Manning's roughness values. Calendar years 2013 and 2014 were chosen to perform routing calibration because they have flow distributions that are representative of the entire simulation period. In an effort to capture the extreme flow variability, SWMM was run for sequential 2-week periods over the 2 years with roughness values being varied between 0.02 and 0.05 in 0.001 increments. The Manning's roughness values that minimized the root mean square error (RMSE) for each 2-week period were averaged to produce a single Manning's roughness value for each river segment. These estimated roughness values (Table A-2) are comparable to those reported by Magirl et al. (2008). Previous routing models for the Colorado River in Grand Canyon suggest that roughness is stage dependent (Graf, 1995; Magirl et al., 2008; Wiele & Smith, 1996), however, given our ability to capture the highly variable flow conditions that occurred over the simulation period and the limited structure in modeled discharge residuals, constant roughness values were applied.

2.3.2.1. Tributary data

Gaged tributaries within the model domain were directly accounted for in the routing and temperature modeling components (Figure 2-2; Table A-1). These tributary gages are located close enough to the Colorado River confluence such that travel time between the gage and confluence were not considered. Most of these tributaries have periods of missing data during the simulation period. Large gaps in the flow record (i.e., greater than 2 days) were filled by assuming flows during that period were equal to the annual median flow. However, in the Little Colorado River (LCR), the largest tributary within Grand Canyon, flow is almost entirely from Blue Springs (Fitzgerald, 1996) and

required this location to be handled differently. To account for periods with missing data at the LCR gage near the confluence (*USGS 09402300*), the gage upstream of Blue Springs (*USGS 09402000 Little Colorado River near Cameron, AZ)* was also used by adding median flow estimates to the upstream gage measurements and applying a constant time offset that represents the approximate travel time between the upstream gage and confluence. The travel time was determined by comparing hydrographs from the two gaging stations. Similarly, temperature gaps were filled such that the heat contribution from tributaries could be better represented during these times. This was done by first calculating the monthly average temperature from the available data. In order to capture the diurnal pattern of temperatures, hourly variability for each month was also calculated. The hourly variability for each month was then added to the monthly average temperatures in order to get a representative temperature series. To compare the relative heat contributions from the tributaries (J_{trib}) to the other heat fluxes in equation 2, the apparent sensible heat flux from the tributaries were calculated following Kurylyk et al. (2016; Text A-5; Eqn. A-6).

2.3.2.2. Distributed flows

Monthly differences in streamflow volume between gaging stations, accounting for gaged tributaries, were computed to close the mass balance and applied to the model as Q_{dist}. A monthly time step was chosen so that travel times between gages and the timing of flash floods from ungaged streams would not greatly influence the volume estimates. This resulted in monthly estimates of Q_{dist} (both positive and negative) for each segment. Because of the uncertainty surrounding the source of gage differences (tributary inflows, groundwater inflows or outflows, or gage error), these estimates were applied

evenly over each model segment with a constant temperature. The mean annual air temperature from within Grand Canyon (Table A-3) was used as an approximate temperature for all distributed inflows (T_{dist}. Eqn. A-7). Similar to the tributary heat contributions, the apparent sensible heat flux from distributed inflows (J_{dist}) was calculated following Kurylyk et al. (2016; Text A-5) for comparison purposes.

2.3.2.3. Meteorological data

Historical climate data used to estimate air-water surface interface heat fluxes were obtained from Page, AZ airport using University of Utah's MesoWest Database (herein referred to as MesoWest; https://mesowest.utah.edu; Figure 2-2). These data include air temperature, wind speed, and relative humidity. Data from Phantom Ranch near RM88 (Table A-3) was not directly used in the model because sub-daily data does not exist for the entire simulation period. Therefore, air temperature data from Page, AZ was regressed to measurements made at Phantom Ranch at hourly intervals. This allowed the use of the longer-term Page, AZ air temperature data while representing the differences in air temperature magnitude and patterns in Grand Canyon (Figure A-3). Similarly, air temperature, wind speed, and relative humidity data from within the canyon were available from the GCMRC (Caster et al., 2014), but again, they do not cover the full simulation period. The air temperature data from GCMRC and Phantom Ranch were, however, used to estimate a mean annual air temperature of 20 °C and to determine how well the regressed air temperature represents other sections of Grand Canyon (Table A-3). While relative humidity and wind speed within the canyon will be significantly different than those from Page, AZ, the values will be highly variable over space and time due to microclimates created within the canyon (Stanitski-Martin, 1996). To avoid

inconsistent forcing data for the simulation period and arbitrary assumptions regarding the applicability of site-specific data collected within the canyon, we applied the Page, AZ regressed air temperature and Page, AZ wind and relatively humidity data uniformly to the entire study area.

Shortwave radiation data measured at wildland fire remote automated weather stations (RAWS) dispersed around the Grand Canyon region were obtained from MesoWest (Figure 2-2; Table A-4). Shortwave radiation measurements at these sites were aggregated into an hourly median time series and used in the model as a single time series ($J_{sn,meas}$; Figure A-4). It was assumed that these sites were free from vegetation or topographic shading so that they could be disaggregated into the various shortwave radiation components as discussed earlier.

2.3.4. Sediment conduction

For sediment conduction (Figure A-1), the depth of the shallow sediment layer (Y_{sed}) was assumed to be 0.5 m and the depth to the ground boundary layer (Y_{gr}) was assumed to be 1 m. The mean annual air temperature was used for the lower boundary condition (T_{gr}).

2.3.5. Radiation balance in Grand Canyon

2.3.5.1. Shortwave radiation

Direct Shortwave Radiation. Topographic shade factors, S_f, were calculated every 100 m along the river centerline following the algorithm described in Text A-2 and averaged over each corresponding model cell before being applied to the direct shortwave radiation term (Eqn. 2-8).

Diffuse Shortwave Radiation. Yard et al. (2005) showed that diffuse radiation made up a significant portion of the annual shortwave radiation budget in Grand Canyon, with some sites receiving no direct shortwave radiation for 194 days. In order to determine which of the models presented by Dervishi and Mahdavi (2012) is best for representing diffuse radiation conditions near Grand Canyon, measurements of shortwave radiation were collected during a 1-month period (May 15 – Jun 27, 2019) in the LCR drainage approximately 6 km upstream from the main channel Colorado River. This site was chosen because of its deep canyon topography and geology that is similar to the Grand Canyon. Two Hukseflux LP02 (Manorville, NY) pyranometers (spectral range = 285-3000 nm) were deployed on the east and west banks, approximately 30 m from the river, in a south-north orientated river segment. These sensors were set up to sample every 5 minutes and record the average shortwave radiation every 15 minutes. This configuration was chosen to identify the differences in magnitude between direct and diffuse shortwave radiation and to capture the timing of morning and evening shade dynamics for comparison against the shade algorithm.

Similar to direct shortwave radiation, following Eqn. 2-9, SV_f was calculated every 100 m along the river centerline and averaged over each model cell in order to determine the amount of diffuse radiation at the water surface (Eqn. 2-10). Given that the river has an average gradient of 0.0015 (Wiele & Smith, 1996) and is comprised of long flat sections separated by short steep rapids (Magirl et al., 2005), our assumption of a zero slope for this calculation was reasonable for most of the canyon.

Land-Reflected Shortwave Radiation. In Grand Canyon, measurements and regional estimates of land surface albedo suggest approximately 20% reflectance

(Stanitski-Martin, 1996). However, the actual portion reflected toward the river is likely small given the complex nature and orientation of the landscape relative to the water surface. Therefore, we applied a constant α_{land} of 1% such that $J_{sn,refl}$ is a very conservative estimate.

2.3.5.2. Longwave radiation

Rock longwave radiation. J_{rock} was estimated using land re-emittance angles computed from terrain within 5 m from the modeled shoreline at flows of approximately 878 m^3/s (Magirl et al., 2008). This was handled by clipping a digital elevation model (DEM) to a 5-m buffer of the river shoreline and computing $SV_{f,5}$ every 100 m along the river centerline and averaging them for each corresponding model cell. An $\mathcal{E}_{lc}$ of 0.9 was chosen for all terrain based off of reported values for limestone and sandstone surfaces (Eqn. 2-12; Brewster, 1992).

2.3.6. Model scenarios

2.3.6.1. Simplified radiation scheme

Shading in canyon-bound rivers has previously been handled using seasonal and reach specific shading factors (e.g., Carron, 2000). In order to understand and demonstrate the importance of a complex radiation balance in canyon-bound rivers, we applied a simplified shading scheme to produce seasonally averaged shade factors for each river segment (Figure 2-2) that was used to scale shortwave radiation values applied in the temperature model. Seasons were divided into Winter (Dec, Jan., and Feb.), Spring (Mar., Apr., and May), Summer (Jun., Jul., and Aug.) and Fall (Sep., Oct., and Nov.). J_{rock} was not accounted for in these simulations, resulting in J_{br} and J_{an} being the only

longwave radiation sources. This model is herein referred to as the “simplified” model, while the model using the complex radiation balance described above is referred to as the “detailed” model.

2.3.6.2. Long term model simulation

An 18-year simulation period for the entire domain (RM0 to RM225) was used to determine the large scale spatial and temporal differences between the simplified and detailed radiation schemes. More broadly, this space and time domain also was used to determine whether accurate predictions of river temperature could be made over long time ranges with highly variable flow and weather conditions over a large spatial extent. The long simulation period also allowed us to test assumptions of constant channel geometries and hydraulic roughness coefficients, which is important when modeling future climate change and/or hydrologic conditions. Additionally, the long-term simulation was used to determine if the assumptions applied to meteorological input data were appropriate for calculating heat fluxes over a large range of conditions. Model performance was evaluated by calculating RMSE and Nash-Sutcliffe Efficiency (NSE) for discharge and temperature at each gaging stations over the entire simulation period by matching model outputs (hourly) to historical observations with a tolerance of ±5 minutes. Histograms of the model residuals were also created to determine whether positive or negative prediction bias was present over time and space.

2.3.6.3. High and low flow comparison

Investigating differences between the simplified and detailed models under different flow regimes can help determine when and where detailed radiation information

becomes important for predicting instream temperatures. We focused comparison on a low flow period that occurred during summer 2000 and a high flow period that occurred during the summer of 2011. During the low flow period releases from Lake Powell were held constant at approximately 226 m^3/s between June and September as part of the Low Summer Steady Flow (LSSF) experiment . During the high flow period discharge was held steady at approximately 700 m^3/s between July and September in order to satisfy water storage agreements via so-called "equalization flows" (an interim operating criteria to equalize storage between Lake Powell and downstream Lake Mead; U.S. Department of the Interior, 2007).

2.3.6.4. Heat flux analysis

Using the results from the detailed long-term model simulation we were able to investigate the dominant heat fluxes controlling river temperatures over space and time in this canyon-bound river. Minimum, mean, and maximum heat flux statistics were calculated for each individual heat flux over the model simulation period and domain. Statistics for the relative contribution (%) were calculated from absolute values for each heat flux over space and time divided by the sum of absolute values for all heat fluxes over space and time. The absolute percent contributions of heat fluxes were also evaluated at individual river segment and month scales to identify if dominant mechanisms changed over the model domain or over the calendar year.

2.3.6.5. Sensitivity analysis

To quantify the sensitivity of individual heat fluxes in the detailed long-term model simulation to perturbations of input time series data, we altered input

meteorological observations (shortwave radiation, wind speed, relative humidity), Q_{BC}, Q_{dist} and T_{dist} arbitrarily by ± 10% to account for measurement uncertainty and spatial representativeness of measurements. Rock temperature (estimated from air temperature) was altered independently from air temperature by ± 10%. We also varied T_{BC} by ± 0.2 °C to account for sensor accuracy. Air temperature was perturbed ± 1.0 °C to account for spatial uncertainty in the regression applied between Page and Phantom Ranch (Figure A-3; Table A-3). The residual between the detailed model and each perturbation was then evaluated to determine if temperature predictions changed significantly compared to the detailed model. This approach can highlight which data are most important and provide insights into how the system may respond to changes in climate, hydrology, or upstream reservoir release temperatures.

3. Results

3.1. Radiation balance

Measurements of shortwave radiation in the LCR ($J_{sn,LCR}$) revealed the timing of shading dynamics and the magnitude of shortwave radiation within the canyon. On a clear-sky day, the timing of direct incidence and shade at the bottom of the canyon was obvious from the data collected (Figure 2-3). For example, on June 19, 2019, our measurement site remained in the shade till 9:30 AM and went back into the shade by 3:30 PM. Our shading model captures this timing within 15 minutes (Figure 2-3). Discrepancy in the timing is likely due to the chosen sampling frequency used in the model and data collection.

Using the correlation equations presented by Dervishi and Mahdavi (2012), we disaggregated $J_{sn,meas}$ into above canyon estimates of $\hat{J}_{sn,dir}$ and $\hat{J}_{sn,diff}$ (i.e., Eqn. 2-5, 2-6,

2-7), that were used to determine the individual components $J_{sn,dir}$, $J_{sn,diff}$, and $J_{sn,refl}$ at the water surface (i.e., Eqn. 2-8, 2-10, 2-11), which sum to get $J_{sn,net}$ (i.e., Eqn 2-3). Comparison of predicted $J_{sn,net}$ to $J_{sn,LCR}$ measurements found that the formulation by Erbs et al. (1982; Text A-1) produced the lowest RMSE over the entire sampling period. For $J_{sn,net}$ during a clear sky day (e.g., Jun. 19, 2019), the model yielded a RMSE of 52.3 W/m^2 (Figure 2-3). Over the entire data collection period (43 days), the RMSE for $J_{sn,net}$ is higher (132.8 W/m^2) because estimates of shortwave radiation were less accurate during local overcast conditions. This result is not a surprise given that the $J_{sn,net}$ value is estimated from $J_{sn,meas}$, which is aggregated from multiple locations spanning the entire Grand Canyon region. Regardless, the timing of shade predicted by our algorithm agrees with the timing observed in the LCR and the magnitude of diffuse radiation in the morning and evening matches what was measured (Figure 2-3). These results illustrate that our method for capturing the timing of shading and the magnitude of diffuse shortwave radiation is appropriate.

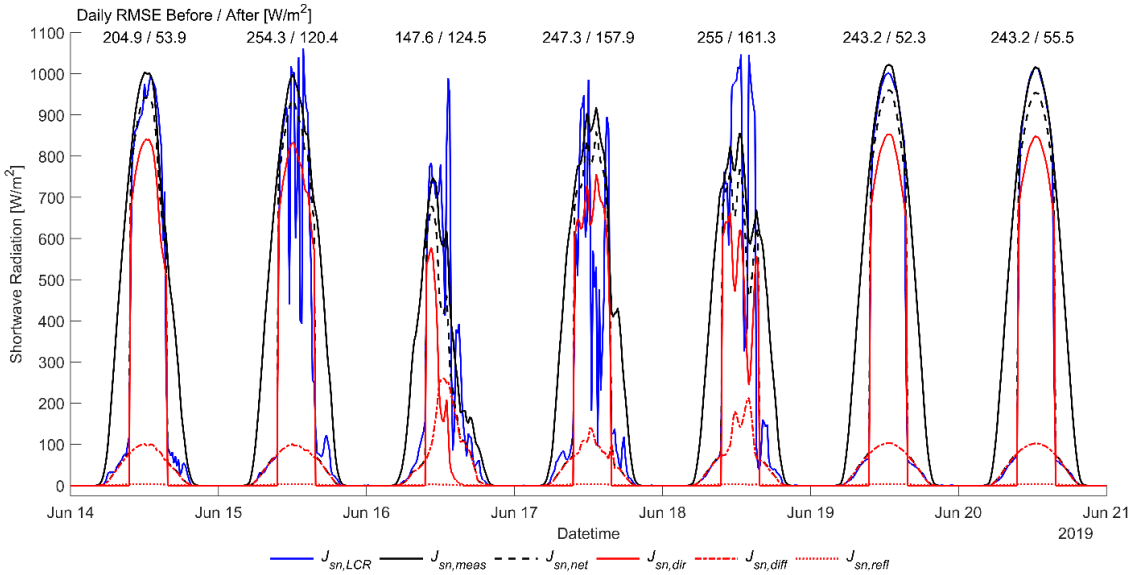

Figure 2-3. Comparison of shortwave radiation measurements from the LCR ($J_{sn,LCR}$) to estimated components of shortwave radiation (i.e., $J_{sn,net}$, $J_{sn,dir}$, $J_{sn,diff}$, $J_{sn,refl}$) derived from the median value of measured shortwave radiation at RAWS network sites ($J_{sn,meas}$) near the study area. Daily RMSE values are provided above each day to illustrate the influence of the diffuse radiation correlation model and correspond to the fit of $J_{sn,meas}$ to $J_{sn,LCR}$ before and after radiation scaling.

3.2. Long-term model results

Modeled discharge. Long-term model results for discharge indicate accurate model predictions given the long simulation period, highly variable flow conditions, and large spatial extent of the model (Figure A-5). The histogram of residuals (observed minus modeled) show that we do not have a positive or negative bias in flows at any of the gaging stations indicating that our approach to closing the flow balance is reasonable. As expected, flow routing prediction errors increase downstream due to the propagation of errors throughout the entire model domain. Overall, the error at the most downstream model element is less than 3% of the average flow. Because there is no apparent temporal drift in the accuracy of the routing predictions, our assumptions of constant channel

roughness coefficients and channel geometry are reasonable for representing the hydraulics over long periods of time and highly variable flow conditions.

Modeled temperature. Long-term model results using the simplified and detailed radiation schemes for temperature predictions at the five main channel gaging stations indicate that high resolution shading dynamics and rock longwave radiation significantly improves model predictions, particularly over large spatial domains (Figure 2-4; Figure A-6). Histograms of the residuals for the detailed simulation are slightly positive with peaks around 0.2 °C for all sites except for RM225, which has a slightly higher bias of approximately 0.5 °C. Bias in the simple model was higher at all sites, with RM225 having a histogram peak around 1.5 °C. These positive residuals indicate a persistent underestimation of temperatures in each river segment. Similar to our discharge results, prediction errors increase downstream as error from upstream segments propagate to downstream segments.

Spatial and temporal model performance. Monthly model residuals reveal that there are also temporal differences between the simple and detailed radiation schemes (Figure A-7). While the detailed model produces underestimates for many months and locations, overestimates do occur in summer months with June being the greatest. During this period, overestimates are increasing downstream up to RM88, but then decrease as you move further downstream. This indicates that local attributes within particular river segments may be influencing river temperature that are not fully captured in the detailed model (e.g., rock longwave radiation or local meteorological conditions). Underestimates of temperature in the detailed model are greatest during late fall and early winter months for all sites. Water temperatures at RM225 have the highest residuals and are

underestimated in all months, but median residuals are below 1 °C (Figure A-7). Residuals from the simple simulation have higher variability over both space and time. The simple model produces significantly lower temperature predictions for nearly all months and locations, with greatest underestimates occurring during late spring, summer, and early fall months, and at the downstream river gages.

3.3. High flow and low flow period model results

Discharges during the summer of 2000 were three times lower than in 2011, with flows during these periods averaging 235 m^3/s and 700 m^3/s, respectively (Figure 2-5). While these significantly different flow regimes alter the volume of water that must be heated or cooled, prediction errors from the detailed model were similar for the two periods at RM61 and RM88, with differences in RMSE within tenths of a degree (Figure 2-5). Larger differences in the detailed model predictions arise downstream of RM88. During the low flow period the RMSE at RM167 jumped to 1.25 °C while the RMSE at RM167 during high flows decreased to 0.47 °C. Temperature data at RM225 is limited to Aug. 6 – Aug. 20 in 2000, and therefore, we do not report an RMSE during this period. However, the RMSE at RM225 during high flows were lower again at 0.34 °C (not shown in Figure 2-5). The simple model had worse, but reasonable results during the high flow period at all sites. During the low flow period the simple model significantly underestimated temperatures at all sites.

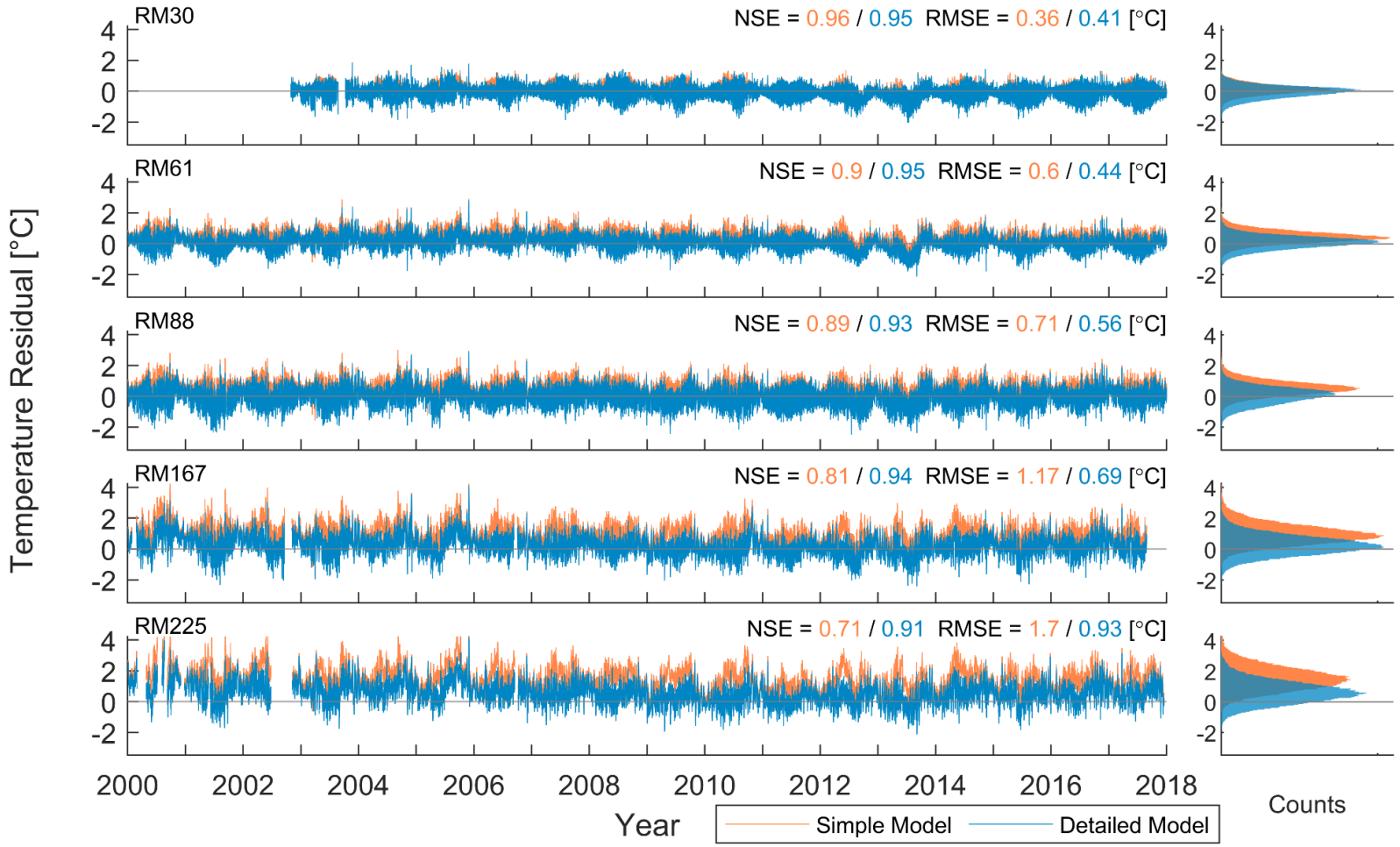

Figure 2-4. Plot of long-term river temperature model residuals (observed minus modeled) for the simple and detailed radiation schemes at 5 gaging stations within Grand Canyon (RM30, RM61, RM88, RM167, and RM225). The right panels show the distribution of residuals between observed and modeled temperatures in °C.

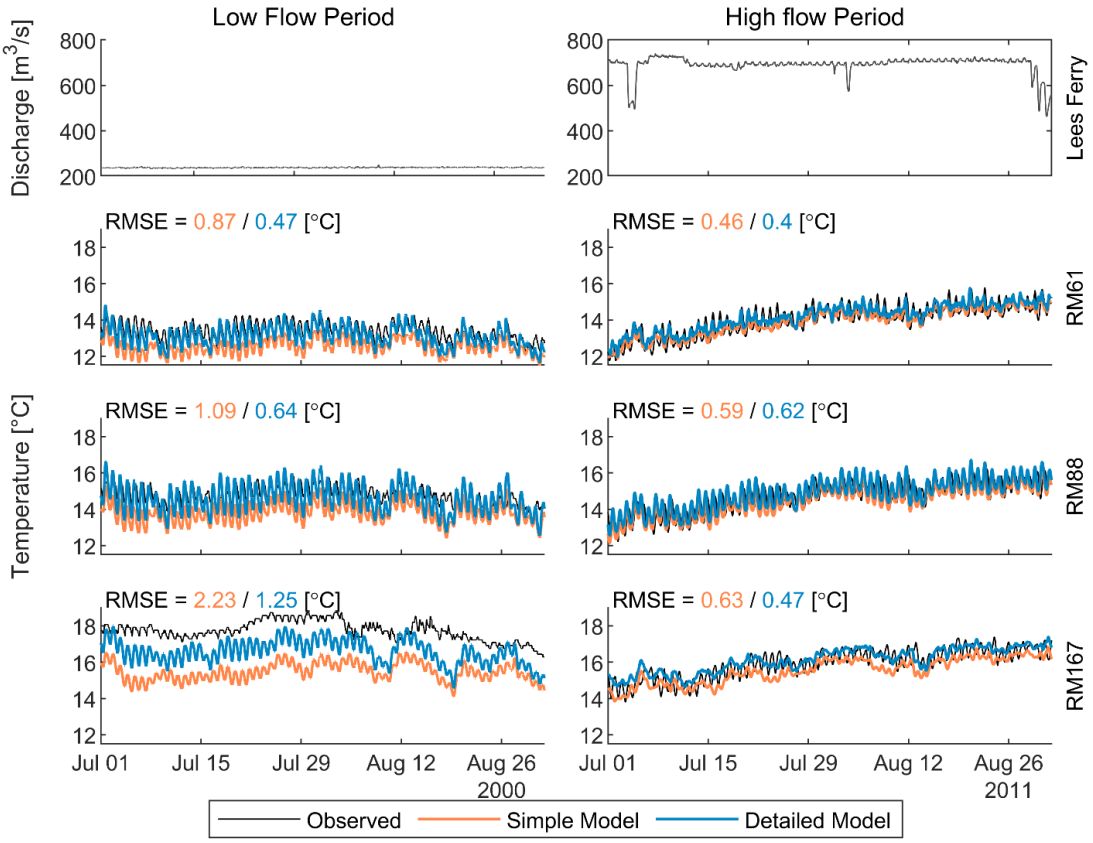

Figure 2-5. Comparison of model results during low flow and high flow summer periods. The left and right columns show model results for July and August of 2000 and 2011, respectively. The top row shows observed discharge at Lees Ferry. Subsequent rows from top to bottom show modeled temperature predictions and observed data at RM61, RM88, and RM167.

3.4. Dominant heat fluxes

3.4.1. All modeled external heat fluxes over time and space

For the detailed simulation, 9 of the 12 evaluated heat fluxes made up a significant portion (> 40%) of the of the total heat budget at any given time over the model domain (Table 2-1). We found that $J_{lw,net}$ (incoming minus outgoing) was on average negative, however, $J_{lw,net}$ switched to a positive flux at times when J_{rock} was relatively high. Sensible (J_c) and latent (J_e) heat fluxes were highly variable and were both positive and negative. High sensible heat fluxes were largely due to periods of high

wind speed coinciding with high air temperature relative to water temperature (> 20 °C difference), which is common due to cold, hypolimnetic releases from Glen Canyon Dam coinciding with warm summer air temperatures. Positive and negative extremes in latent heat values, which correspond to greater condensation or evaporation, respectively, occurred when there were relatively large differences between air temperature and water temperature (> 20 °C) coinciding with high relative humidity (~78%) or low relative humidity (~4%), respectively. Surprisingly, friction had the largest maximum heat flux magnitude of 2047 W/m^2, which occurred under a high flow experiment on Nov. 12, 2012, where flows exceeded 1250 m^3/s in a model cell that has an approximate slope of 0.7% and width of 41 m at this discharge. However, the average contribution for J_f was modest and similar to sensible heat. Lateral heat fluxes provided by tributaries and distributed inflows were both positive and negative. Negative lateral heat fluxes occurred when river temperature was warmer than the temperature of the source or when distributed flows (Q_{dist}) were negative. J_{trib} had the second largest maximum heat flux magnitude of 1475 W/m^2, which occurred during a flash flood event.

The high maximum relative contribution from most of the heat fluxes indicates that mechanisms for heating and cooling are highly dynamic over both space and time (Table 2-1). This is further illustrated by the change in relative contribution of heat fluxes for the five model segments during each season of the year averaged over the entire simulation period (Figure 2-6). Relative contributions from $J_{sn,net}$ are lowest during the winter and increase in the summer, corresponding with patterns in solar zenith angles throughout the year. $J_{sn,net}$ contributions are smallest in East Central Grand Canyon during winter, which is due to a predominant East – West orientation and particularly high

elevation angles when compared to other river segments (Figure A-8). $J_{lw,net}$ contributions are highest in winter, when other heat fluxes are small, and lowest in summer, when J_e and J_c become more dominant. J_{sed} contributions do not vary significantly over space or time. The relative contributions from J_{lat} (sum of J_{trib} and J_{dist}) are highly variable over space and time, where again, the largest contributions corresponded with flash floods.

Table 2-1. Statistics for modeled external heat fluxes (W/m^2) and percent of total external heat fluxes for the Colorado River in Grand Canyon between Jan 1, 2000 and Jan 1, 2018. Statistics for the relative contribution (%) were calculated from the absolute values for each heat flux over space and time divided by the sum of absolute values for all heat fluxes over space and time.

		$J_{sn,dir}$	$J_{sn,diff}$	$J_{sn,refl}$	J_{an}	J_{br}	J_{rock}	J_e	J_c	J_f	J_{sed}	J_{trib}	J_{dist}
Heat Flux [W/m^2]	Min	0	0	0	116	-408	0	-722	-380	0	-3	-509	-2
	Mean	127	32	1	267	-365	10	-84	69	78	7	0	25
	Max	1009	404	7	393	-331	125	526	1062	2047	25	1475	769
Relative Contribution [%]	Min	0	0	0	5	9	0	0	0	0	0	0	0
	Mean	8	2	0	27	37	1	8	6	7	1	0	3
	Max	56	32	1	45	61	12	46	56	77	4	66	47

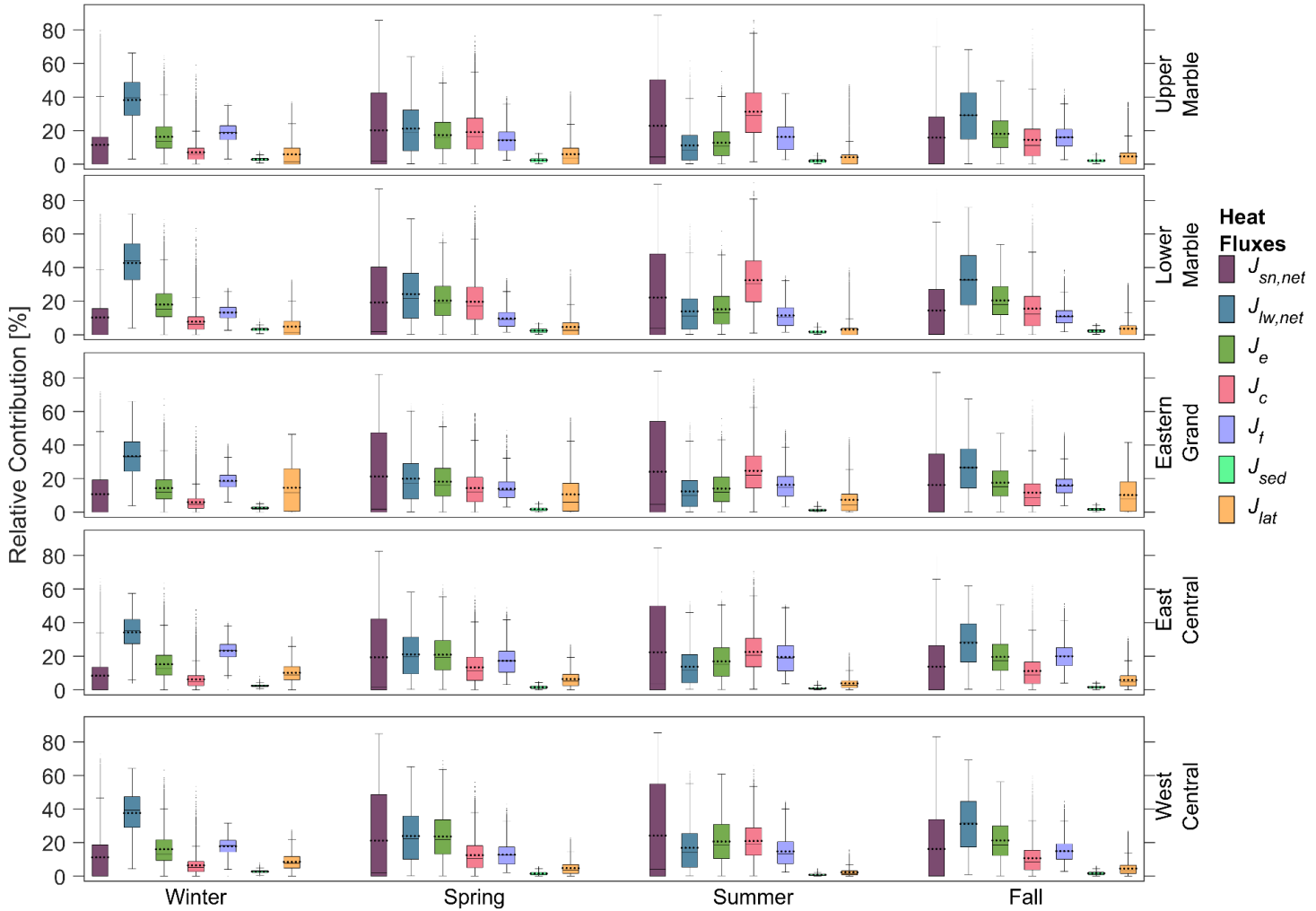

Figure 2-6. Boxplot of relative contribution of heat fluxes averaged over each model segment (shown in Figure 2-1) and each season of the year (Winter = Dec.-Feb., Spring = Mar.-May, Summer = Jun.-Aug., and Fall = Sep.-Nov.) for the entire simulation period. Mean values are included as horizontal dots. Shortwave and longwave radiative heat fluxes and lateral sources have been combined for readability. Variables being compared are net shortwave radiation ($J_{sn,net}$), net longwave radiation ($J_{lw,net}$), latent heat (J_e), sensible heat (J_c), friction (J_f), bed conduction (J_{sed}), and the apparent sensible heat from lateral sources (J_{lat}).

3.4.2. Fluxes during high and low flows

Between high and low flow periods the relative contributions were relatively similar for most heat fluxes (Figure A-9). Friction heat (J_f) had the largest change in percent contribution by more than doubling between these two periods (~10% during low flows and ~21% during high flows) due to the nearly three-fold difference in discharge. $J_{sn,net}$ remained the dominant heat flux under high and low flow conditions. The relative contribution of $J_{lw,net}$, J_e, and J_c decreased during the high flow period even though the surface area of the river increased 17%. While width increased under high flows, it was relatively small compared to the increase in volume.

3.5. Sensitivity analysis

Temperature predictions from the detailed model were compared to subsequent simulations where input data were perturbed to determine the sensitivity of forcing data on temperatures through space and time (Figure 2-7; Figure A-10). Positive and negative residuals generally increased further downstream for all perturbations except for changes to T_{BC}, which on average has lowest temperature residuals at RM225, regardless of season. Positive perturbations of input data often resulted in negative temperature residuals (predictions greater than those in the detailed model) except for Q_{BC} and wind speed, which resulted in positive temperature residuals during most seasons. At the most upstream location chosen for comparison (RM30), the perturbation in T_{BC} (± 0.2 °C) creates the greatest residual between the detailed model than any other perturbation. This suggests that water in the first 30 miles is moving through this segment at a rate fast enough (approximately 7 hours) to not be influenced by climate variables and the model is mostly propagating T_{BC} for any time of year. At RM88, perturbation of T_{BC} still

produces the largest median residual between the detailed model and any other perturbation during winter and fall. However, perturbations of $J_{sn,net}$, T_{air}, Q_{BC}, and T_{BC} have residuals of comparable magnitude during spring and summer. Water travels from Lees Ferry to RM88 in approximately 20 hours, which allows more time for external heat sources and sinks to influence river temperatures. Further downstream at RM225, the influence of T_{BC} becomes less pronounced and the perturbations of Q_{BC} and climate variables have even higher magnitude residuals, with $J_{sn,net}$, T_{air}, and Q_{BC} perturbations creating the largest deviations from the detailed model temperature predictions during summer. At each location and during all seasons Q_{BC} has the most variability as indicated by the broad distribution of residuals. Perturbations in wind speed, T_{rock}, Q_{dist}, and T_{dist} result in only minor differences from the detailed model suggesting that warming or cooling of the river is less sensitive to these variables. Q_{trib} (not shown) was also perturbed by ±10% but was found to be less influential on river temperatures than the variables show here.

Sensitivity analyses constrained to the high and low flow periods show that river temperatures during high flows are sensitive to T_{BC} throughout the entire canyon (Figure A-11). Under high flows the influence of other inputs is relatively small at RM30, but the role of $J_{sn,net}$, T_{air}, and Q_{BC} increase downstream, creating the largest temperature residuals at RM225. River temperatures during low flows are most sensitive to perturbations of T_{BC} at RM30, but that sensitivity is reduced downstream and $J_{sn,net}$, T_{air}, Q_{BC}, and relative humidity become more sensitive. Between RM30 and RM225, all inputs create higher magnitude residuals during the low flow period when compared to the high flow period, with the exception of T_{BC} at RM225. This indicates that temperature

of water released from the dam is altered more during low flow and the rate of change is controlled by a wide variety of heat fluxes.

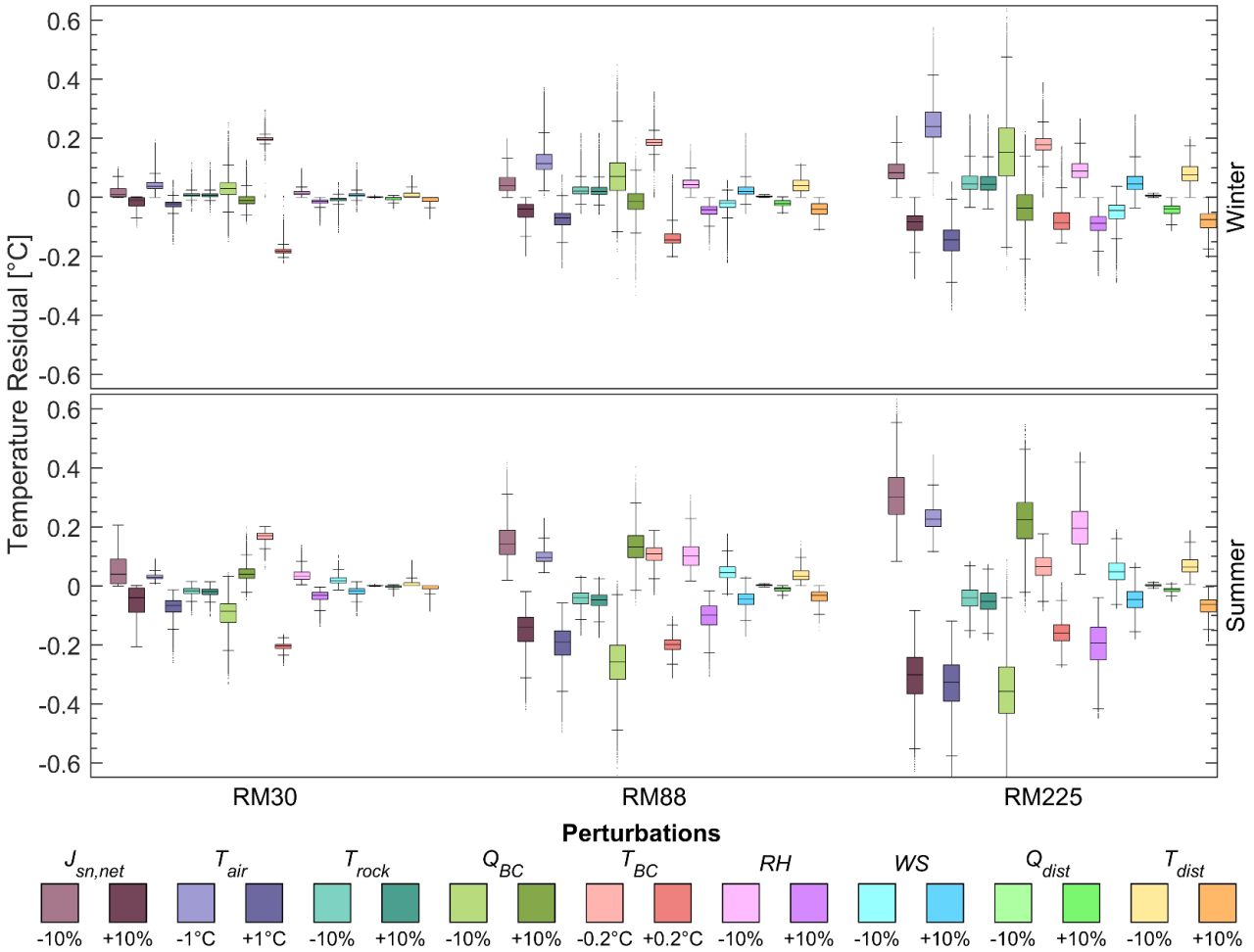

Figure 2-7. Sensitivity analysis of river temperature to input data perturbations at three locations during Winter and Summer averaged over the entire simulation time (Winter = Dec.-Feb., Summer = Jun.-Aug.). The residual is calculated as the detailed model minus scenario. Variables being compared are net shortwave radiation ($J_{sn,net}$), air temperature (T_{air}), rock temperature (T_{rock}), upstream boundary flow (Q_{BC}), upstream boundary condition temperature (T_{BC}), relative humidity (RH), wind speed (WS), distributed flows (Q_{dist}), distributed flow temperatures (T_{dist}). Box plot order follows that of the legend. Figure A-10 depicts sensitivity analysis results for Spring and Fall.

4. Discussion

Consistent with our hypothesis, the results from this work show that the dominant heat fluxes in canyon-bound rivers are highly dynamic over space and time. As with other systems, shortwave radiation is the dominant heat flux when considering the entire simulation period and model domain. However, the influence of typically smaller air-water heat fluxes become more important during fall and winter periods when portions of the river experience more shading and have limited direct shortwave radiation. Flow regulation is also a major control on river temperatures in the Colorado River, as pointed out by Anderson and Wright (2007). We expect other canyon-bound rivers to experience similar variability in dominant heat fluxes, but when and where these changes occur would be based on a combination of site-specific influences (e.g., variability in spatial orientation, flow, complexity of surrounding topography).

4.1. Radiation balance

Our approach to incorporating shade predicts the onset and departure of direct shortwave radiation within 15 minutes when compared with measured conditions in the LCR study area (Figure 2-3). This method is computationally simplistic, but estimates are completed at sufficiently high resolution to account for the spatial and temporal shading dynamics within Grand Canyon. While others have used similar approaches to predict shade in temperature models (Chen et al., 1998b; Cox & Bolte, 2007), our method for determining elevation angles and the timing of shade is computationally similar to Yard et al. (2005; Text A-2) with nearly identical predictions (Figure A-12). However, the key difference between our approach and Yard et al. (2005) is our use of shortwave radiation

from outside of the canyon to estimate the amount received at the water surface. Our results illustrate that accurate predictions of shade timing are critical for estimating direct shortwave radiation ($J_{sn,dir}$), and ultimately estimating river temperatures.

Diffuse shortwave radiation ($J_{sn,diff}$) is also an important component of the radiation balance (Table 2-1). While some river temperature models have partitioned shortwave radiation data, either as a fixed ratio (Rutherford et al., 1997; Westhoff et al., 2007) or using an approach similar to the one implemented here (Chen, et al., 1998b; Leach & Moore, 2010), applications rarely have access to measured data to evaluate the best empirical approach. Loinaz et al. (2013) is the only example found where measured diffuse shortwave radiation was directly applied in a model, however, this work provided no details as to how these measurements were made. Here, we found that having physical measurements to help us choose an appropriate correlation equation for partitioning $J_{sn,meas}$ to be important, especially since $J_{sn,diff}$ had a generally high maximum relative contribution of up to 32% at times (Table 2-1).

Reflected shortwave radiation ($J_{sn,refl}$) provides negligible amounts of heat to this large river. Our approach to estimating $J_{sn,refl}$ was relatively simple and we acknowledge the complexity in obtaining more detailed flux estimates. We anticipate the need for these advanced methods for narrower and lower flow canyon-bound streams.

Longwave radiation from the rock walls contributes a small amount of heat to most of the river in Grand Canyon. While never a major heat flux to the river, longwave radiation from rock walls increased during summer in the narrowest parts of Grand Canyon. Given that air temperature likely underestimates the actual temperature of the rock walls (Larson et al., 2000), and that rock temperatures likely lag behind the timing

of air temperatures due to the significantly higher specific heat capacity, the J_{rock} estimates do not fully represent the diverse conditions within the canyon. Furthermore, view angle estimates computed from the center of the river, as opposed to calculating it from several points along a transect, could produce underestimates of $SV_{f,c,5}$. In some situations, there may also be a need to account for detailed longwave radiation from riparian vegetation.

4.2. Long term model results

The results from the 18-year simulation period and 362 km long model domain, demonstrate that a detailed radiation scheme is important when predicting over large spatial extents and different times of the year (Figure 2-4). The temperature RMSE for the detailed radiation model simulation over the entire period at RM225 is 0.93 °C, however, temperature predictions are underestimated most of the time. The persistent under prediction of temperature indicates a missing heat source within the model or a misrepresentation of the heat fluxes included. A main source of error may be due to changes in local meteorology within the canyon deviating from the meteorological conditions at Page, AZ (the source for relative humidity, wind speed) and potential errors in the regressed air temperatures (Table A-3). This conclusion is supported by the sensitivity analysis, which shows that perturbations in T_{air} causes some of the most significant residuals at RM225 for all periods (Figures 2-7 and A-10). Inclusion of additional weather stations was considered, however, they were omitted to avoid inconsistent forcing data for the simulation period and arbitrary assumptions regarding the applicability of site-specific data to other areas within the canyon. Similarly,

overestimation of temperatures in the upstream river segments during summer months, particularly in June (Figure A-6), were potentially due in part to inaccurate estimates of shortwave radiation from aggregating all radiation measurements above the rim into a single time series. In other words, we are not accounting for longitudinal differences among sites and this influences the timing and magnitude of $J_{sn,meas}$ that is scaled within the model. To address these meteorological challenges, future modeling efforts should investigate the feasibility of alternative data sources (such as remote sensing or climate reanalysis products) for acquiring input meteorological variables and applying them over remote, topographically complex regions.

Lateral inflows from seeps, springs, or ungaged tributaries may also be adding more or less heat than anticipated. Between Lees Ferry and RM225 the river gains approximately 30.4 m^3/s annually, half of which is accounted for in the gaged record of tributaries, leaving 14.6 m^3/s (4% of the total annual flow) being contributed to the river from unknown sources (Figure A-2). While we accounted for the additional flow from unknown sources within river segments as evenly distributed inflows at a constant water temperature of 20 °C, most of these flows likely come from small ungaged tributaries that have different thermal characteristics. Lateral inflow heat fluxes (Eqn. A-5) make up 5% of heat exchange on average (Figure A-9) but can be higher during different times and at different locations due to flash floods (Figure 2-6; Table 2-1). Therefore, a better understanding of seeps, springs, or ungaged tributaries and associated inflow temperatures may improve temperature predictions. Temperature prediction errors could also be rooted in our flow routing errors. The sensitivity analysis results show that by RM88 a 10% perturbation in flow could result in up to ± 0.5 °C change in temperature

predictions relative to the detailed model run for most seasons (Figures 2-7 and A-10). While our flow routing predictions are well within 10% of the observed flows, better routing may improve river temperature predictions.

Lastly, a few heat transfer mechanisms were intentionally omitted from this model, including groundwater exchanges, hyporheic exchange, and surface transient storage. While each of these processes likely occur to some degree, these were ultimately left out of the model because they were expected to be negligible based on findings in the literature or site-specific conditions (Text A-6).

4.3. High flow and low flow periods

Our results from modeling high flow and low flow periods with a detailed radiation scheme agrees with the conclusions made by Anderson & Wright (2007), that the river temperatures are significantly influenced by the advection of heat during high flow periods. However, this work expands on previous river temperature modeling studies within Grand Canyon (Text A-4) by evaluating the change in relative contribution from individual heat fluxes between different flow regimes. We found that the heat contribution from friction more than doubled under high flows, which had approximately three times more discharge than the low flow period. With the increase in flow, it would be expected that the surface area would also increase, allowing for greater contributions of air-water interface heat fluxes. However, the high flow period only resulted in a 17% increase of surface area when compared to the low flow period due to the confining channel margins. Poor predictions at RM167 for the low flow period (Figure 2-5) were likely due to limited information about tributary flow and temperatures for Bright Angel

Creek, Kanab Creek and Havasu Creek (all within the East Central Grand Canyon segment) during this time. As a result, our estimates of median flows and application of monthly average tributary temperatures used during this period resulted in overestimates of discharge at the most downstream gage (RM225) and contributed to underestimates of temperatures for those segments. Temperature predictions using a simple radiation scheme were much worse during the low flow period, exemplifying the need to have detailed radiation in rivers with significant flow variability.

4.4. Estimated heat fluxes

While some of the heat fluxes reported here (e.g., J_f, J_e, J_c) seem very large compared to values published in the literature (e.g., Meier et al., 2003; Webb & Zhang, 2004), the conditions present in the Colorado River within Grand Canyon are somewhat unique (e.g., high air temperature and cold hypolimnetic releases, large variability in discharge, and a very deep canyon that limits solar warming). Particularly, heat generated from internal fluid shear friction is often considered an insignificant source of heat in process-based river temperature models (Dugdale et al., 2017; Moore et al., 2005; Theurer et al., 1984). However, we found this flux to be important given the relatively large discharges in Grand Canyon. On average, friction made up 7% of the total heat budget, which is similar to the contributions from J_e and J_c (Table 2-1). Webb and Zhang (1997) found that friction provided significant heat for many streams when they conducted a heat budget analysis for 11 river segments in the Exe Basin of Devon, UK. Their work showed that average daily values of heat gained from friction accounted for 1.7 to 81.4% of the total heat energy gains to the rivers. Similarly, Meier et al. (2003)

reported friction being significant in streams steeper than 5 to 10%, with a mean flux of 1812 W/m^2 in the Brenno del Lucomagno. While the average gradient of the Colorado River is 0.0015 in Grand Canyon (Wiele & Smith, 1996), the relatively high discharge compared to that of steep mountain streams (e.g., natural discharge of Brenno del Lucomagno is 2.5 m^3/s), results in similar magnitudes and relative contributions of friction reported in these studies (Table 2-1).

4.5. Sensitivity analysis

Perturbations in T_{BC}, averaged seasonally over the entire simulation period, have the most influence over river temperature between Lees Ferry and RM30, before the system has had sufficient exposure to weather inputs (Figure 2-7; Figure A-10). However, at further downstream locations, changes of ± 10% in Q_{BC} resulted in a high variability in temperature residuals and often larger magnitude minimum and maximum residuals than other perturbations. Depending on the season, $J_{sn,net}$ or T_{air} can become the most influential input influencing river temperatures at RM225, as indicated by their median values. It is important to note, however, that the temperature variability caused by perturbations of these parameters is typically less than the temperature variability from ± 10% Q_{BC}. The high temperature variability from ± 10% Q_{BC} highlights the importance of correctly handling the flow balance. Similarly, the observed seasonal influence of $J_{sn,net}$, combined with the comparison between simple and detailed models (Figures 2-4 and A-7), further illustrates the need for detailed spatiotemporal estimates of individual shortwave radiation terms when considering canyon-bound rivers.

With concerns of ecosystem management prevalent in Grand Canyon, knowing the spatial ramifications of perturbations of inputs can help interpret results and inform management decisions. Our results show that seasonal and hydrologic characteristics play a large role in determining which parameter, namely Q_{BC}, $J_{sn,net}$, or T_{air}, has the largest influence on river temperatures in downstream segments (e.g., RM225). However, perturbations of T_{BC} had the greatest effect on river temperatures near RM61, regardless of season, which is a primary habitat location of federally endangered native humpback chub *Gila cypha*. This suggests that management decisions at Glen Canyon Dam could be designed to produce beneficial temperatures for native fish habitat within these upper sections of the river. The Glen Canyon Dam Adaptive Management Program (GCDAMP) have conducted experimental flow operations to investigate the creation of habitat such as sandbars and associated backwaters to promote juvenile fish growth and survival (Schmidt et al., 2007; Trammell et al., 2002). However, Dodrill et al. (2015) found that only a small proportion of the entire juvenile humpback chub population resided within backwaters. Dodrill et al. (2015) also pointed out that the observed increases in humpback chub population since 2006 (Van Haverbeke et al., 2013) occurred during a period of low backwater abundance, suggesting that population increases are likely linked to other factors such as temperature, non-native salmonid abundances, food availability, and/or turbidity. Research directly focused on growth and survival of juvenile humpback chub (Yackulic et al., 2018) and growth of sub-adult humpback chub (Dzul et al., 2016), has shown that temperature is the dominant physical factor influencing early life history demography in this river segment and success at these vulnerable life stages is essential for a healthy humpback chub population (Yackulic et al., 2014).

Within the Colorado River basin, climate change will impact the reservoir storage levels in Lake Powell as annual snowfall totals are reduced, the timing of spring snowmelt runoff shifts to earlier in the year, and overall basin runoff is decreased (Dettinger et al., 2015; Udall & Overpeck, 2017). Additionally, while efficiency trends have curtailed consumptive water use nationally since 1980 (Georgakakos et al., 2014; Maupin et al., 2014), water demands are projected to increase as population growth and climate change continue (Brown et al., 2013). With the anticipated changes to basin hydrology combined with changes in water demand, it is expected that many reservoirs will face high variability in water storage and may be relatively low for long periods of time (Barnett et al., 2004). This leaves uncertainty in the downstream thermal regime of the river as Lake Powell levels decline, resulting in warm water releases out of Glen Canyon Dam. While warm water releases are generally thought as being beneficial to native fish species that evolved under warmer thermal regimes, there are still unknown risks associated with increasing water temperatures in regard to non-native fish species. Specifically, warmer river temperatures may result in expanding the distribution and abundance of warm water non-native fishes (i.e., smallmouth bass *Micropterus dolomieu*, green sunfish *Lepomis cyanellus*, and walleye *Stizostedion vitreum*) within Grand Canyon that could swim upstream from Lake Mead, come down from Lake Powell through hydropower penstocks, or enter through accidental introductions at tributary headwaters. While the ecosystem impacts of different thermal regimes remain uncertain, understanding which mechanisms control downstream river temperature changes provides a framework for evaluating the potential ecosystem responses to changing climate and hydrology.

5. Conclusions

Canyon-bound rivers are disproportionally affected by water development, often resulting in dramatic changes to the natural downstream hydrologic and thermal characteristics, and by extension, the downstream aquatic ecosystems. As ongoing climate change exposes dammed systems to new hydrologic patterns and thermal regimes, downstream river segments may be further altered. In order to anticipate the associated changes in aquatic ecosystems, the dominant heat transfer mechanisms in canyon-bound rivers, particularly below reservoirs, need to be understood. Using process-based modeling that incorporates the influences of complex topography on radiation balances, we predicted discharge and temperature throughout the Grand Canyon over an 18-year period. The relative contribution from most of the heat fluxes (9 of the 12) represented within the model were highly variable over time and space, indicating the dynamic nature of heating and cooling mechanisms in these systems. This is largely due to the wide range of conditions experienced over the long simulation time, the controls on net shortwave radiation (i.e., $J_{sn\text{-}net}$) due to topographic shading, and the high variability in flow releases (i.e., Q_{BC}) out of Glen Canyon Dam. In the upper portion of the model domain (RM30 and RM61), perturbations to the boundary condition water temperature (i.e., T_{BC}) had the most influence on river temperatures regardless of the time of year, while further downstream (RM88, RM167, and RM225), perturbations to the boundary condition flow (Q_{BC}), net shortwave radiation, and air temperature were dominant, but varied significantly by season. Evaluating high and low flow periods revealed that the model performed well during either condition, but highlighted the importance of having accurate tributary information during the low flow period.

Overall, the sensitivity analysis to input climate and hydrologic parameters provides a means for understanding the temporal and spatial variation in heat flux contributions in a canyon-bound river. Terrain in these environments can dramatically reduce the amount of shortwave radiation and elevate the importance of other radiative or typically less influential heat flux mechanisms. Other rivers around the world are situated similarly in deep canyons or mountainous terrain with flows highly influenced by upstream reservoir operations. These systems and their downstream segments face similar ecosystem challenges imposed by climate change as reservoir levels decline and release temperatures increase. The modeling approach presented here provides insight regarding potential climate change impacts to canyon-bound rivers and allows for thorough planning among diverse stakeholders.

Acknowledgements

Funding was provided by the Walton Family Foundation, David Bonderman, My Good Fund, and the National Science Foundation (EAR- 1343861). Any use of trade, product, or firm names is for descriptive purposes only and does not imply endorsement by the U.S. Government. Thanks to the GCMRC staff for assistance in data collection (Maria Dzul), insights and discussions on data and modeling results (Kimberly Dibble, Theodore Kennedy, Nick Voichick, and Bridget Deemer) and help with our shading model (Mike Yard and Glenn Bennett). Additional thanks to Joshua Walston at the DRI for help in acquiring shortwave radiation data. Data and models are provided online at https://www.hydroshare.org/resource/5199f53238134cc9bf4c4e997312125b/.

References

Alvarez, L. V., & Schmeeckle, M. W. (2013). Erosion of river sandbars by diurnal stage fluctuations in the Colorado River in the Marble and Grand Canyons: Full-scale laboratory experiments. River Research and Applications, 29(7), 839–854. https://doi.org/10.1002/rra.2576

Anderson, C. R., & Wright, S. A. (2007). Development and application of a water temperature model for the Colorado River below Glen Canyon Dam, Arizona. Proceedings of the American Institute of Hydrology, 23, 1–11.

Barnett, T., Malone, R., Pennell, W., Stammer, D., Semtner, B., & Washington, W. (2004). The effects of climate change on water resources in the west: Introduction and overview. Climatic Change, 62(1–3), 1–11. https://doi.org/10.1023/B:CLIM.0000013695.21726.b8

Behn, K. E., Kennedy, T. A., & Hall, R. O. J. (2010). Basal resources in backwaters of the Colorado River below Glen Canyon Dam - Effects of discharge regimes and comparison with mainstem depositional environments. U.S. Geological Survey Open-File Report 2010-1075, 25. http://pubs.usgs.gov/of/2010/1075/

Benyahya, L., Caissie, D., Satish, M. G., & El-Jabi, N. (2012). Long-wave radiation and heat flux estimates within a small tributary in Catamaran Brook (New Brunswick, Canada). Hydrological Processes, 26(4), 475–484. https://doi.org/10.1002/hyp.8141

Brazel, A. J., & Marcus, M. G. (1987). Heat enhancement by longwave wall emittance. Geographical Review, 77(4), 440. https://doi.org/10.2307/214283

Brewster, Q. M. (1992). Thermal radiative transfer and properties. John Wiley & Sons Ltd.

Brown, T. C., Foti, R., & Ramirez, J. A. (2013). Projected freshwater withdrawals in the United States under a changing climate. Water Resources Research, 49(3), 1259–1276. https://doi.org/10.1002/wrcr.20076

Buahin, C. A., & Horsburgh, J. S. (2018). Advancing the Open Modeling Interface (OpenMI) for integrated water resources modeling. Environmental Modelling & Software, 108(April), 133–153. https://doi.org/10.1016/j.envsoft.2018.07.015

Buahin, C. A., Horsburgh, J. S., & Neilson, B. T. (2019). Parallel multi-objective calibration of a component-based river temperature model. Environmental Modelling & Software, 116(February), 57–71. https://doi.org/10.1016/j.envsoft.2019.02.012

Budhu, M., & Gobin, R. (1995). Seepage-induced slope failures on sandbars in Grand Canyon. Journal of Geotechnical Engineering, 121(August), 601–609.

Buendia, C., Sabater, S., Palau, A., Batalla, R. J., & Marcé, R. (2015). Using equilibrium temperature to assess thermal disturbances in rivers. Hydrological Processes, 29(19), 4350–4360. https://doi.org/10.1002/hyp.10489

Caissie, D. (2006). The thermal regime of rivers: A review. Freshwater Biology, 51(8), 1389–1406. https://doi.org/10.1111/j.1365-2427.2006.01597.x

Caissie, D. (2016). River evaporation, condensation and heat fluxes within a first-order tributary of Catamaran Brook (New Brunswick, Canada). Hydrological Processes, 30(12), 1872–1883. https://doi.org/10.1002/hyp.10744

Cardenas, M. B., Doering, M., Rivas, D. S., Galdeano, C., Neilson, B. T., & Robinson, C. T. (2014). Analysis of the temperature dynamics of a proglacial river using time-lapse thermal imaging and energy balance modeling. Journal of Hydrology, 519(PB), 1963–1973. https://doi.org/10.1016/j.jhydrol.2014.09.079

Carpenter, M. C., Crosswhite, J. A., & Carruth, R. L. (1995). Water-level fluctuations, water temperatures, and tilts in sandbars -6.5R, 43.1L, and 172.3L, Grand Canyon, Arizona, 1990-93. Open-File Report 94-485, 17.

Carron, J. C. (2000). Simulation and optimization of unsteady flow and water temperature in reservoir regulated rivers. Civil, Environmental and Architectual Engineering Ph.D. Thesis, University of Colorado, Boulder CO., 159.

Carron, J. C., & Rajaram, H. (2001). Impact of variable reservoir releases on management of downstream water temperatures. Water Resources Research, 37(6), 1733–1743. https://doi.org/10.1029/2000WR900390

Caster, J. J., Dealy, T. P., Andrews, T., Fairley, H., Draut, A. E., Sankey, J. B., & Bedford, D. R. (2014). Meteorological data for selected sites along the Colorado River Corridor, Arizona, 2011-2013. U.S. Geological Survey Open-File Report 2014-1247, 56. https://doi.org/http://dx.doi.org/10.3133/ofr20141247

Caster, J. J., & Sankey, J. B. (2016). Variability in rainfall at monitoring stations and derivation of a long-term rainfall intensity record in the Grand Canyon Region, Arizona, USA. In Scientific Investigations Report. https://doi.org/10.3133/sir20165012

Chapra, S. C. (1997). Surface water-quality modeling. In McGraw-Hill Series in Water Resources and Environmental Engineering.

Chen, Y. D., Carsel, R. F., McCutcheon, S. C., & Nutter, W. L. (1998a). Stream temperature simulation of forested riparian areas: I. Watershed-scale model development. Journal of Environmental Engineering, 124(4), 304–315. https://doi.org/10.1061/(ASCE)0733-9372(1998)124:4(304)

Chen, Y. D., McCutcheon, S. C., Norton, D. J., & Nutter, W. L. (1998b). Stream temperature simulation of forested riparian areas: II. Model application. Journal of Environmental Engineering, 124(4), 316–328. https://doi.org/10.1061/(ASCE)0733-9372(1998)124:4(316)

Chen, Y., Hall, A., & Liou, K. N. (2006). Application of three-dimensional solar radiative transfer to mountains. Journal of Geophysical Research, 111(D21), D21111. https://doi.org/10.1029/2006JD007163

Collier, M., Webb, R. H., & Schmidt, J. C. (1996). Dams and rivers: a primer on the downstream effects of dams. US Geological Survey Circular, 1126. https://doi.org/10.3133/cir1126

Cox, M. M., & Bolte, J. P. (2007). A spatially explicit network-based model for estimating stream temperature distribution. Environmental Modelling and Software, 22(4), 502–514. https://doi.org/10.1016/j.envsoft.2006.02.011

Dervishi, S., & Mahdavi, A. (2012). Computing diffuse fraction of global horizontal solar radiation: A model comparison. Solar Energy, 86(6), 1796–1802. https://doi.org/10.1016/j.solener.2012.03.008

Dettinger, M., Udall, B., & Georgakakos, A. (2015). Western water and climate change. Ecological Applications, 25(8), 2069–2093. https://doi.org/10.1890/15-0938.1

Dodrill, M. J., Yackulic, C. B., Gerig, B., Pine, W. E., Korman, J., & Finch, C. (2015). Do management actions to restore rare habitat benefit native fish conservation? distribution of juvenile native fish among shoreline habitats of the Colorado River. River Research and Applications, 31(10), 1203–1217. https://doi.org/10.1002/rra.2842

Dozier, J., & Frew, J. (1990). Rapid calculation of terrain parameters for radiation modeling from digital elevation data. IEEE Transactions on Geoscience and Remote Sensing, 28(5), 963–969. https://doi.org/10.1109/36.58986

Draut, A. E., & Rubin, D. M. (2006). Measurements of wind, aeolian sand transport, and precipitation in the Colorado River corridor, Grand Canyon, Arizona; January 2005 to January 2006. In Open-File Report (Revised an). https://doi.org/10.3133/ofr20061188

Dubayah, R., & Rich, P. M. (1995). Topographic solar radiation models for GIS. International Journal of Geographical Information Systems, 9(4), 405–419. https://doi.org/10.1080/02693799508902046

Dugdale, S. J., Hannah, D. M., & Malcolm, I. A. (2017). River temperature modelling: A review of process-based approaches and future directions. Earth-Science Reviews, 175(October), 97–113. https://doi.org/10.1016/j.earscirev.2017.10.009

Dzul, M. C., C. B. Yackulic, J. Korman, M. D. Yard, & J. D. Muehlbauer. (2016). Incorporating temporal heterogeneity in environmental conditions into a somatic growth model. Canadian Journal of Fisheries and Aquatic Sciences:1-11

Edinger, J. E., Duttweiler, D. W., & Geyer, J. C. (1968). The response of water temperatures to meteorological conditions. Water Resources Research. https://doi.org/10.1029/WR004i005p01137

Erbs, D. G., Klein, S. A., & Duffie, J. A. (1982). Estimation of the diffuse radiation fraction for hourly, daily and monthly-average global radiation. Solar Energy. https://doi.org/10.1016/0038-092X(82)90302-4

Ferencz, S. B., Cardenas, M. B., & Neilson, B. T. (2019). Analysis of the effects of dam release properties and ambient groundwater flow on surface water-groundwater exchange over a 100-km-long reach. Water Resources Research, 55(11), 8526–8546. https://doi.org/10.1029/2019WR025210

Ferrari, R. (1987). Colorado River water temperature modeling below Glen Canyon Dam. *Glen Canyon Environmental Studies*.

Fitzgerald, J. (1996). Residence time of groundwater issuing from the South Rim Aquifer in the eastern Grand Canyon. Department of Geoscience MSc Thesis, University of Nevada, Las Vegas.

Garrett, D., Baron, J., Dale, V., Gunderson, L., Hulse, D., Kitchell, J., Loomis, J., Palmer, M., Parker, R., Robertson, D., Schwartz, D., & Watkins, J. (2003). Evaluating a Glen Canyon Dam temperature control device to enhance native fish habitat in the Colorado River: A risk assessment. Upper Colorado Region, Bureau of Reclamation, June.

Gates, D. M. (1980). Biophysical ecology. Springer New York, 611p. https://doi.org/10.1007/978-1-4612-6024-0

Georgakakos, A., Fleming, P., Dettinger, M., Peters-Lidard, C., Richmond, T. (T. C. ., Reckhow, K., White, K., & Yates, D. (2014). Ch. 3: Water resources. Climate change impacts in the United States: The third national climate assessment. https://doi.org/10.7930/J0G44N6T

Gloss, S., Lovich, J., & Melis, T. (2005). The State of the Colorado River Ecosystem in Grand Canyon: USGS Circular 1282.

Goings, D. B. (1985). Spring flow in a portion of Grand Canyon National Park, Arizona. Department of Geoscience MSc Thesis, University of Nevada, Las Vegas.

Graf, J. B. (1995). Measured and Predicted Velocity and Longitudinal Dispersion At Steady and Unsteady-Flow, Colorado River, Glen Canyon Dam To Lake Mead. Water Resources Bulletin, 31(2), 265–281.

Graff, W. (1999). Dam Nation: A Geographic Census of American Dams and Their Large-Scale Hydrologic Impacts. 35(4), 1305–1311.

Grams, P., Schmidt, J., Wright, S., Topping, D., Melis, T., & Rubin, D. (2015). Building sandbars in the Grand Canyon. Eos, 96. https://doi.org/10.1029/2015EO030349

Gu, R., Montgomery, S., & Austin, T. AL. (1998). Quantifying the effects of stream discharge on summer river temperature. Hydrological Sciences Journal, 43(6), 885–904. https://doi.org/10.1080/02626669809492185

Hoch, S. W., & David Whiteman, C. (2010). Topographic effects on the surface radiation balance in and around Arizona's Meteor crater. Journal of Applied Meteorology and Climatology, 49(6), 1114–1128. https://doi.org/10.1175/2010JAMC2353.1

Hoffnagle, T. L. (2001). Changes in water temperature of backwaters during fluctuating vs. short-term steady flows in the Colorado River, Grand Canyon. Proceedings of the Fifth Biennial Conference of Research on the Colorado Plateau, June, 103–118.

Huning, L. S., & Margulis, S. A. (2015). Watershed modeling applications with a modular physically-based and spatially-distributed watershed educational toolbox. Environmental Modelling & Software, 68, 55–69. https://doi.org/10.1016/j.envsoft.2015.02.008

Huntoon, P. W. (1974). The karstic groundwater basins of the Kaibab Plateau, Arizona. Water Resources Research, 10(3), 579–590. https://doi.org/10.1029/WR010i003p00579

Karlstrom, K. E., Timmons, J. M., & Crossey, L. J. (2012). Introduction to Grand Canyon geology. Special Paper of the Geological Society of America, 489(November), 1–6. https://doi.org/10.1130/2012.2489(00)

King, T. V., & Neilson, B. T. (2019). Quantifying reach-average effects of hyporheic exchange on arctic river temperatures in an area of continuous permafrost. Water Resources Research, 1–21. https://doi.org/10.1029/2018WR023463

Kurylyk, B. L., Moore, R. D., & Macquarrie, K. T. B. (2016). Scientific briefing: Quantifying streambed heat advection associated with groundwater-surface water interactions. Hydrological Processes. https://doi.org/10.1002/hyp.10709

Lam, J. C., & Li, D. H. W. (1996). Correlation between global solar radiation and its direct and diffuse components. Building and Environment, 31(6), 527–535. https://doi.org/10.1016/0360-1323(96)00026-1

Larson, D. W., Matthes, U., & Kelly, P. E. (2000). Cliff ecology: pattern and process in cliff ecosystems. Cambridge, 360p. https://doi.org/10.5860/CHOICE.37-6277

Leach, J. A., & Moore, R. D. (2010). Above-stream microclimate and stream surface energy exchanges in a wildfire-disturbed riparian zone. Hydrological Processes, 24(17), 2369–2381. https://doi.org/10.1002/hyp.7639

Leeder, M. R. (2010). Sedimentology and sedimentary basins: From turbulence to tectonics. *Wiley*.

Loinaz, M. C., Davidsen, H. K., Butts, M., & Bauer-Gottwein, P. (2013). Integrated flow and temperature modeling at the catchment scale. Journal of Hydrology, 495, 238–251. https://doi.org/10.1016/j.jhydrol.2013.04.039

Lowney, C. L. (2000). Stream temperature variation in regulated rivers: Evidence for a spatial pattern in daily minimum and maximum magnitudes. Water Resources Research, 36(10), 2947–2955. https://doi.org/10.1029/2000WR900142

MacDonald, R. J., Boon, S., & Byrne, J. M. (2014). A process-based stream temperature modelling approach for mountain regions. Journal of Hydrology, 511, 920–931. https://doi.org/10.1016/j.jhydrol.2014.02.009

Magirl, C. S., Breedlove, Mi. J., Webb, R. H., & Griffitsh, P. G. (2008). Modeling water-surface elevations and virtual shorelines for the Colorado River in Grand Canyon, Arizona. U.S. Geological Survey, Scientific Investigations Report, 2008–5075, 1–32.

Magirl, C. S., Webb, R. H., & Griffiths, P. G. (2005). Changes in the water surface profile of the Colorado River in Grand Canyon, Arizona, between 1923 and 2000. Water Resources Research, 41(5), 1–10. https://doi.org/10.1029/2003WR002519

Matzinger, N., Andretta, M., van Gorsel, E., Vogt, R., Ohmura, A., & Rotach, M. W. (2003). Surface radiation budget in an alpine valley. Quarterly Journal of the Royal Meteorological Society, 129(588), 877–895. https://doi.org/10.1256/qj.02.44

Maupin, M. A., Kenny, J. F., Hutson, S. S., Lovelace, J. K., Barber, N. L., & Linsey, K. S. (2014). Estimated use of water in the United States in 2010. https://doi.org/http://dx.doi.org/10.3133/cir1405

McMahon, A., & Moore, R. D. (2017). Influence of turbidity and aeration on the albedo of mountain streams. Hydrological Processes, 31(25), 4477–4491. https://doi.org/10.1002/hyp.11370

Meier, W., Bonjour, C., Wüest, A., & Reichert, P. (2003). Modeling the effect of water diversion on the temperature of mountain streams. Journal of Environmental Engineering, 129(8), 755–764. https://doi.org/10.1061/(ASCE)0733-9372(2003)129:8(755)

Melis, T. S. (Editor) (2011). Effects of three high-flow experiments on the Colorado River ecosystem downstream from Glen Canyon Dam, Arizona. U.S. Geological Survey Circular, 1366 (February), 147 p. http://pubs.usgs.gov/circ/1366/

Moore, R. D., Leach, J. A., & Knudson, J. M. (2014). Geometric calculation of view factors for stream surface radiation modelling in the presence of riparian forest. Hydrological Processes, 28(6), 2975–2986. https://doi.org/10.1002/hyp.9848

Moore, R. D., Spittlehouse, D. L., & Story, A. (2005). Riparian microclimate and stream temperature response to forest harvesting: A review. Journal of the American Water Resources Association, 41(4), 813–834. https://doi.org/10.1111/j.1752-1688.2005.tb03772.x

Neilson, B. T., Stevens, D. K., Chapra, S. C., & Bandaragoda, C. (2009). Data collection methodology for dynamic temperature model testing and corroboration. Hydrological Processes, 23(20), 2902–2914. https://doi.org/10.1002/hyp.7381

Neilson, B. T., Stevens, D. K., Chapra, S. C., & Bandaragoda, C. (2010). Two-zone transient storage modeling using temperature and solute data with multiobjective calibration: 1. Temperature. Water Resources Research, 46(12), 1–17. https://doi.org/10.1029/2009WR008759

Nilsson, C., & Renöfält, B. M. (2008). Linking Flow Regime and Water Quality in Rivers: a Challenge to Adaptive Catchment Management. Ecology and Society, 13(2), art18. https://doi.org/10.5751/ES-02588-130218

Olden, J. D., & Naiman, R. J. (2010). Incorporating thermal regimes into environmental flows assessments: Modifying dam operations to restore freshwater ecosystem integrity. Freshwater Biology, 55(1), 86–107. https://doi.org/10.1111/j.1365-2427.2009.02179.x

Olyphant, G. A. (1986). Longwave radiation in mountainous areas and its influence on the energy balance of alpine snowfields. Water Resources Research, 22(1), 62–66. https://doi.org/10.1029/WR022i001p00062

Orgill, J. F., & Hollands, K. G. T. (1977). Correlation equation for hourly diffuse radiation on a horizontal surface. Solar Energy, 19(4), 357–359. https://doi.org/10.1016/0038-092X(77)90006-8

Petersen, J. H., & Paukert, C. P. (2005). Development of a bioenergetics model for humpback chub and evaluation of water temperature changes in the Grand Canyon, Colorado River. Transactions of the American Fisheries Society, 134(4), 960–974. https://doi.org/10.1577/T04-090.1

Plüss, C., & Ohmura, A. (1997). Longwave radiation on snow-covered mountainous surfaces. Journal of Applied Meteorology, 36(6), 818–824. https://doi.org/10.1175/1520-0450-36.6.818

Polehn, R. A., & Kinsel, W. C. (1997). Transient temperature solution for stream flow from a controlled temperature source. Water Resources Research, 33(1), 261–265. https://doi.org/10.1029/96WR03016

Risley, J. C., Constantz, J., Essaid, H., & Rounds, S. (2010). Effects of upstream dams versus groundwater pumping on stream temperature under varying climate conditions. Water Resources Research, 46(6). https://doi.org/10.1029/2009WR008587

Ross, R. P., & Vernieu, W. S. (2013). Nearshore temperature findings for the Colorado River in Grand Canyon, Arizona - Possible implications for native fish. U.S. Geological Survey Fact Sheet 2013–3104. https://doi.org/10.3133/fs20133104

Rossman, L. A. (2006). Storm water management model quality assurance report: Dynamic wave flow routing. Storm Water Management Model Quality Assurance Report, EPA/600/R-06/097, 1–115. http://www.epa.gov/water-research/storm-water-management-model-swmm

Roth, T. R., Westhoff, M. C., Huwald, H., Huff, J. A., Rubin, J. F., Barrenetxea, G., Vetterli, M., Parriaux, A., Selker, J. S., & Parlange, M. B. (2010). Stream temperature response to three riparian vegetation scenarios by use of a distributed temperature validated model. Environmental Science & Technology, 44(6), 2072–2078. https://doi.org/10.1021/es902654f

Rutherford, J. C., Blackett, S., Blackett, C., Saito, L., & Davies-Colley, R. J. (1997). Predicting the effects of shade on water temperature in small streams. New Zealand Journal of Marine and Freshwater Research, 31(5), 707–721. https://doi.org/10.1080/00288330.1997.9516801

Sabol, T. A., & Springer, A. E. (2013). Transient simulation of groundwater levels within a sandbar of the Colorado River, Marble Canyon, Arizona, 2004. U.S. Geological Survey Open-File Report 2013-1277, 22. https://doi.org/http://dx.doi.org/10.3133/ofr20131277

Schmidt, J. C., Topping, D. J., Rubin, D. M., Hazel, J. E., Kaplinski, M., Wiele, S. M., & Goeking, S. A. (2007). Streamflow and sediment data collected to determine the effects of low summer steady flows and habitual maintenance flows in 2000 on the Colorado River between Lees Ferry and Bright Angel Creek, Arizona. U.S. Geological Survey Open-File Report 2007-1268, 79 p. http://pubs.usgs.gov/of/2007/1268/

Sridhar, V., Sansone, A. L., LaMarche, J., Dubin, T., & Lettenmaier, D. P. (2004). Prediction of stream temperature in forested watersheds. Journal of the American Water Resources Association, 40(1), 197–213. https://doi.org/10.1111/j.1752-1688.2004.tb01019.x

Stanitski-Martin, D. (1996). Seasonal energy balance relationships over the Colorado River and adjacent riparian habitat: Glen Canyon, Arizona. Ph.D. Dissertation, Arizona State University, Tempe. https://doi.org/10.16953/deusbed.74839

Theurer, F. D., Voos, K. A., & Miller, W. J. (1984). Instream water temperature model. Instream Flow Information Paper 16. In FWS/OBS. http://pubs.er.usgs.gov/publication/fwsobs84_15

Topping, D. J., Rubin, D. M., & Vierra, L. E. (2000). Colorado River sediment transport: 1. Natural sediment supply limitation and the influence of Glen Canyon Dam. Water Resources Research, 36(2), 515–542. https://doi.org/10.1029/1999WR900285

Topping, D. J., Schmidt, J. C., & Vierra Jr., L. E. (2003). Computation and analysis of the instantaneous-discharge record for the Colorado River at Lees Ferry, Arizona : May 8, 1921, through September 30, 2000. In Professional Paper. https://doi.org/10.3133/pp1677

Trammell, M. A., Valdez, R. A., Carothers, S. W., & Ryel, R. J. (2002). Effects of a low steady summer flow experiment on native fishes of the Colorado River in Grand Canyon, Arizona. SWCA Environmental Consultants.

U.S. Bureau of Reclamation. (1999). Glen Canyon Dam modifications to control downstream temperatures - plan and draft environmental assessment. Department of the Interior.

U.S. Bureau of Reclamation. (2012). Colorado River Basin Water Supply and Demand Study. 85.

Udall, B., & Overpeck, J. (2017). The twenty-first century Colorado River hot drought and implications for the future. Water Resources Research, 53(3), 2404–2418. https://doi.org/10.1002/2016WR019638

U.S. Department of the Interior. (2007). Recod of decision: Colorado River interim guidelines for lower basin shortages and the coordinated operations for Lake Powell and Lake Mead, Final environmental impact statement. Office of the Secretary of Interior, Washington, D.C.

Valdez, R. A., Speas, D. W., & Kubly, D. M. (2013). Benefits and risks of temperature modification at Glen Canyon Dam to aquatic resources of the Colorado River in the Grand Canyon. U.S. Bureau of Reclamation, Upper Colorado Region, Salt Lake City, UT.

Van Haverbeke, D. R., Stone, D. M., Coggins, L. G., & Pillow, M. J. (2013). Long-term monitoring of an endangered desert fish and factors influencing population dynamics. Journal of Fish and Wildlife Management, 4(1), 163–177. https://doi.org/10.3996/082012-JFWM-071

Vernieu, W. S., & Anderson, C. R. (2013). Water temperatures in select nearshore environments of the Colorado River in Grand Canyon, Arizona, during the low steady summer flow experiment of 2000. U.S. Geological Survey Open- File Report 2013–1066, 44.

Vernieu, W. S., Hueftle, S. J., & Gloss, S. P. (2005). Water quality in Lake Powell and the Colorado River. In S. P. Gloss, J. E. Lovich, & T. S. Melis (Eds.), State of the Colorado River Ecosystem (pp. 69–85). U.S. Geological Survey Circular 1282.

Ward, J. V., & Stanford, J. A. (1983). The serial discontinuity concept of lotic ecosystems.

Wawrzyniak, V., Allemand, P., Bailly, S., Lejot, J., & Piégay, H. (2017). Coupling LiDAR and thermal imagery to model the effects of riparian vegetation shade and groundwater inputs on summer river temperature. Science of the Total Environment, 592, 616–626. https://doi.org/10.1016/j.scitotenv.2017.03.019

Webb, B. W., Hannah, D. M., Moore, R. D., Brown, L. E., & Nobilis, F. (2008). Recent advances in stream and river temperature research. Hydrological Processes, 22(7), 902–918. https://doi.org/10.1002/hyp.6994

Webb, B. W., & Walling, D. E. (1993). Temporal variability in the impact of river regulation on thermal regime and some biological implications. Freshwater Biology, 29(1), 167–182. https://doi.org/10.1111/j.1365-2427.1993.tb00752.x

Webb, B. W., & Zhang, Y. (1997). Spatial and seasonal variability in the components of the river heat budget. Hydrological Processes, 11(1), 79–101. https://doi.org/10.1002/(SICI)1099-1085(199701)11:1<79::AID-HYP404>3.0.CO;2-N

Webb, B. W., & Zhang, Y. (2004). Intra-annual variability in the non-advective heat energy budget of Devon streams and rivers. Hydrological Processes, 18(11), 2117–2146. https://doi.org/10.1002/hyp.1463

Wenzel, L. K., & Fishel, V. C. (1942). Methods for determining permeability of water-bearing materials, with special reference to discharging-well methods, with a section on direct laboratory methods and bibliography on permeability and laminar flow. USGS Water Supply Paper 887. https://doi.org/10.3133/wsp887

Westhoff, M. C., Savenije, H. H. G., Luxemburg, W. M. J., Stelling, G. S., van de Giesen, N. C., Selker, J. S., Pfister, L., & Uhlenbrook, S. (2007). A distributed stream temperature model using high resolution temperature observations. Hydrology and Earth System Sciences Discussions, 4(1), 125–149. https://doi.org/10.5194/hessd-4-125-2007

Whiteman, C. D., Allwine, K. J., Fritschen, L. J., Orgill, M. M., & Simpson, J. R. (1989). Deep valley radiation and surface energy budget microclimates. Part I: Radiation.

Journal of Applied Meteorology, 28(6), 414–426. https://doi.org/10.1175/1520-0450(1989)028<0414:DVRASE>2.0.CO;2

Wiele, S. M., & Griffin, E. R. (1997). Modification to a one-dimensional model of unsteady flow in the Colorado River through the Grand Canyon, Arizona. Water-Resouces Investigations Report 97-4046, 17.

Wiele, S. M., & Smith, J. D. (1996). A reach-averaged model of diurnal discharge wave propagation down the Colorado River through the Grand Canyon. Water Resources Research, 32(5), 1375–1386. https://doi.org/10.1029/96WR00199

Wright, S. A., Anderson, C. R., & Voichick, N. (2009). A simplified water temperature model for the Colorado River below Glen Canyon Dam. River Research and Applications, 25(6), 675–686. https://doi.org/10.1002/rra.1179

Wright, S. A., Melis, T. S., Topping, D. J., & Rubin, D. M. (2005). Influence of Glen Canyon Dam operations on downstream sand resources of the Colorado River in Grand Canyon. In S. P. Gloss, J. E. Lovich, & T. S. Melis (Eds.), State of the Colorado River Ecosystem (pp. 17–31). U.S. Geological Survey Circular 1282.

Yackulic, C. B., M. D. Yard, J. Korman, & D. R. Van Haverbeke. (2014). A quantitative life history of endangered humpback chub that spawn in the Little Colorado River: variation in movement, growth, and survival. Ecology and Evolution 4:1006-1018.

Yackulic, C. B., J. Korman, M. D. Yard, & M. Dzul. (2018). Inferring species interactions through joint mark–recapture analysis. Ecology 99:812-821.

Yard, M. D., Bennett, G. E., Mietz, S. N., Coggins, L. G., Stevens, L. E., Hueftle, S., & Blinn, D. W. (2005). Influence of topographic complexity on solar insolation estimates for the Colorado River, Grand Canyon, AZ. Ecological Modelling, 183(2–3), 157–172. https://doi.org/10.1016/j.ecolmodel.2004.07.027

Zhang, Y. L., Li, X., Cheng, G. D., Jin, H. J., Yang, D. W., Flerchinger, G. N., Chang, X. L., Wang, X., & Liang, J. (2018). Influences of topographic shadows on the thermal and hydrological processes in a cold region mountainous watershed in northwest China. Journal of Advances in Modeling Earth Systems, 10(7), 1439–1457. https://doi.org/10.1029/2017MS001264

Zukosky, K. A. (1995). An assessment of the potential to use water chemistry parameters to define ground water flow pathways at Grand Canyon National Park , Arizona. Department of Geoscience MSc Thesis, University of Nevada, Las Vegas.

CHAPTER 3[1]

EVALUATION OF THE ERA5-LAND REANALYSIS DATASET FOR PROCESS-BASED RIVER TEMPERATURE MODELING OVER DATA SPARSE AND TOPOGRAPHICALLY COMPLEX REGIONS

Abstract

Models developed to capture underlying river processes over long historical periods and varying hydrologic conditions provide confidence for subsequent forecasting applications. However, many areas lack the weather data needed to develop process-based models over these long periods. Climate reanalysis datasets (CRDs) are increasingly used as surrogates for historical meteorology, but use in river temperature models is still relatively new and untested. Testing of temperature models using CRDs in rivers experiencing a range of instream flow, weather, and topographic conditions is needed to validate the application of these datasets. Focusing on the ERA5-Land CRD, correction methods that relate weather variables and elevation were tested using weather stations surrounding and adjacent to the Colorado River in Grand Canyon. Our findings show that elevation corrections improved air temperature and relative humidity, but negatively impacted wind speed estimates. Two-year river temperature model simulations in a 387-km segment of the Colorado River in Grand Canyon and a 576-km segment of the Green River showed that using elevation corrected ERA5-Land inputs produced lower mean errors at downstream river locations when compared to predictions using elevation corrected ground-based inputs. Better river temperature predictions when using ERA5-Land are attributed to the ability to represent spatial variability in weather

[1]Coauthored by Bryce A. Mihalevich, Bethany T. Neilson, Caleb A. Buahin

conditions over these large areas. These promising results persisted when spatially coarsened ERA5-Land inputs were used. This study highlights the importance of having spatially varying weather information, even at relatively coarse resolutions, when modeling physical processes over large spatial scales and suggests confidence in using CRDs for obtaining this information.

1. Introduction

Process-based river temperature models are integral in understanding the dominant heat flux mechanisms controlling river thermal regimes and allow us to evaluate how systems may be altered with changes in climate, hydrology, or management practices (King & Neilson, 2019; Meier et al., 2003; Webb & Zhang, 2004). These types of models estimate the energy and water fluxes responsible for temperature patterns using hydraulic (i.e., stream width, depth, gradient, and roughness) and meteorological information (i.e., air temperature, relative humidity, wind speed, and solar radiation). As such, prior river temperature modeling efforts have relied on existing weather station networks (e.g., King et al., 2016; Loinaz et al., 2013; Mihalevich et al., 2020) or installed stream microclimate and ground-based meteorological stations (e.g., Benyahya et al., 2010; Caissie, 2016; Leach & Moore, 2010). However, the number of long-term hydrological and meteorological networks has been highly variable over the last two decades and some regions lack observations altogether (Lins, 2008; Menne et al., 2018; NASA-GISS, 2019). While data limitations reduce our ability to develop process-based models, quantifying heat flux dynamics is still needed to resolve climate related impacts on aquatic thermal regimes (Arismendi et al., 2014; Diabat et al., 2013; Dugdale et al.,

2017; Leach & Moore, 2019). Therefore, to overcome the challenges of river temperature modeling in regions with limited weather data, new data products need to be evaluated.

Runoff modelers have faced similar challenges related to the availability of weather data and many have resorted to climate reanalysis datasets to supply weather inputs over data limited regions at large scales (e.g., Bogaart et al., 2003; Essou et al., 2017; Krogh et al., 2015; Mizukami et al., 2014; Tarek et al., 2019). Climate reanalysis datasets (CRDs) consist of gridded representations of historical meteorology and land surface conditions. They are created from general circulation models and data assimilation systems using historical observations as a means to "reanalyze" the past (Copernicus Climate Change Service, 2019; Kalnay et al., 1996). The result is a set of predictions for atmosphere, land surface, and ocean conditions over several decades and at continental or global scales. One advantage of these datasets is the inherent consistency in spatial and temporal resolution, whereas ground-based observations can be disparate when considering large spatial and temporal domains. Furthermore, there has been an increasing number of high spatial (e.g., 4–32 km) and temporal (1–3 hour time steps) resolution CRDs that include the necessary variables for process-based river temperature modeling (Table 3-1). However, systematic biases are common, and therefore datasets need to be validated and are often transformed (i.e., bias corrected) to better represent observational data before application (Teutschbein & Seibert, 2012). Despite this caveat, CRDs are becoming more frequent in hydrological applications (e.g., Essou et al., 2017; Frassl et al., 2018; Krogh et al., 2015), but there are only a few examples of CRD's being used in river temperature models (Daniels & Danner, 2020; Li et al., 2015; Van Beek et al., 2012; Van Vliet et al., 2012).

Table 3-1. Select climate reanalysis datasets that contain meteorological information (i.e., air temperature, solar radiation, relative humidity, and wind speed) with high spatial and temporal resolutions suitable for process-based river temperature modeling.

Dataset name	Approximate grid size	Minimum temporal resolution	Data years	Spatial Coverage	Source
ERA5-Land	9 x 9 km	1 hr	1950-present	Global	ECMWF[a]
ERA5	30 x 30 km	1 hr	1979- present	Global	ECMWF
Climate Forecast System Reanalysis (CFSR)	38 x 38 km	1 hr	1979-2014	Global	NCEP[b]
Climate Forecast System version 2 (CFSv2)	22.2 x 22.2 km	1 hr	2011-present	Global	NCEP
North American Regional Reanalysis (NARR)	32 x 32 km	3 hr	1979-present	North America	NCEP
North America Land Data Assimilation System version 2 (NLDAS-2)	12 x 12 km	1 hr	1979-pressent	Central North America	NASA[c]
Global Land Data Assimilation System version 2.1 (GLDAS-2.1)	27 x 27 km	3 hr	2000-present	Global	NASA
Physical Solar Model version 3 (PSMv3)	4 x 4 km	0.5 hr	1998-2020	Non-polar latitudes of North and South America	NREL[d]

[a] European Center for Medium-range Weather Forecasts
[b] National Centers for Environmental Prediction
[c] National Aeronautics and Space Administration
[d] National Renewable Energy Laboratory

Most applications of CRDs to process-based river temperature models have been limited to coupled land surface-hydrologic models that generalize many river-specific characteristics (Van Beek et al., 2012; Van Vliet et al., 2012). While these river temperature models provide reasonable predictions at large spatial and temporal scales, they do not account for local influences (e.g., diversions, shading dynamics, reservoir release elevations), which can be significant determinants of thermal regimes at smaller scales. One of the few examples of a CRD in a process-based river temperature model that includes local scale heat transfer processes used the North American Regional Reanalysis dataset (NARR, 2004) to predict river temperatures over 338 km of Sacramento River below Keswick Dam, a low-relief region in California's Central Valley (Daniels and Danner, 2020). In their application, the NARR dataset was bias corrected using empirical quantile mapping, which has been shown to be an effective transformation technique in several studies (e.g., Chen et al., 2013; Li et al., 2019; Teutschbein & Seibert, 2012). However, statistical bias correction methods depend on ground-based observations, which may not be possible in data limited regions, and at best, result in extrapolation of site-specific bias corrections to new locations. Statistical bias corrections also assume that the relationships calculated using historical data do not change, and therefore, may not be transferable to future climate extremes. Alternatively, correction methods that remove elevation induced biases based on physical relationships have been shown to improve reanalysis estimates over complex terrain and can be used in the absence of ground-based observations (Gao et al., 2012; Sen Gupta & Tarboton, 2016; You et al., 2019; Zhao et al., 2008). Application of these elevation-based correction methods are limited to comparisons between ground-based observations and distributed

hydrologic models. This combined with the limited application of CRDs in process-based river temperature modeling leaves many unknowns about their feasibility and the spatial resolution needed to ensure reasonable river temperature predictions.

To evaluate the effectiveness of using CRDs with elevation corrections for predicting river temperatures in remote and topographically complex regions, we developed models for two parts of the Colorado River basin and tested these with the ERA5-Land dataset (Table 3-1) and ground-based observations. With the variety of different spatial resolutions offered among available datasets (Table 3-1), we also tested the influence of coarsening the spatial resolution of ERA5-Land on river temperature predictions. We first evaluated the application of elevation corrections to ERA5-Land weather data at different spatial resolutions on the highly regulated Grand Canyon reach of the Colorado River. Due to the extensive hydrological and meteorological data in the Grand Canyon region, this provided a means to test the validity of elevation corrections and the use of ERA5-Land over highly variable terrain. We then tested the use of ERA5-Land in a river temperature model at larger spatial scales within the Colorado River basin by modeling the Green River below Flaming Gorge Dam where weather data are sparse, and the topography is more varied.

2. Methods

2.1. Study Area

The Colorado River basin provides water for 40 million people in the United States and Mexico (U.S. Bureau of Reclamation, 2012) and critical habitat for three federally listed endangered fish species (U.S. Fish and Wildlife Service, 1987). To increase the reliability of water supply across the basin, more than 7.4×10^{10} m^3 (60

million acre-feet) of water storage has been developed. The dams constructed to provide this storage have also dramatically changed the hydrologic and thermal characteristics of the reaches downstream from each reservoir (Vernieu et al., 2005). The result of these changes, as well as introduction of nonnative competing species, has been a decline, and in some cases extirpation, of endemic fish species (Gloss & Coggins, 2005; Bestgen & Hill, 2016; Dibble et al., 2021; Martinez et al., 2014; Olden et al., 2006). As the basin continues to grapple with the on-going Millennium Drought (2000-present; Salehabadi et al., 2020; Wheeler et al., 2021) and the reduction of flows due to a warming climate (Dettinger et al., 2015; Udall & Overpeck, 2017), reservoirs have fallen to unprecedented low levels. If reservoir elevations, thermal stratification patterns, or operational procedures change significantly, the downstream river segments and ecosystems may once again be altered (Null et al., 2013). In order to address the concerns of future temperature impacts on both native and nonnative fish communities in the Colorado River basin, the development of large-scale process-based river temperature models are needed to provide insight regarding the thermal implications of water management decisions and influences of climate change.

Weather data are critical in process-based river temperature models, however, these data are spatially and temporally limited in sections of the Colorado River basin. Given the large spatial extents of the Colorado and Green Rivers (Figure 3-1), significant variability in weather occurs due to changes in latitude, elevation, and surrounding topography. For instance, weather in the Grand Canyon region can be highly variable with cooler air temperatures closer to Lake Powell, hotter conditions further west towards Lake Mead, and more summer monsoon rains around the Little Colorado River

confluence. While these patterns are recorded by numerous weather stations around Grand Canyon (Caster et al., 2014; Caster & Sankey, 2016), most sites have inconsistent observational periods making them inadequate for long-term model simulations (Figure B-1). Within the Grand Canyon, observations of air temperature, relative humidity, and wind speed at the river elevation have been collected intermittently by the Grand Canyon Monitoring and Research Center (GCMRC) since 2003 (Caster et al., 2014; Draut & Rubin, 2006). However, only limited solar radiation measurements have been made (Mihalevich et al., 2020; Stanitski-Martin, 1996). While these GCMRC weather station data (referred to as GCMRC-WS here) provide valuable insights into the microclimates along the river corridor, they are too temporally sparse for simulating longer term river temperatures in Grand Canyon (Figure B-2). Meteorological information in the Green River, is even more limited and sparsely distributed, with most weather stations located around municipal areas (Figure B-3). Weather stations are particularly limited in remote sections of the watershed such as the semi-arid Tavaputs Plateau and the arid Canyonlands region. The 664 km section of the Green River between Flaming Gorge Dam and the Colorado River confluence (Figure 3-1) also experiences highly variable climate, with lower latitudes experiencing warmer air temperature, more solar radiation, and lower relative humidity in relation to higher latitude locations (Figure B-4). The lack of meteorological information and variability of weather conditions in the Colorado River basin highlights the need to test CRDs for larger scale river temperature modeling applications.

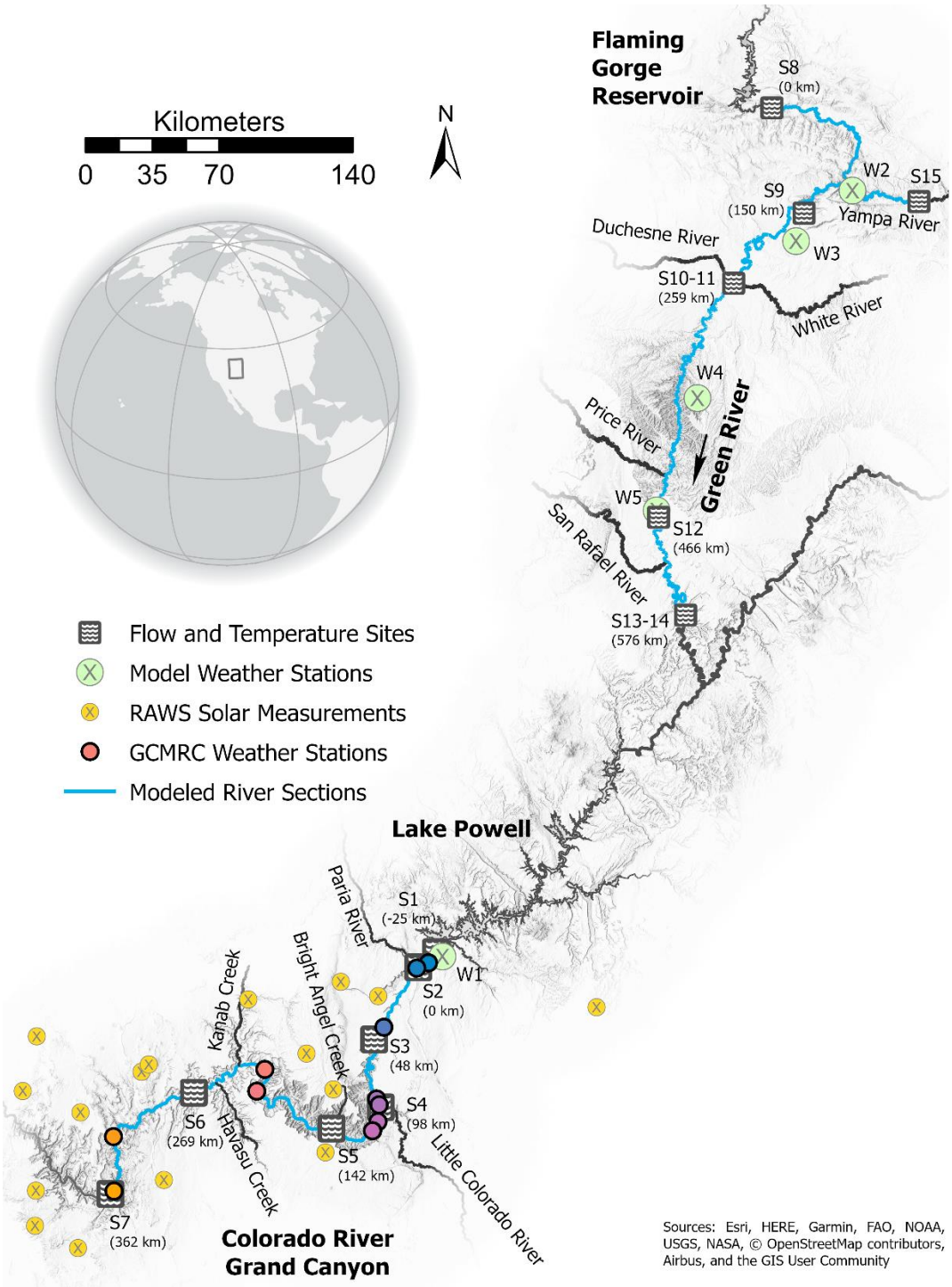

Figure 3-1. Map of the study area depicting the location of monitoring sites used in analyses and river temperature models for the Green River and Colorado River in Grand Canyon. Stream flow and temperature locations are indicated with a "S" and weather stations used in the modeling are indicated with a "W" and correspond to the information presented in Table 3-2. Yellow circles with X's are the location of the solar radiation stations aggregated in the Grand Canyon model described by Mihalevich et al. (2020). Colored circles along the river show the location of GCMRC weather stations (GCMRC-

WS) and correspond to the colors used in Figure B-2. Only tributaries with active monitoring stations are shown.

Table 3-2. Sites along the mainstem branches used for boundary conditions, inflows, and evaluating model predictions in the Colorado and Green River models. Stream flow and temperature locations are indicated with a "S" and weather stations are indicated with a "W" and correspond to the locations mapped in Figure 3-1. The river kilometer indicates the approximate location of flow and river temperature sites and for weather stations they represent the range over which data were applied in the model domain.

No.	Site Name[1]	Site ID	River KM(s)	Variables[2]
Colorado River Model				
S1	Colorado River below Glen Canyon Dam	09379901	-25	Flow, WT
S2	Colorado River at Lees Ferry	09380000	0	Flow, WT
S3	Colorado River near river mile 30	09393050	48	Flow, WT
S4	Colorado River above Little Colorado River	09383100	98	Flow, WT
S5	Colorado River near Grand Canyon	09402500	142	Flow, WT
S6	Colorado River above National Canyon	09404120	269	Flow, WT
S7	Colorado River above Diamond Creek	09404200	362	Flow, WT
W1	Page Municipal Airport	KPGA	-25 - 362	AT, RH, WS
N/A	Remote automated weather stations (RAWS)	N/A	-25 - 362	SR
Green River Model				
S8	Green River near Greendale UT (immediately below Flaming Gorge Dam)	09234500	0	Flow, WT
S9	Green River near Jensen UT	09261000	150	Flow, WT
S10	USFWS Green River near Ouray	N/A	248	WT
S11	Green River at Ouray UT	09272400	259	Flow
S12	Green River at Green River UT	09315000	466	Flow
S13	Green River at Mineral Bottom near Canyonlands National Park	09328920	576	Flow
S14	UTDNR Green River at Mineral Bottoms	N/A	576	WT
S15	Yampa River at Deerlodge Park CO	09260050	-75	Flow, WT
W2	Dinosaur NM Success	SURC2	0 - 150	AT, RH, WS, SR
W3	Split Mountain	SPMU1	151 - 259	AT, RH, WS, SR
W4	Wildhorse	WHBU1	260 - 466	AT, RH, WS, SR
W5	Green River	GREU1	467 - 576	AT, RH, WS, SR

[1]Data were retrieved from USGS and MesoWest online databases or through personal communications with U.S. Fish and Wildlife Service (USFWS) and Utah Department of Natural Resources (UTDNR) staff.
[2]Abbreviations used are WT (water temperature), AT (air temperature), RH (relative humidity), WS (wind speed), and SR (solar radiation).

2.2. River Temperature Model

In order to address our research questions regarding the influence of different weather inputs on river temperature predictions, we applied a one-dimensional, dynamic,

process-based routing and river temperature model within HydroCouple (Buahin et al., 2019; Buahin & Horsburgh, 2018). This HydroCouple application includes an EPA SWMM (Storm Water Management Model; Rossman, 2006) component for dynamic wave flow routing, the channel solute and heat transport (CSH) component for channel advection and dispersion, and sensible and latent heat fluxes; the radiative heat exchange (RHE) component used for shortwave and longwave radiation terms; the hyporheic transient storage (HTS) component used for sediment conduction; and the time series provider component to apply externally calculated scaling factors to select heat flux terms (i.e., spatial and temporal shading factors). Similar to Mihalevich et al. (2020), the heat fluxes included are net shortwave radiation ($J_{sn,net}$), atmospheric longwave radiation (J_{an}), water longwave radiation (J_{br}), bedrock longwave radiation (J_{rock}), sensible heat (conduction and convection; J_c), latent heat (evaporation and condensation; J_e), internal fluid shear friction (J_f), and sediment conduction (J_{sed}). Heat from tributary inflows is accounted for directly in both the hydraulic and heat transfer modeling components. Air-water interface heat fluxes, as described in Buahin et al. (2019) (i.e., J_{br}, J_e, J_c) and Mihalevich et al. (2020) (i.e., $J_{sn,net}$, J_{an}, and J_{rock}), are estimated from solar radiation, air temperature, relative humidity, and wind speed information as detailed in Text B-1 and Figure B-5. Multiple weather time series can be used in the CSH and RHE components, allowing for spatially varying weather information over the modeling domain.

This model framework was originally applied in the Grand Canyon as described by Mihalevich et al. (2020). The model had approximately 1-km long elements and accounted for complex shading and radiation characteristics present in this part of the Colorado River. Similar to previous modeling work by Anderson & Wright, (2007),

Mihalevich et al. (2020) found that discharge is a major determinant of river temperatures, but also found that topographic shading plays a significant role in controlling the amount of heat exchanged at the air-water interface of the river. Mihalevich et al. (2020) also noted that the controls on solar radiation increased the relative importance of heat fluxes that are generally small in large rivers, highlighting the importance of having good estimates of meteorological conditions when modeling over topographically complex regions. Here, we modified the Mihalevich et al. (2020) Grand Canyon model by extending it 25 km upstream to include the section of river between Glen Canyon Dam (S1) and Lees Ferry (S2), making the total length of river downstream from the dam to be approximately 387 km (Figure 3-1; Table 3-2). This allowed for the use of flow and temperature information immediately downstream from Glen Canyon Dam as our upstream boundary condition. The reader is referred to Mihalevich et al. (2020) for other specifics regarding model formulation, calibration, and input data.

The section of the Green River between Flaming Gorge Dam and the confluence with the Yampa River (Figure 3-1) was previously modeled by Carron & Rajaram (2001) to identify management regimes that provide optimal temperatures for trout (daily maximum < 16 °C) over the first 45 km downstream from the dam and for Colorado pikeminnow (daily maximum > 20 °C) at the Yampa River confluence. Carron & Rajaram (2001) found that the only way to achieve this objective was to attenuate atmospheric heating during the hottest part of the day by diurnally fluctuating flow rates. Understanding how river management may impact the highly migratory and endangered Colorado pikeminnow throughout the Green River is still a relevant issue (Bestgen et al., 2018; Dibble et al., 2021). However, no process-based temperature model has been

developed for sections of the Green River downstream of the Yampa River, limiting our ability to evaluate temperature impacts on Colorado pikeminnow in other critical river segments. To overcome this gap and further test the use of different weather data sets for river temperature predictions, we applied the same coupled modeling framework from Mihalevich et al. (2020) to the Green River. The goal was to predict sub-daily river flow and temperature between Flaming Gorge Dam (S8) and Mineral Bottom (S14), a river segment that is approximately 576-km long (Figure 3-1; Table 3-2). We also simulated flow and temperature for 75 km of the Yampa River from Deerlodge Park (S15) to its confluence with the Green River. Each model element had a length of 1 km and received unique time-varying shading and radiation factors used to scale solar radiation and compute $J_{rock,}$ using the methods described in Mihalevich et al. (2020) (Text B-2). Further details on model tributary data, distributed inflows, sediment heat flux, bedrock longwave radiation and flow routing calibration are available in the supplemental information (Text B-2).

2.3. Input Meteorological Data

2.3.1. Ground-based weather data

Previous modeling efforts in the Grand Canyon have relied on weather information from the Page, AZ municipal airport (e.g., Anderson & Wright, 2007; Mihalevich et al., 2020; Wright et al., 2009; Table 3-2 W1). This weather station has consistent long-term observations of air temperature, relative humidity, and wind speed, but does not have solar radiation measurements. For this reason, Mihalevich et al. (2020) obtained solar radiation observations from remote automated weather stations (RAWS) dispersed around the Grand Canyon (Figure 3-1) and aggregated all data into a median

time series. For consistency with previous studies, we used the same weather information from Page, AZ and the solar radiation dataset described in Mihalevich et. al. (2020), which we collectively refer to as the "CR-WS" dataset and apply these data uniformly across the Grand Canyon model domain.

The modeling study by Carron & Rajaram (2001) used meteorological data from two weather stations and estimated solar radiation for calculating atmospheric heat fluxes over the 105 km of river immediately downstream from Flaming Gorge Dam. However, their model relied on minimum and maximum air temperatures, instantaneous dry and wet bulb temperatures, and daily values of wind speed and precipitation. To obtain higher resolution meteorological information for our application in the Green River, we searched for weather stations using the University of Utah MesoWest database (herein referred to as MesoWest; https://mesowest.utah.edu) of current and archived weather observations. We established a criteria wherein weather stations had to be within 16.1 km (10 miles) of the river corridor, have hourly or sub-hourly time steps, and contain all four key weather variables (i.e., air temperature, shortwave radiation, wind speed, and relative humidity or dew point temperature) to be selected. Weather data from specific stations were applied uniformly to their closest river section, which are defined as the river segments between each USGS gaging station. For example, the coverage area of weather station W2 only includes model elements between Flaming Gorge Dam and Jensen, UT, or river kilometers 0 and 150 (Table 3-2). If multiple weather stations met our selection criteria and corresponded to the same river section, each weather dataset was tested and the station producing the lowest temperature prediction error was selected. The selected

weather information for the Green River model domain (W2 through W5 in Table 3-2) is collectively referred to as the “GR-WS” dataset.

2.3.2. Climate reanalysis data

We selected the ERA5-Land climate reanalysis dataset to provide spatially varying (i.e., gridded) hourly inputs of solar radiation, air temperature, relative humidity, and wind speed (Sabater, 2019). ERA5 is the fifth generation model for atmospheric reanalysis of global climate from the European Center for Medium-Range Weather Forecasts (ECMWF; Hersbach et al., 2018). ERA5-Land is a derivative of ERA5 with finer spatial resolution (approximately 0.1° x 0.1° versus 0.25° x 0.25° latitude and longitude grids) and a series of improvements making it more accurate for applications involving land surface processes. Currently, the temporal coverage of ERA5-Land is between 1950-present. Other climate reanalysis datasets also contain the necessary variables for river temperature models (Table 3-1), however, ERA5-Land was selected over other datasets because of its relatively high spatial and temporal resolution. Here, we refer to models using this input dataset as “ERA5-010”. Since values corresponding to a grid do not have within-grid spatial variability, assignment of ERA5-010 information to model elements was carried out by simply identifying the ERA5-010 grid that directly overlapped a model element.

Spatial aggregation of climate reanalysis data

The spatial resolution of the reanalysis grid determines the amount of input data used within the temperature model, which in turn influences model initialization periods and overall model simulation times. When running large scale models under multiple

hydrologic and climate scenarios, the faster simulation times achieved through coarser resolution inputs may be a compelling tradeoff to the potential improvement in prediction accuracy that may occur with finer resolution inputs.

To test the influence of coarser resolution data, we aggregated ERA5-Land grids to a 1.0 ° x 1.0° latitude and longitude resolution. This corresponds with the coarsest resolution of most CMIP5 climate projection models. Like the Spatial Aggregation method in ArcGIS Insights ®, version 2021.1 (ESRI, Redlands, CA), we calculated a new grid value using the average values among overlapping grids of the original resolution, with areal fractions of each overlapping grid used as weighting factors (Figure B-6). Here we refer to models using upscaled ERA5-Land data as "ERA5-100". As with ERA5-010, assignment of ERA5-100 information to model element was carried out by simply identifying the model elements contained within each ERA5-100 grid.

2.4. Elevation corrections

Weather data can have large spatial variations in topographically complex terrain, especially in the vertical dimension. A well-known phenomenon is the air temperature lapse rate, which describes the nearly linear increase in air temperature with decrease in altitude. Elevation can also influence relative humidity and wind speed (Liston & Elder, 2006; Sen Gupta & Tarboton, 2016; TVA, 1972), although these relationships are not as linear. Nevertheless, when predicting river temperatures in mountainous or canyon-bound regions, the input weather data may be improved by applying parameter specific elevations corrections that relate weather station elevation or the reference elevation of CRD grids to the actual river elevation. Here, we describe elevation corrections for air temperature, relative humidity, and wind speed and apply these corrections to each input

meteorological data set described in Section 2.3. While there are methods for elevation correcting solar radiation (Berg et al., 2003; Liston & Elder, 2006; Mizukami et al., 2014; Sen Gupta & Tarboton, 2016), the lack of solar radiation data at river elevations in our study area limits the validation of these methods, and therefore, they were not tested.

Air temperature

Air temperature is commonly elevation corrected by applying the linear environmental lapse rate of 6.5 °C km^{-1} (Berg et al., 2003; Iizumi et al., 2017; Krogh et al., 2015; Mizukami et al., 2014). However, since lapse rates vary widely over space and time, some refinement can be gained by varying lapse rates monthly (Liston and Elder, 2006). Lapse rates can also be calculated using air temperature profiles over vertical pressure levels (Gao et al., 2012; Sen Gupta & Tarboton, 2016; You et al., 2019), however not all CRD's provide this information (e.g., Table 3-1: ERA5-Land and PSMv3). Therefore, air temperature was corrected to the river elevation with a constant monthly lapse rate as:

$$T_a = T_{a,0} - \Gamma_{a,m}(Z - Z_0) \quad (3\text{-}1)$$

where $T_{a,0}$ is the raw, uncorrected air temperature (°C) at the reference elevation, Z_0 (m), T_a is the air temperature (°C) corrected to the river elevation, Z (m) and is the value supplied to the river temperature model, and $\Gamma_{a,m}$ is the air temperature lapse rate for month m converted to °C m^{-1}, from Table B-1 (Kunkel, 1989).

Relative Humidity

Relative humidity was elevation corrected using air and dew point temperature lapse rates. Dew point temperature was elevation corrected as:

$$T_d = T_{d,0} - \Gamma_{d,m}(Z - Z_0) \quad (3\text{-}2)$$

where $T_{d,0}$ is the raw, uncorrected dew point temperature (°C) at the reference elevation, Z_0 (m), and T_d is the dew point temperature (°C) corrected to the river elevation, Z (m), and $\Gamma_{d,m}$ is the dew point temperature lapse rate for month m converted to °C m^{-1}, from Table B1 (Kunkel, 1989). Following air temperature and dew point temperature elevation corrections, the vapor pressure, e (mmHg), is calculated as a function of temperature:

$$e(T) = 4.596 \exp\left[\frac{17.27T}{237.3+T}\right] \quad (3\text{-}3)$$

where T is either the air temperature (T_a) or the dew point temperature (T_d). Relative humidity, RH (%) is then calculated as the ratio of actual vapor pressure and saturation vapor pressure as:

$$RH = \frac{e(T_d)}{e(T_a)} 100 \quad (3\text{-}4)$$

Wind Speed

For some datasets, wind information is supplied as the zonal, U_0 (m s^{-1}) and meridional, V_0 (m s^{-1}) components. These components can be used to calculate the horizontal wind speed, W_0 (m s^{-1}) at the reference elevation, Z_0 (m) using Pythagoras' equation:

$$W_0 = \sqrt{U_{ERA5}^2 + V_{ERA5}^2} \quad (3\text{-}5)$$

A few different methods exist for correcting wind speeds based on physical properties. One such method proposed by Liston & Sturm, (1998) adjusts wind speeds and directions as a function of terrain slope and curvature using a digital elevation model. However, application of this method by Sen Gupta & Tarboton (2016) resulted in a weak relationship to ground-based observations relative to correlations of other corrected

climate variables (air temperature, shortwave radiation, and relative humidity). Therefore, we opted to use a simpler method that reduces measured wind speed from one elevation to another based on the exponential wind law (TVA, 1972) as:

$$W = W_0 \left(\frac{Z_{mh}}{|Z-(Z_0+Z_{mh,0})|} \right)^n \quad (3\text{-}6)$$

where W is the corrected wind speed (m s^{-1}) for a measurement height of Z_{mh} (m) above the river surface, Z (m), $Z_{mh,0}$ (m) is the measurement height of W_0, and the exponent n is assumed to be 0.15. The wind function in the CSH component assumes wind speed is measured 2 m above the water surface (Buahin et al., 2019), thus, Z_{mh} was set to 2 m.

2.5. Model Simulation period

For Colorado River simulations in Grand Canyon, weather and boundary condition flow and temperature data are available to conduct model runs between January 1, 2000, and January 1, 2020. However, in the Green River, the simulation period is limited by the available weather data coinciding with available river temperature data at downstream locations used for evaluating temperature model performance and spans January 1, 2015, to January 1, 2017. During this time, river temperature information is available at Mineral Bottom (S14), the most downstream monitoring location (Figure 3-1, Table 3-2). This period contains both low and high flow years, providing an opportunity to test our approach over varied flow conditions. Here, we evaluate both the Grand Canyon and Green River models over the same two-year period for consistency in our analyses.

2.6. Analyses

2.6.1. Testing of elevation corrections in Grand Canyon

We first used GCMRC-WS data to test the appropriateness of the elevation corrections (Equations 1-6) when applied to weather time series from CR-WS, ERA5-010, and ERA5-100 datasets. This comparison established how well each model input dataset resemble air temperature, wind speed, and relative humidity observations near the water surface. Assignment of ERA5-010 and ERA5-100 information to individual GCMRC-WS sites was carried out by identifying which specific ERA5-Land grid overlaps with each GCMRC-WS station. The mean error was then calculated to evaluate accuracy by matching times stamps between GCMRC-WS data and CR-WS, ERA5-010 or ERA5-100 datasets.

2.6.2. Differences in elevation corrected weather data

To determine when, where, and for which parameters the weather datasets varied, we subtracted each time series of ERA5-010 from CR-WS and subtracted ERA5-010 from ERA5-100 to produce residual surface heatmaps that show the differences in weather inputs over the Grand Canyon model domain during the simulation period. This was repeated in the Green River model domain, where we subtracted each time series of ERA5-010 from GR-WS and subtracted ERA5-010 from ERA5-100. The residual surface was calculated using elevation corrected daily average weather data for both the Grand Canyon and Green River.

2.6.3. Model performance using different weather data products

We evaluated the accuracy of river temperature predictions made using each set of weather data by comparing temperature predictions to temperature observations at multiple river locations based on available observational data and ecological importance.

In the Grand Canyon, we analyzed predictions at S4, S6, and S7 and in the Green River we analyzed predictions at S9, S10, and S14 (Table 3-2). The mean error, root mean squared error (RMSE), and Nash-Sutcliffe efficiency (NSE) was calculated for each location by matching times between model outputs and river temperature observations.

To determine when and where river temperature predictions deviated when using different weather input datasets, we calculated residual surface heatmaps from model outputs. The residual surface was calculated using daily average water temperature predictions in both the Grand Canyon and Green River. To identify the drivers between model prediction differences we performed a sensitivity analysis of spatially varying model inputs. This was done by conducting four additional two-year model simulations in the Grand Canyon and Green River, where for each run a ground-based weather variable (from CR-WS or GR-WS) was substituted with ERA5-010 elevation corrected time series. The effect of replacing each of the four weather inputs were tested independently.

3. Results

3.1. Grand Canyon

3.1.1. Testing of elevation corrections in Grand Canyon

The GCMRC-WS data indicate that air temperature within Grand Canyon has large seasonal variation and increases in the downstream direction (Figure B-2). Not surprisingly, CR-WS cannot exhibit these spatial changes because it is based on a single measurement location, but the air temperature elevation corrections do improve the representation of CR-WS at most GCMRC-WS locations (Table 3-3; Figure B-7). ERA5-010, on the other hand, does exhibit spatial patterns and has similar air temperature

patterns compared to GCMRC-WS observations. Elevation corrections applied to ERA5-010 air temperature improved representation at all GCMRC-WS locations (Table 3-3).

Relative humidity within Grand Canyon does not have a distinct spatial pattern like air temperature but does experience a seasonal trend with higher values from December to February and lower values between May and July (Figure B-2). Both CR-WS and ERA5-010 exhibits similar temporal variations in relative humidity and both overestimate GCMRC-WS observations (Table 3-3). Applying relative humidity elevation corrections slightly improved mean errors for both input weather datasets.

Like relative humidity, wind speed magnitudes within Grand Canyon experience a seasonal trend, with highest values occurring between April and June, but do not have an apparent spatial pattern (Figure B-2). This temporal pattern exists in both CR-WS and ERA5-010, but the raw, uncorrected datasets overestimate within canyon wind speeds (Table 3-3). Elevation corrections for wind speed increased errors when compared to uncorrected data for both input weather datasets, and now underestimate nearly all GCMRC-WS locations (Table 3-3).

No long-term measurements of solar radiation are available from within Grand Canyon. Therefore, we compared ERA5-010 solar radiation values to the individual RAWS stations that make up the median solar radiation time series used in the CR-WS dataset (Table B-2). This comparison indicated that ERA5-010 overestimated most solar radiation measurement locations with a mean error and standard deviation of 11.8 ±105.9 W/m^2. Seasonally, overestimates were the lowest between October and January and highest in July and August coinciding with the Arizona monsoon season. This indicates

that ERA5-010 does not represent seasonally cloudy periods as well but does capture some of the variability during these times.

Table 3-3. Mean error (ME) between GCMRC-WS data and input weather data used in the river temperature models before (Pre) and after (Post) elevation corrections were applied. Errors are calculated as the input weather data (i.e., CR-WS, ERA5-010, or ERA5-100) minus GCMRC-WS, where positive errors are overestimates of ground-based observations. Post elevation correction values that were the same or greater than pre elevation corrections values, based on the absolute ME, are shaded in light gray. The bottom two rows represent the mean error and standard deviation (σ) of all GCMRC-WS sites combined.

Grand Canyon Weather Stations (GCMRC-WS)	Air Temperature ME [°C]					Relative Humidity ME [%]					Wind Speed ME [m/s]				
	CR-WS		ERA5-010		ERA5-100	CR-WS		ERA5-010		ERA5-100	CR-WS		ERA5-010		ERA5-100
	Pre	Post	Pre	Post	Post	Pre	Post	Pre	Post	Post	Pre	Post	Pre	Post	Post
Mile -10	-1.4	3.7	-2.4	-0.2	0.0	0.6	-1.6	7.4	7.0	6.1	0.8	-0.7	0.1	-0.8	-0.7
Mile 0.5	-0.7	3.7	-2.6	0.4	0.6	-4.5	-5.5	3.3	2.5	3.0	0.6	-0.6	0.2	-0.7	-0.5
Mile 24.5 Upper	-2.9	1.9	-5.6	-1.4	-1.7	3.2	1.6	12.8	11.5	9.1	1.1	-0.3	0.8	-0.4	-0.3
Mile 24.5 Lower	-4.1	0.4	-5.6	-1.4	-1.6	7.1	5.9	12.2	11.0	8.5	0.9	-0.4	0.9	-0.4	-0.3
Mile 58 Upper	-4.3	-0.4	-5.9	-1.0	-0.6	11.8	11.2	8.6	7.5	5.1	-0.1	-1.4	-0.3	-1.4	-0.9
Mile 58 Lower	-4.3	-0.3	-5.3	-0.4	0.0	11.9	11.3	6.4	5.3	2.9	0.5	-0.8	0.4	-0.7	-0.2
Mile 60	-4.8	-0.3	-6.2	-1.2	-0.8	8.1	6.8	8.7	7.5	5.1	0.6	-0.6	0.4	-0.6	-0.2
Mile 66	-5.3	-0.9	-6.4	-1.5	-1.7	10.0	9.0	10.0	9.1	7.7	-0.6	-1.7	-0.9	-1.9	-1.4
Mile 70 Upper	-3.2	1.7	-5.3	-0.2	-0.5	-0.2	-2.4	6.3	5.0	4.0	0.6	-0.7	-0.1	-1.1	-0.6
Mile 70 Lower	-4.6	-0.2	-5.4	-0.4	-0.6	7.9	6.8	6.7	5.7	4.2	-0.1	-1.2	-0.2	-1.2	-0.8
Mile 88	-3.7	0.7	-5.7	-0.1	0.4	-3.0	-3.6	3.7	2.4	2.3	1.7	0.5	0.9	0.1	0.6
Mile 125.5	-4.5	0.0	-6.2	-0.6	-0.8	-1.4	-2.5	6.9	5.1	5.7	0.5	-0.7	-0.1	-1.0	-0.7
Mile 135	-5.8	-1.4	-7.1	-0.9	-1.4	6.5	5.5	6.4	5.6	6.2	0.2	-0.9	0.2	-0.8	-0.4
Mile 203	-7.1	-2.6	-6.7	-0.1	0.2	10.6	9.4	3.2	2.4	4.0	0.8	-0.5	0.3	-0.7	-0.4
Mile 223	-6.1	-1.7	-6.1	0.1	0.1	1.3	0.3	4.9	3.8	4.4	0.7	-0.5	0.6	-0.6	-0.5
ME	-3.7	0.7	-5.7	-0.6	-0.6	-1.5	-2.4	7.3	6.2	5.3	1.3	0.1	0.3	-0.8	-0.5
σ	2.9	3.2	3.3	3.5	3.3	12.9	12.6	14.2	14.2	13.1	1.8	1.1	1.4	1.2	1.2

3.1.2. Differences in input weather data

The most notable difference between CR-WS and ERA5-010 datasets is the spatial variation in air temperature provided by ERA5-010 (Figure 3-2A). In general, CR-WS is providing warmer air temperatures in the 100 km immediately downstream from Glen Canyon Dam and cooler air temperatures over the last 100 km of the model domain (Figure 3-2A). Similar spatial variation is present between ERA5-100 and ERA5-010 (Figure 3-2B) because of the four different ERA5-100 grids that cover the model domain (Figure B-8), however, the average difference between upstream and downstream river kilometers is less. For relative humidity there is both spatial and temporal variation between CR-WS and ERA5-010, with lower CR-WS values in the upstream 100 km and during winter periods (Figure 3-2C). Between ERA5-100 and ERA5-010, there are smaller differences in relative humidity (Figure 3-2D). Differences in wind speed between CR-WS and ERA5-010 are primarily in the spatial dimension, with CR-WS providing higher values in the central part of Grand Canyon (100 – 250 km) and mixed differences occurring over the first 100 kilometers (Figure 3-2E). Interestingly, ERA5-100 provides higher wind speed values than ERA5-010, with spatial variation occurring at the transition of ERA5-100 grid cells (Figure 3-2F). Little spatial variation in solar radiation exists between CR-WS and ERA5-010, but CR-WS generally provides lower values with greatest differences during summer (Figure 3-2G). There are virtually no meaningful differences in solar radiation between ERA5-100 and ERA5-010 (Figure 3-2H).

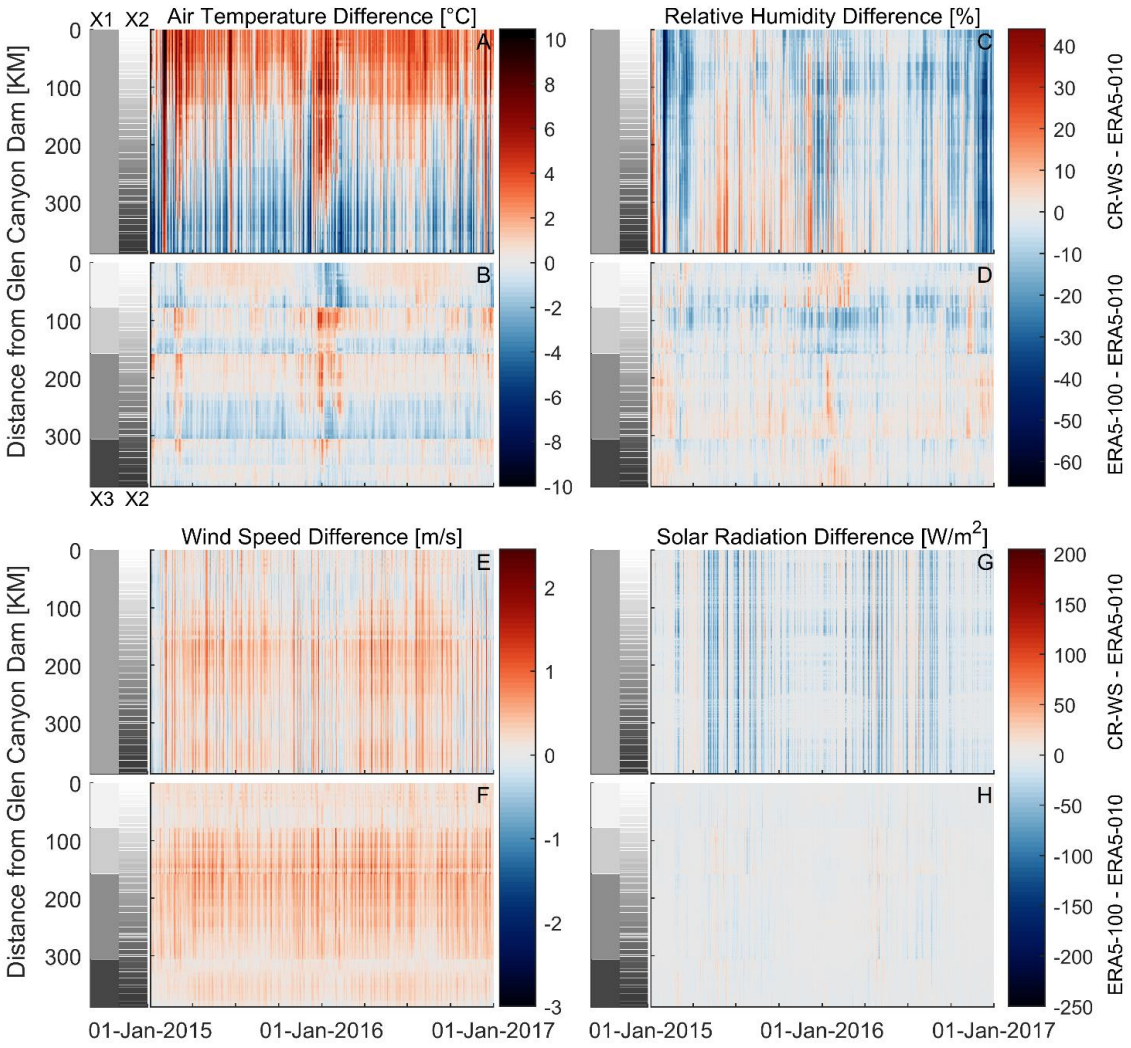

Figure 3-2. Spatial and temporal differences between weather input data for each variable. Values in plots A, C, E, and G are calculated as CR-WS minus ERA5-010. Values in plots B, D, F, and H are calculated as ERA5-100 minus ERA5-010. Black and white bars to the left of each plot show the spatial resolution of weather inputs from CR-WS (X1), ERA5-010 (X2) and ERA5-100 (X3), with each shade indicating a different weather station or ERA5-Land grid. Data were averaged from hourly to daily resolution for illustration.

3.1.3. Model accuracy using tested weather inputs

Temperature predictions in the Colorado River using CR-WS, ERA5-010, and ERA5-100 weather input datasets were evaluated against temperature observations at S4, S6, and S7. The significance of different model inputs on temperature predictions was

determined using a one-way ANOVA test followed by a Tukey's Honest Significant Difference test (Figure B-9). At S4, all three input weather datasets produce positive median residuals, but most of these overestimations occur between July and September (Figure 3-3). Here, ERA5-010 and ERA5-100 prediction errors are lower and statistically different from CR-WS predictions. At S6 median residuals are still positive for all three input weather datasets, but errors have reduced for each. At this location all three models have statistically similar temperature predictions. At the most downstream monitoring location, S7, differences among model predictions are greatest and each model under estimates observed river temperatures, which occurs most often between September and November. Here, ERA5-010 and ERA5-100 prediction errors are lower and statistically different from CR-WS predictions.

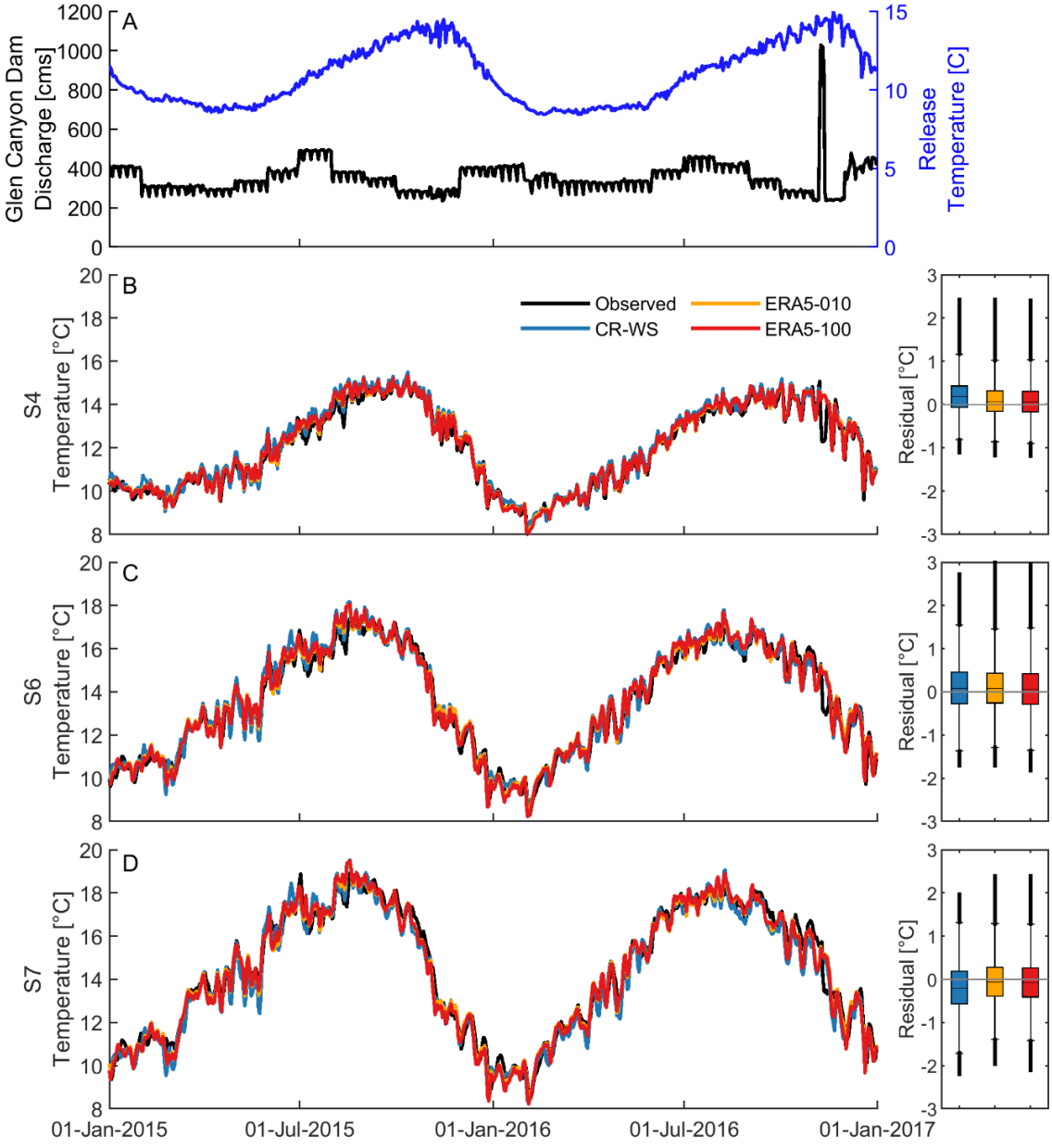

Figure 3-3. Figure showing boundary condition flow and temperature for the Colorado River (A) with river temperature predictions at downstream monitoring locations (B, C, and D) shown in Figure 3-1. Boxplots on the right-hand side show model residuals calculated as modeled minus observed. Time series data were aggregated into daily average values for illustration purposes.

3.1.4. Differences between model predictions

Similarities and differences in river temperature predictions were identified by subtracting ERA5-010 results from CR-WS and ERA5-100. In the 25 km immediately downstream from Glen Canyon Dam, river temperature predictions using CR-WS and ERA5-010 are essentially the same, illustrating the influence of boundary condition flow and temperatures (Figure 3-4A). The spatial patterns observed between river temperature predictions (Figure 3-4A) closely resemble observed differences in air temperatures (Figure 3-2A). The sensitivity analysis, where ERA5-Land time series were substituted one at a time into the CR-WS model, further showed that prediction differences are sensitive to spatially varying air temperature, shortwave radiation, and relative humidity (Figure B-10). The relative impact of these variables differs seasonally, particularly for shortwave radiation, which is significantly reduced during fall and winter due to topographic shading within the canyon.

Between ERA5-100 and ERA5-010, there is minimal spatial variation despite the variations noted for input air temperature and wind speed (Figure 3-4B). However, there are significant seasonal differences in river temperature predictions using ERA5-100 and ERA5-010, which is due to seasonal differences in air temperature and relative humidity inputs.

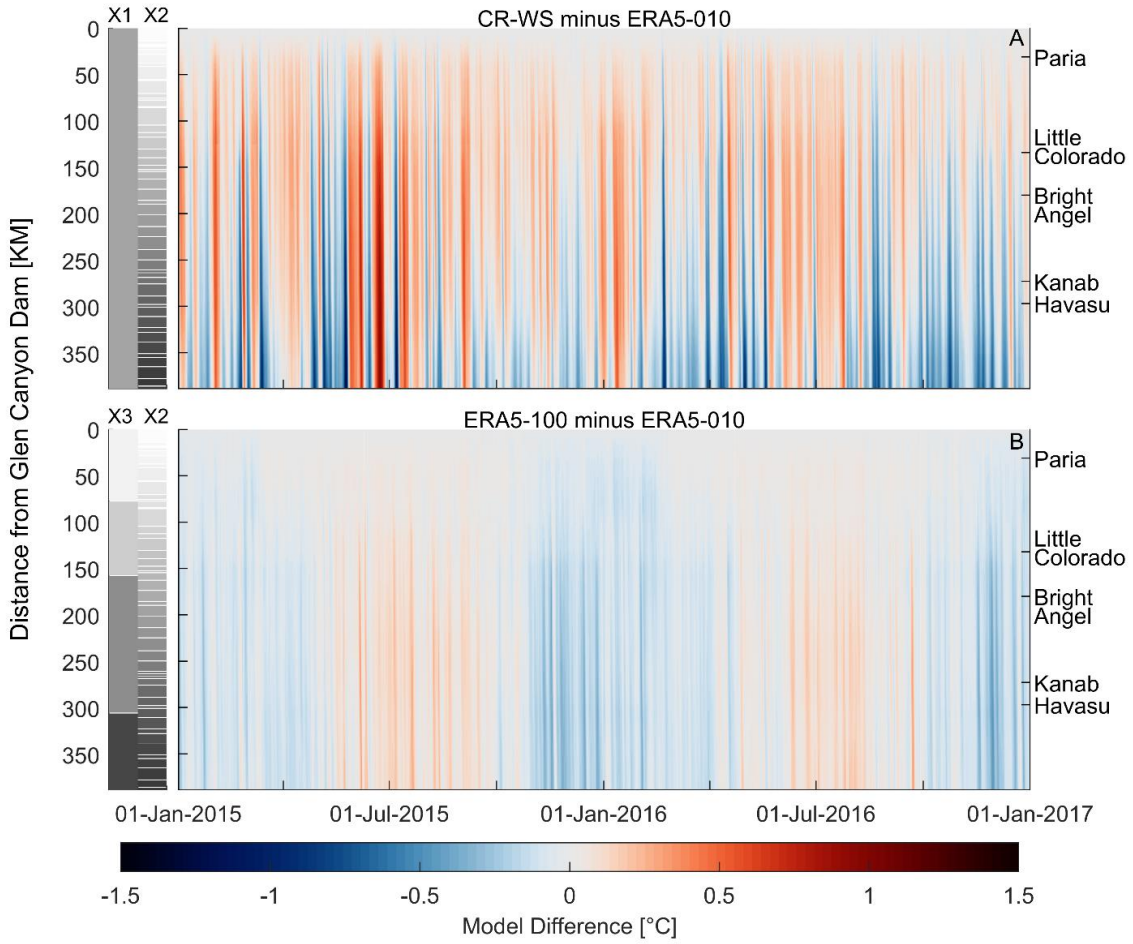

Figure 3-4. Spatial and temporal differences between river temperature model predictions in the Colorado River. Values in plot A are calculated as CR-WS minus ERA5-010, and values in plot B are calculated as ERA5-100 minus ERA5-010. Black and white bars to the left of each plot show the spatial variability of weather inputs from CR-WS (X1), ERA5-010 (X2) and ERA5-100 (X3), with each shade indicating a different weather station or ERA5-Land grid. Labels on the right denote tributary locations.

3.2. Green River

3.2.1. Differences in input weather data

In the Green River, GR-WS and ERA5-010 weather inputs differ on many fronts. For air temperature, spatial variation is most prominent in the first 150 km below Flaming Gorge Dam and between river kilometers 260-466 (Figure 3-5A). There are also temporal variations over these two reaches, with GR-WS providing warmer temperatures

in the winter months. More spatial variability in air temperature exists between ERA5-100 and ERA5-010, with ERA5-010 providing cooler upstream and warmer downstream values within the respective coverage area of ERA5-100 grids (Figure 3-5B). Similar to the Grand Canyon application, there are four different ERA5-100 grids that cover the Green River model domain (Figure B-11).

The residual surface for relative humidity indicates that GR-WS has lower upstream and higher downstream values compared to ERA5-010, and that GR-WS typically has greater values in summer in much of the study area (Figure 3-5C). Like GR-WS, differences between ERA5-100 and ERA5-010 also show spatial variation with ERA5-100 having lower upstream and higher downstream relative humidity values within respective spatial coverage areas (Figure 3-5D). There is also spatial variability of ERA5-010 within the respective coverage area of ERA5-100 grids. However, there are no apparent temporal patterns between ERA5-100 and ERA5-010 relative humidity.

Spatial differences between GR-WS and ERA5-010 wind speed exist throughout the model domain, with significance shifts occurring at the transition of weather station coverage areas (Figure 3-5E). This indicates that wind speed differences are largely determined by site specific characteristics or wind speed elevation corrections among the GR-WS locations. A similar pattern is present between ERA5-100 and ERA5-010 wind speeds, where positive or negative differences mostly fall within the coverage area of ERA5-100 grids, indicating the spatial variability of ERA5-010 grids (Figure 3-5F).

A seasonal pattern is present in solar radiation differences between GR-WS and ERA5-010, with GR-WS supplying more solar radiation during the fall and winter and less during spring and summer months (Figure 3-5G). There is also spatial variability in

ERA5-010 solar radiation, most notably around river km 100-150 and river km 350-400 (Figure 3-5G). There are negligible differences in solar radiation between ERA5-100 and ERA5-010 (Figure 3-5H).

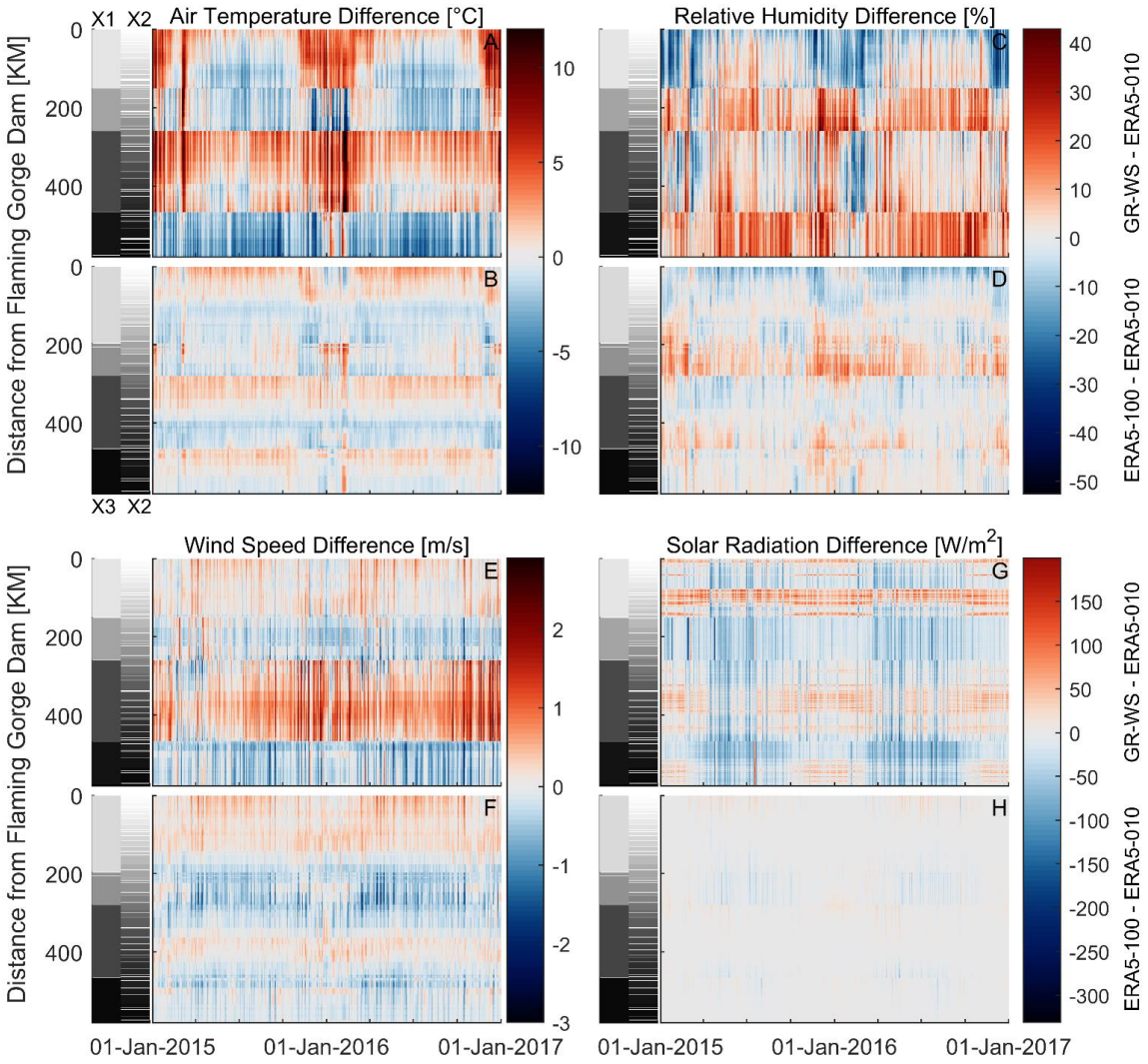

Figure 3-5. Spatial and temporal differences between weather input data for each variable. Values in plots A, C, E, and G are calculated as GR-WS minus ERA5-010. Values in plots B, D, F, and H are calculated as ERA5-100 minus ERA5-010. Black and white bars to the left of each plot show the spatial variability of weather inputs from GR-WS (X1), ERA5-010 (X2) and ERA5-100 (X3), with each shade indicating a different weather station or ERA5-Land grid.

3.2.2. Model accuracy using tested weather inputs

Temperature predictions in the Green River using GR-WS, ERA5-010, and ERA5-100 weather input datasets were evaluated against observations at S9, S10, and S14. The significance of different input weather datasets on model predictions was determined using a one-way ANOVA test followed by a Tukey's Honest Significant Difference test. At S9, the first monitoring location closest to Flaming Gorge Dam, all three input weather datasets generally underestimate river temperatures, with most of the error variability coinciding with reduced flows during late summer and fall periods. Here, ERA5-010 is statistically similar to GR-WS and ERA5-100 datasets while, GR-WS and ERA5-100 are statistically different from each other (Figure B-12). At this location ERA5-010 and GR-WS produce the lowest errors (Figure 3-6). At S10, 98 km downstream of S9, under estimates of temperatures are greater for all three input weather datasets, with ERA5-010 and ERA5-100 predictions producing lower errors and statistically different predictions from GR-WS. At S14, the furthest downstream monitoring location, ERA5-100 predictions produce the lowest error and is statistically different from GR-WS and ERA5-010 predictions.

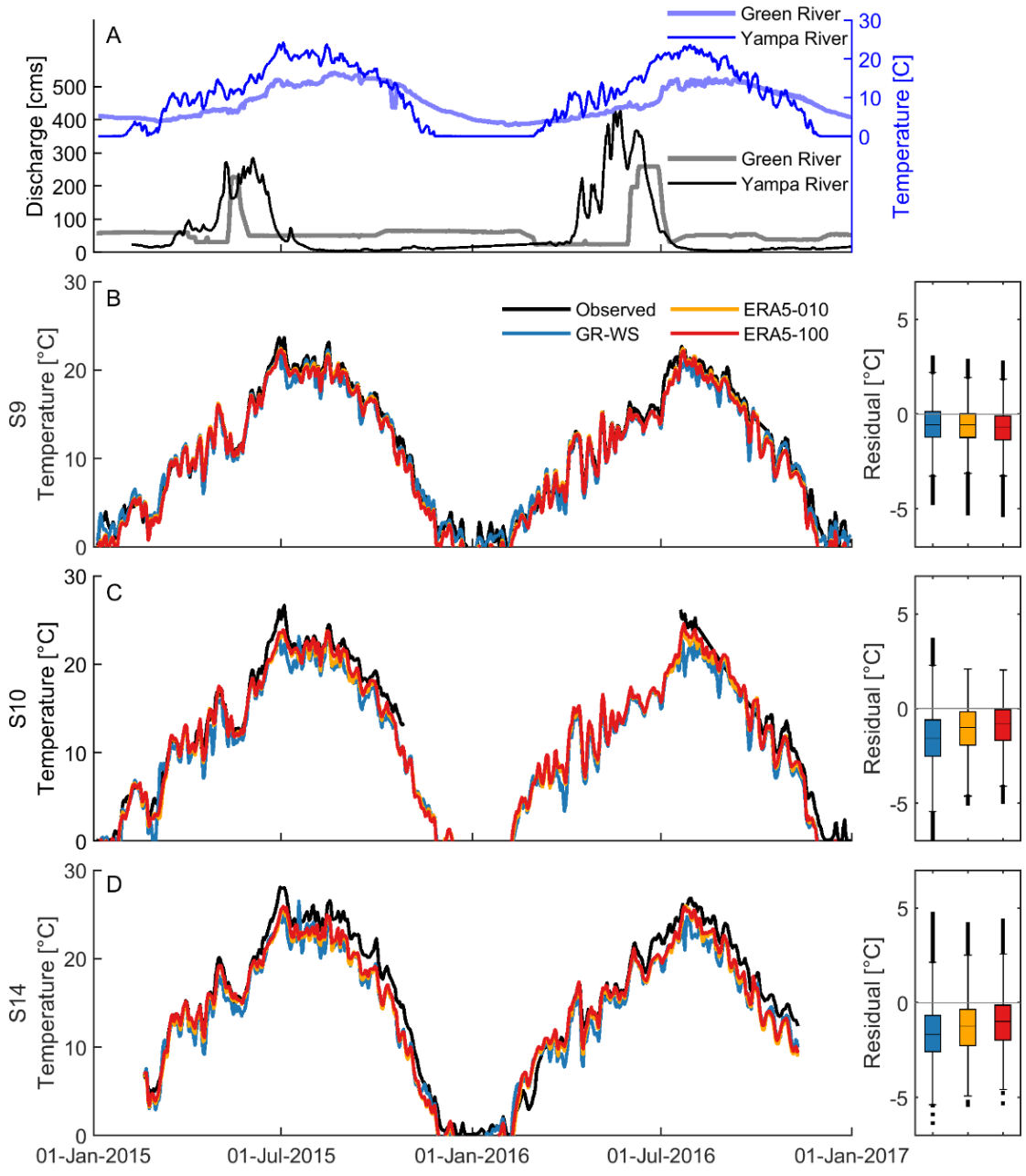

Figure 3-6. Figure showing boundary condition flow and temperature for the Yampa and Green Rivers (A) with river temperature predictions at downstream monitoring locations (B, C, and D) shown in Figure 3-1. Boxplots on the right-hand side show model residuals calculated as modeled minus observed. Time series data were aggregated into daily averaged values for illustration purposes.

3.2.3. Differences between model predictions

Similarities and differences in river temperature predictions were identified by subtracting GR-WS and ERA5-100 by ERA5-010. Differences between GR-WS and ERA5-010 model predictions have significant seasonal variability, with GR-WS predicting warmer river temperatures over fall and winter periods and cooler temperatures during spring and summer months (Figure 3-7A). Tributaries in the Green River contribute proportionally more stream flow than the tributaries in the Grand Canyon, resulting in a greater influence on river temperatures and bringing predictions from GR-WS and ERA5-010 closer together for short distances downstream. In comparing Figure 3-7A to Figure 3-5A and 3-5G, it appears that river temperature predictions resemble observed differences in air temperature and solar radiation inputs. Further inspection into the influence of specific weather inputs on model predictions, determined by performing a sensitivity analysis, showed that all four weather inputs are important at certain times and locations (Figure B-13). Notably, substituting in spatially varying air temperature has the greatest impact on predictions over winter while substituting in spatially varying solar radiation mostly influenced spring and summer predictions. Spatially varying relative humidity has a large effect on summer and fall predictions, and is most influential at the downstream river location (i.e., S14). The influence of spatially varying wind speed does not change much between seasons, but is important at the downstream river location.

River temperature prediction differences between ERA5-100 and ERA5-010 are mostly in the spatial dimension, with ERA5-100 producing cooler predictions in the upstream 200 km, but warmer predictions further downstream (Figure 3-7B). This pattern

is similar to the observed differences in wind speed and air temperature (Figure 3-5B and 3-5F). Temporal variations between ERA5-100 and ERA5-010 predictions appear to be mostly influenced by changes in flow, with smallest differences coinciding with months that have higher flows.

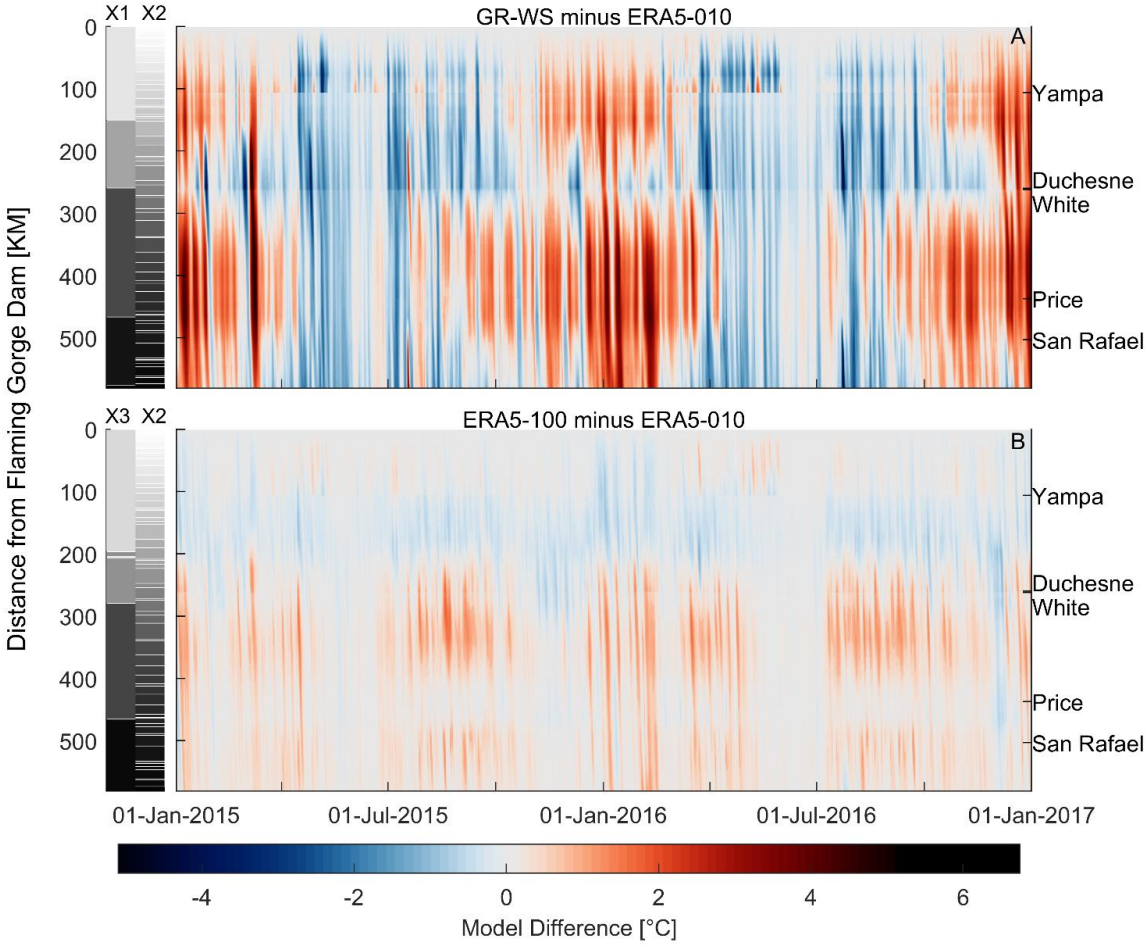

Figure 3-7. Spatial and temporal differences between river temperature model predictions where (A) represents GR-WS minus ERA5-010, and (B) represents ERA5-100 minus ERA5-010. Black and white bars to the left of each plot show the spatial variability of weather inputs from GR-WS (X1), ERA5-010 (X2) and ERA5-100 (X3), with each shade indicating a different weather station or ERA5-Land grid. Labels on the right denote tributary locations.

4. Discussion

4.1. Comparison of ERA5-010 dataset to ground-based weather data

Elevation corrections applied to CR-WS and ERA5-010 improved the within-canyon estimates of air temperature and relative humidity, but negatively influenced wind speed estimates when compared to GCMRC-WS observations (Table 3-3). While we used the mean error for this analysis to indicate over and under estimations, the Nash-Sutcliffe Efficiency (NSE) and Root Mean Square Error (RMSE) goodness-of-fit metrics show similar trends (Table B-3, Table B-4). The shift from both input meteorological datasets overestimating to underestimating wind speeds before and after elevation corrections suggest that the equation applied here (i.e., Eqn. 3-6) over-reduces wind velocities. Furthermore, the NSE for pre- and post-elevation corrected wind speed is negative at most locations (Table B-3), indicating that error variance of estimated wind speeds is greater than the error variance of observed GCMRC-WS data. In contrast, NSE values for both air temperature and relative humidity estimates are positive at almost all GCMRC-WS locations.

Poor representation of wind speed reanalysis data after elevation correction has also been noted in comparisons between downscaled daily mean MERRA (NASA's Modern-Era Retrospective Analysis for Research and Applications) data and Natural Resource Conservation Service SNOTEL observations in the mountainous Logan River watershed, despite arguably more complex wind speed reduction methods (Sen Gupta & Tarboton, 2016). Several semi-empirical approaches that account for slope and curvature of the land surface with calibrated coefficients have also been applied with varying levels of success (Liston & Sturm, 1998; Winstral et al., 2009). More commonly, wind speed reanalysis data are corrected using statistical approaches (e.g., Iizumi et al., 2017; Li et al., 2019), however, these methods required ground-based observations which limits their

broad application. This highlights the continued need of improving wind speed corrections methods that are based solely on physical properties, particularly over topographically complex regions where differences in elevation between reanalysis grids and river locations may be large.

4.2. Differences in input weather data

The heatmaps produced allowed us to visualize and quantify spatiotemporal differences and infer how these differences may impact river temperature predictions. One of the most dramatic differences was between CR-WS and ERA5-010 air temperatures in the Grand Canyon (Figure 3-2A), which suggested that the model using CR-WS inputs may overestimate river temperatures over the upstream 100 km and underestimate in the last 100 km of the Colorado River in Grand Canyon. This indeed was the case as shown in Figure 3-3 at sites S4 and S7. A similar spatial pattern in air temperatures between ERA5-100 and ERA5-010 was also observed, but was contained within the respective coverage area of ERA5-100 grids. While differences also exist between wind speed and relative humidity inputs, they are of lesser concern because Grand Canyon temperatures are not very sensitive to these variables (Mihalevich et al., 2020).

In the Green River, the heatmaps comparing differences among input weather datasets (Figure 3-5) highlight the issues associated with using somewhat arbitrarily selected weather stations based purely on the proximity to the river and availability of data. This resulted in large differences between GR-WS and ERA5-010 for all parameters and river segments. While we tested the model with all available weather stations in each river segment and selected the one that produced lowest RMSE, the lack of data within

some reaches forced us to use weather stations that required large elevation corrections (i.e., weather station W4) or were not centrally located within the assigned reach (i.e., weather station W5). Unlike in Grand Canyon, no microclimate data exists along the Green River to validate these input datasets. The large spatial domains of ERA5-100 grids also miss some of the variability exhibited by ERA5-010. An inherent effect of coarsening ERA5-Land is larger elevation differences due to averaging grids that include locations further away from the river (e.g., higher elevations). This results in higher air temperature inputs after elevation corrections, which can be seen in Figure 3-5B.

4.3. Model accuracy using tested weather inputs

Overall, the influence of spatially varying meteorological input data is most noticeable when looking at model residuals at the farthest downstream monitoring location (i.e., S7 and S14) over the entire simulation period (Figure 3-3, Figure 3-6). In Grand Canyon, ERA5-010 and ERA5-100 input data resulted in the lowest errors at the upstream (S4) and downstream (S7) monitoring locations. Despite the averaging and related impacts of elevation corrections, coarsening ERA5-Land data to 1°x1° longitude and latitude grids (ERA5-100) resulted in similar river temperature prediction accuracy when compared to predictions using ERA-010. River temperature predictions using CR-WS was sometimes better than ERA5-010 and ERA5-100 over shorter time (e.g., weekly or monthly) periods. This indicates that ERA5-Land may not always be a better substitute for ground-based observations, but could still be used to fill in data gaps within existing sensor networks to create long term data series (Lompar et al., 2019).

The results from the Green River are similar to the findings made for the Grand Canyon, in that all three input weather datasets produce similar river temperature

predictions. Here, GR-WS and ERA5-010 produce the smallest errors at S9, and ERA5-100 produces the smallest error at S14, with all weather datasets resulting in underestimates at all three locations. We attribute underpredictions of temperature to over estimates in discharge, which subsequently increases the rivers thermal inertia making it less resistant to meteorological forcing influences during summer periods. While we closed our flow balance using lateral inflows calculated using a 10-day moving average of daily flow difference between upstream and downstream gages (see Text B-2), our flow routing in the Green River (Figure B-14) still produces over estimates of discharge. Flow errors are largely attributed to the difficulty in capturing the effects of irrigation diversions and return flows throughout the Green River. Flow routing errors are much smaller in Grand Canyon (Figure B-15), where diversions and return flows are negligible.

4.4. Differences between model predictions

Comparing predictions directly (Figure 3-4, Figure 3-7) highlighted how sensitive river temperatures are to changes in input weather information and how far downstream reservoir release discharges and temperatures drive instream temperatures. In both the Grand Canyon and Green River, predictions were approximately the same over the first 25 km even though reservoir discharges from Flaming Gorge Dam and Glen Canyon Dam are significantly different. Comparing predictions also revealed the influence of tributary inflows in the Green River. At times where tributary inflows were high and meteorological inputs noticeably different, tributary flows acted as thermal resets in that river temperatures from the two models were shifted to nearly the same values (Figure 3-7A). Differences between models were greatest in downstream river segments due to the cumulative differences from all four weather variables. This was highlighted by the

sensitivity analysis performed in the Grand Canyon and Green River models (Figure B-10; Figure B-13).

4.5. Future considerations

While we show that a coarsened resolution of ERA5-Land datasets works well for predicting temperatures in the relatively large Colorado and Green Rivers, the native ERA5-Land resolution or even higher spatial resolutions may be needed to predict river temperature in smaller rivers. For example, Benyahya et al. (2010) showed that having microclimate data is essential for making accurate temperature predictions in a small sheltered stream, but also found that in a larger river, temperature predictions were nearly the same when using microclimate and remote weather station data. This alludes to the influence of thermal inertia, in that larger streams are less sensitive to meteorological data because more energy is required to alter water temperatures as volumes increase (Gu et al., 1998). Therefore, river specific characteristics may constrain the use of climate reanalysis datasets, but more testing of CRDs in different systems is needed to determine such limitations. Furthermore, the formulations underlying each reanalysis dataset are different, with some producing better estimates in certain regions (Angélil et al., 2016; Keller & Wahl, 2021), which highlights the need to evaluate multiple CRDs (e.g., Table 3-1) in future applications.

4.6. Broader Impacts

A number of process-based river temperature modeling studies have noted limitations in modeling certain regions or specific heat fluxes due to the lack of weather data or inadequate spatial resolution of existing observations for their study area (e.g.,

Benyahya et al., 2012; Dugdale et al., 2017; Leach & Moore, 2019; MacDonald et al., 2014; Mihalevich et al., 2020). Recently, Leach & Moore (2019) stressed the need for developing process-based models that capture the underlying mechanisms controlling thermal regimes when anticipating climate change impacts as empirical relationships may underestimate stream temperature responses. However, the lack of long-term wind speed and vapor pressure in their study reach resulted in the omission of sensible and latent heat fluxes, which were assumed to be negligible based on previous modeling studies in similar forested catchments. In another example, MacDonald et al. (2014) described a modeling framework for estimating stream energy processes in mountainous regions that have limited hydrometeorological data by implementing the Generate Earth Systems Science inputs (GENESYS) model (MacDonald et al., 2009). Yet, the GENESYS model relies on observed data to extrapolate conditions over adjacent terrain which may not be suitable in landscapes where local weather is highly variability (MacDonald et al., 2009) or where measurements are significantly far from the study area. In the review by Dugdale et al. (2017), they expressed that a significant advancement for process-based modeling studies will be overcoming the challenges of limited meteorological data in remote locations. They went on to point out that modeling studies often rely on a single ground-based weather station that may not capture the spatial variability of meteorology in the respective study area. As a result, they emphasized the need to develop approaches that acquire weather information and apply appropriate upscaling/downscaling routines that enable process-based river temperature modeling in inaccessible regions. The work presented here is a step towards fulfilling this knowledge gap.

In the context of the Colorado River basin, overcoming data limitations allows for the evaluation of future temperature impacts on ecosystems brought on by changes in climate and hydrology. In the recent report by Wheeler et al. (2021) that focused on understanding different management alternatives on water supply throughout the basin, they determined that a water scarcity crisis cannot be avoided under current or modified reservoir storage strategies, stressing that current uses of the Colorado River are not sustainable. They did, however, conclude that operational changes in reservoir storage could provide ecosystem benefits in key river sections, as storage levels largely determine downstream river temperatures for portions of the Colorado and Green Rivers (Anderson & Wright, 2007; Carron & Rajaram, 2001; Dibble et al., 2021; Mihalevich et al., 2020). Bruckerhoff et al. (in review) used the results from Wheeler et al. (2021) to evaluate ecosystem outcomes within Grand Canyon, finding that future river temperatures will likely be warmer and more suitable for several native and non-native fish species, but the interactions between species with overlapping habitat remains uncertain. Similar analysis of ecosystem outcomes in the Upper Colorado River basin resulting from current or modified management operations has yet to be conducted in part because sparse weather data previously limited the development of process-based river temperature models over this large region. The predictions shown here for the Green River illustrate the utility of elevation corrected CRDs to represent conditions in weather data sparse portions of the Colorado River basin. These data and modeling tools can help facilitate future investigations of ecosystem outcomes throughout the basin. However, strategies to predict future release temperatures and volumes from Colorado River basin reservoirs are still needed. Beyond the scope of the Colorado River basin, the data

analysis and modeling methods presented here bridge some of the existing data and knowledge gaps and stand to advance our understanding of the drivers of temperatures in rivers and streams around the world.

5. Conclusion

This study presented techniques for elevation correcting climate reanalysis data and validated these methods and data in two relatively large process-based river temperature models in the Colorado River basin. The results showed that ERA5-Land can be used as an input meteorological dataset in the absence of historical weather information. In the Colorado River in Grand Canyon, the use of native resolution ERA5-Land (ERA5-010) improved river temperature predictions when compared to the same model using ground-based weather information from Page, AZ (CR-WS). ERA5-010 reasonably captures the magnitudes and spatial and temporal variability of most weather variables within Grand Canyon. However, the model improvements are largely attributed to the ERA5-010's ability to capture the highly spatially variable air temperature in the Grand Canyon model domain. In the Green River, temperature prediction errors were lowest when using a coarsened spatial resolution of ERA5-Land (ERA5-100). Elevation corrections to ERA5-100 inflated air temperatures relative to other input datasets (i.e., ERA5-010 and GR-WS ground observations). However, differences in temperature predictions between ERA5-010 and ERA5-100 were minimal. This indicates that using coarser climate reanalysis datasets is likely acceptable for large river basin temperature predictions.

With the advancement of remotely sensed metrological data products, the limitations of data availability in remote areas are becoming easier to overcome. As such,

river temperature models may be able to be developed in regions that have no, or very limited, historical weather information. This in turn allows for greater assessment of climate related impacts on aquatic thermal regimes and the ability to design effective management strategies to mitigate negative ecosystem responses.

Acknowledgements

This work is part of the Future of the Colorado River Project, an interdisciplinary project from Utah State University's Center for Colorado River Studies. Funding was provided by Walton Family Foundation, the Utah Water Research Laboratory at Utah State University, David Bonderman, My Good Fund, and the National Science Foundation (EAR- 1343861). Any use of trade, product, or firm names is for descriptive purposes only and does not imply endorsement by the U.S. Government. Thanks to Joshua Caster and Joel Sankey of the U.S.G.S. Grand Canyon Monitoring and Research Center for providing weather data. I am grateful for the comments from Charles Yackulic, David Tarboton, and Jack Schmidt on earlier drafts that greatly improved this manuscript. Data and models are provided online at http://www.hydroshare.org/resource/71cb6a96a74f4207b2a879fb1f34f27a/.

References

Anderson, C. R., & Wright, S. A. (2007). Development and application of a water temperature model for the Colorado River below Glen Canyon Dam, Arizona. Proceedings of the American Institute of Hydrology, 23, 1–11.

Angélil, O., Perkins-Kirkpatrick, S., Alexander, L. V., Stone, D., Donat, M. G., Wehner, M., Shiogama, H., Ciavarella, A., & Christidis, N. (2016). Comparing regional precipitation and temperature extremes in climate model and reanalysis products. Weather and Climate Extremes, 13, 35–43. https://doi.org/10.1016/j.wace.2016.07.001

Arismendi, I., Safeeq, M., Dunham, J. B., & Johnson, S. L. (2014). Can air temperature be used to project influences of climate change on stream temperature? Environmental Research Letters, 9(8), 084015. https://doi.org/10.1088/1748-9326/9/8/084015

Benyahya, L., Caissie, D., El-Jabi, N., & Satish, M. G. (2010). Comparison of microclimate vs. remote meteorological data and results applied to a water temperature model (Miramichi River, Canada). Journal of Hydrology, 380(3–4), 247–259. https://doi.org/10.1016/j.jhydrol.2009.10.039

Benyahya, L., Caissie, D., Satish, M. G., & El-Jabi, N. (2012). Long-wave radiation and heat flux estimates within a small tributary in Catamaran Brook (New Brunswick, Canada). Hydrological Processes, 26(4), 475–484. https://doi.org/10.1002/hyp.8141

Berg, A. A., Famiglietti, J. S., Walker, J. P., & Houser, P. R. (2003). Impact of bias correction to reanalysis products on simulations of North American soil moisture and hydrological fluxes. Journal of Geophysical Research D: Atmospheres, 108(16), 1–15. https://doi.org/10.1029/2002jd003334

Bestgen, K. R., & Hill, A. A. (2016). River regulation affects reproduction, early growth, and suppression strategies for invasive smallmouth bass in the upper Colorado River basin. April, 84. http://www.coloradoriverrecovery.org/documents-publications/technical-reports/nna/Projects_FR115-140_2016.pdf

Bestgen, K. R., Walford, C. D., White, G. C., Hawkins, J. A., Jones, M. T., Webber, P. A., Breen, M., Skorupski Jr., J. A., Howard, J., Creighton, K., Logan, J., Battige, K., & Wright, F. B. (2018). Population Status and Trends of Colorado pikeminnow in the Green River Sub-Basin, Utah and Colorado, 2000-2013. April, 152. https://doi.org/10.13140/RG.2.2.34757.35048

Bogaart, P. W., Van Balen, R. T., Kasse, C., & Vandenberghe, J. (2003). Process-based modelling of fluvial system response to rapid climate change - I: Model formulation and generic applications. Quaternary Science Reviews, 22(20), 2077–2095. https://doi.org/10.1016/S0277-3791(03)00143-4

Bruckerhoff, L., Wheeler, K. G., Dibble, K. L., Mihalevich, B. A., Neilson, B. T., Wang, J., Yackulic, C. B., & Schmidt, J. C. (in review). Water Storage Decisions and Consumptive Use May Constrain Ecosystem Management under Severe Sustained Drought. Journal of the American Water Resources Association.

Buahin, C. A., & Horsburgh, J. S. (2018). Advancing the Open Modeling Interface (OpenMI) for integrated water resources modeling. Environmental Modelling & Software, 108(April), 133–153. https://doi.org/10.1016/j.envsoft.2018.07.015

Buahin, C. A., Horsburgh, J. S., & Neilson, B. T. (2019). Parallel multi-objective calibration of a component-based river temperature model. Environmental Modelling & Software, 116(February), 57–71. https://doi.org/10.1016/j.envsoft.2019.02.012

Caissie, D. (2016). River evaporation, condensation and heat fluxes within a first-order tributary of Catamaran Brook (New Brunswick, Canada). Hydrological Processes, 30(12), 1872–1883. https://doi.org/10.1002/hyp.10744

Carron, J. C., & Rajaram, H. (2001). Impact of variable reservoir releases on management of downstream water temperatures. Water Resources Research, 37(6), 1733–1743. https://doi.org/10.1029/2000WR900390

Caster, J. J., Dealy, T. P., Andrews, T., Fairley, H., Draut, A. E., Sankey, J. B., & Bedford, D. R. (2014). Meteorological data for selected sites along the Colorado River Corridor, Arizona, 2011-2013. U.S. Geological Survey Open-File Report 2014-1247, 56. https://doi.org/http://dx.doi.org/10.3133/ofr20141247

Caster, J. J., & Sankey, J. B. (2016). Variability in rainfall at monitoring stations and derivation of a long-term rainfall intensity record in the Grand Canyon Region, Arizona, USA. In Scientific Investigations Report. https://doi.org/10.3133/sir20165012

Chen, J., Brissette, F. P., Chaumont, D., & Braun, M. (2013). Finding appropriate bias correction methods in downscaling precipitation for hydrologic impact studies over North America. Water Resources Research, 49(7), 4187–4205. https://doi.org/10.1002/wrcr.20331

Copernicus Climate Change Service. (2019). ERA5-Land reanalysis. https://cds.climate.copernicus.eu/cdsapp#!/home

Daniels, M. E., & Danner, E. M. (2020). The Drivers of River Temperatures Below a Large Dam. Water Resources Research, 56(5), 1–15. https://doi.org/10.1029/2019wr026751

Dettinger, M., Udall, B., & Georgakakos, A. (2015). Western water and climate change. Ecological Applications, 25(8), 2069–2093. https://doi.org/10.1890/15-0938.1

Diabat, M., Haggerty, R., & Wondzell, S. M. (2013). Diurnal timing of warmer air under climate change affects magnitude, timing and duration of stream temperature change. Hydrological Processes, 27(16), 2367–2378. https://doi.org/10.1002/hyp.9533

Dibble, K. L., Yackulic, C. B., Kennedy, T. A., Bestgen, K. R., & Schmidt, J. C. (2021). Water storage decisions will determine the distribution and persistence of imperiled river fishes. Ecological Applications, 31(2), 1–9. https://doi.org/10.1002/eap.2279

Draut, A. E., & Rubin, D. M. (2006). Measurements of wind, aeolian sand transport, and precipitation in the Colorado River corridor, Grand Canyon, Arizona; January 2005 to January 2006. In Open-File Report (Revised an). https://doi.org/10.3133/ofr20061188

Dugdale, S. J., Hannah, D. M., & Malcolm, I. A. (2017). River temperature modelling: A review of process-based approaches and future directions. Earth-Science Reviews, 175(October), 97–113. https://doi.org/10.1016/j.earscirev.2017.10.009

Essou, G. R. C., Brissette, F., & Lucas-Picher, P. (2017). The use of reanalyses and gridded observations as weather input data for a hydrological model: Comparison of performances of simulated river flows based on the density of weather stations. Journal of Hydrometeorology, 18(2), 497–513. https://doi.org/10.1175/JHM-D-16-0088.1

Frassl, M. A., Boehrer, B., Holtermann, P. L., Hu, W., Klingbeil, K., Peng, Z., Zhu, J., & Rinke, K. (2018). Opportunities and limits of using meteorological reanalysis data for simulating seasonal to sub-daily water temperature dynamics in a large shallow lake. Water (Switzerland), 10(5), 1–17. https://doi.org/10.3390/w10050594

Gao, L., Bernhardt, M., & Schulz, K. (2012). Elevation correction of ERA-Interim temperature data in complex terrain. Hydrology and Earth System Sciences, 16(12), 4661–4673. https://doi.org/10.5194/hess-16-4661-2012

Gu, R., Montgomery, S., & Austin, T. AL. (1998). Quantifying the effects of stream discharge on summer river temperature. Hydrological Sciences Journal, 43(6), 885–904. https://doi.org/10.1080/02626669809492185

Hersbach, H., Bell, B., Berrisford, P., Biavati, G., Horányi, A., Sabater, M. J., Nicolas, J., Peubey, C., Radu, R., Rozum, I., Schepers, D., Simmons, A., Soci, C., Dee, D., & Thépaut, J.-N. (2018). ERA5 hourly data on pressure levels from 1979 to present. Copernicus Climate Change Service (C3S) Climate Data Store (CDS). https://doi.org/10.24381/cds.bd0915c6

Iizumi, T., Takikawa, H., Hirabayashi, Y., Hanasaki, N., & Nishimori, M. (2017). Contributions of different bias-correction methods and reference meteorological forcing data sets to uncertainty in projected temperature and precipitation extremes. Journal of Geophysical Research, 122(15), 7800–7819. https://doi.org/10.1002/2017JD026613

Kalnay, E., Kanamitsu, M., Kistler, R., Collins, W., Deaven, D., Gandin, L., Iredell, M., Saha, S., White, G., Woollen, J., Zhu, Y., Leetmaa, A., Reynolds, R., Chelliah, M., Ebisuzaki, W., Higgins, W., Janowiak, J., Mo, K. C., Ropelewski, C., … Joseph, D. (1996). The NCEP/NCAR 40-Year Reanalysis Project. Bulletin of the American Meteorological Society, 77(3), 437–471. https://doi.org/10.1175/1520-0477(1996)077<0437:TNYRP>2.0.CO;2

Keller, J. D., & Wahl, S. (2021). Representation of climate in reanalyses: An intercomparison for Europe and North America. Journal of Climate, 34(5), 1667–1684. https://doi.org/10.1175/JCLI-D-20-0609.1

King, T. V., & Neilson, B. T. (2019). Quantifying reach-average effects of hyporheic exchange on arctic river temperatures in an area of continuous permafrost. Water Resources Research, 1–21. https://doi.org/10.1029/2018WR023463

King, T. V., Neilson, B. T., Overbeck, L. D., & Kane, D. L. (2016). Water temperature controls in low arctic rivers. Water Resources Research, 52(6), 4358–4376. https://doi.org/10.1002/2015WR017965

Krogh, S. A., Pomeroy, J. W., & McPhee, J. (2015). Physically based mountain hydrological modeling using reanalysis data in Patagonia. Journal of Hydrometeorology, 16(1), 172–193. https://doi.org/10.1175/JHM-D-13-0178.1

Kunkel, K. E. (1989). Simple Procedures for Extrapolation of Humidity Variables in the Mountainous Western United States. Journal of Climate, 2(7), 656–670. https://doi.org/10.1175/1520-0442(1989)002<0656:SPFEOH>2.0.CO;2

Leach, J. A., & Moore, R. D. (2010). Above-stream microclimate and stream surface energy exchanges in a wildfire-disturbed riparian zone. Hydrological Processes, 24(17), 2369–2381. https://doi.org/10.1002/hyp.7639

Leach, J. A., & Moore, R. D. (2019). Empirical stream thermal sensitivities may underestimate stream temperature response to climate warming. Water Resources Research, 2018WR024236. https://doi.org/10.1029/2018WR024236

Li, D., Feng, J., Xu, Z., Yin, B., Shi, H., & Qi, J. (2019). Statistical Bias Correction for Simulated Wind Speeds Over CORDEX-East Asia. Earth and Space Science, 6(2), 200–211. https://doi.org/10.1029/2018EA000493

Li, H.-Y., Ruby Leung, L., Tesfa, T., Voisin, N., Hejazi, M., Liu, L., Liu, Y., Rice, J., Wu, H., & Yang, X. (2015). Modeling stream temperature in the Anthropocene: An earth system modeling approach. Journal of Advances in Modeling Earth Systems, 7(4), 1661–1679. https://doi.org/10.1002/2015MS000471

Lins, H. F. (2008). Challenges to hydrological observations. WMO Bulletin, 57(January), 55–58.

Liston, G. E., & Elder, K. (2006). A meteorological distribution system for high-resolution terrestrial modeling (MicroMet). Journal of Hydrometeorology, 7(2), 217–234. https://doi.org/10.1175/JHM486.1

Liston, G. E., & Sturm, M. (1998). A snow-transport model for complex terrain. Journal of Glaciology, 44(148), 498–516. https://doi.org/10.3189/S0022143000002021

Loinaz, M. C., Davidsen, H. K., Butts, M., & Bauer-Gottwein, P. (2013). Integrated flow and temperature modeling at the catchment scale. Journal of Hydrology, 495, 238–251. https://doi.org/10.1016/j.jhydrol.2013.04.039

Lompar, M., Lalić, B., Dekić, L., & Petrić, M. (2019). Filling gaps in hourly air temperature data using debiased ERA5 data. Atmosphere, 10(1), 11–13. https://doi.org/10.3390/atmos10010013

MacDonald, R. J., Boon, S., & Byrne, J. M. (2014). A process-based stream temperature modelling approach for mountain regions. Journal of Hydrology, 511, 920–931. https://doi.org/10.1016/j.jhydrol.2014.02.009

MacDonald, R. J., Byrne, J. M., & Kienzle, S. W. (2009). A physically based daily hydrometeorological model for complex mountain terrain. Journal of Hydrometeorology, 10(6), 1430–1446. https://doi.org/10.1175/2009JHM1093.1

Martinez, P., Wilson, K., Cavalli, P., Crockett, H., Speas, D., Trammell, M., Albrecht, B., & Ryden, D. (2014). Upper Colorado River Basin Nonnative and Invasive Aquatic Species Prevention and Control Strategy. February. http://www.coloradoriverrecovery.org/general-information/program-elements/nonnative-fish-management.html

Meier, W., Bonjour, C., Wüest, A., & Reichert, P. (2003). Modeling the effect of water diversion on the temperature of mountain streams. Journal of Environmental Engineering, 129(8), 755–764. https://doi.org/10.1061/(ASCE)0733-9372(2003)129:8(755)

Menne, M. J., Williams, C. N., Gleason, B. E., Jared Rennie, J., & Lawrimore, J. H. (2018). The Global Historical Climatology Network Monthly Temperature Dataset, Version 4. Journal of Climate, 31(24), 9835–9854. https://doi.org/10.1175/JCLI-D-18-0094.1

Mihalevich, B. A., Neilson, B. T., Buahin, C. A., Yackulic, C. B., & Schmidt, J. C. (2020). Water temperature controls for regulated canyon-bound rivers. Water Resources Research, 1–24. https://doi.org/10.1029/2020wr027566

Mizukami, N., Clark, M. P., Slater, A. G., Brekke, L. D., Elsner, M. M., Arnold, J. R., & Gangopadhyay, S. (2014). Hydrologic implications of different large-scale meteorological model forcing datasets in mountainous regions. Journal of Hydrometeorology, 15(1), 474–488. https://doi.org/10.1175/JHM-D-13-036.1

NASA-GISS. (2019). GISS Surface Temperature Analysis Station Data: GHCN v3 and SCAR. https://data.giss.nasa.gov/gistemp/stdata/

Null, S. E., Ligare, S. T., & Viers, J. H. (2013). A Method to Consider Whether Dams Mitigate Climate Change Effects on Stream Temperatures. Journal of the American Water Resources Association, 49(6), 1456–1472. https://doi.org/10.1111/jawr.12102

Olden, J. D., Leroy Poff, N., & Bestgen, K. R. (2006). Life-history strategies predict fish invasions and extirpations in the Colorado River Basin. Ecological Monographs, 76(1), 25–40. https://doi.org/10.1890/05-0330

Sabater, M. J. (2019). ERA5-Land hourly data from 1981 to present. Copernicus Climate Change Service (C3S) Climate Data Store (CDS). (Accessed on 01-Oct-2020). https://doi.org/10.24381/cds.e2161bac

Salehabadi, H., Tarboton, D., Kuhn, E., Udall, B., Wheeler, K., Rosenberg, D., Goeking, S., Schmidt, J. C., Salehabadi, H., Tarboton, D., Kuhn, E., Udall, B., Wheeler, K., Rosenberg, D., Goeking, S., Schmidt, J. C., & Summary, E. (2020). The Future Hydrology of the Colorado River Basin. Center for Colorado River Studies, white paper no. 4, 108.

Sen Gupta, A., & Tarboton, D. G. (2016). A tool for downscaling weather data from large-grid reanalysis products to finer spatial scales for distributed hydrological applications. Environmental Modelling and Software, 84, 50–69. https://doi.org/10.1016/j.envsoft.2016.06.014

Stanitski-Martin, D. (1996). Seasonal energy balance relationships over the Colorado River and adjacent riparian habitat: Glen Canyon, Arizona. Ph.D. Dissertation, Arizona State University, Tempe. https://doi.org/10.16953/deusbed.74839

Tarek, M., Brissette, F. P., & Arsenault, R. (2019). Evaluation of the ERA5 reanalysis as a potential reference dataset for hydrological modeling over North-America. Hydrology and Earth System Sciences Discussions, July, 1–35. https://doi.org/10.5194/hess-2019-316

Teutschbein, C., & Seibert, J. (2012). Bias correction of regional climate model simulations for hydrological climate-change impact studies: Review and evaluation of different methods. Journal of Hydrology, 456–457, 12–29. https://doi.org/10.1016/j.jhydrol.2012.05.052

TVA. (1972). Heat and mass transfer between a water surface and the atmosphere. In Water Resources Research, Laboratory Report No. 14. Engineering Laboratory, Division of Water Control Planning, Tennessee Valley Authority, Norris TN.

U.S. Bureau of Reclamation. (2012). Colorado River Basin Water Supply and Demand Study-Executive Summary. December, 34.

U.S. Fish and Wildlife Service. (1987). Recovery Implementation Program for Endangered Fish Species in the Upper Colorado River Basin.

Udall, B., & Overpeck, J. (2017). The twenty-first century Colorado River hot drought and implications for the future. Water Resources Research, 53(3), 2404–2418. https://doi.org/10.1002/2016WR019638

Van Beek, L. P. H., Eikelboom, T., Van Vliet, M. T. H., & Bierkens, M. F. P. (2012). A physically based model of global freshwater surface temperature. Water Resources Research, 48(9). https://doi.org/10.1029/2012WR011819

Van Vliet, M. T. H., Yearsley, J. R., Franssen, W. H. P., Ludwig, F., Haddeland, I., Lettenmaier, D. P., & Kabat, P. (2012). Coupled daily streamflow and water temperature modelling in large river basins. Hydrology and Earth System Sciences, 16(11), 4303–4321. https://doi.org/10.5194/hess-16-4303-2012

Vernieu, W. S., Hueftle, S. J., & Gloss, S. P. (2005). Water quality in Lake Powell and the Colorado River. In S. P. Gloss, J. E. Lovich, & T. S. Melis (Eds.), State of the Colorado River Ecosystem (pp. 69–85). U.S. Geological Survey Circular 1282.

Webb, B. W., & Zhang, Y. (2004). Intra-annual variability in the non-advective heat energy budget of Devon streams and rivers. Hydrological Processes, 18(11), 2117–2146. https://doi.org/10.1002/hyp.1463

Wheeler, K., Kuhn, E., Bruckerhoff, L., Udall, B., Wang, J., Gilbert, L., Goeking, S., Mihalevich, B., Neilson, B., Salehabadi, H., & Schmidt, J. C. (2021). Alternative Management Paradigms for the Future of the Colorado and Green Rivers. Center for Colorado River Studies, white paper no. 6, 91.

Winstral, A., Marks, D., & Gurney, R. (2009). An efficient method for distributing wind speeds over heterogeneous terrain. Hydrological Processes, 23(17), 2526–2535. https://doi.org/10.1002/hyp.7141

Wright, S. A., Anderson, C. R., & Voichick, N. (2009). A simplified water temperature model for the Colorado River below Glen Canyon Dam. River Research and Applications, 25(6), 675–686. https://doi.org/10.1002/rra.1179

You, Q., Bao, Y., Jiang, Z., Pepin, N., & Moore, G. W. K. (2019). Surface pressure and elevation correction from observation and multiple reanalyses over the Tibetan Plateau. Climate Dynamics, 53(9–10), 5893–5908. https://doi.org/10.1007/s00382-019-04905-y

Zhao, T. B., Guo, W. D., & Fu, C. Bin. (2008). Calibrating and evaluating reanalysis surface temperature error by topographic correction. Journal of Climate, 21(6), 1440–1446. https://doi.org/10.1175/2007JCLI1463.1

CHAPTER 4

DATA INTEGRATION AND COUPLED MODELING TO EVALUATE RIVER TEMPERATURE RESPONSES TO WATER MANAGEMENT DECISIONS

Abstract

Dams constructed to increase the reliability of water supply have dramatically changed downstream hydrologic and thermal regimes as well as many other river characteristics. In some rivers, the result has been a decline of native fish species. As the western United States continues to grapple with on-going drought and the reduction of flows due to a warming climate, reservoirs have fallen to unprecedented low levels. As reservoir elevations, thermal stratification patterns, and operational procedures adapt, the downstream riverine ecosystems may once again be altered. Anticipating changes in aquatic ecosystems over large spatial scales requires an understanding of thermal responses to basin-scale management decisions. Yet, existing water management tools used for allocating water amongst users generally have limited, if any, predictive capacity of ecosystem outcomes to management strategies. Furthermore, spatial and temporal resolution mismatches between system-operation models and river temperature models inhibits direct linking of these tools. To evaluate climate and management related impacts on aquatic thermal regimes, we developed a modeling framework that integrates a water management model, climate reanalysis and forecast datasets, and coupled process-based river and reservoir temperature models while addressing data requirement and management issues. This framework was tested using the Bureau of Reclamation's Colorado River Simulation System (CRSS) water management model over 1,000 km of

the Green and Colorado Rivers between Flaming Gorge and Lake Mead reservoir. To illustrate the utility of high spatial and temporal resolution river temperature predictions associated with current water management strategies, but future hydrologic conditions, select ecosystem metrics were quantified in critical habitat locations. While we use this framework to provide insight into the ecological implications of future climate and water management strategies in the Colorado River basin, these methods are adaptive and transferable to other rivers facing ecological concerns as the climate and water management requirements change.

1. Introduction

In the western United States, 53% of annual streamflow comes from snowfall that accumulates in mountainous regions during the winter and early spring (Li et al., 2017). This resource is critical for agriculture, municipal and industrial use, recreation, and ecosystems. In order to ensure the availability of this resource, more than 6,500 dams have been built west of the U.S. continental divide (USACE, 2019). However, the reliability of this infrastructure may be stressed as on-going climate change is expected to alter hydrologic patterns by reducing annual snowfall totals, shifting the timing of spring snowmelt runoff to earlier in the year, and decreasing overall basin runoff (Dettinger et al., 2015; Udall and Overpeck, 2017). Furthermore, water demands are projected to increase as population growth and climate change continues (Brown et al., 2013). With the anticipated changes to basin hydrology combined with changes in water demand, it is expected that many reservoirs will face high variability in water storage and predictions suggest relatively low reservoir levels for long periods of time (Barnett et al., 2004; Wheeler et al., 2020). The decisions water managers make to address these changes are

anticipated to alter downstream flow characteristics (Ehsani et al., 2017). However, negotiations on how available water is stored and redistributed during times of surplus or drought often do not consider the potential impacts on water quality and aquatic ecosystems (e.g., Dibble et al., 2021; Colorado River Drought Contingency Plan Authorization Act, 2019). Therefore, existing water supply planning tools need to incorporate models that assist in evaluating the associated water quality and ecological outcomes so that a more holistic understanding can be realized during negotiations.

Water resources decision makers often employ planning models (e.g., IQQM, Simons et al., 1996; MODSIM DSS, Fredericks et al., 1998; RiverWare, Zagona et al., 2001) that codify current water management policies to simulate how water is allocated throughout a river basin and provide predictions of water at specific locations (e.g., nodes), such as storage and releases from major reservoirs or diversions and return flows to and from specific stakeholders (Figure 4-1A). For long term planning, these models often use estimates of future consumptive uses combined with historical runoff information to serve as future hydrologic conditions. Because these models were developed primarily to serve water supply planning needs, the spatial and temporal resolution included in these models are typically at coarse scales where basin-wide management decisions are practical. However, finer resolution information is often needed to resolve some ecological questions (such as minimum flow requirements, temperature degree days, etc.).

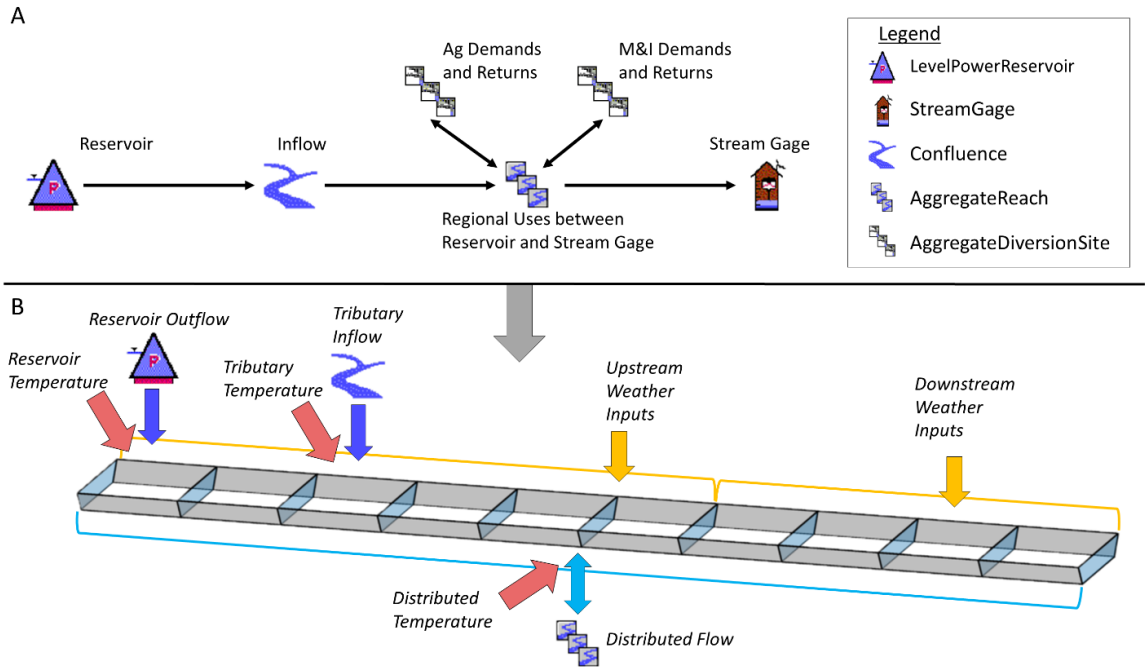

Figure 4-1. (A) Example stream network representation in a water resources management model (RiverWare). Each icon represents a "node" which can be a specific location (i.e., stream gage, inflow, or reservoir) or a non-descript delineation of abstractions and redistributions within a river segment (i.e., regional uses). (B) Conceptual schematic of how the water management model in Figure 4-1A is linked to a process-based river temperature model. Each trapezoidal prism is considered a model element (or cell) and can be many meters to many kilometers long. The dark blue directional arrow represents a point inflow while light blue bidirectional arrows represent distributed flow (either in or out of the model). Distributed flows can be calculated as the aggregate of all regional uses, shown above in Figure 4-1A. Red directional arrows represent the temperature associated with the point or distributed inflow (distributed outflows are given the instream temperature). Yellow directional arrows indicate weather information inputs which are applied to each model cell and can come from multiple sources.

To enable holistic water resources problem solving, coupled decision support modeling platforms have been developed that link water quality and aquatic ecosystem response models to water management models. This coupled modeling involves sequentially running independently developed models and passing outputs from one model to the next. This approach takes advantage of already developed models, speeding up implementation. For example, Bovee et al. (2008) developed the Yakima River Decision Support System (YRDSS) which linked the Bureau of Reclamation's (hereafter

Reclamation) systems operation model in River-Ware to a series of Microsoft Excel workbooks that calculate and summarize 14 water quality and ecosystem variables in 5 important flood plain reaches. Similarly Campbell et al. (2001) linked a MODSIM systems operation model for the Klamath River Basin to a HEC-5Q water quality model to test alternative operations and determine if improvements to summer and fall water temperatures could be achieved to benefit fish populations. However, these coupled modeling examples both exhibit limited spatial and temporal resolution of ecologically relevant outputs. For instance, both applications produce daily outputs, missing within day extremes that are important for understanding ecosystem impacts (Alexander et al., 2013; Kennedy et al., 2016). Furthermore, both HEC-5Q and YRDSS are calibrated to provide water quality predictions at specific locations that coincide with nodes in the systems operation model and do not provide information between node locations. Because ecologically important locations are often different than operational nodes, there are spatial mismatches between ecosystem and water management models. This highlights the need to develop more robust tools that overcome inter-model compatibility issues that arise due to spatial resolution mismatches while providing predictions at temporal resolutions relevant to ecosystems.

Process-based river routing and water quality models can be used to overcome these spatial and temporal resolution limitations and provide information necessary to calculate ecosystem responses to water management efforts. The drawback is that these models have large data requirements which impose additional challenges especially when forecasting and necessitates transferable and widely applicable methods for generating required input data. Towards this end, we describe a generic coupled modeling and data

assembly approach that enables process-based water temperature forecasts at high spatial and temporal resolutions necessary to establish aquatic ecosystem indicators from coarse resolution water management model forecasts. While these methods can be applied to other constituents, we focus on predicting water temperature, since temperature is often considered the "master" water quality variable that drives rates of chemical reactions and controls biological life history traits (Caissie, 2006; Webb et al., 2008). To validate our methods, we test the proposed modeling approach using an existing water resources management model for the Colorado River basin. We focus on a highly managed portion of the basin that includes the Green River, Lake Powell, and the Colorado River in Grand Canyon, where critical habitat exists for a number of endangered and threatened native fish species. The on-going drought in this basin continues to create great interest in determining management approaches that maintain these ecosystems while meeting downstream water supply needs.

2. Modeling Approach

Dynamic process-based river routing and temperature models are integral in understanding the dominant heat flux mechanisms controlling river thermal regimes and allow us to evaluate how systems may change with changes in climate, hydrology, or management practices (King and Neilson, 2019; Meier et al., 2003; Mihalevich et al., 2020; Webb and Zhang, 2004). Similarly, process-based reservoir models enhance our understanding of thermal stratification patterns and the influence of operational procedures on release temperatures (Williams, 2009), which can have large impacts on downstream river thermal regimes (Collier et al., 1996; Graff, 1999; Lowney, 2000) and by extension aquatic ecosystems (Nilsson and Renöfält, 2008; Olden and Naiman, 2010;

Ward and Stanford, 1983). Process-based models rely on boundary conditions (e.g., upstream gage flow and temperature data), other inflows or outflows (e.g., tributary inputs, agricultural withdrawals or returns, etc.), and weather information to predict water temperatures. In order to link water management model forecasts to river and reservoir temperature forecasts, the information requirements of process-based models must also be produced for future conditions. The combined complications of overcoming spatial and temporal mismatches between multiple model types and forecasting required data inputs at appropriate resolutions requires a detailed conceptualization for linking models (Figure 4-1B).

2.1. Process-based models

2.1.1. River Temperature Model

In this application, we used a component-based, one-dimensional, dynamic, process-based routing and river temperature model applied within the HydroCouple framework (Buahin et al., 2019; Buahin and Horsburgh, 2018). Similar to Chapters 1 and 2, we coupled the EPA SWMM (Storm Water Management Model; Rossman, 2006) component for dynamic wave flow routing, the channel solute and heat transport (CSH) component for channel advection and dispersion, and sensible and latent heat fluxes; the radiative heat exchange (RHE) component used for shortwave and longwave radiation terms; the hyporheic transient storage (HTS) component used for sediment conduction; and the time series provider component to apply externally calculated scaling factors to select heat flux terms (i.e., spatial and temporal shading factors) (Mihalevich et al., 2020). The heat fluxes included in these components were net shortwave radiation ($J_{sn,net}$), atmospheric longwave radiation (J_{an}), water longwave radiation (J_{br}), bedrock

longwave radiation (J_{rock}), sensible heat (conduction and convection; J_c), latent heat (evaporation and condensation; J_e), internal fluid shear friction (J_f), and sediment conduction (J_{sed}) (Figure C-1). Heat from tributary inflows, calculated from temperature and flow time series data, are accounted for directly in both the hydraulic and heat transfer modeling components. Air-water interface heat fluxes, as described in Buahin et al. (2019) (i.e., J_{br}, J_e, J_c) and Mihalevich et al. (2020) (i.e., $J_{sn,net}$, J_{an}, and J_{rock}), are estimated from solar radiation, air temperature, relative humidity, and wind speed information provided as model inputs. Weather time series used by the model can vary by model element in both the CSH and RHE components, allowing for spatially varying weather information over the modeling domain.

2.1.2. Reservoir Temperature model

To simulate reservoir temperatures we applied the CE-QUAL-W2 model (Cole and Wells, 2003). CE-QUAL-W2 is a two dimensional, longitudinal/vertical, hydrodynamic, and water quality model that has been broadly applied to more than 300 reservoirs, including Lake Powell, Lake Mead, and Flaming Gorge in the Colorado River basin. CE-QUAL-W2 simulates reservoir temperatures and stratification by calculating heat fluxes and densities. Evaporative heat loss is always included in the heat budget, but evaporative mass losses can be turned off in CE-QUAL-W2, which can be important when coupling to water management models that already account for evaporative mass losses. Flow in and out of reservoirs are boundary conditions provided by the model user. Inflow temperatures are also required inputs. Multiple release structures (e.g., temperature control devices, penstocks, bypasses, etc.) can be included in the model at

specified elevations, allowing for predicted release temperatures to vary as water levels, stratification depths and management decisions change.

2.2. Linking Water Management Models to Process-Based Models

Flow information is one of the most important variables in predicting river temperatures because flow influences the amount of energy required to alter temperatures given the total volume of water in the channel (i.e., thermal inertia; Gu et al., 1998) and the surface area to volume ratio influencing heat transfer rates at the air-water interface (Polehn and Kinsel, 1997; Risley et al., 2010; Schmadel et al., 2015). However, future watershed hydrology is also one of the largest uncertainties when conducting water resources planning (Wang et al., 2020). Water management modelers typically develop future hydrologic scenarios based on historical conditions under the premise that, if it has happened in the past, it is plausible it can happen in the future (Salehabadi et al., 2020; U.S. Bureau of Reclamation, 2012). Under this approach, past hydrologic conditions can be resampled multiple times, either randomly or sequentially, to generate an ensemble (10's to 100's) of plausible hydrologic sequences (herein referred to as "traces") that characterize a range of future hydrologic conditions (Wheeler et al., 2019; Salehabadi et al., 2020; Table C-1). Using plausible future hydrologic traces, water management models make predictions of water volumes at key river locations such as major reservoirs and tributaries (Figure 4-1A). This accounts for future or possible regional demands and return flows based on projected demand curves that describe consumptive uses. These models typically simulate flow at nodes at daily or monthly time steps to serve water supply and distribution planning needs.

Linking flow information from water management models to the process-based river and reservoir models is required to enable predictions of higher spatial and temporal resolution of flow and temperature information throughout the river system. To properly link these two models, flow information from the water management model must first be categorized. In general, flow information from a water management model can be categorized as either *point* or *distributed flows*. Point flows describe sources that have a real-world geographic location, such as reservoir outflows, tributary inflows, or headwater gages. In a process-based model, point flow sources get applied to a single element (e.g., dark blue directional arrow in Figure 4-1B). Distributed flows describe sources that do not have specific geographic locations, such as reservoir evaporation or regional diversions and return flows. Distributed flow sources get applied to multiple elements in the process-based model (e.g., light blue bidirectional arrows in Figure 4-1B).

The temporal resolution of flow information must also be addressed to ensure the process-based models maintain the correct flow balance of the water management model. For example, monthly flow predictions represent the average value for that month at either the start or end of the month. To ensure the flow balance is maintained within the process-based model this information needs to be repeated to create stepwise inputs (Figure C-2). Without a stepwise input flow series, most process-based models would interpolate between monthly flow volumes resulting in an incorrect flow balance.

2.3. Linking Forcing Data to Process-Based Models

Representative boundary condition water temperature and distributed weather information is also critical for predicting river and reservoir temperatures. For example, in reservoirs with relatively high outflows (e.g., > 100 cms), release temperatures can

influence the downstream river for 100s of kilometers (Anderson and Wright, 2007; Carron and Rajaram, 2001; Daniels and Danner, 2020). With regards to weather information, Chapter 3 showed that Colorado River temperature predictions in Grand Canyon were improved after switching from a single weather station to distributed (i.e., gridded) weather information as forcing data to the model.

Similar studies that needed to obtain future weather conditions have stochastically generated weather information (Sapin et al., 2017) while others have directly resampled historical data based on similar flow years (Williams, 2009). For consistency between hydrologic conditions, weather, and boundary condition temperatures, we adopted the latter approach of directly resampling historical weather and input temperature data. Therefore, historical water temperature and weather data were resampled based on the hydrology resampling used in the water management model (e.g., Table C-1). This approach maintained the native resolution of the input data to be incorporated in river temperature predictions, which provided information regarding within day variability.

3. Case Study: Colorado River Basin

3.1. Study Area

The Colorado River basin (Figure 4-2) provides water for 40 million people in the United States and Mexico (U.S. Bureau of Reclamation, 2012) and critical habitat for three federally listed endangered fish species (U.S. Fish and Wildlife Service, 1987). To increase the reliability of water supply across the basin, more than 7.4×10^{10} m^3 (60 million acre-feet) of water storage has been developed. The dams constructed to provide this storage have also dramatically changed the hydrologic and thermal regimes, sediment supply, carbon cycles, and migration characteristics of the reaches downstream from each

reservoir (Vernieu et al., 2005). The result of these changes, as well as introduction of nonnative competing species, has been a decline, and in some cases extirpation, of fish species (Gloss & Coggins, 2005; Bestgen & Hill, 2016; Dibble et al., 2021; Martinez et al., 2014; Olden et al., 2006). As the basin continues to grapple with the on-going Millennium Drought (2000-present; Salehabadi et al., 2020; Wheeler et al., 2021) and the reduction of flows due to a warming climate (Dettinger et al., 2015; McCabe et al., 2017; Udall and Overpeck, 2017; Woodhouse et al., 2016), reservoirs have fallen to unprecedented low levels. To mitigate the impacts of the on-going drought the United States Congress passed the Colorado River Drought Contingency Plan (DCP) Authorization Act in April of 2019 (Colorado River Drought Contingency Plan Authorization Act, 2019), which set water supply cutbacks to states that receive Colorado River water if reservoir levels continue to drop. These cutbacks are combined with the shortage guidelines described in the Colorado River 2007 Interim Guidelines (U.S. Department of the Interior, 2007). The DCP joins the assemblage of bi-national treaties, interstate compacts, federal laws, administrative agreements and records-of-decision associated with environmental impact statements that collectively determine how water is managed within the basin and are informally referred to as the *Law of the River*. Despite these measures to conserve water, if reservoir elevations, thermal stratification patterns, or operational procedures change significantly, the downstream river segments and ecosystems may once again be altered (Null et al., 2013). In order to address the concerns of future temperature impacts on both native and nonnative fish communities in the Colorado River basin, the development of large-scale process-based river temperature

models are needed to provide insight regarding the thermal implications of water management decisions under future climate and hydrologic changes.

3.2. Models

The model coupling for our approach was sequential and directional. This means that each model was run only once and there was no feedback loop to influence subsequently simulated traces. The order of running models starts with the water management model followed by process-based river and reservoir models that run from upstream to downstream (Figure 4-3). The flow information from key nodes in the water management model was processed and passed to the reservoir and river temperature models. Flow and river temperature information was passed from the Upper Basin model to the Lake Powell model, and reservoir release flow and temperature information was passed from the Lake Powell model to the Colorado River Grand Canyon model.

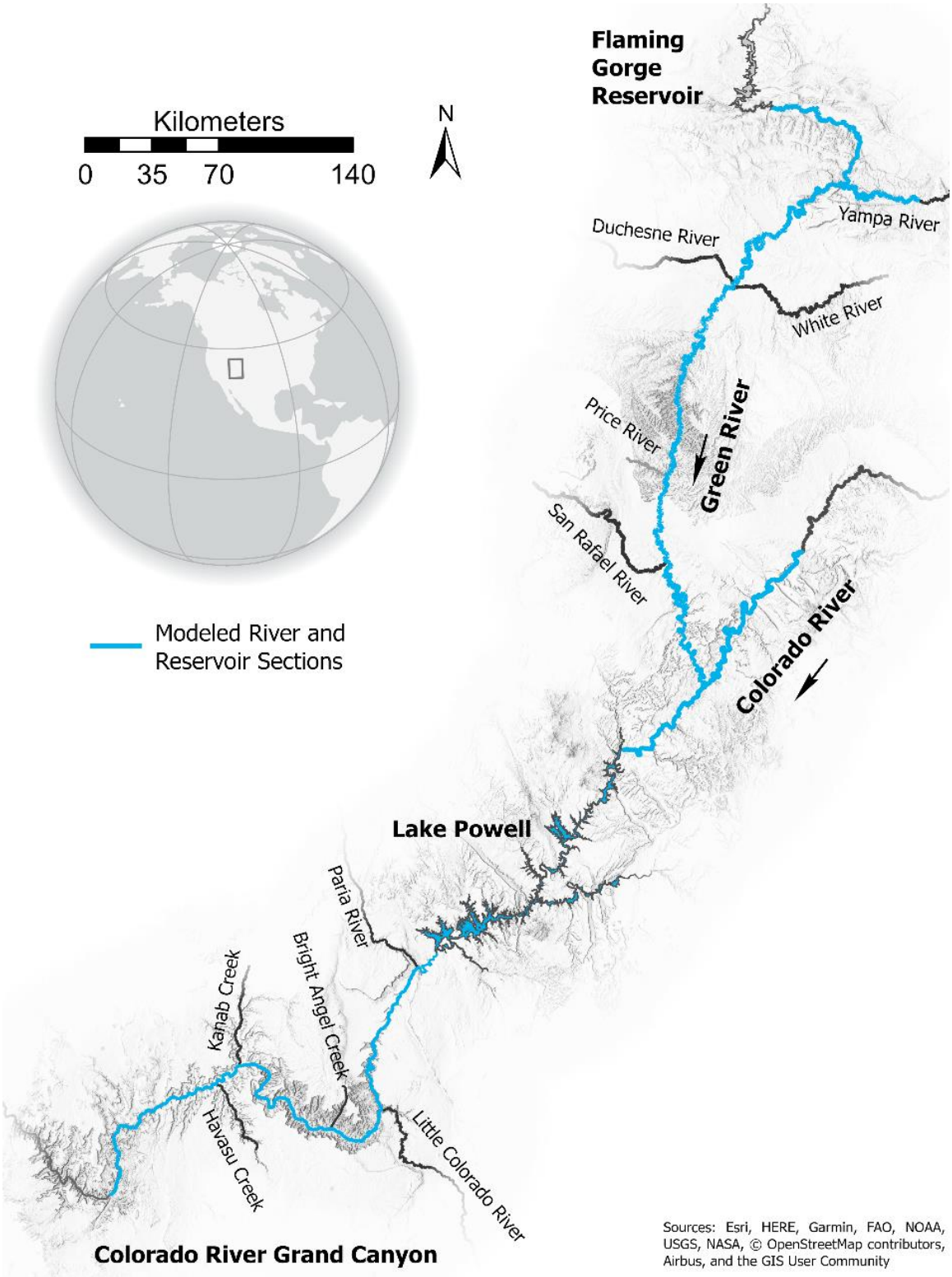

Figure 4-2. Map of the study area depicting the sections Colorado River basin modeled using process-based river and reservoir models.

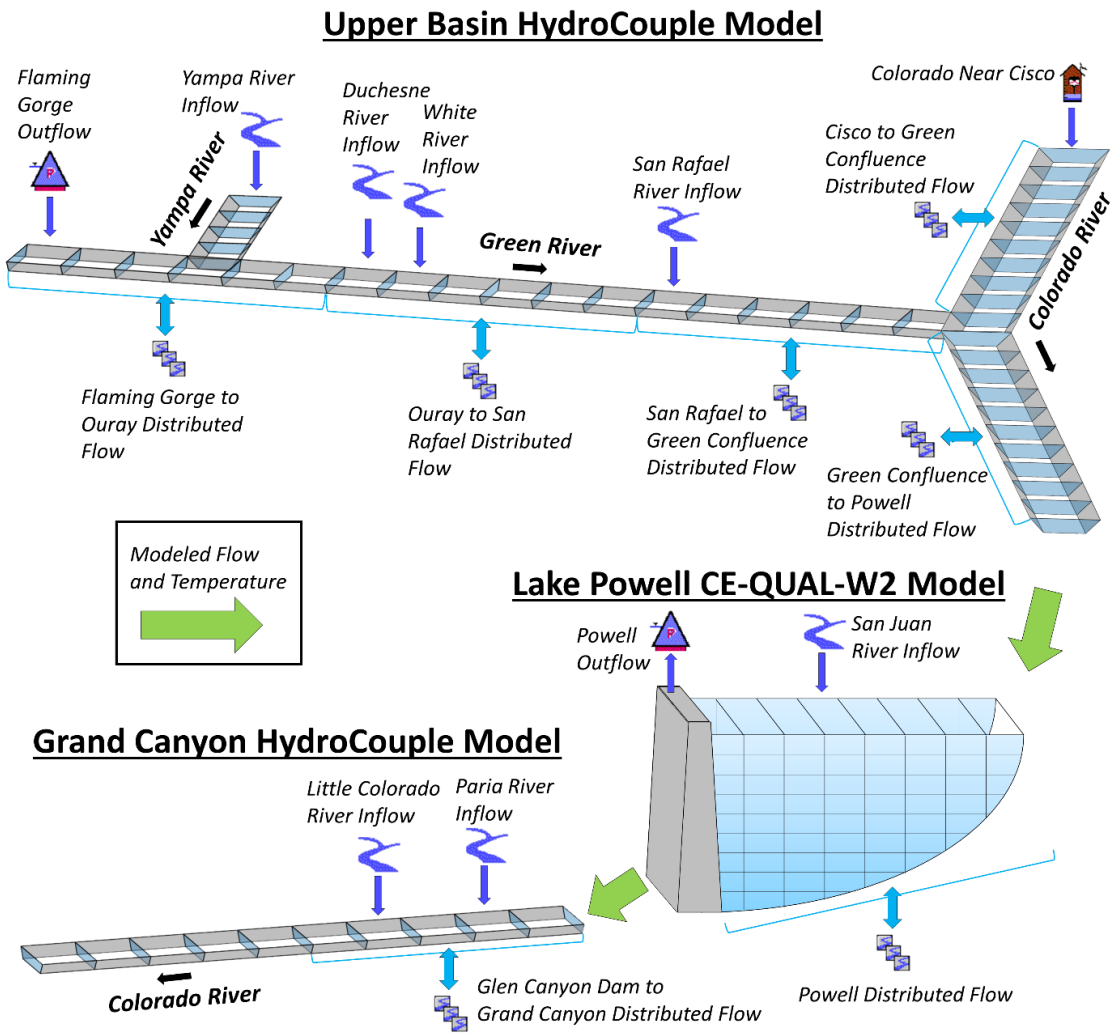

Figure 4-3. Model coupling sequence (green arrows) used to conduct river routing and water temperature predictions throughout the Colorado River basin. RiverWare icons are used to illustrate how point inflow (dark blue directional arrows) and distributed flow (light blue bidirectional arrows) from the water management model are assigned to process-based model cells. Note that the process-based models are comprised of 100's of model cells, but have been reduced here for illustrative purposes.

3.2.1. Colorado River Simulation System (CRSS)

The Colorado River Simulation System (CRSS; for full description see Alexander et al., 2013; Wheeler et al., 2019) developed by Reclamation and implemented in RiverWare software (Zagona et al., 2001) simulates how water is allocated throughout the basin based on the present interpretation of the Law of the River. Reclamation's

implementation of CRSS codifies the current water management policies to predict water storage, reservoir elevations and releases, and the volume of water exchanged at specific demand points (i.e., nodes) on a monthly time step. To test our modeling approach, we selected a subset of the CRSS model domain (see Figure C-3 for a full CRSS model schematic) to focus on river segments that are highly influenced by management decisions and provide critical habitat to endangered and threatened fish species (Table C-2, Figure C-4).

This model application requires several CRSS nodes, which include diversion and return flows for individual state uses, allocations for water quality improvement projects (WQIP), local inflows (e.g., tributaries and intervening flows), reservoir evaporation, and anticipated future depletions (Figure C-4). To account for the gains and losses in volume from regional diversion, return, and intervening flows we applied all "AggregateReach" nodes (Figure 4-1) as *distributed* flows (Table 4-1). These nodes are the summation of all sub-branched nodes (shown in Figure C-4) which can include "AggregateDiversionSite" and "Confluence" nodes. It also includes some "LevelPowerReservoir" Objects, such as reservoir evaporation, which is applied as *distributed* flows as noted in the equations in Text C-1. All other nodes were applied as *point* flows. To ensure that the flow balance was closed in this application, we transformed monthly CRSS time steps to a stepwise series by duplicating flow information and shifting time steps to the first day of the month with a time of 00:00:00 and the last day of the month with a time of 23:59:59 (Figure C-2).

Table 4-1. Subset of CRSS nodes used to model river temperatures in the Colorado River basin. CRSS Objects have been combined and renamed for readability. A complete list of CRSS nodes used in this study is shown in Table C-2. The river kilometer indicates the approximate location of where CRSS point inflows were assigned or the range over which distributed flows were assigned in the process-based models.

RiverWare Object Type	CRSS Object	River KM(s)	Spatial Resolution
Green River		(Distance from FGD)	
LevelPowerReservoir	Flaming Gorge Outflow	0	Point
Confluence	Yampa River Inflows	-74[1]	Point
Confluence	Duchesne River Inflow	260	Point
Confluence	White River Inflow	262	Point
Confluence	San Rafael River Inflow	504	Point
AggregateReach	Flaming Gorge to Ouray Distributed Flow	0-259	Distributed
AggregateReach	Ouray to San Rafael Distributed Flow	259-503	Distributed
AggregateReach	San Rafael to Green River Confluence Distributed Flow	503-661	Distributed
Colorado River above Lake Powell		(Distance from Cisco)	
StreamGage	Colorado River near Cisco	0	Point
AggregateReach	Cisco to Green Confluence Distributed Flow	0-153	Distributed
AggregateReach	Green Confluence to Powell Distributed Flow	153-231	Distributed
Lake Powell and San Juan River Inflows		(Distance from Hite, UT)	
Confluence	San Juan River Inflow	186	Point
LevelPowerReservoir	Powell Outflow	278	Point
AggregateReach	Powell Distributed Flow[2]	0-278	Distributed
Colorado River in Grand Canyon		(Distance from GCD)	
Confluence	Paria River Inflow	27	Point
Confluence	Little Colorado River Inflow	125	Point
AggregateReach	Grand Canyon Distributed Flow	0-167	Distributed

[1]Distance of the Yampa River is calculated from the confluence with the Green River.
[2]Includes *evaporation* and *change in bank storage* terms associated with the LevelPowerReservoir node.

The CRSS simulations were based on the Millennium Drought hydrology developed by Salehabadi et al. (2020). This hydrologic scenario was created by sampling naturalized flow at Lees Ferry between the years 2000 and 2018 at random, with replacement (each year may be repeated), to construct 100 40-year traces for use in CRSS to project flows from 2022 to 2060 (Salehabadi et al., 2020). We randomly selected 50 of the 100 CRSS traces to test. These traces represent a highly variable range of flows that drastically impacted Lake Powell water elevations over the 10-year period simulated in the process-based models (Figure 4-4).

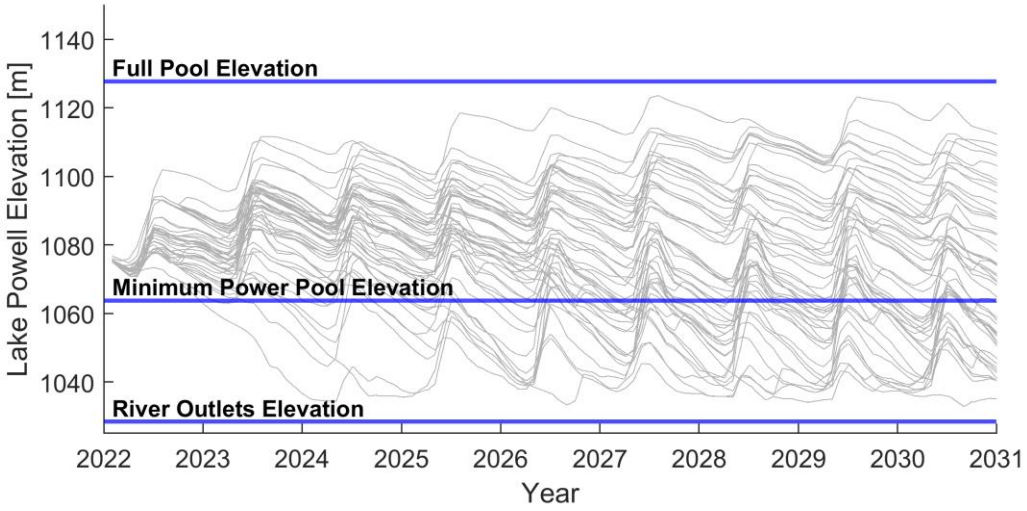

Figure 4-4. Variability in Lake Powell water elevation for the 50 traces (grey lines) selected from the Millennium Drought hydrology (Salehabadi et al., 2020). The "Minimum Power Pool Elevation" is the elevation needed to generate hydropower. The "River Outlets Elevation" refers to the elevation at which water is drawn from the bypass tubes, which are used when elevations drop below minimum power pool.

3.2.2. HydroCouple

Upper Basin Model

To simulate river temperatures throughout the Colorado River basin we adopted the modeling approach applied to the Green River, described in Chapter 3, that was

developed within HydroCouple. This required the development of routing and temperature models for a portion of the Upper Colorado River basin (Figure 4-2). This model includes 576 km of the Green River between Flaming Gorge Dam and Mineral Bottom in Canyonlands National Park and 74 km of the Yampa River using approximately 2-km long elements. Flow and temperature inputs from 4 tributaries were accounted for, including the Duchesne River, White River, Price River, and San Rafael River. Here we modified this model to also include 86 km of the Green River between Mineral Bottom and the confluence with the Colorado River and 232 km of the Colorado River between the USGS river gage near Cisco, UT and the upper end of Lake Powell near Hite, UT. Topographic shading and radiation characteristics were determined following methods described by Mihalevich et al. (2020) for all elements in the model. Herein we refer to this model as the "Upper Basin" model (Figure 4-3).

The linking of CRSS outputs to the Upper Basin model is illustrated in Figure 4-3. We used the CRSS outputs *Flaming Gorge Outflow*, *Yampa River Inflow*, and *Colorado near Cisco* as the upstream boundary condition flows for the Green, Yampa, and Colorado rivers, respectively. Tributary inflows for the Duchesne, White, and San Rafael rivers come from their respective CRSS nodes (Table 4-1). Inflows from the Price River were not accounted for directly in this application because they are not represented by a specific CRSS node. Five AggregateReach nodes were used to apply distributed flow in different river sections within the Upper Basin model (Figure 4-3). Note that *Flaming Gorge to Ouray Distributed Flow* was not applied to Yampa River model elements because this river segment has no meaningful diversions or return flows (Colorado's Decision Support Systems, 2021).

Grand Canyon Model

The HydroCouple model downstream of Lake Powell simulated 387 km of the Colorado River between Glen Canyon Dam and Diamond Creek using approximately 1-km long elements. This model accounted for flow and temperature inputs from 5 tributaries, which include the Paria River, Little Colorado River, Bright Angel Creek, Kanab Creek, and Havasu Creek. Similar to the Upper Basin model, all model elements received unique topographic shading and radiation information (Mihalevich et al., 2020). Herein we refer to this model as the "Grand Canyon" model.

The linking of CRSS outputs to the Grand Canyon model is illustrated in Figure 4-3. These nodes only account for water between Glen Canyon Dam and the USGS gage near Grand Canyon, AZ (approximately river mile 88) just upstream of Bright Angel Creek (Figure 4-2). CRSS nodes downstream of this location were excluded in our case study. The AggregateReach node between Glen Canyon Dam and the USGS gage near Grand Canyon was used to determine distributed flows for this river segment (Figure 4-2). Tributary inflows for the Paria and Little Colorado river are provided by CRSS nodes directly. Flows from tributaries downstream of the USGS gage near Grand Canyon (i.e., Bright Angel Creek, Kanab Creek, and Havasu Creek) are not represented by CRSS nodes but can be significant sources of intervening flow (Wang and Schmidt, 2020). Since these inputs are beyond the most downstream CRSS node in our modeling domain, and therefore do not affect the flow balance, we decided to include these inflows using the monthly average discharge determined from historical USGS gage data for each tributary.

Weather Data

We selected the ERA5-Land climate reanalysis dataset to provide spatially varying (i.e., gridded) hourly inputs of solar radiation, air temperature, relative humidity, and wind speed (Sabater, 2019) required by the river and reservoir models. ERA5-Land does not provide relative humidity directly and therefore was estimated using air temperature and dew point temperature terms from the dataset. Air temperature, dew point temperature, relative humidity, and wind speed were also elevation corrected following methods presented in Chapter 3 to account for spatial variation in the vertical dimension that arises due to the topographically complex terrain in the Colorado River basin.

Currently, the temporal coverage of ERA5-Land is between 1950-present and has a spatial resolution of 0.1° x 0.1° latitude and longitude grids. We coarsened the spatial resolution of ERA5-Land to 1.0° x 1.0° latitude and longitude grids. As Chapter 3 showed, this has negligible influence on river temperature predictions and reduces data requirements and simulation times for these river sections. ERA5-Land information grids were assigned to river temperature model elements by simply identifying the model elements contained within each ERA5-Land grid.

Similar to water temperature inputs, ERA5-Land weather data were resampled based on the sequence of historical years in each hydrologic trace (Table C-1). An additional step was taken to impose future climate projections on air temperature inputs for each ERA5-Land grid. This was carried out by adding the monthly air temperature increases relative to 2021 to the resampled ERA5-Land air temperatures based on the ensemble mean of Reclamation’s Bias Corrected and Spatially Disaggregated (BCSD)

CMIP5 projections (1.0° x 1.0° latitude and longitude grids) with a RCP 4.5 emissions pathway (Udall, personal communications; Figure C-5). We opted to use historical ERA5-Land information over using CMIP5 to ensure input meteorology was closely linked to the hydrologic scenario applied here.

Water Temperature Data

Historical water temperature data from USGS gages were used at upstream boundary conditions and tributary inflows (Table C-3). These data were resampled based on the sequence of historical years in each hydrologic trace (Salehabadi et al., 2020; Table C-1). The gages used for continuous inputs (Table C-3) started measuring water temperature in 2004 (Green River near Greendale UT) and 2007 (Yampa River at Deerlodge Park, CO and Colorado River near Cisco, UT) which is later than the historical flow information used in the hydrologic sequences (2000-2018). Therefore, when hydrologic sequences contained historical flow years that predate the available water temperature information at specific gage sites, then similar flow years within the data availability range were substituted into the hydrologic sequence to enable resampling. Similar flow years were determined by comparing the total annual discharge volume at Lees Ferry using Reclamation's natural flows database (U.S. Bureau of Reclamation, 2021). Large data gaps in historical records, if present, were filled using monthly averages. Monthly average temperatures were determined from historical USGS gages and used for smaller tributaries that do not have long term records (Table C-3). Water temperature associated with distributed inflows were assumed to be the average air temperature between 2000 – 2018, which were determined using the ERA5-Land climate reanalysis dataset and varied over space. Temperatures assigned to the ground boundary

condition (Figure C-4) were assumed to be the annual average of resampled air temperature inputs (i.e., varying each year), which were also determined using the ERA5-Land climate reanalysis dataset and varied over space. Water temperatures at the upstream boundary of the Grand Canyon model were predicted using the Lake Powell model.

3.2.3. CE-QUAL-W2

Lake Powell Model

To simulate temperatures within and released from Lake Powell, we used the Reclamation's (BOR) Lake Powell CE-QUAL-W2 model (Williams, 2007). Lake Powell bathymetry data, in the form of a digital elevation model, was used to generate the computational grid. The computational grid consists of 9 branches which represent the main Lake Powell water body and 8 tributaries (Figure C-6). Branches are represented by a total of 99 longitudinal segments and 97 vertical layers. The segments range from 1 km to more than 10 km in length and all layers are 1.75 m thick (Williams, 2007). There are five tributary inflows accounted for within the model. All of the branches and tributaries require inflow discharge and temperature information.

In order to use CRSS projections as inputs to the Lake Powell model, minor modifications were needed. Initial model testing with CRSS projections resulted in simulation errors due to low reservoir levels experienced in extreme drought scenarios and the stepwise change in inflows associated with monthly CRSS inputs. To improve numerical stability, we increased longitudinal segmentation of the tributary branches by dividing cells in half. This changed the total number of longitudinal segments from 99 to 129. Testing of this new segmentation during historical periods resulted in improved

release temperature predictions when compared to observations. This improvement was likely due to the reduced averaging over long longitudinal segments in tributary branches.

Linking CRSS outputs to CE-QUAL-W2 is shown in Figure 4-3. Colorado River inflows to Lake Powell are provided by the Upper Basin model. Tributary inflows for the San Juan River and outflows from Glen Canyon Dam are provided by CRSS nodes directly. When projected Lake Powell elevations from CRSS fell below 1063.75 m (3490 ft), which is the minimum elevation needed for hydropower generation, releases were switched from the penstocks to the bypass tubes (Figure 4-4). All distributed sources associated with Lake Powell nodes were represented by the *Powell Distributed Flow* term and were aggregated together into a single time series and applied to the main Colorado River branch in the Lake Powell model (Figure 4-3). *Powell Distributed Flow* was not applied to tributary branches (e.g., Escalante, Wahweap, etc., Figure C-6) to be consistent with Reclamation's current approach for handling distributed flows in the Lake Powell model. Note that there are several tributaries accounted for in the Lake Powell model as constant inflows. To maintain tributary flow sources, which influence reservoir mixing, the volumes were subtracted from the *Powell Distributed Flow* term (Text C-1). Evaporative mass losses were turned off in CE-QUAL-W2 since it is included in the CRSS mass balance.

Weather Data

Similar to the HydroCouple models, we opted to use the ERA5-Land climate reanalysis dataset to provide high temporal resolution inputs for solar radiation, air temperature, dew point temperature, wind speed, wind direction and cloud cover (Sabater, 2019). Cloud cover is not provided by ERA5-Land directly and was instead

calculated using additional variables within the dataset (Text C-2). Currently, the Lake Powell model is configured to only use a single source of weather information. Therefore, all ERA5-Land grids (in the native resolution) overlapping the spatial extent of Lake Powell were averaged together before being applied to the CE-QUAL-W2 model. Future air temperature increases estimated using Reclamation's BCSD CMIP5 projections with a RCP 4.5 emissions pathway were also imposed on the resampled ERA5-Land air temperature inputs. The closest BCSD grid to Lake Powell (centroid of 37.5 Latitude, -110.5 Longitude) was used to determine the relative air temperature increases.

Water Temperature Data

Water temperature associated with *Colorado River Inflow to Powell* comes from the predicted river temperature at the most downstream element in the Upper Basin HydroCouple model. Historical continuous water temperature data for the San Juan River (Table C-3) was resampled based on the sequence of historical years in each hydrologic trace and applied at upstream boundary in the San Juan River branch. Water temperature data from smaller tributaries do not exist. Therefore, resampled water temperatures from the San Juan were assigned to these sources, which is consistent with current practices used by the Reclamation. The *Powell Distributed Flow* term is also assigned resampled San Juan River temperatures to be consistent with Reclamation methods. Temperature of the ground (sediment) boundary, 12 °C, was not changed from the original Lake Powell model.

3.5. Results and Discussion

The 50 hydrologic traces simulated in the river and reservoir temperature models resulted in high spatial and temporal resolution temperature predictions throughout the modeling domain (Figure 4-5). These predictions can be used to quantify specific ecosystem metrics, such as temperature degree days, or to understand changes in seasonal temperatures throughout the modeling domain under future reservoir conditions. Although Figure 4-5 only shows results over the 2030 calendar year, the outputs can be used to evaluate year-to-year changes in river temperatures and ecosystem metrics. While it is outside the scope of this paper to exhaustively calculate all ecosystem metrics, we evaluate two simple metrics to illustrate the capabilities of this modeling approach.

One ecosystem metric suggested by Alexander et al. (2013) is the difference in water temperature between the Green River and Yampa River near their confluence. As Colorado pikeminnow larvae drift downstream in the Yampa River, they may be exposed to colder water temperatures in the Green River and may experience cold "shock", reducing survival (Muth et al., 2000). Tyus (1991) found that pikeminnow recruitment increased when Green and Yampa river temperatures differed by ≤ 2 °C. Using the 50 hydrologic traces simulated over 10 years we evaluated the percent probability that temperature differences at the confluence are less than 2 °C during spawning months (June, July, and August; Figure 4-6). Later months have higher chances of being less than 2 °C. Over the 10-year simulation the overall probability increases owing to higher water temperatures in the Green River (Figure 4-6).

Another ecosystem metric that can be calculated from the model results is the number of thermally suitable days (TSD) for specific fish species. To illustrate this we used the model developed by Dibble et al. (2021) and associated data (Dibble et al.,

2020) to calculate the TSD for threatened humpback chub at within Grand Canyon. A minor modification was made to the Dibble et al. (2021) model to calculate TSD using hourly temperature predictions, as opposed to monthly average temperatures (Text C-3). We evaluated TSD at two river locations: at the confluence with the Little Colorado River, and immediately upstream from the confluence with Diamond Creek (Figure 4-2). These locations were chosen because they represent a gradient of temperature change throughout the canyon and are ecologically significant for humpback chub populations (Van Haverbeke et al., 2017, 2020; Kegerries et al., 2020; Yackulic et al., 2014). Our results from calculating this metric show that farther downstream locations have higher, but less variable TSD (Figure 4-7). The high amount of variability in TSD at the Little Colorado River alludes to the impact of Glen Canyon Dam release temperatures on downstream river temperatures, which are most influential up to Bright Angle Creek (Figure 4-2), after which other factors, such as discharge, air temperature, and solar radiation, are more dominant (Mihalevich et al., 2020).

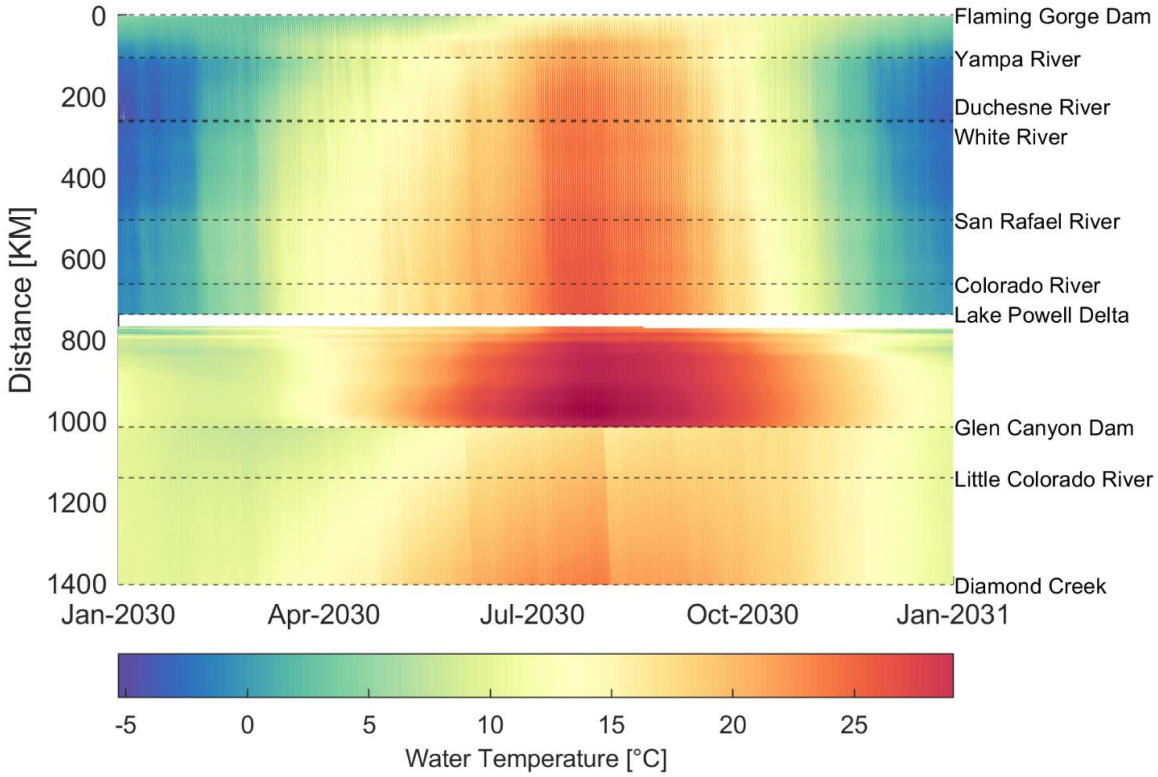

Figure 4-5. Modeled river and reservoir temperatures in the Green River, Lake Powell, and Grand Canyon river sections for the forecast year 2030. Temperatures are the mean of all 50 traces simulated. Surface water (epilimnion) temperatures are shown for Lake Powell (approximately 800 km to 1000 km).

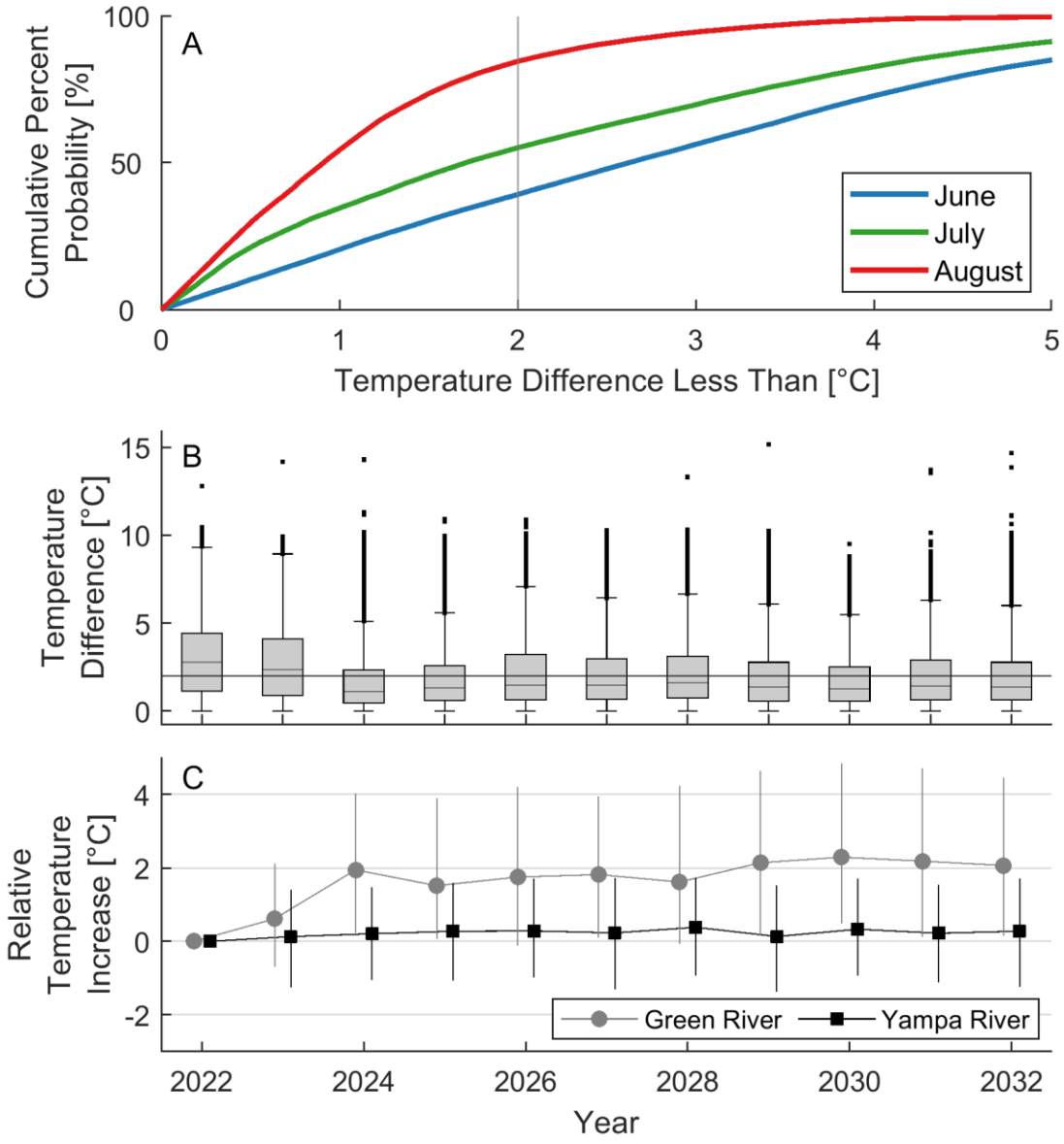

Figure 4-6. Plot showing the cumulative percent probability that temperature differences between the Yampa River and Green River near their confluence are within certain temperature thresholds during summer months (A). Change in temperature differences between the Green and Yampa river temperatures at their confluence for summer months (June, July, and August) (B). The relative increase in river temperatures since 2022 for summer months in the Green and Yampa rivers immediately upstream of their confluence (C)

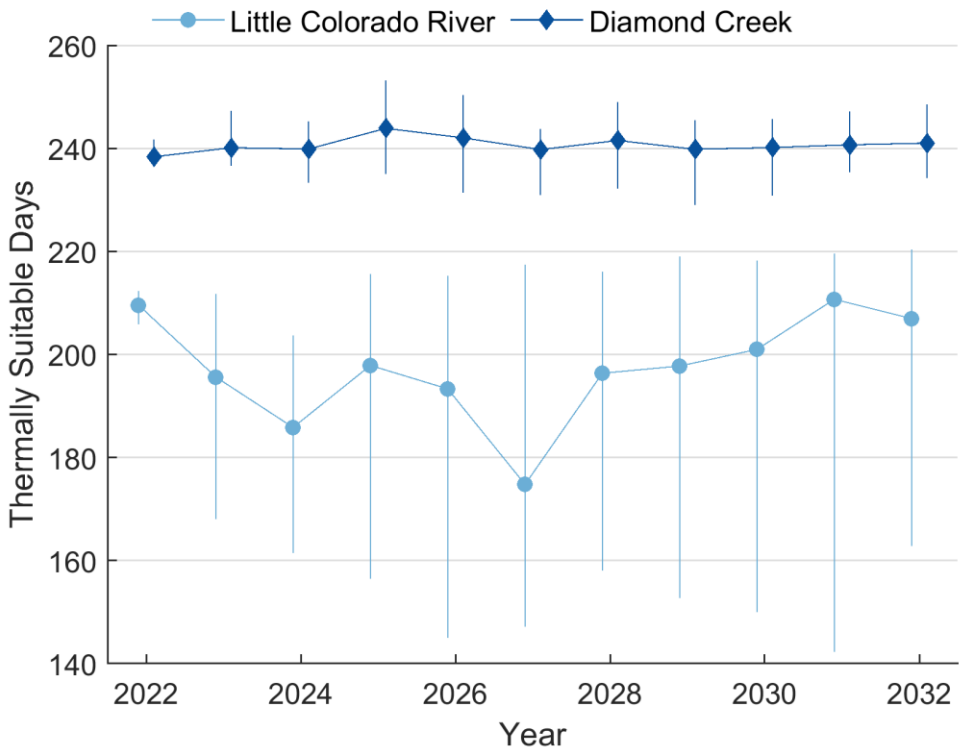

Figure 4-7. Thermally suitable days for humpback chub at three locations within Grand Canyon. Vertical lines on each series indicates the 25th and 75th percentiles and markers indicate the median for all 50 traces simulated.

The amount of river temperature variability is highly dynamic throughout the river basin for the 50 traces we simulated, with the greatest range of summer temperatures occurring in the Grand Canyon model (Figure 4-8). The influence of Lake Powell on downstream river temperature highlights the importance of establishing connections between water management models and water quality responses. Even more so, these results highlight the influence of the applied hydrology and the amount of uncertainty that remains in predicting river temperatures in certain portions of the Colorado River basin several years from now. Therefore, it may be more applicable to focus on shorter-term hydraulic and river temperature responses to specific flow regimes. While our model application used stepwise monthly flow information, sub-daily flow information could applied by resampling historical flows or developing idealized flow

patterns (Carron and Rajaram 2001) as long as monthly flow volumes remained the same. Sub-daily hydraulic variability would enable the evaluation of more ecosystem outcomes, such as spawning and nesting disruptions due to high velocities (Bestgen and Hill 2016; Martinez et al. 2014) or aquatic insect egg desiccation due to short-term hydropeaking effects on water levels (Kennedy et al. 2016). Alexander et al. (2013) also recommended ecosystem metrics that rely solely on flow information, such as spring peak daily flows from Flaming Gorge Dam to assess indicators for in-channel habitats and floodplain inundation to determine cottonwood recruitment in the lower Green River.

The methodology described here for handling distributed flows may also be improved in future updates. Assumptions about the location of distributed flows (applied uniformly throughout an entire reach) made here were needed due to the lack of spatial information in the water management model. However, some "common sense" restrictions could be placed on the locations these flows are applied to. For example, it is reasonable to assume that canyon-bound reaches have nearly zero diversion and return flows. As such, distributed inflows were not applied to the Yampa River branch. While this was done mainly for numerical stability (so the Yampa River would not go dry in late summer months), this is also a reasonable assumption as there is only one small water rights holder within this reach (Colorado's Decision Support System, 2021). More investigation into the geographic location of water rights holders could be made to justify restricting distributed flows to specific river reaches.

Lastly, an issue we ran into when simulating monthly flows over long river sections was an imperfect flow balances resulting from travel times. For example, modeled end of month volumes for inflow to Lake Powell we consistently different than

CRSS inflows due to 6-7 day travel times between the model boundaries (i.e., Flaming Gorge Dam, Yampa River near Deerlodge Park, and Colorado River near Cisco, UT) and Lake Powell. However, since the model coupling here is directional (i.e., no feed back to the water management model) this has little impact on the ability to assesses ecosystem metrics using process-based models and the methodology still allows for the quantification of heat flux dynamics that are needed to resolve climate change related impacts on aquatic thermal regimes (Arismendi et al., 2014; Diabat et al., 2013; Dugdale et al., 2017; Leach and Moore, 2019).

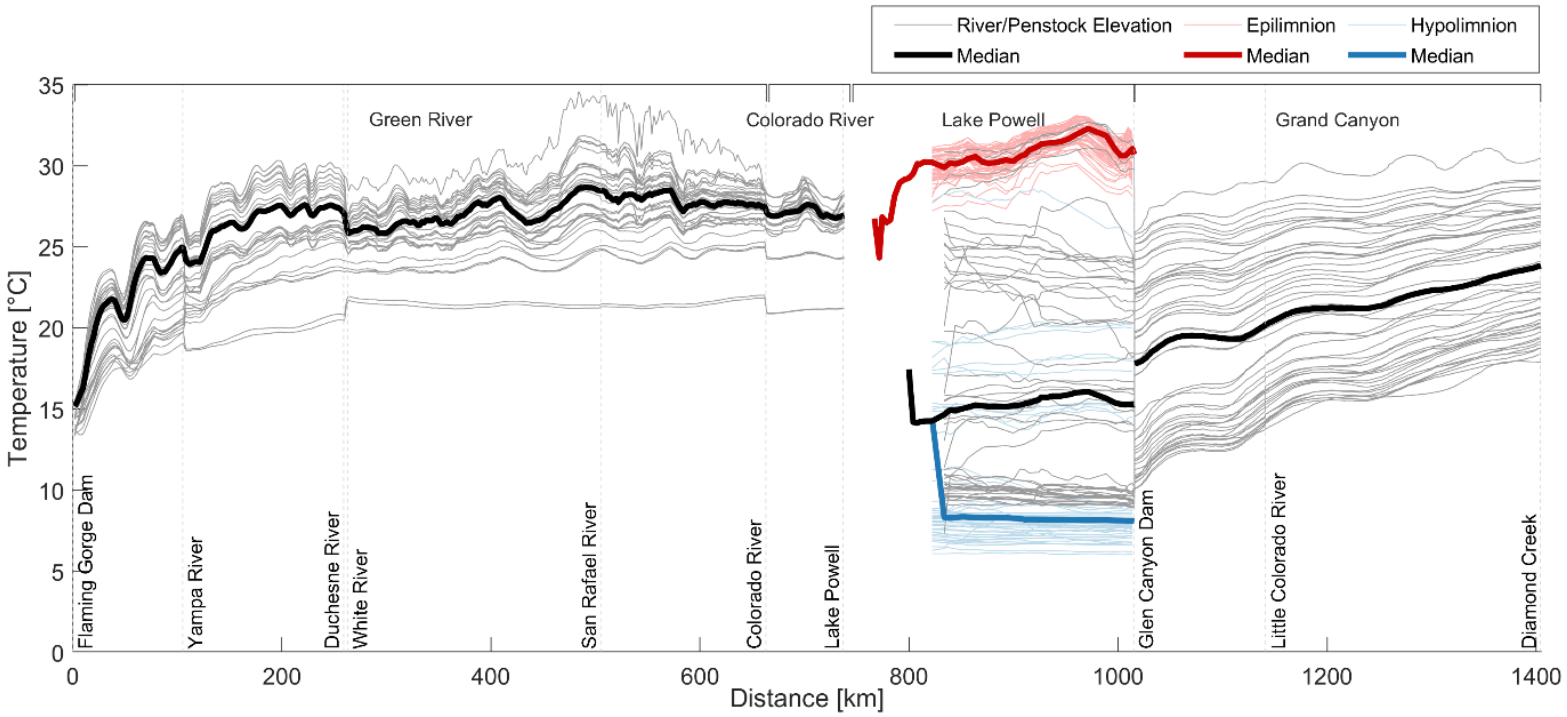

Figure 4-8. Longitudinal plot of temperature predictions for all 50 hydrologic traces on July 15, 2030, 6:00 pm. The date was arbitrarily chosen for illustration purposes. Our model was not setup to report temperatures of reservoir model cells that go dry due to reservoir drawdown, resulting in a gap between approximately 725 km and 825 km. Epilimnion lines (red) represent the variability in surface water temperatures. Hypolimnion lines (blue) represent the variability of temperatures deep in the reservoir, which was assumed to be at the bypass elevation (1028 m). Release temperatures from Lake Powell become the upstream boundary condition in the Grand Canyon model, which are slightly different than the penstock elevation (1058 m) temperatures shown here (gray) because release temperatures are calculated from multiple vertical cells near the penstocks.

4. Conclusion

While climate plays a major role in determining thermal regimes around the world, in regulated river basins, management decisions also play a significant part in determining thermal responses. Historically management decisions have focused on providing flood control, hydropower, irrigation, and flow regulation to downstream users. However, as water levels in reservoirs continue to be depleted as a result of higher demand and climate change induced drought, more attention has been given to the downstream consequences of warm water releases on aquatic ecosystems. Yet, there is relatively limited understanding of the spatial and temporal effects management decisions have on river temperatures throughout large river basins. Since anticipating changes in aquatic ecosystems over large spatial scales ultimately requires understanding the thermal responses to basin scale management decisions, it is important to have tools that interface with systems operation models. The model coupling and data assimilation approach presented here accomplishes this. Specifically, to overcome the spatial mismatches between the water management model and process-based temperature models we assigned two different flow categories (i.e., *point* or *distributed*) to the output flow information for simplistic linking to river and reservoir model elements. To ensure the flow balance was maintained within the process-based model, we repeated flow information and shifted time steps to create stepwise inputs that prevent interpolation between monthly flow volumes. We directly resampled historical weather and input temperature data based on the sequence of past flow years used in the water management model to provide consistency between hydrologic conditions, weather, and boundary condition and inflow temperatures required by the river and reservoir models. Lastly, we

tested this approach in a large section of the Colorado River basin and quantified select ecosystem indicators to illustrate the utility of high spatial and temporal resolution river temperature predictions. Overall, this approach is expected to enhance our understanding of temperature responses to management scenarios throughout a river basin. In addition, understanding temperature responses at high spatial and temporal resolutions bridges the known gaps between management and ecosystem modeling frameworks and allows for investigating climate and management implications to riverine ecosystems.

Acknowledgments

This work is part of the Future of the Colorado River Project, an interdisciplinary project from Utah State University's Center for Colorado River Studies. Funding was provided by the Walton Family Foundation, Utah Water Research Laboratory at Utah State University, David Bonderman, My Good Fund, and the National Science Foundation (EAR- 1343861). Any use of trade, product, or firm names is for descriptive purposes only and does not imply endorsement by the U.S. Government. Thanks to Jian Wang, Kevin Wheeler, Homa Salehabadi, and Brad Udall for help with modeling outputs and implementation. I am grateful for the comments from Charles Yackulic, David Tarboton, Caleb Buahin, and Jack Schmidt on earlier drafts that greatly improved this chapter.

References

Alexander, C., Olson, E., Carron, J., & Conservancy, P. by E. T. L. and H. C. for the C. R. P. of T. N. (2013). Integrated Water Management in the Colorado River Basin Evaluation of Decision Support Platforms and Tools Final Report. January 2013, 107.

Anderson, C. R., & Wright, S. A. (2007). Development and application of a water temperature model for the Colorado River below Glen Canyon Dam, Arizona. Proceedings of the American Institute of Hydrology, 23, 1–11.

Arismendi, I., Safeeq, M., Dunham, J. B., & Johnson, S. L. (2014). Can air temperature be used to project influences of climate change on stream temperature? Environmental Research Letters, 9(8), 084015. https://doi.org/10.1088/1748-9326/9/8/084015

Barnett, T., Malone, R., Pennell, W., Stammer, D., Semtner, B., & Washington, W. (2004). The effects of climate change on water resources in the west: Introduction and overview. Climatic Change, 62(1–3), 1–11. https://doi.org/10.1023/B:CLIM.0000013695.21726.b8

Bestgen, K. R., & Hill, A. A. (2016). River regulation affects reproduction, early growth, and suppression strategies for invasive smallmouth bass in the upper Colorado River basin. April, 84. http://www.coloradoriverrecovery.org/documents-publications/technical-reports/nna/Projects_FR115-140_2016.pdf

Bovee, K., Waddle, T., Talbert, C., Hatten, J., & Batt, T. (2008). Development and application of a decision support system for water management investigations in the upper Yakima River, Washington. 289.

Brown, T. C., Foti, R., & Ramirez, J. A. (2013). Projected freshwater withdrawals in the United States under a changing climate. Water Resources Research, 49(3), 1259–1276. https://doi.org/10.1002/wrcr.20076

Buahin, C. A., & Horsburgh, J. S. (2018). Advancing the Open Modeling Interface (OpenMI) for integrated water resources modeling. Environmental Modelling & Software, 108(April), 133–153. https://doi.org/10.1016/j.envsoft.2018.07.015

Buahin, C. A., Horsburgh, J. S., & Neilson, B. T. (2019). Parallel multi-objective calibration of a component-based river temperature model. Environmental Modelling & Software, 116(February), 57–71. https://doi.org/10.1016/j.envsoft.2019.02.012

Campbell, S. G., Hanna, R. B., Flug, M., & Scott, J. F. (2001). Modeling Klamath River System Operations for Quantity and Quality. Journal of Water Resources Planning and Management, 127(5), 284–294. https://doi.org/10.1061/(ASCE)0733-9496(2001)127:5(284)

Carron, J. C., & Rajaram, H. (2001). Impact of variable reservoir releases on management of downstream water temperatures. Water Resources Research, 37(6), 1733–1743. https://doi.org/10.1029/2000WR900390

Cole, T. M., & Wells, S. A. (2003). CE-QUAL-W2—A two- dimensional, laterally averaged, hydrodynamic and water quality model, version 3.2. U.S. Army Engineering and Research Development Center, Instruction Report EL-03-01.

Collier, M., Webb, R. H., & Schmidt, J. C. (1996). Dams and rivers: a primer on the downstream effects of dams. US Geological Survey Circular, 1126. https://doi.org/10.3133/cir1126

Colorado's Decision Support System. (2021). Division 6 Irrigated Lands Geodatabase. Colorado Department of Natural Resources. https://cdss.colorado.gov/gis-data/division-6-yampa/white/dist-47-north-platte

Daniels, M. E., & Danner, E. M. (2020). The Drivers of River Temperatures Below a Large Dam. Water Resources Research, 56(5), 1–15. https://doi.org/10.1029/2019wr026751

Dettinger, M., Udall, B., & Georgakakos, A. (2015). Western water and climate change. Ecological Applications, 25(8), 2069–2093. https://doi.org/10.1890/15-0938.1

Diabat, M., Haggerty, R., & Wondzell, S. M. (2013). Diurnal timing of warmer air under climate change affects magnitude, timing and duration of stream temperature change. Hydrological Processes, 27(16), 2367–2378. https://doi.org/10.1002/hyp.9533

Dibble, K. L., Yackulic, C. B., & Bestgen, K. R. (2020). Water temperature models, data and code for the Colorado, Green, San Juan, Yampa, and White rivers in the Colorado River basin. U.S. Geological Survey Data Release. https://doi.org/https://doi.org/10.5066/P9HFKV7Q

Dibble, K. L., Yackulic, C. B., Kennedy, T. A., Bestgen, K. R., & Schmidt, J. C. (2021). Water storage decisions will determine the distribution and persistence of imperiled river fishes. Ecological Applications, 31(2), 1–9. https://doi.org/10.1002/eap.2279

Dugdale, S. J., Hannah, D. M., & Malcolm, I. A. (2017). River temperature modelling: A review of process-based approaches and future directions. Earth-Science Reviews, 175(October), 97–113. https://doi.org/10.1016/j.earscirev.2017.10.009

Ehsani, N., Vörösmarty, C. J., Fekete, B. M., & Stakhiv, E. Z. (2017). Reservoir operations under climate change: Storage capacity options to mitigate risk. Journal of Hydrology, 555, 435–446. https://doi.org/10.1016/j.jhydrol.2017.09.008

Fredericks, B. J. W., Labadie, J. W., & Altenhofen, J. M. (1998). DECISION SUPPORT SYSTEM FOR CONJUNCTIVE STREAM-AQUIFER MANAGEMENT By

Jeffrey W. Fredericks; Member, ASCE, John W. Labadie,2 Member, ASCE, and Jon M. Altenhofen,3 Member, ASCE. 124(2), 69–78.

Gloss, S. P., & Coggins, L. G. (2005). Fishes of Grand Canyon. In S. P. Gloss, J. E. Lovich, & T. S. Melis (Eds.), State of the Colorado River Ecosystem (pp. 33–56). U.S. Geological Survey Circular 1282.

Graff, W. (1999). Dam Nation: A Geographic Census of American Dams and Their Large-Scale Hydrologic Impacts. 35(4), 1305–1311.

Gu, R., Montgomery, S., & Austin, T. AL. (1998). Quantifying the effects of stream discharge on summer river temperature. Hydrological Sciences Journal, 43(6), 885–904. https://doi.org/10.1080/02626669809492185

H.R.2030 - 116th Congress. (2019). Colorado River Drought Contingency Plan Authorization Act. (2019, April 16). https://www.congress.gov/bill/116th-congress/house-bill/2030/

Kegerries, R. B., Albrecht, B., McKinstry, M. C., Rogers, R. J., Valdez, R. A., Barkalow, A. L., Gilbert, E. I., Mohn, H. E., Healy, B., & Smith, E. O. (2020). Small-Bodied Fish Surveys Demonstrate Native Fish Dominance Over 300 Kilometers of the Colorado River Through Grand Canyon, Arizona. Western North American Naturalist, 80(2), 146. https://doi.org/10.3398/064.080.0202

Kennedy, T. A., Muehlbauer, J. D., Yackulic, C. B., Lytle, D. A., Miller, S. W., Dibble, K. L., Kortenhoeven, E. W., Metcalfe, A. N., & Baxter, C. V. (2016). Flow management for hydropower extirpates aquatic insects, undermining river food webs. BioScience, 66(7), 561–575. https://doi.org/10.1093/biosci/biw059

King, T. V., & Neilson, B. T. (2019). Quantifying reach-average effects of hyporheic exchange on arctic river temperatures in an area of continuous permafrost. Water Resources Research, 1–21. https://doi.org/10.1029/2018WR023463

Leach, J. A., & Moore, R. D. (2019). Empirical stream thermal sensitivities may underestimate stream temperature response to climate warming. Water Resources Research, 2018WR024236. https://doi.org/10.1029/2018WR024236

Li, D., Wrzesien, M. L., Durand, M., Adam, J., & Lettenmaier, D. P. (2017). How much runoff originates as snow in the western United States, and how will that change in the future? Geophysical Research Letters, 44(12), 6163–6172. https://doi.org/10.1002/2017GL073551

Lowney, C. L. (2000). Stream temperature variation in regulated rivers: Evidence for a spatial pattern in daily minimum and maximum magnitudes. Water Resources Research, 36(10), 2947–2955. https://doi.org/10.1029/2000WR900142

Martinez, P., Wilson, K., Cavalli, P., Crockett, H., Speas, D., Trammell, M., Albrecht, B., & Ryden, D. (2014). Upper Colorado River Basin Nonnative and Invasive Aquatic

Species Prevention and Control Strategy. February. http://www.coloradoriverrecovery.org/general-information/program-elements/nonnative-fish-management.html

McCabe, G. J., Wolock, D. M., Pederson, G. T., Woodhouse, C. A., & McAfee, S. (2017). Evidence that recent warming is reducing upper Colorado river flows. Earth Interactions, 21(10), 1–14. https://doi.org/10.1175/EI-D-17-0007.1

Meier, W., Bonjour, C., Wüest, A., & Reichert, P. (2003). Modeling the effect of water diversion on the temperature of mountain streams. Journal of Environmental Engineering, 129(8), 755–764. https://doi.org/10.1061/(ASCE)0733-9372(2003)129:8(755)

Mihalevich, B. A., Neilson, B. T., Buahin, C. A., Yackulic, C. B., & Schmidt, J. C. (2020). Water temperature controls for regulated canyon-bound rivers. Water Resources Research, 1–24. https://doi.org/10.1029/2020wr027566

Muth, R. T., Crist, L. W., LaGory, K. E., Hayse, J. W., Bestgen, K. R., Ryan, T. P., Lyons, J. K., & Valdez, R. A. (2000). Flow and Temperature Recommendations for Endangered Fishes in the Green River Downstream of Flaming Gorge Dam. September, 344.

Nilsson, C., & Renöfält, B. M. (2008). Linking Flow Regime and Water Quality in Rivers: a Challenge to Adaptive Catchment Management. Ecology and Society, 13(2), art18. https://doi.org/10.5751/ES-02588-130218

Null, S. E., Ligare, S. T., & Viers, J. H. (2013). A Method to Consider Whether Dams Mitigate Climate Change Effects on Stream Temperatures. Journal of the American Water Resources Association, 49(6), 1456–1472. https://doi.org/10.1111/jawr.12102

Olden, J. D., Leroy Poff, N., & Bestgen, K. R. (2006). Life-history strategies predict fish invasions and extirpations in the Colorado River Basin. Ecological Monographs, 76(1), 25–40. https://doi.org/10.1890/05-0330

Olden, J. D., & Naiman, R. J. (2010). Incorporating thermal regimes into environmental flows assessments: Modifying dam operations to restore freshwater ecosystem integrity. Freshwater Biology, 55(1), 86–107. https://doi.org/10.1111/j.1365-2427.2009.02179.x

Polehn, R. A., & Kinsel, W. C. (1997). Transient temperature solution for stream flow from a controlled temperature source. Water Resources Research, 33(1), 261–265. https://doi.org/10.1029/96WR03016

Risley, J. C., Constantz, J., Essaid, H., & Rounds, S. (2010). Effects of upstream dams versus groundwater pumping on stream temperature under varying climate conditions. Water Resources Research, 46(6). https://doi.org/10.1029/2009WR008587

Rossman, L. A. (2006). Storm water management model quality assurance report: Dynamic wave flow routing. Storm Water Management Model Quality Assurance Report, EPA/600/R-06/097, 1–115. http://www.epa.gov/water-research/storm-water-management-model-swmm

Sabater, M. J. (2019). ERA5-Land hourly data from 1981 to present. Copernicus Climate Change Service (C3S) Climate Data Store (CDS). (Accessed on 01-Oct-2020). https://doi.org/10.24381/cds.e2161bac

Salehabadi, H., Tarboton, D., Kuhn, E., Udall, B., Wheeler, K., Rosenberg, D., Goeking, S., Schmidt, J. C., Salehabadi, H., Tarboton, D., Kuhn, E., Udall, B., Wheeler, K., Rosenberg, D., Goeking, S., Schmidt, J. C., & Summary, E. (2020). The Future Hydrology of the Colorado River Basin. Center for Colorado River Studies, white paper no. 4, 108.

Sapin, J. R., Saito, L., Dai, A., Rajagopalan, B., Blair Hanna, R., & Kauneckis, D. (2017). Demonstration of Integrated Reservoir Operations and Extreme Hydroclimate Modeling of Water Temperatures for Fish Sustainability below Shasta Lake. Journal of Water Resources Planning and Management, 143(10), 04017062. https://doi.org/10.1061/(ASCE)WR.1943-5452.0000834

Schmadel, N. M., Neilson, B. T., & Heavilin, J. E. (2015). Spatial considerations of stream hydraulics in reach scale temperature modeling. Water Resources Research, 51(7), 5566–5581. https://doi.org/10.1002/2015WR016931

Simons, M., Podger, G., & Cooke, R. (1996). IQQM - A hydrologic modelling tool for water resource and salinity management. Environmental Software, 11(1–3), 185–192. https://doi.org/10.1016/S0266-9838(96)00019-6

Tyus, H. M. (1991). Ecology and management of Colorado squawfish. In W. L. Minckley & J. E. Deacon (Eds.), Battle against extinction: native fish management in the American Southwest (pp. 379–402). University of Arizona Press.

U.S. Bureau of Reclamation. (2012). Colorado River Basin Water Supply and Demand Study. 85.

U.S. Bureau of Reclamation. (2021). Colorado River Basin Natual Flow and Salt Data. Colorado River Basin Natural Flow Database. https://www.usbr.gov/lc/region/g4000/NaturalFlow/current.html

U.S. Department of the Interior. (2007). Recod of decision: Colorado River interim guidelines for lower basin shortages and the coordinated operations for Lake Powell and Lake Mead, Final environmental impact statement. Office of the Secretary of Interior, Washington, D.C.

U.S. Fish and Wildlife Service. (1987). Recovery Implementation Program for Endangered Fish Species in the Upper Colorado River Basin.

Udall, B., & Overpeck, J. (2017). The twenty-first century Colorado River hot drought and implications for the future. Water Resources Research, 53(3), 2404–2418. https://doi.org/10.1002/2016WR019638

USACE. (2019). U.S. Army Corps of Engineers: National Inventory of Dams. http://nid.usace.army.mil/cm_apex/f?p5838:12

Van Haverbeke, D. R., Stone, D. M., Dodrill, M. J., Young, K. L., & Pillow, M. J. (2017). Population Expansion of Humpback Chub In Western Grand Canyon and Hypothesized Mechanisms. The Southwestern Naturalist, 62(4), 285–292. https://doi.org/10.1894/0038-4909-62.4.285

Van Haverbeke, D. R., Young, K. L., Pillow, M. J., & Williams, O. (2020). Monitoring humpback chub in the Little Colorado River and Colorado River, Grand Canyon, Fall 2019. Arizona Fish and Wildlife Conservation Office, Flagstaff, Arizona, USFWS Docu(August).

Vernieu, W. S., Hueftle, S. J., & Gloss, S. P. (2005). Water quality in Lake Powell and the Colorado River. In S. P. Gloss, J. E. Lovich, & T. S. Melis (Eds.), State of the Colorado River Ecosystem (pp. 69–85). U.S. Geological Survey Circular 1282.

Wang, J., Rosenberg, D. E., Wheeler, K. G., & Schmidt, J. C. (2020). Managing the Colorado River for an Uncertain Future. Center for Colorado River Studies, white paper no. 3, 1–30. https://tinyurl.com/ColoradoUncertaintyFeedback

Wang, J., & Schmidt, J. C. (2020). Stream flow and Losses of the Colorado River in the Southern Colorado Plateau. Center for Colorado River Studies, white paper no. 5, 26.

Ward, J. V., & Stanford, J. A. (1983). The serial discontinuity concept of lotic ecosystems.

Webb, B. W., & Zhang, Y. (2004). Intra-annual variability in the non-advective heat energy budget of Devon streams and rivers. Hydrological Processes, 18(11), 2117–2146. https://doi.org/10.1002/hyp.1463

Wheeler, K. G., Schmidt, J. C., Rosenberg, D. E., & Tarboton, D. G. (2019). Water Resource Modelling of the Colorado River - Present and Future Strategies (Issue 2).

Wheeler, K., Kuhn, E., Bruckerhoff, L., Udall, B., Wang, J., Gilbert, L., Goeking, S., Mihalevich, B., Neilson, B., Salehabadi, H., & Schmidt, J. C. (2021). Alternative Management Paradigms for the Future of the Colorado and Green Rivers. Center for Colorado River Studies, white paper no. 6, 91.

Williams, N. T. (2007). Modeling dissolved oxygen in Lake Powell using CE-QUAL-W2. Civil and Environmental Engineering M.S. Thesis, Brigham Young University, Provo UT., 120.

Williams, N. T. (2009). Projecting Temperature in Lake Powell and the Glen Canyon Dam Tailrace. Proceedings of the Colorado River Basin Science and Resource Management Symposium, 9.

Woodhouse, C. A., Pederson, G. T., Morino, K., McAfee, S. A., & McCabe, G. J. (2016). Increasing influence of air temperature on upper Colorado River streamflow. Geophysical Research Letters, 43(5), 2174–2181. https://doi.org/10.1002/2015GL067613

Yackulic, C. B., Yard, M. D., Korman, J., & Haverbeke, D. R. (2014). A quantitative life history of endangered humpback chub that spawn in the <scp>L</scp> ittle <scp>C</scp> olorado <scp>R</scp> iver: variation in movement, growth, and survival. Ecology and Evolution, 4(7), 1006–1018. https://doi.org/10.1002/ece3.990

Zagona, E. A., Fulp, T. J., Shane, R., Magee, T., & Goranflo, H. M. (2001). RIVERWARE: A GENERALIZED TOOL FOR COMPLEX RESERVOIR SYSTEM MODELING1. JAWRA Journal of the American Water Resources Association, 37(4), 913–929. https://doi.org/10.1111/j.1752-1688.2001.tb05522.x

CHAPTER 5

CONCLUSION

A primary determinant of habitat suitability for aquatic ecosystems is instream temperature. However, anthropogenic alterations to riverine environments have caused significant disturbances to natural flow and temperature regimes. Going forward, the decisions water managers make, such as where to store water and how much water to divert, to address declines in annual runoff due to climate change may reshape existing habitat and food chain connections. Through the development of new modeling approaches that are integrated into process-based river and reservoir temperature models, this dissertation provides a framework for connecting water management decisions to water temperature responses over topographically complex river basins with limited weather data. Specifically, this dissertation describes the development and application of a process-based river temperature model in the canyon-bound Colorado River in Grand Canyon to estimate dominant heat fluxes and understand the influence of topographic shading (Chapter 2), evaluates new data products to enable detailed river temperature modeling over large, weather data sparse regions (Chapter 3), and develops a data assembly and coupled modeling approach for linking water management models to basin scale river and reservoir temperature models (Chapter 4).

In Chapter 2, the dominant heat fluxes controlling river temperature in the Colorado River in Grand Canyon are identified. In the upstream portion of the model domain (RM30 and RM61), boundary condition water temperature was found to be the most influential on river temperatures regardless of the time of year, while further down-

stream (RM88, RM167, and RM225), boundary condition flow, net shortwave radiation, and air temperature were dominant, but varied significantly by season. The topographic controls on shortwave radiation were accurately estimated using the algorithm developed to predict shade. Topographic shading increased the relative importance of heat fluxes that are generally small in large temperate rivers. The relative contribution from most of the heat fluxes (9 of the 12) represented within the model were highly variable over time and space, indicating the dynamic nature of heating and cooling mechanisms in these systems. While the model performed well over high and low flow periods, predictions during low flow periods highlighted the importance of having accurate tributary information and the need for spatially varying meteorological information.

Building on the key findings in Chapter 2, Chapter 3 evaluated the feasibility of climate reanalysis datasets (CRDs) for supplying spatially varying weather inputs to river temperature models for the Grand Canyon and Green River while considering CRD spatial resolution influences. Focusing on the ERA5-Land CRD, this work first determined that physics-based elevation corrections improved the representation of certain variables when compared to observations at weather stations on the rim and adjacent to the Colorado River in Grand Canyon. Particularly, elevation corrections improved air temperature and relative humidity, but negatively impacted wind speed estimates. River temperature predictions in Grand Canyon were found to have lower errors when using elevation corrected ERA5-Land inputs versus the ground-based counterparts. When applied to the Green River, temperature prediction errors were lowest and statistically different when using a coarsened spatial resolution of ERA5-Land, which was attributed to elevation corrections inflating air temperatures and lowering wind

speeds relative to other input datasets. While ERA5-Land was coarsened from 0.1° to 1.0° longitude and latitude grids, differences in temperature predictions between the two inputs were minimal, signaling that data requirements may be reduced when modeling over significantly large domains.

With an understanding of temperature controls in canyon-bound rivers (Chapter 2) and ability to model temperatures over large geographic regions (Chapter 3), the focus of Chapter 4 was aimed at linking water management models to river and reservoir temperature predictions across entire basins. This included the development of a model coupling and data assimilation approach that enables long-term river temperature forecasts based on outputs from a water management model. Spatial mismatches between the water management model and process-based temperature models were overcome by assigning two different flow categories (i.e., *point* or *distributed*) to the output flow information for simplistic linking to river and reservoir model elements. The temporal resolution of flow information was also repeated to create stepwise inputs to be used within the process-based models to prevent interpolation between monthly flow volumes. Historical weather and input temperature data were directly resampled based on the sequence of past flow years used in the water management model to provide consistency between hydrologic conditions, weather, and boundary condition and inflow temperatures required by the river and reservoir models. This approach was tested over large river sections of the Colorado River basin and select ecosystem metrics were quantified to illustrate the utility of high spatial and temporal resolution river temperature predictions.

Combining the methods and findings from this dissertation allow us to link water management decisions impacts on instream water quality over large, data limited and

topographically complex regions. While this research was focused on the characteristics and existing challenges in the Colorado River basin, many basins face similar water resources and ecosystem concerns. The work here provides a foundation for water managers and ecologists to better understand how future changes in climate, hydrology, and management decisions may impact aquatic ecosystems in any river system.

CHAPTER 6

ENGINEERING SIGNIFICANCE

The work presented in this dissertation makes significant contributions in linking the fields of water resources engineering and water quality modeling. The development of advanced dynamic river temperature modeling methods that account for the detailed influences of topography provides insight into mechanistic controls on water temperatures in deep canyons. Incorporating spatially varying weather information with physics-based correction methods that relate weather variables and elevation provides even greater insight regarding spatial and temporal patterns where data are commonly not available. Linking these tools with water management models advanced our understanding of how water management decisions in large, highly regulated basins influences thermal regimes historically and under future management scenarios. Furthermore, these river and reservoir temperature modeling tools and frameworks are adaptive and transferable to other river systems.

Complex topography is not unique to the Colorado River basin and many other rivers around the world flow through deep canyons or mountainous valleys. These landscape features play a significant role in altering shortwave radiation inputs to rivers and streams. Namely, topographic shading can be highly variable and can greatly reduce the amount of direct shortwave radiation received at the water surface. The orientation of the river, time of year, and time of day are all factors that determine the amount of shortwave radiation received at any given time. Similarly, the steep landscape features (e.g., cliff walls) common in canyon-bound rivers can contribute longwave radiation to

the water surface. These radiative factors can dramatically influence the thermal responses of rivers. To provide more complete estimates of the radiative heat balance, this work developed algorithms for estimating spatiotemporal shading dynamics and methods for incorporating these factors in a process-based modeling framework. This included a methodology for partitioning shortwave radiation into individual components (direct, diffuse, land-reflected) to improve our understanding of the importance of diffuse shortwave radiation in canyon bound rivers, such as the Grand Canyon portion of the Colorado River. The incorporation of longwave radiation from terrain features into the model also highlighted that these sources contribute a small, but not insignificant, amount of heat to the river and justifies inclusion of these fluxes in other systems to provide a more holistic representation of the factors controlling river temperatures.

This research also evaluated the application of climate reanalysis datasets for input weather data to process-based models. These models traditionally rely on locally measured meteorological data, however, the number of long-term hydrological and meteorological networks has been highly variable over the last two decades and some regions lack observations all together. While such data limitations reduce our ability to confidently apply process-based models, quantifying heat flux dynamics is still needed to resolve climate related impacts on aquatic thermal regimes. The methods for elevation correcting climate reanalysis data can be applied consistently over topographically complex terrain and were validated over large geographic regions in the Colorado River basin. The findings of this work indicate that climate reanalysis datasets are a reasonable surrogate for providing historical meteorology when ground-based weather data are limited. Further, these data can even improve river temperature predictions. These results

bridge existing data gaps which stand to advance our understanding of temperature drivers and ecosystem responses in rivers around the world. For example, river temperature models can be developed in regions that have no, or very limited, historical weather information. This in turn allows for greater assessment of climate related impacts on aquatic thermal regimes and the ability to design effective management strategies to mitigate negative ecosystem outcomes.

While climate plays a major role in determining thermal regimes around the world, in regulated river basins, management decisions also play a significant part in determining thermal responses at hourly and daily scales. However, water managers use tools to guide decisions that generally have coarser spatial and temporal (e.g., monthly) scales that are more practical for making large basin-wide decisions regarding water supply distribution. As climate change induced drought is likely to change hydrologic patterns in many parts of the world, water managers may need to rethink where water is stored and the timing of abstractions and redistributions throughout a basin. This highlights the disconnect between water management and aquatic ecosystems. Particularly, what are the consequences of management decisions on instream temperatures at temporal resolutions relevant to aquatic ecosystems (i.e., daily or hourly)? There have been limited advances toward linking water management models to process-based river and reservoir temperature models for the purpose of obtaining high resolution hydraulic and water quality information. The methods presented in this dissertation fills this gap by describing a generic model coupling and data assembly approach for forecasting river and reservoir temperatures based on water management model forecasts. While this framework was tested in the Colorado River basin, these

methods are adaptive and transferable to other rivers enabling greater assessment of flow regulation and climate change impacts on ecosystems around the world.

In the context of the Colorado River basin specifically, the work here is expected to help water managers and ecologists better understand the ecological implications of future climate and hydrologic patterns. The basin provides critical habitat to three federally listed endangered native fish species but is also host to several warm and cold water nonnative fish communities, some of which are of economic value. Particularly, the introduction of brown and rainbow trout downstream from large reservoirs with hypolimnetic releases provides unique and desirable fishing opportunities in geographic regions that could otherwise not support cold water species. However, this also introduces resource competition and predation between native and nonnative fishes. While climate change is anticipated to warm river temperatures throughout the basin, potentially benefiting the native fishes that evolved under warmer thermal regimes, there are still unknown risks to both native and nonnative fish species. For example, warmer river temperatures may result in expanding the distribution and abundance of warm water nonnative fishes (i.e., smallmouth bass *Micropterus dolomieu*, green sunfish *Lepomis cyanellus*, and walleye *Stizostedion vitreum*) increasing the strain on existing native fish habitats. While the ecosystem impacts of different thermal regimes remain uncertain, understanding how different management decisions impact release temperatures from large reservoirs, such as Flaming Gorge and Lake Powell, while understanding the mechanisms that control downstream river temperature provides a framework for evaluating the potential ecosystem responses to changing climate and hydrology.

CHAPTER 7

RECOMMENDATIONS FOR FUTURE WORK

Chapter 2 of this dissertation provides an initial assessment of the dominant heat fluxes responsible for controlling river temperatures in highly regulated systems that flow through topographically complex and geographically remote regions. River temperature predictions were significantly improved when using high spatiotemporal resolution shading factors. Using these detailed shading estimates, the heat fluxes controlling temperatures in Grand Canyon were found to be highly variable over space and time, primarily due to the altered shortwave radiation dynamics and hydropeaking flow conditions. This analysis should be extended to similar rivers to determine whether the findings presented here are consistent in other systems. Specific to the Grand Canyon model, further investigation into intervening flows and associated temperatures from springs or other groundwater contributions could be warranted. Springs in Grand Canyon contribute approximately 8% of the total annual flow, however, only 4% of this flow is gaged (Chapter 2; Wang and Schmidt, 2020). Identifying the source locations, quantity, and temperatures of the remaining 4% may improve river temperature predictions at some locations, particularly during low flow periods.

A clear extension of Chapter 3, where the ERA5-Land Climate Reanalysis dataset was used to supply weather information to river temperature models in Grand Canyon and the Green River, is to evaluate the viability of using this dataset to model temperatures in smaller tributaries or other smaller river basins. Smaller streams and rivers are more sensitive to climate inputs because there is less thermal inertia. Validating

the ERA5-Land Climate Reanalysis dataset in smaller rivers may improve the ability to forecast temperature changes in variable sized rivers situated in data sparse regions (e.g., arctic regions, developing nations, etc.). Furthermore, other climate reanalysis datasets should be tested to determine the variability between reanalysis products on water temperature predictions. This is crucial because some datasets may be better suited over others due to their coverage, resolution, and accessibility. Lastly, improvements to wind speed elevation correction methods could be addressed to better estimate latent and sensible heat fluxes. While these heat fluxes are generally small, wind speed representation may improve river temperature predictions over specific seasons, specifically in the Grand Canyon. Furthermore, better wind speed and direction estimates may make these datasets more applicable to process-based reservoir models, such as CE-QUAL-W2, which are sensitive to wind induced mixing.

Building on the water management and temperature modeling approach described in Chapter 4, development of algorithms that transform monthly average flow volumes from the water management model to historical discharge patterns at hourly or daily resolution should be conducted. Higher temporal resolution flow information at some model boundary conditions (e.g., below reservoirs) would enable greater insights into discharge related ecosystem metrics, such as nest disrupting velocities or insect egg desecration (Bestgen and Hill, 2016; Kennedy et al., 2016), throughout the Colorado River basin. The spatial representation of distributed inflows could also be improved upon by analyzing water rights data for various states. Water rights geodatabases could be used to identify locations that have the most abstractions and diversions. This analysis

could be used to assign distributed flows from the water management model to more appropriate and “common-sense” locations (i.e., exclude canyon reaches).

Lastly, more attention to reservoir modeling is needed. Improving the representation of mixing dynamics in the Lake Powell model could be conducted to evaluate additional ecosystem and water quality related metrics. For example, improved predictions of salinity (collectively pooled as TDS) are needed given the potential increase in concentration as reservoir levels are reduced, which poses a significant threat to drinking water, irrigation, and aquatic habitats (Deemer et al., 2020). Furthermore, incorporation of the Flaming Gorge Reservoir model among the development of new reservoir models could be used to expand the modeling domain used in Chapter 4. This would enable an even more holistic understanding of management decisions in other critical habitat areas of the Colorado River basin.

References

Bestgen, K. R., and Hill, A. A. (2016). “River regulation affects reproduction, early growth, and suppression strategies for invasive smallmouth bass in the upper Colorado River basin.” (April), 84.

Deemer, B. R., Stets, E. G., and Yackulic, C. B. (2020). “Calcite precipitation in Lake Powell reduces alkalinity and total salt loading to the Lower Colorado River Basin.” Limnology and Oceanography, 65(7), 1439–1455.

Kennedy, T. A., Muehlbauer, J. D., Yackulic, C. B., Lytle, D. A., Miller, S. W., Dibble, K. L., Kortenhoeven, E. W., Metcalfe, A. N., and Baxter, C. V. (2016). “Flow management for hydropower extirpates aquatic insects, undermining river food webs.” BioScience, 66(7), 561–575.

Wang, J., and Schmidt, J. C. (2020). “Stream flow and Losses of the Colorado River in the Southern Colorado Plateau.” Center for Colorado River Studies, (white paper no. 5), 26.

APPENDICES

APPENDIX A

Supporting Information for Chapter 2

Text A-1: Fraction of diffuse shortwave radiation

Measured shortwave radiation outside of the canyon was disaggregated into direct ($\hat{J}_{sn,dir}$) and diffuse ($\hat{J}_{sn,diff}$) components using a correlation equation that predicts the fraction of diffuse radiation (k_d; Eqn. 2-7) based on the clearness index (k_t; Eqn. 2-6). The correlation equations tested include:

Erbs et al. (1982):

$$k_d = \begin{cases} 1 - 0.09k_t, & k_t \leq 0.22 \\ 0.9511 - 0.1604k_t + 4.39k_t^2 - 16.64k_t^3 + 12.34k_t^4, & 0.22 < k_t \leq 0.8 \\ 0.165, & k_t > 0.80 \end{cases} \quad \text{(A-1)}$$

Orgill & Hollands (1977):

$$k_d = \begin{cases} 1 - 0.249k_t, & k_t \leq 0.35 \\ 1.577 - 1.84k_t, & 0.35 < k_t \leq 0.75 \\ 0.177, & k_t > 0.75 \end{cases} \quad \text{(A-2)}$$

Lam & Li (1996):

$$k_d = \begin{cases} 0.977, & k_t \leq 0.15 \\ 1.273 - 1.361k_t, & 0.15 < k_t \leq 0.70 \\ 0.273, & k_t > 0.70 \end{cases} \quad \text{(A-3)}$$

Text A-2: Shading algorithm

Our approach to computing spatiotemporal shade factors is based on the procedure described by Yard et al. (2005), but modified slightly so that the entire shortwave radiation spectrum can be scaled. The first step computes elevation angles (Ψ_E; Figure 2-1) at locations spaced every 100 m along the river centerline. Ψ_E is defined as the largest angle measured from the water surface to the highest topographic feature. At each point, Ψ_E is determined at 1° increments over a 360° azimuth circle using a 10-m resolution digital elevation model (DEM) clipped to a 10-km buffer of the river centerline. This process returns a matrix containing 360 Ψ_E values for every location along the river centerline. The second step computes solar geometries of zenith angles (θ)

and azimuth angles (Φ) for each location at 15-minute increments for each day of the year using the Modular Distributed Watershed Educational Toolbox (MOD-WET; (Huning and Margulis 2015). For each time step (t), the algorithm returns Ψ_E in the direction of Φ, interpolating when needed. Because Ψ_E is based on a different datum than θ, Ψ_E is subtracted from 90° to get an angle measured from the vertical datum, referred to as illumination angle (Ψ_I). Ψ_I is then compared directly to θ at time t (i.e., θ_t), where $\Psi_I > \theta_t$ indicates no shade and $\Psi_I < \theta_t$ indicates shade. This results in a binary matrix where each x,y location has a time series of Boolean values that can be repeated for any year. Lastly, the binary values are averaged over space for their respective model cell (typically 1-km long) resulting in a shade factor ($S_{f,c}$) that represents the fraction of a cell being shaded at a given time.

Text A-3: Fluid friction flux

Heat generated through internal fluid friction was not in the original channel solute and heat (CSH) component of HydroCouple. We adapted the CSH component to include this heat flux by following the formulation by Theurer et al. (1984) as:

$$J_f = 9805\ Q\ \frac{S}{B} \qquad \text{(A-4)}$$

where J_f is the fluid friction flux (W/m^2), Q is the stream discharge (m^3/s), S is the stream gradient, and B is the channel top width (m).

Text A-4: Background on the Colorado River in Grand Canyon

The completion of Glen Canyon Dam (GCD) in 1963 and subsequent filling of Lake Powell has significantly affected the downstream aquatic environment because the Colorado River's flow regime through Grand Canyon is entirely determined by releases

from the reservoir. The annual release schedule is set by the Law of the River, which is the informally named assemblage of bi-national treaties, interstate compacts, federal laws, administrative agreements, and records-of-decision associated with environmental impact statements. In the Colorado River basin, water volumes are commonly measured and reported in million acre-feet (MAF). Annual releases are managed to be 8.23 MAF (322 m^3/s), but can vary year-to-year depending on operational tiers established by the 2007 interim guidelines (U.S. Department of the Interior 2007). Monthly and daily reservoir releases are primarily determined by regional demands for hydroelectricity generated at the large dams and agreements that restrict the efficiency of hydropower production in order to minimize adverse impacts to downstream ecosystems. In the Colorado River network, the largest demands for hydroelectricity are in winter and summer, and the lowest demands are in spring and fall (Wright et al. 2005). Consequently, in the Grand Canyon, monthly total streamflow is typically largest in December, January, July, and August.

In addition to the changes in the flow and sediment supply regimes that have been extensively described (e.g., Grams et al., 2015; Topping et al., 2000, 2003), regulation has also dramatically changed the thermal regime of the Colorado River from a seasonally warm river in summer to a predominantly cold river in summer (Vernieu et al. 2005). The Colorado River once had ice on its surface in some places during winter, but this no longer occurs. Pre-dam temperatures of the Colorado River at Lees Ferry (Figure 2-2) averaged 14 °C, ranging from 0 °C to 27 °C (Anderson and Wright 2007; Vernieu et al. 2005). Since 1980, when the reservoir reached capacity for the first time, temperatures at Lees Ferry have averaged 10.3 °C, ranging from 7.0 °C to 16.5 °C. Colder downstream

temperatures in the post-dam era are due to penstock withdrawals from the hypolimnion, which maintains temperatures between 6 °C and 9 °C when the reservoir is relatively deep (Vernieu et al., 2005; Figure A-13). Instead of the warmest river temperatures occurring in July or August, as was the case in the pre-dam era, downstream temperatures are now highest between October and December when reservoir levels are generally lower and fall turnover mixes the relatively warm epilimnion with the hypolimnion. For instance, the warmest temperature at Lees Ferry (16.5 °C) occurred in October of 2005, coinciding with the lowest reservoir levels in Lake Powell since filling. Seasonal river temperature patterns still exist today, however, releases from the relatively stable hypolimnion has greatly reduced the annual variation (Vernieu et al., 2005; Figure A-13). Several endemic fish species from Grand Canyon, including two federally listed fish species (i.e., humpback chub (*Gila cypha*) and razorback sucker (*Xyrauchen texanus*) and three extirpated fish species (i.e., Colorado pikeminnow (*Ptychocheilus lucius*), roundtail chub (*Gila robusta*) and bonytail chub (*Gila elegans*), have declined in response to introduction of non-native fish and the direct impacts of the current regulated flow and post-dam water temperature regime.

Many datasets have also been published for Grand Canyon due to the need to understand the aquatic ecosystem within the national park, making the region very data rich. Flow measurements at Lees Ferry and above Bright Angle Creek (approximately 141 km downstream) started in the early 1920's. Additional main channel gages were established decades later in the 1980's. Continuous measurements of river temperature began in the early 1990's with 10 stations spaced approximately 50 km apart. Tributaries to the Colorado River have also been monitored to provide flow, water temperature, and

sediment flux data. Main channel and tributary data have been used to inform and evaluate experimental reservoir releases (unrelated to hydropower production) implemented to improve beaches for recreational users and benefit fish populations. One implementation of this was during the summer of 2000 and fall of 2001, where low steady flows were released to raise summer river temperature to benefit native fish (Schmidt et al. 2007; Trammell et al. 2002). In the mid 2000's the number of main channel and tributary monitoring sites were reduced. Currently, active monitoring includes five main channel flow gaging sites, 9 main channel water temperature sites, and 5 tributary sites recording flow and water temperature measurements (Figure 2-2; Table A-1). More information about monitoring efforts can be found in Vernieu et al. (2005) and data can be obtained from the US Geological Survey Grand Canyon Monitoring and Research Center (GCMRC; www.gcmrc.gov).

In addition to the rich amount of data associated with the Colorado River, extensive weather data from within Grand Canyon and surrounding region also exist. Meteorological observations of air temperature and precipitation have been recorded at daily and sub-daily resolution as part of the National Weather Service Cooperative Observer (COOP) network at Lees Ferry since 1928, in Phantom Ranch (located approximately 1 km upstream from the main channel in Bright Angle Creek) since 1935, and at Page, Arizona since 1957 (Figure 2-2; Caster & Sankey, 2016). Additional parameters of wind speed and relative humidity were added to these sites at later dates. Weather data has also been collected by the GCMRC within Grand Canyon at the river elevation intermittently since 2003 to relate geomorphic changes to meteorological events (Caster et al. 2014; Draut and Rubin 2006). Along the north and south rim of Grand

Canyon are several weather stations that are part of the wildland fire remote automated weather station (RAWS) network. Some RAWS network sites have existed since the early 1990's and are to our knowledge, the only sources for sub-daily shortwave radiation measurements within the region (Figure 2-2; Table A-4).

Accompanying the extensive amount of data for the Grand Canyon region are models to estimate Colorado River flow, river temperature, sediment transport, and bioenergetics downstream of Glen Canyon Dam. The first river temperature model, motivated by the need to determine the influence of water release temperatures from Glen Canyon Damon downstream river temperatures, looked into the effect of a multi-level penstock withdraw structure to warm reservoir releases and promote downstream warming (Ferrari 1987). They found that warming would occur, but not to pre-dam levels. The addition of a temperature control device (TCD) at Glen Canyon Damhas been the subject of many subsequent studies (Garrett et al. 2003; Petersen and Paukert 2005; U.S. Bureau of Reclamation 1999). Anderson and Wright (2007) developed a temperature model to explore the effects of dam operations on the downstream thermal regime at an hourly time step. Their model was based on the equilibrium temperature concept, which is the water temperature reached when the sum of the heat fluxes across the air–water interface equals zero (Buendia et al. 2015; Edinger et al. 1968). Anderson and Wright (2007) used Lake Powell release flow and water temperature, air temperature, and wind speed as model inputs. To account for longitudinal dispersion of flow velocities in Grand Canyon (Graf 1995), they used the unsteady-flow model from Wiele and Griffin (1997). Their key finding was that flow volumes play the most substantial role in determining water temperature patterns downstream. Later, Wright et al. (2009) created a

less sophisticated version of the Anderson & Wright (2007) model, estimating river temperature at a monthly time step to allow for simplified evaluations of alternative dam operations considered by the Glen Canyon Adaptive Management Program (GCDAMP). Most recently, Valdez et al. (2013) assessed the effects of adding a TCD to Glen Canyon Dam on downstream river temperatures, similar to Ferrari (1987), but also looked at potential water temperature effects on native and nonnative fish species.

Text A-5: Heat from lateral inflows

In order for lateral inflow contributions to be comparable with other heat fluxes, the energy contributed from tributaries (J_{trib}) and distributed inflows (J_{dist}) was calculated as the apparent sensible heat flux (Kurylyk et al. 2016). This approach uses the main channel temperature as a relative thermal datum allowing for the influence of lateral inflows on instream temperature to be quantified. The formulation for this approach is:

$$J_{lat,c} = J_{trib,c} + J_{dist,c} \quad \text{(A-5)}$$

$$J_{trib,c} = \frac{\rho_w c_p Q_{trib,c}(T_{trib,c} - T_c)}{A_{s,c}} \quad \text{(A-6)}$$

$$J_{dist,c} = \frac{\rho_w c_p Q_{dist,c}(\mathrm{T}_{dist,c} - T_c)}{A_{s,c}} \quad \text{(A-7)}$$

where (c) is the model cell index, $J_{lat,c}$, $J_{trib,c}$, $J_{dist,c}$ is the heat flux (positive or negative) being contributed to the model cell (W/m^2), Q_{trib} is the external flow from a tributary (m^3/s), Q_{dist} is the distributed flow (m^3/s), T_{trib} is the tributary temperature (°C), T_{dist} is the distributed flow temperature (°C; assumed to be the mean annual air temperature from within Grand Canyon, Table A-3), T_c is the water temperature of the model cell (°C), ρ_w is the water density (kg/m^3), c_p is the specific heat capacity of water (J/kg/°C), and $A_{s,c}$ is the surface area (m^2) of the model cell.

Text A-6: Excluded heat transfer mechanisms

Other mechanisms could be explored and potentially incorporated within the model in order to improve temperature predictions. Additionally, investigation of model residuals at sub-daily time scales may provide further insight into missing or misrepresented processes. These include groundwater exchanges, hyporheic exchange, surface transient storage, and time-varying albedo. While each of these processes likely occur to some degree, these were ultimately left out of the model because they were expected to be negligible based on findings in the literature or site-specific conditions. For example, groundwater exchange could be occurring in portions of the Grand Canyon, particularly where the river flows over or is adjacent to karst limestone layers (e.g., Redwall Limestone and Muav Limestone formations; Huntoon, 1974; Leeder, 2010) which occur in both upper and lower segments within the canyon. However, these exchanges are likely minimized by the surrounding bed rock and the sensitivity analysis of Q_{dist} suggests that further efforts along these lines may not be warranted.

Exchange of surface water with banks and sandbars could be another mechanism as water levels fluctuate in response hydropeaking operations. This results in infiltration into sandbars during the rising limb and a slower exfiltration out of the sandbars after the peak of the flow wave passes over long distances downstream (Alvarez and Schmeeckle 2013; Budhu and Gobin 1995; Ferencz et al. 2019; Sabol and Springer 2013). This exchange of water between the river and sandbars within Grand Canyon does influence temperatures within these shallow aquifers (Carpenter et al. 1995). However, when water seeps back into the river as river water levels decrease, there are only small thermal gradients (< 0.2 °C) between the near shore and main channel temperatures (Ross and

Vernieu 2013). This suggests that these exchanges likely add negligible amounts of heat to the river.

Influences from surface transient storage could be occurring when backwater areas fill during high flows and drain during low flows. These areas are prominent throughout the Grand Canyon and differentially warm compared to the temperatures in the main channel because they typically have low-velocity flows and are intermittently isolated from the river (Behn et al. 2010; Trammell et al. 2002). Work has been done to evaluate water temperatures in these nearshore environments (Hoffnagle 2001; Trammell et al. 2002; Vernieu and Anderson 2013), however, it is not clear if there are large enough volumes of water in these areas relative to that in the main channel to result in significant heating to the river. Furthermore, these influences likely decrease downstream as the amplitude of the hydropeaking wave, backwater inundation, and total amount of volume exchanged decreases.

Lastly, variability in water surface albedo over space and time could change the radiation balance, but was not considered here. Albedo changes throughout each day as a function of the solar zenith angle with greater albedo values occurring when the sun is close to the horizon (high zenith angle; Hoch & Whiteman, 2010; Matzinger et al., 2003). Given the interference of the steep canyon walls when solar zenith angles are high, the periods of high reflection were not a factor. The times when the river receives $J_{sn,dir}$ during the middle of the day, the zenith angles are low and the reflection off the water surface is limited when dealing with relatively clear water. In settings like the Colorado River, however, high turbidity can influence the amount of solar radiation that is reflected off the water surface (e.g., Neilson et al. 2009) and will change the amount of $J_{sn,net}$

absorbed by the river (e.g., McMahon & Moore, 2017). Some additional work regarding the influences of the temporal and spatial turbidity patterns on solar radiation reflection throughout the Grand Canyon would be warranted.

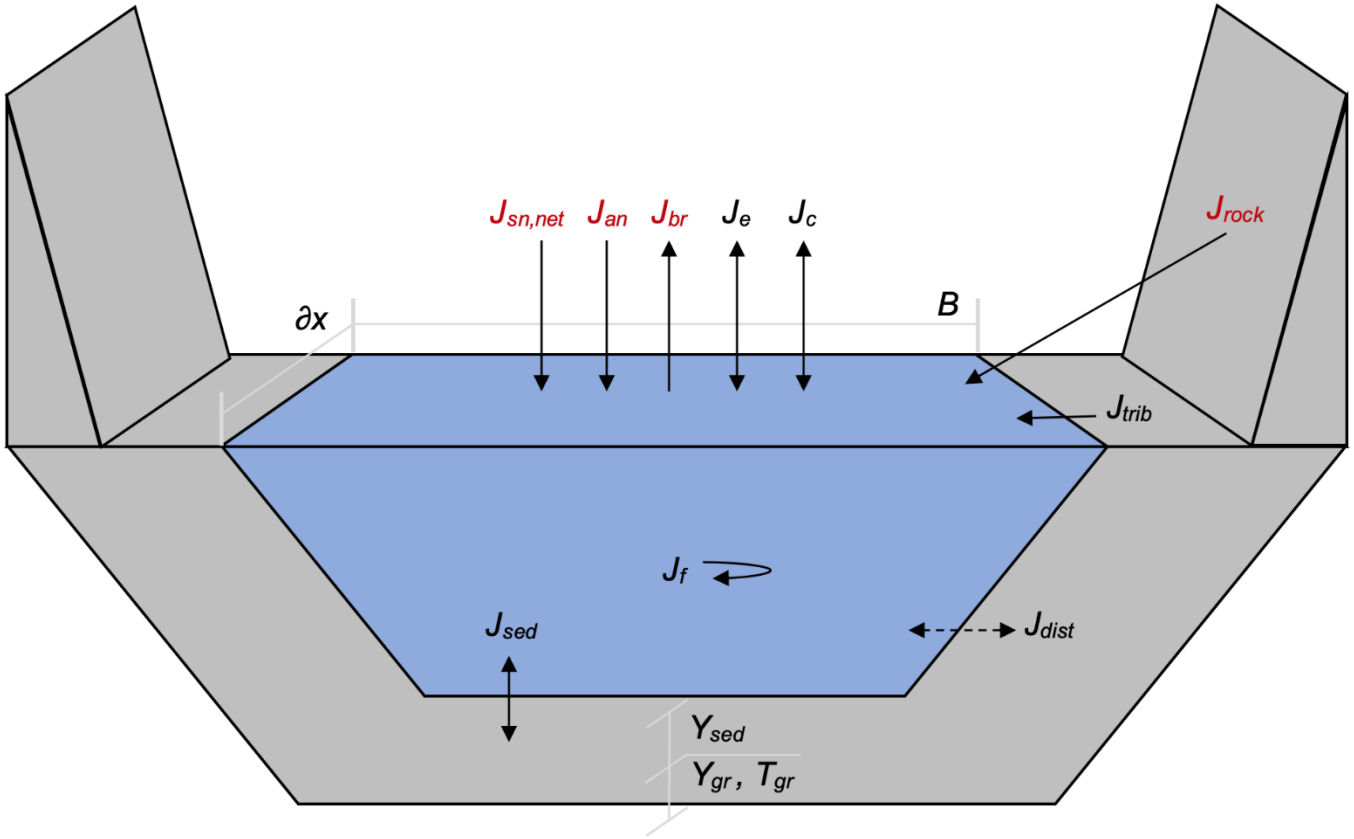

Figure A-1. Simple schematic of external heat fluxes and lateral inflows accounted for in the river temperature model. Included terms are net shortwave radiation (Jsn,net), atmospheric longwave radiation (Jan), water longwave radiation (Jbr), bedrock longwave radiation (Jrock), sensible heat (conduction and convection; Jc), latent heat (evaporation and condensation; Je), internal fluid shear friction (Jf), sediment conduction (Jsed), tributary flows (Jtrib) and distributed flows (Jdist). Radiative terms are shown in red (Jsn,net, Jan, Jbr, and Jrock) and are described and illustrated in greater detail in the manuscript. Ysed is the depth of the shallow sediment layer, and Ygr is the depth to the ground boundary layer. Tsed is the temperature of the shallow sediment layer and Tgr is the temperature of the ground boundary layer.

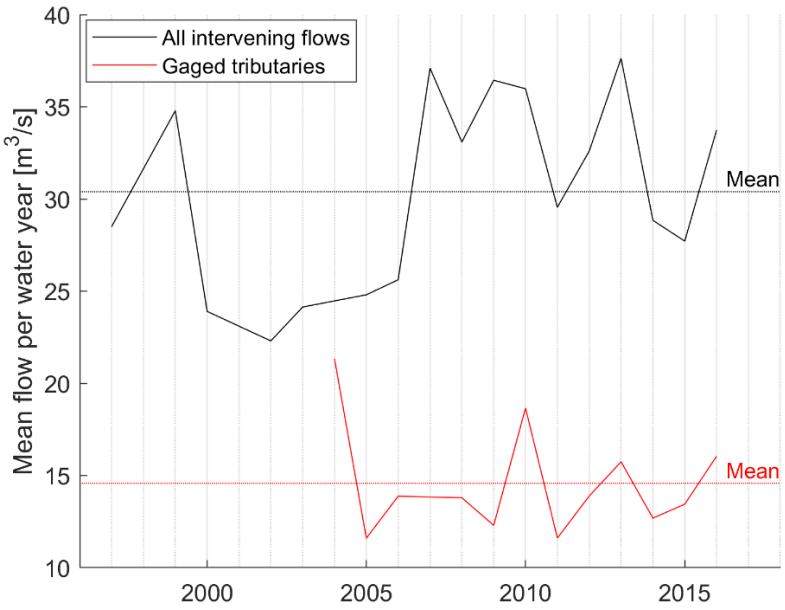

Figure A-2. Flow gained per water year in Grand Canyon between Lees Ferry (RM0) and RM225. The mean annual intervening flow is 30.4 m^3/s. The contribution from gaged tributaries is roughly half, with a mean annual flow of 14.6 m^3/s.

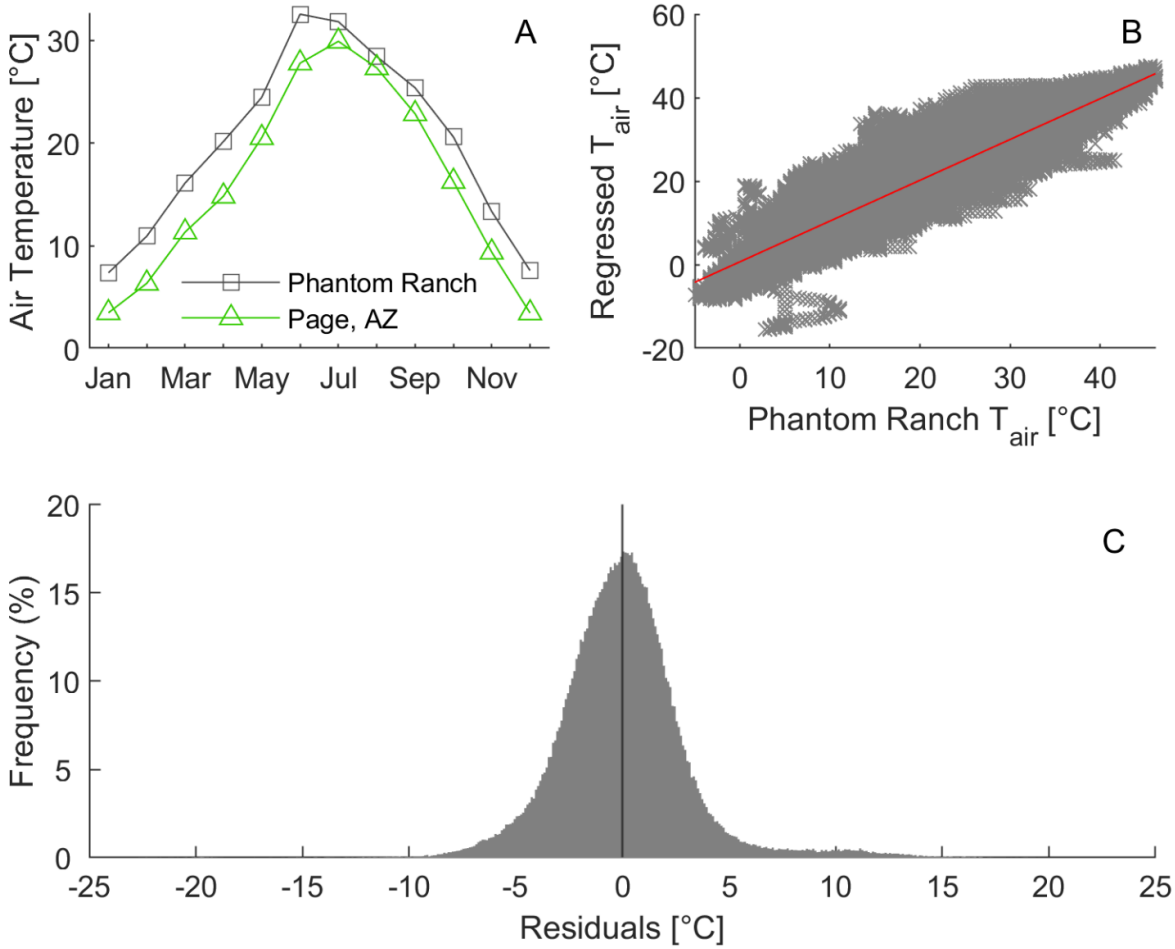

Figure A-3. Comparison between monthly average air temperature at Page, AZ municipal airport and Phantom Ranch within Grand Canyon to illustrate the general difference between the two locations (A). Relationship between sub-hourly air temperature measured at Phantom Ranch and air temperature regressed to Phantom Ranch using measured air temperature at Page, AZ (B). Histogram of residuals between measured and regressed air temperature data (C). The residuals have a mean of 0.0 and a standard deviation of 3.02 °C. The 99% confidence interval of the residuals are ± 0.012 °C.

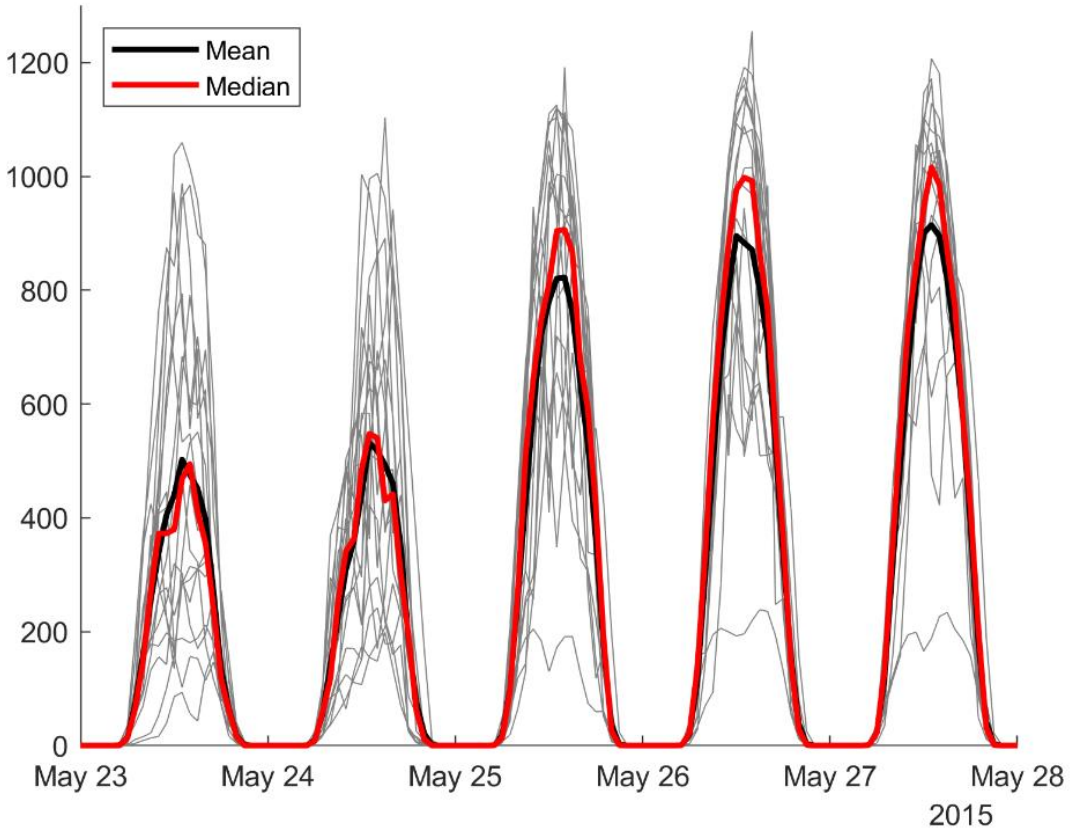

Figure A-4. Comparison of all shortwave radiation measurements from remote automated weather station network sites (grey lines) within the Grand Canyon region over a 5-day period. The Page, AZ municipal airport weather station characterizes the first two days as being overcast with light to moderate rain. The third day was mostly clear with periods of cloud cover. The last two days were clear conditions.

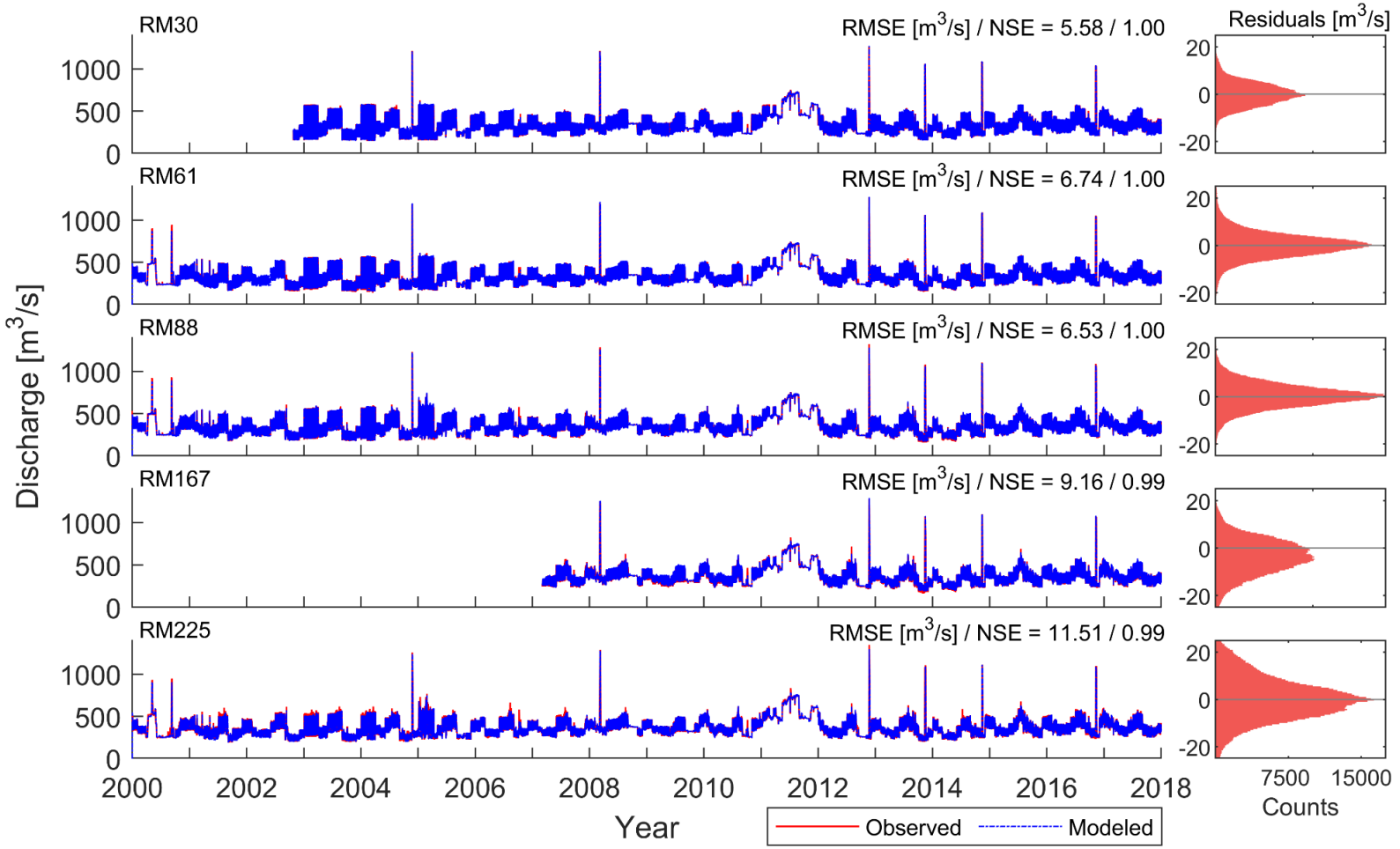

Figure A-5. Plot of long-term observations and model predictions of discharge at five gaging stations within Grand Canyon (RM30, RM61, RM88, RM167, and RM225). The right panels show the distribution of residuals between observed and modeled discharge in cubic meters per second.

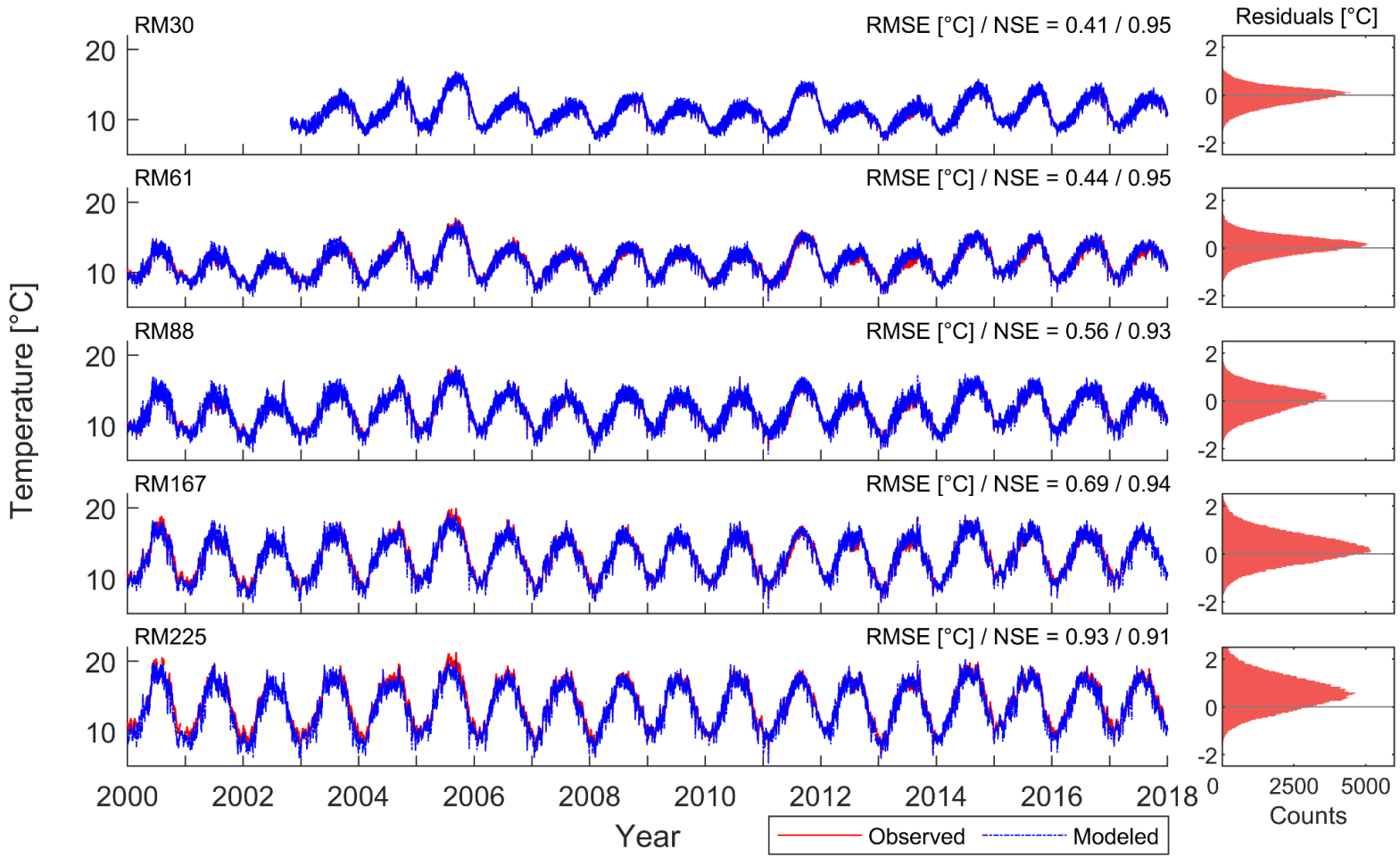

Figure A-6. Plot of long-term observations and model predictions of temperature at five gaging stations within Grand Canyon (RM30, RM61, RM88, RM167, and RM225). The right panels show the distribution of residuals between observed and modeled temperature.

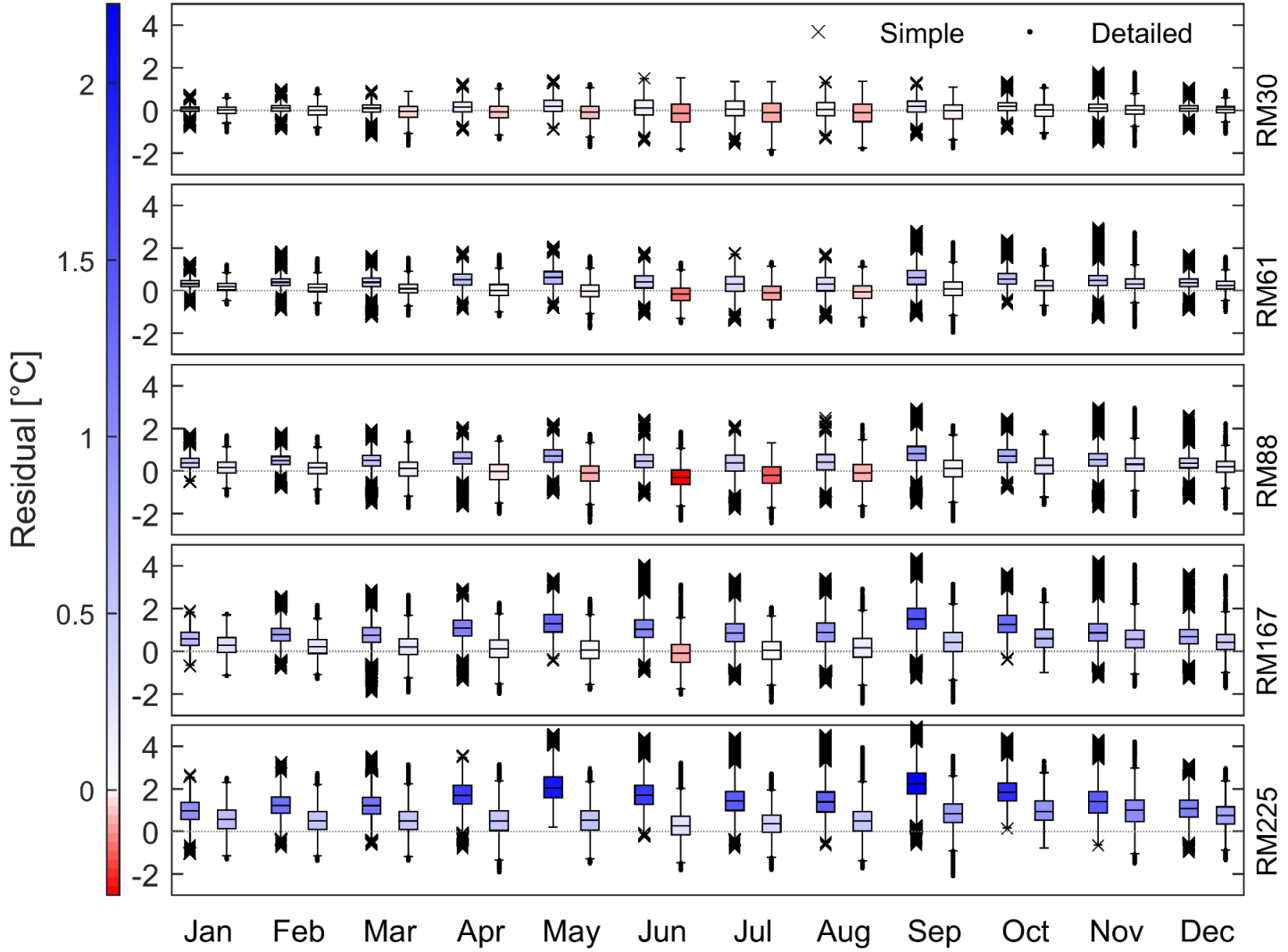

Figure A-7. Boxplot of temperature model residuals for simple and detailed radiation schemes by month for five gaging stations within Grand Canyon. Residuals were calculated as observed minus modeled temperatures. Colors correspond to the median value of a box where blue color/positive values represent model underestimated temperatures and red color/negative values represent over estimated temperatures.

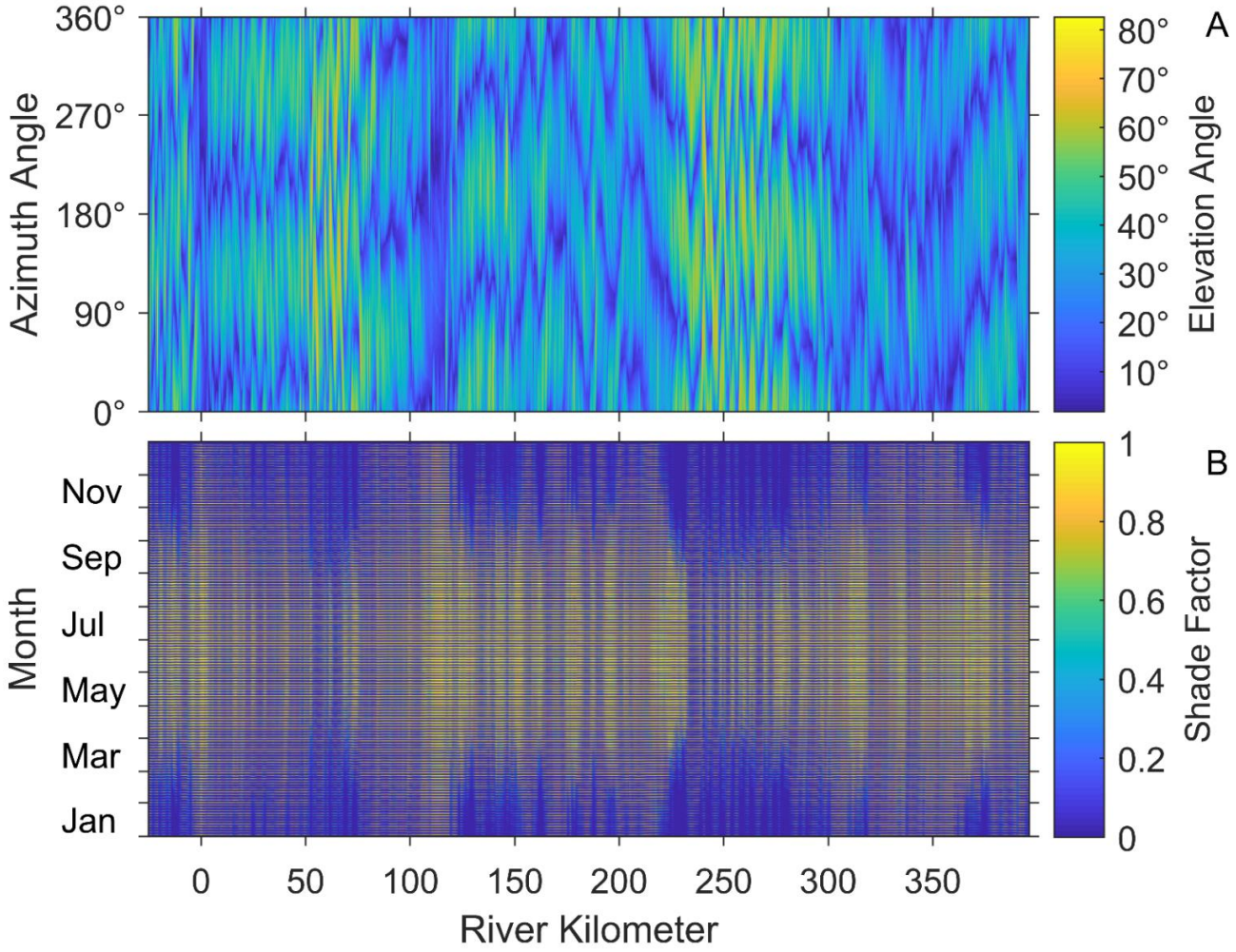

Figure A-8. Illustration of calculated elevation angles (Ψ_E) from Glen Canyon Dam (24.1 km upstream of Lees Ferry) to Spencer Creek (395.9 km downstream of Lees Ferry) that were used to calculate spatiotemporal topographic shading (see Text A-2) (A). Shading factors (S_f) for each model cell at hourly resolution over a 1-year period used to scale incoming shortwave radiation ($\hat{J}_{sn,dir}$) using Eqn. 2-8 (B). A shade factor of zero indicates no direct shortwave radiation. Note that 15-minute resolution S_f was used in the temperature model (i.e., Text A-2).

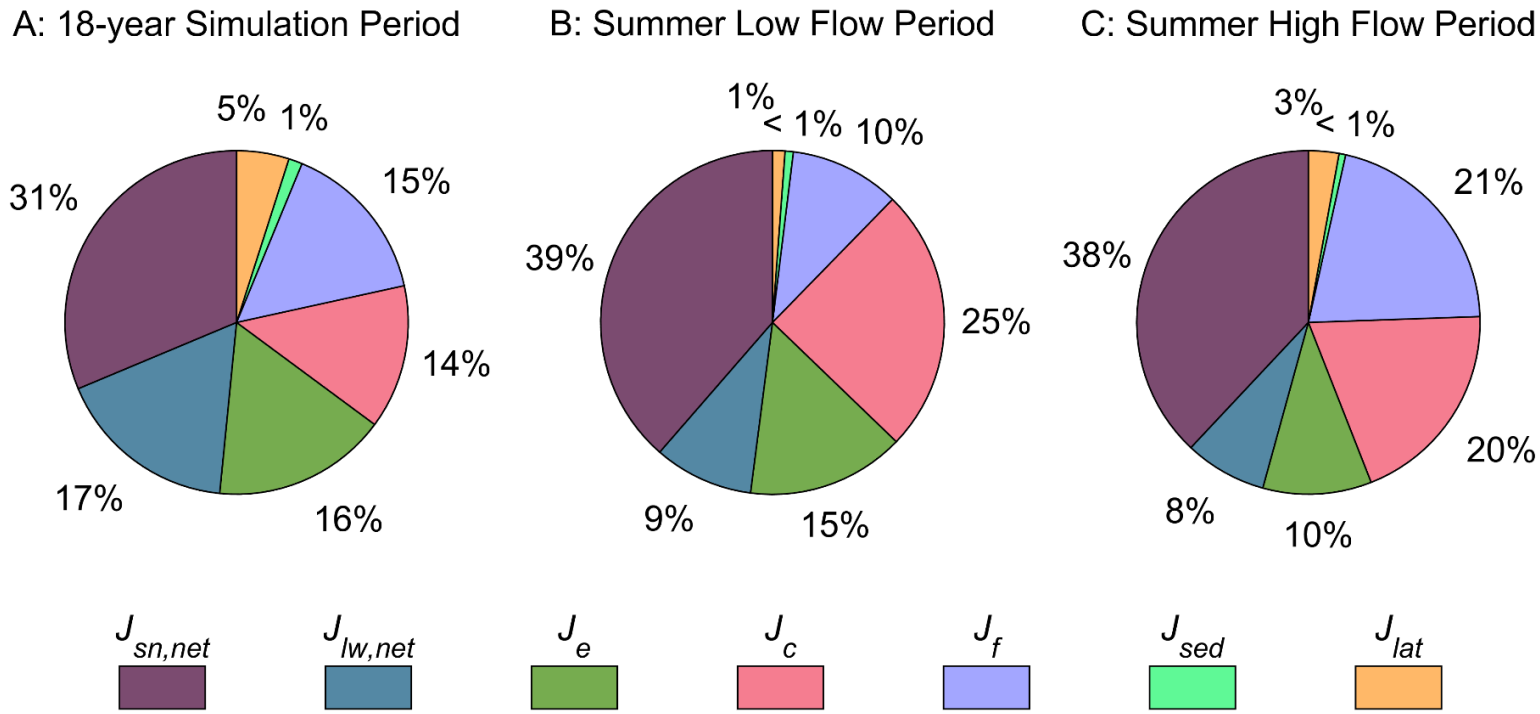

Figure A-9. Pie charts comparing the relative contribution of external heat fluxes from the detailed model during the entire simulation period (A), the summer of 2000 low flow period (B) and the summer of 2011 high flow period during (C). Variables being compared are net shortwave radiation ($J_{sn,net}$), net longwave radiation ($J_{lw,net}$), latent heat (J_e), sensible heat (J_c), friction (J_f), bed conduction (J_{sed}), and heat from lateral sources (J_{lat}). Percent contributions are calculated from the absolute value of the average for each flux over space and time. Each pie represents the fraction of the total heat exchanged, with $J_{lw,net}$ and J_e having negative average fluxes for each period shown.

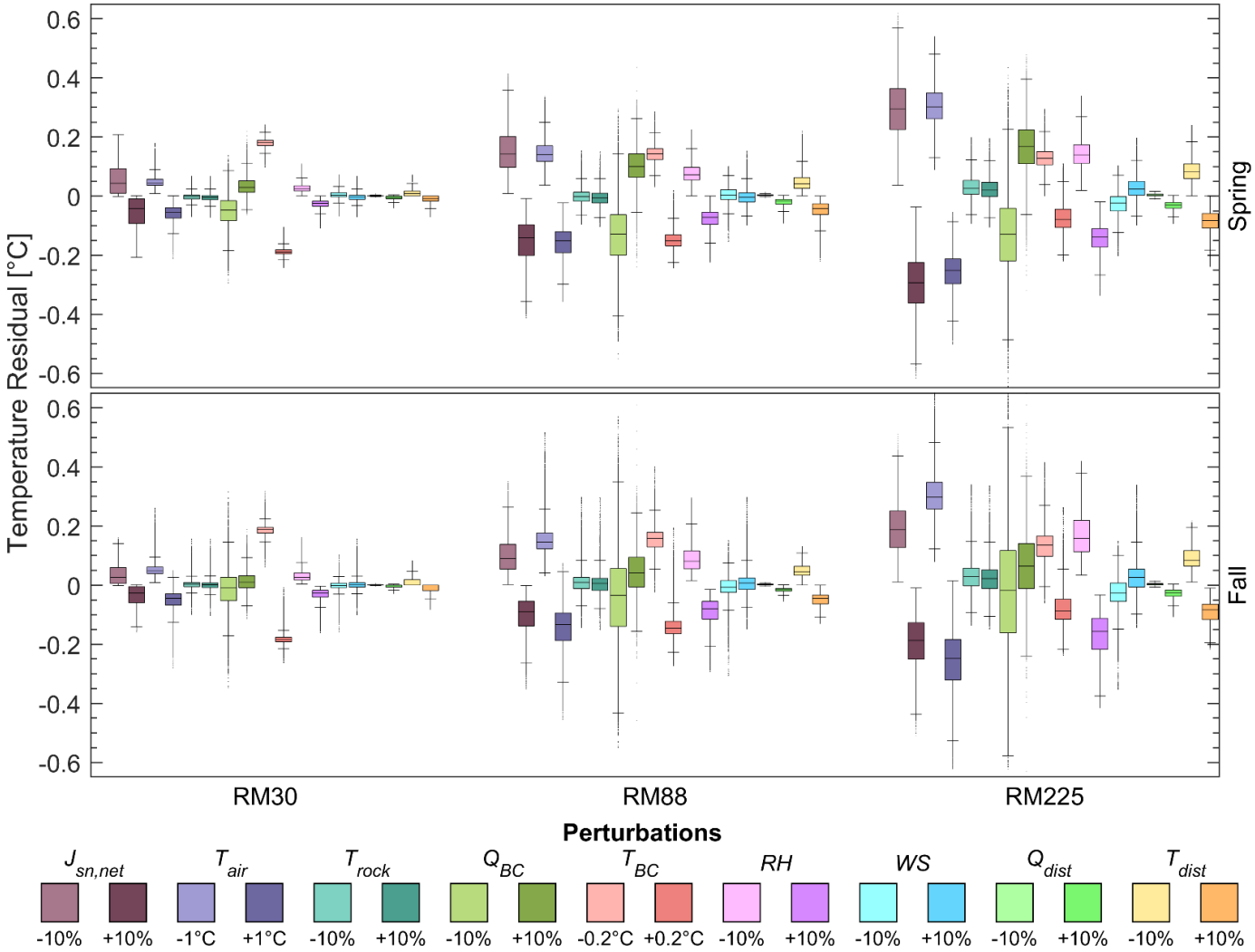

Figure A-10. Sensitivity analysis of river temperature to input data perturbations at three locations during Fall and Spring averaged over the entire simulation time (Spring = Mar.-May, Fall = Sep.-Nov.). The residual is calculated as the detailed model minus scenario. Variables being compared are net shortwave radiation ($J_{sn,net}$), air temperature (T_{air}), bedrock temperature (T_{rock}), upstream boundary flow (Q_{BC}), upstream boundary condition temperature (T_{BC}), relative humidity (RH), wind speed (WS), distributed flows (Q_{dist}), distributed flow temperatures (T_{dist}). Box plot order follows that of the legend.

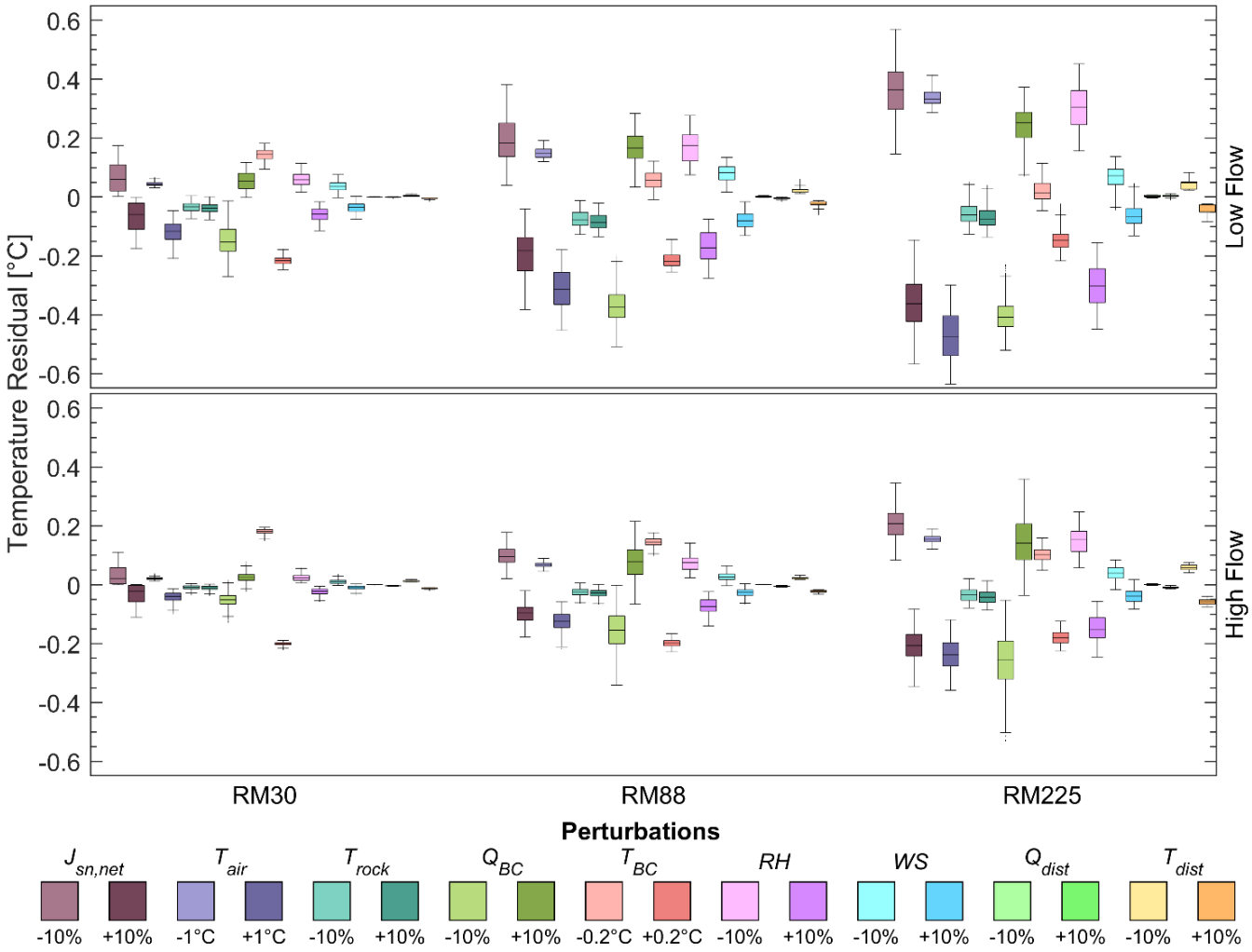

Figure A-11. Sensitivity analysis of river temperature to input data perturbations at three locations during low flow (July 1, 2000 – Sept. 1, 2000) and high flow (July 1, 2011 – Sept. 1, 2011) periods. The residual is calculated as the detailed model minus scenario. Variables being compared are net shortwave radiation ($J_{sn,net}$), air temperature (T_{air}), rock temperature (T_{rock}), upstream boundary flow (Q_{BC}), upstream boundary condition temperature (T_{BC}), relative humidity (RH), wind speed (WS), distributed flows (Q_{dist}), distributed flow temperatures (T_{dist}). Box plot order follows that of the legend.

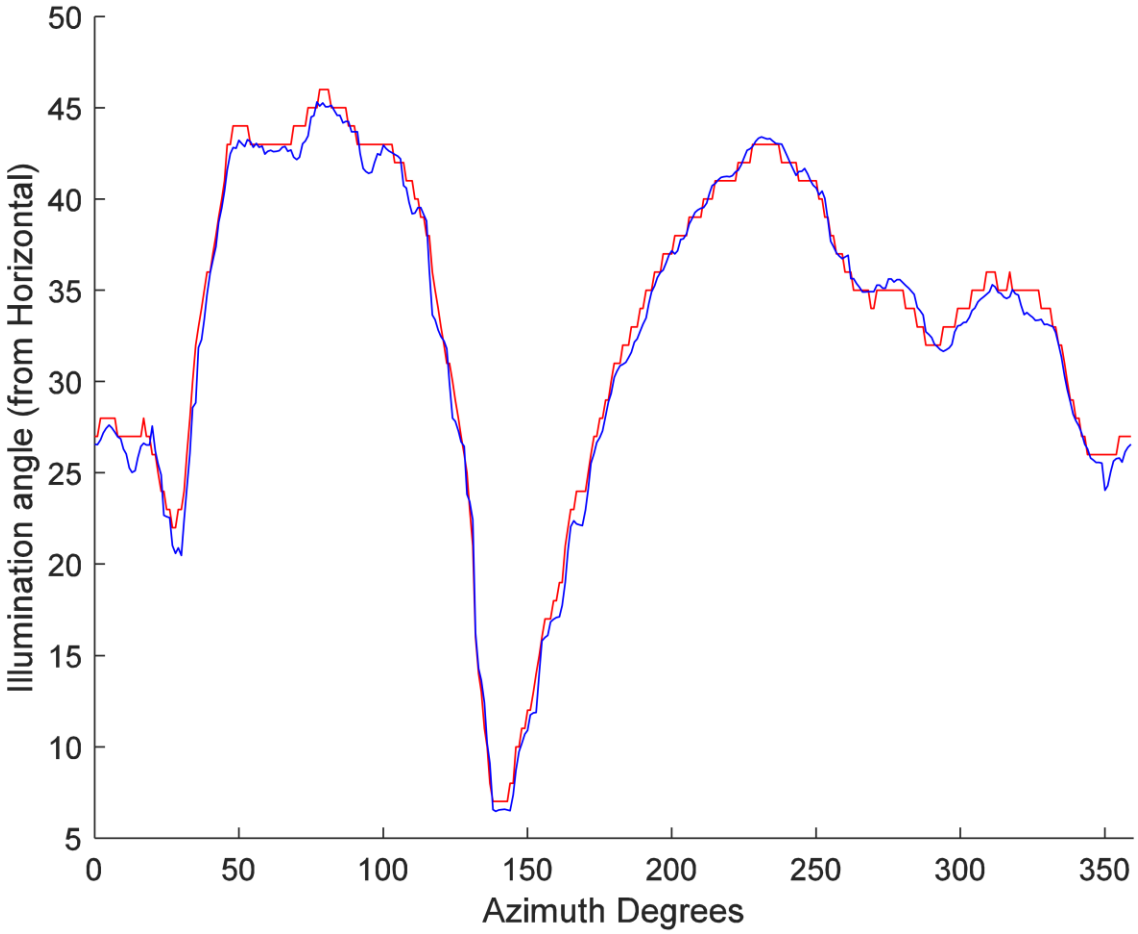

Figure A-12. Comparison of predicted illumination angles 8.1 km upstream from Lees Ferry (i.e., RM -5) using the model presented by Yard et al. (2005) (red line) and the algorithm used here (i.e., Text A-2) (blue line). Root mean square error between the two models is 0.884 degrees of illumination angle.

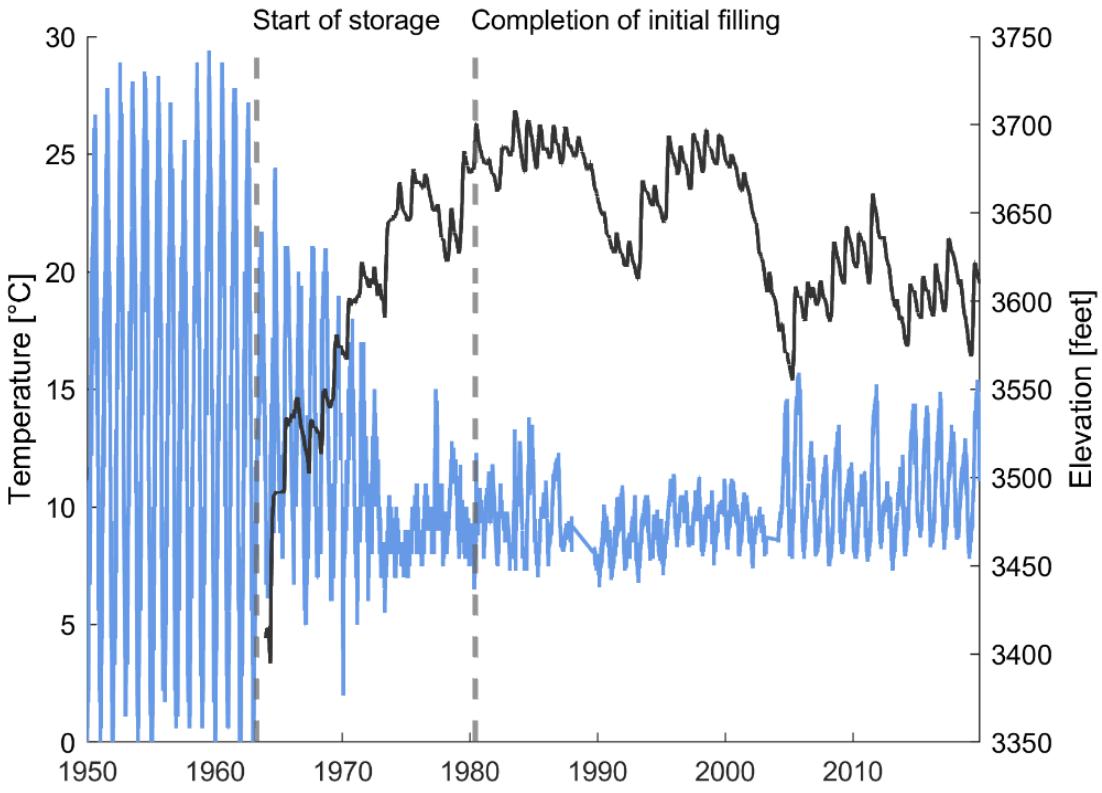

Figure A-13. Historical daily water temperature at Lees Ferry (blue line) and daily elevation at Lake Powell (black line). Start of initial storage is approximately April 13, 1963 and completion of initial filling is approximately June 6, 1980.

Table A-1. Current and historical Colorado River monitoring stations within Grand Canyon in order of river kilometer. Bold font indicates stations that were used in this model.

Name	USGS Gage Name	Approximate river mile (km)	Active ?	Parameters
Main Channel, Colorado River				
Glen Canyon Dam	09379901	-15 (-24.1)	Yes	Water Temperature, *, †, ‡,
at Lees Ferry	09380000	0 (0)	Yes	Flow, Water Temperature, *, †, ‡, §
near river mile 30	09383050	30 (48.3)	Yes	Flow, Water Temperature, *, †, ‡, §
near river mile 33	Riv Mi 33	33 (53.1)	No	Water Temperature
above Little Colorado River	09383100	61 (98.2)	Yes	Flow, Water Temperature, *, †, ‡, §
near river mile 66	09402352	66 (106.2)	Yes	Water Temperature
near river mile 76	09402430	76 (122.3)	No	Water Temperature
near Grand Canyon	09402500	88 (141.6)	Yes	Flow, Water Temperature, *, †, ‡, §
below 127 Mile Creek	09403270	127 (204.4)	Yes	Water Temperature
near river mile 132	Riv Mi 132	132 (212.4)	No	Water Temperature
near river mile 149	Riv Mi 149	149 (239.8)	No	Water Temperature
above National Canyon	09404120	167 (268.8)	Yes	Flow, Water Temperature, *, †, ‡, §
near river mile 194	Riv Mi 194	194 (312.2)	No	Water Temperature
above Diamond Creek	09404200	225 (362.1)	Yes	Flow, Water Temperature, *, †, ‡, §
near river mile 246	09404220	246 (395.9)	Yes	Water Temperature
Tributaries				
Paria River	09382000	0.9 (1.4)	Yes	Flow, Water Temperature, §
Nankoweap Creek	Nankoweap Ck Mouth	52.5 (84.5)	No	Water Temperature
Little Colorado River	09402300	62 (99.8)	Yes	Flow, Water Temperature, §
Bright Angle Creek	09403000	88.4 (142.3)	Yes	Flow, Water Temperature, ‡, §
Shinumo Creek	Shinumo Ck	109.3 (175.9)	No	Water Temperature
Tapeats Creek	Tapeats Ck Mouth	134.4 (216.3)	No	Water Temperature
Kanab Creek	09403850	144 (231.7)	Yes	Flow, Water Temperature, ‡, §
Havasu Creek	09404115	157.3 (253.1)	Yes	Flow, Water Temperature, ‡, §

Additional monitoring parameters:
* Dissolved Oxygen
† Turbidity

‡ Specific Conductance
§ Suspended Sediment (sand, silt, and clay)

Table A-2. Calibrated roughness values for each segment of the Colorado River in Grand Canyon.

1. REACH NAME	Reach Length miles (km)	Downstream Gage	Roughness
Upper Marble Canyon	30 (48.3)	RM30	0.033
Lower Marble Canyon	31 (49.9)	RM61	0.040
Eastern Grand Canyon	27 (43.5)	RM88	0.038
East-Central Grand Canyon	79 (127.1)	RM167	0.040
West-Central Grand Canyon	58 (93.3)	RM225	0.033

Table A-3. Comparison of air temperature data from weather stations within Grand Canyon and at Page, AZ. The mean air temperature from within Grand Canyon (excluding Page, AZ and Regressed Air Temperature) is 19.95 °C.

Station Name	Source[a]	Years of data	Approximate river mile (km)	Mean air temperature (C)	Mean residual air temperature[b] (C)
Page Municipal Airport	MesoWest	21.1	-15 (-24.1)	16.03	-3.73
AZ C:02:0071	GCMRC	2.8	-10 (-16.1)	16.45	-0.81
AZ C:02:0070	GCMRC	3.6	0.5 (0.8)	17.85	-2.44
AZ C:05:0031 Upper	GCMRC	0.2	24.5 (39.4)	20.23	-0.39
AZ C:05:0031 Lower	GCMRC	4.4	24.5 (39.4)	19.37	-0.49
AZ C:13:0365 Upper	GCMRC	3.5	58 (93.3)	19.49	0.48
AZ C:13:0365 Lower	GCMRC	3.5	58 (93.3)	18.90	0.42
AZ C:13:0006	GCMRC	4.3	60 (96.6)	19.87	0.17
AZ C:13:0336	GCMRC	4.4	66 (106.2)	19.80	0.73
AZ C:13:0346 Upper	GCMRC	9.7	70 (112.7)	20.53	0.22
AZ C:13:0346 Lower	GCMRC	4.7	70 (112.7)	19.09	0.01
WX7FGZ-1 Phantom Ranch	MesoWest	7.5	88 (141.6)	20.49	0.18
Regressed Air Temperature at Phantom Ranch	Calculated	21.1	88 (141.6)	19.76	0.00
AZ B:10:0225	GCMRC	3.7	125.5 (202)	22.75	1.60
AZ B:11:0281	GCMRC	4.0	135 (217.3)	19.82	1.23
AZ A:15:0033	GCMRC	4.4	203 (326.7)	21.94	2.56
AZ G:03:0072	GCMRC	9.8	223 (358.9)	22.75	2.80

[a] See Caster et al. (2014) for description of US Geological Survey Grand Canyon Monitoring and Research Center (GCMRC) stations.

[b] Residual air temperature is observed air temperature minus regressed air temperature at Phantom Ranch.

Table A-4. Remote automated weather station (RAWS) network sites used to aggregate measured shortwave radiation into a hourly median time series ($J_{sn,meas}$).

SiteCode	Station Name	Latitude	Longitude	Elevation (ft)
AZPA3	AZTCA_PORT1	35.51488	-113.543	4468
QDPA3	DRY PARK	36.45308	-112.238	8706
QFSA3	FOUR SPRINGS	36.79361	-112.043	6560
FZWA3	FRAZIER WELLS	35.84551	-113.055	6796
QGSA3	GUNSIGHT	36.70444	-112.583	5280
QLBA3	LINDBERGH HILL	36.28556	-112.079	8800
QMLA3	MOUNT LOGAN	36.35306	-113.199	7605
QMMA3	MUSIC MOUNTAIN	35.61497	-113.794	5375
NVRA3	NEVERSHINE	36.24753	-113.889	2165
QNFA3	NIXON FLATS	36.38833	-113.158	6500
QOKA3	OLAF KNOLLS	36.50722	-113.816	2900
QPPA3	PARIA POINT	36.72778	-111.822	7235
TCRA3	TRUXTON CANYON	35.78013	-113.796	5304
QTUA3	TUSAYAN	35.98833	-112.121	6570
QYJA3	YELLOW JOHN MOUNTAIN	36.155	-113.549	6160
QNMA3	NAVAJO MONUMENT	36.67692	-110.541	7279
QHIA3	HOPI	35.86292	-110.615	5579
KAGU1	KANE GULCH	37.52472	-109.893	6500

References

Alvarez, L. V., & Schmeeckle, M. W. (2013). Erosion of river sandbars by diurnal stage fluctuations in the Colorado River in the Marble and Grand Canyons: Full-scale laboratory experiments. River Research and Applications, 29(7), 839–854. https://doi.org/10.1002/rra.2576

Anderson, C. R., & Wright, S. A. (2007). Development and application of a water temperature model for the Colorado River below Glen Canyon Dam, Arizona. Proceedings of the American Institute of Hydrology, 23, 1–11.

Behn, K. E., Kennedy, T. A., & Hall, R. O. J. (2010). Basal resources in backwaters of the Colorado River below Glen Canyon Dam - Effects of discharge regimes and comparison with mainstem depositional environments. U.S. Geological Survey Open-File Report 2010-1075, 25. http://pubs.usgs.gov/of/2010/1075/

Budhu, M., & Gobin, R. (1995). Seepage-induced slope failures on sandbars in Grand Canyon. Journal of Geotechnical Engineering, 121(August), 601–609.

Buendia, C., Sabater, S., Palau, A., Batalla, R. J., & Marcé, R. (2015). Using equilibrium temperature to assess thermal disturbances in rivers. Hydrological Processes, 29(19), 4350–4360. https://doi.org/10.1002/hyp.10489

Carpenter, M. C., Crosswhite, J. A., & Carruth, R. L. (1995). Water-level fluctuations, water temperatures, and tilts in sandbars -6.5R, 43.1L, and 172.3L, Grand Canyon, Arizona, 1990-93. Open-File Report 94-485, 17.

Caster, J. J., Dealy, T. P., Andrews, T., Fairley, H., Draut, A. E., Sankey, J. B., & Bedford, D. R. (2014). Meteorological data for selected sites along the Colorado River Corridor, Arizona, 2011-2013. U.S. Geological Survey Open-File Report 2014-1247, 56. https://doi.org/http://dx.doi.org/10.3133/ofr20141247

Caster, J. J., & Sankey, J. B. (2016). Variability in rainfall at monitoring stations and derivation of a long-term rainfall intensity record in the Grand Canyon Region, Arizona, USA. In Scientific Investigations Report. https://doi.org/10.3133/sir20165012

Draut, A. E., & Rubin, D. M. (2006). Measurements of wind, aeolian sand transport, and precipitation in the Colorado River corridor, Grand Canyon, Arizona; January 2005 to January 2006. In Open-File Report (Revised an). https://doi.org/10.3133/ofr20061188

Edinger, J. E., Duttweiler, D. W., & Geyer, J. C. (1968). The response of water temperatures to meteorological conditions. Water Resources Research. https://doi.org/10.1029/WR004i005p01137

Erbs, D. G., Klein, S. A., & Duffie, J. A. (1982). Estimation of the diffuse radiation fraction for hourly, daily and monthly-average global radiation. Solar Energy. https://doi.org/10.1016/0038-092X(82)90302-4

Ferencz, S. B., Cardenas, M. B., & Neilson, B. T. (2019). Analysis of the effects of dam release properties and ambient groundwater flow on surface water-groundwater exchange over a

100-km-long reach. Water Resources Research, 55(11), 8526–8546. https://doi.org/10.1029/2019WR025210

Ferrari, R. (1987). Colorado River water temperature modeling below Glen Canyon Dam. *Glen Canyon Environmental Studies*.

Garrett, D., Baron, J., Dale, V., Gunderson, L., Hulse, D., Kitchell, J., Loomis, J., Palmer, M., Parker, R., Robertson, D., Schwartz, D., & Watkins, J. (2003). Evaluating a Glen Canyon Dam temperature control device to enhance native fish habitat in the Colorado River: A risk assessment. Upper Colorado Region, Bureau of Reclamation, June.

Graf, J. B. (1995). Measured and Predicted Velocity and Longitudinal Dispersion At Steady and Unsteady-Flow, Colorado River, Glen Canyon Dam To Lake Mead. Water Resources Bulletin, 31(2), 265–281.

Grams, P., Schmidt, J., Wright, S., Topping, D., Melis, T., & Rubin, D. (2015). Building sandbars in the Grand Canyon. Eos, 96. https://doi.org/10.1029/2015EO030349

Hoch, S. W., & David Whiteman, C. (2010). Topographic effects on the surface radiation balance in and around Arizona's Meteor crater. Journal of Applied Meteorology and Climatology, 49(6), 1114–1128. https://doi.org/10.1175/2010JAMC2353.1

Hoffnagle, T. L. (2001). Changes in water temperature of backwaters during fluctuating vs. short-term steady flows in the Colorado River, Grand Canyon. Proceedings of the Fifth Biennial Conference of Research on the Colorado Plateau, June, 103–118.

Huning, L. S., & Margulis, S. A. (2015). Watershed modeling applications with a modular physically-based and spatially-distributed watershed educational toolbox. Environmental Modelling & Software, 68, 55–69. https://doi.org/10.1016/j.envsoft.2015.02.008

Huntoon, P. W. (1974). The karstic groundwater basins of the Kaibab Plateau, Arizona. Water Resources Research, 10(3), 579–590. https://doi.org/10.1029/WR010i003p00579

Kurylyk, B. L., Moore, R. D., & Macquarrie, K. T. B. (2016). Scientific briefing: Quantifying streambed heat advection associated with groundwater-surface water interactions. Hydrological Processes. https://doi.org/10.1002/hyp.10709

Lam, J. C., & Li, D. H. W. (1996). Correlation between global solar radiation and its direct and diffuse components. Building and Environment, 31(6), 527–535. https://doi.org/10.1016/0360-1323(96)00026-1

Leeder, M. R. (2010). Sedimentology and sedimentary basins: From turbulence to tectonics. *Wiley*.

Matzinger, N., Andretta, M., van Gorsel, E., Vogt, R., Ohmura, A., & Rotach, M. W. (2003). Surface radiation budget in an alpine valley. Quarterly Journal of the Royal Meteorological Society, 129(588), 877–895. https://doi.org/10.1256/qj.02.44

McMahon, A., & Moore, R. D. (2017). Influence of turbidity and aeration on the albedo of mountain streams. Hydrological Processes, 31(25), 4477–4491. https://doi.org/10.1002/hyp.11370

Neilson, B. T., Stevens, D. K., Chapra, S. C., & Bandaragoda, C. (2009). Data collection methodology for dynamic temperature model testing and corroboration. Hydrological Processes, 23(20), 2902–2914. https://doi.org/10.1002/hyp.7381

Orgill, J. F., & Hollands, K. G. T. (1977). Correlation equation for hourly diffuse radiation on a horizontal surface. Solar Energy, 19(4), 357–359. https://doi.org/10.1016/0038-092X(77)90006-8

Petersen, J. H., & Paukert, C. P. (2005). Development of a bioenergetics model for humpback chub and evaluation of water temperature changes in the Grand Canyon, Colorado River. Transactions of the American Fisheries Society, 134(4), 960–974. https://doi.org/10.1577/T04-090.1

Ross, R. P., & Vernieu, W. S. (2013). Nearshore temperature findings for the Colorado River in Grand Canyon, Arizona - Possible implications for native fish. U.S. Geological Survey Fact Sheet 2013–3104. https://doi.org/10.3133/fs20133104

Sabol, T. A., & Springer, A. E. (2013). Transient simulation of groundwater levels within a sandbar of the Colorado River, Marble Canyon, Arizona, 2004. U.S. Geological Survey Open-File Report 2013-1277, 22. https://doi.org/http://dx.doi.org/10.3133/ofr20131277

Schmidt, J. C., Topping, D. J., Rubin, D. M., Hazel, J. E., Kaplinski, M., Wiele, S. M., & Goeking, S. A. (2007). Streamflow and sediment data collected to determine the effects of low summer steady flows and habitual maintenance flows in 2000 on the Colorado River between Lees Ferry and Bright Angel Creek, Arizona. U.S. Geological Survey Open-File Report 2007-1268, 79 p. http://pubs.usgs.gov/of/2007/1268/

Theurer, F. D., Voos, K. A., & Miller, W. J. (1984). Instream water temperature model. Instream Flow Information Paper 16. In FWS/OBS. http://pubs.er.usgs.gov/publication/fwsobs84_15

Topping, D. J., Rubin, D. M., & Vierra, L. E. (2000). Colorado River sediment transport: 1. Natural sediment supply limitation and the influence of Glen Canyon Dam. Water Resources Research, 36(2), 515–542. https://doi.org/10.1029/1999WR900285

Topping, D. J., Schmidt, J. C., & Vierra Jr., L. E. (2003). Computation and analysis of the instantaneous-discharge record for the Colorado River at Lees Ferry, Arizona : May 8, 1921, through September 30, 2000. In Professional Paper. https://doi.org/10.3133/pp1677

Trammell, M. A., Valdez, R. A., Carothers, S. W., & Ryel, R. J. (2002). Effects of a low steady summer flow experiment on native fishes of the Colorado River in Grand Canyon, Arizona. SWCA Environmental Consultants.

U.S. Bureau of Reclamation. (1999). Glen Canyon Dam modifications to control downstream temperatures - plan and draft environmental assessment. Department of the Interior.

U.S. Department of the Interior. (2007). Recod of decision: Colorado River interim guidelines for lower basin shortages and the coordinated operations for Lake Powell and Lake Mead, Final environmental impact statement. Office of the Secretary of Interior, Washington, D.C.

Valdez, R. A., Speas, D. W., & Kubly, D. M. (2013). Benefits and risks of temperature modification at Glen Canyon Dam to aquatic resources of the Colorado River in the Grand Canyon. U.S. Bureau of Reclamation, Upper Colorado Region, Salt Lake City, UT.

Vernieu, W. S., & Anderson, C. R. (2013). Water temperatures in select nearshore environments of the Colorado River in Grand Canyon, Arizona, during the low steady summer flow experiment of 2000. U.S. Geological Survey Open- File Report 2013–1066, 44.

Vernieu, W. S., Hueftle, S. J., & Gloss, S. P. (2005). Water quality in Lake Powell and the Colorado River. In S. P. Gloss, J. E. Lovich, & T. S. Melis (Eds.), State of the Colorado River Ecosystem (pp. 69–85). U.S. Geological Survey Circular 1282.

Wiele, S. M., & Griffin, E. R. (1997). Modification to a one-dimensional model of unsteady flow in the Colorado River through the Grand Canyon, Arizona. Water-Resouces Investigations Report 97-4046, 17.

Wright, S. A., Anderson, C. R., & Voichick, N. (2009). A simplified water temperature model for the Colorado River below Glen Canyon Dam. River Research and Applications, 25(6), 675–686. https://doi.org/10.1002/rra.1179

Wright, S. A., Melis, T. S., Topping, D. J., & Rubin, D. M. (2005). Influence of Glen Canyon Dam operations on downstream sand resources of the Colorado River in Grand Canyon. In S. P. Gloss, J. E. Lovich, & T. S. Melis (Eds.), State of the Colorado River Ecosystem (pp. 17–31). U.S. Geological Survey Circular 1282.

Yard, M. D., Bennett, G. E., Mietz, S. N., Coggins, L. G., Stevens, L. E., Hueftle, S., & Blinn, D. W. (2005). Influence of topographic complexity on solar insolation estimates for the Colorado River, Grand Canyon, AZ. Ecological Modelling, 183(2–3), 157–172. https://doi.org/10.1016/j.ecolmodel.2004.07.027

APPENDIX B

Supporting Information for Chapter 3

Text B-1: Air-water interface heat flux calculations

The descriptions of calculated heat fluxes are taken directly from Buahin et al. (2019) and Mihalevich et al. (2020).

Evaporation and Condensation Heat Fluxes

Evaporation/condensation (J_e) is calculated as a function of the sensible heat carried with the evaporated water, the latent heat of evaporation, density of water, and the evaporative rate as expressed in Eqn B-1 (Boyd and Kasper 2003; Evans et al. 1998; Webb and Zhang 1997b).

$$\mathrm{J}_e = -\rho_w L_e E \tag{B-1}$$

where L_e is the latent heat of vaporization $\left(\frac{J}{kg}\right)$ and E is the evaporative rate $\left(\frac{m}{s}\right)$. The latent heat of vaporization is estimated as a weak function of water temperature using Eqn B-2 (Martin and McCutcheon 1998).

$$L_e = 1000(2499 - 2.36T) \tag{B-2}$$

where T is the water temperature in the channel (℃). Following Dingman (2008), the evaporative rate is estimated using Eqn B-3.

$$E = f(\vec{w})(e_s^w - e_a) \tag{B-3}$$

where e_s^w is the saturation vapor pressure of the evaporating surface (kPa), e_a is the actual vapor pressure (kPa), and $f(\vec{w})$ is a wind function used to estimate the adiabatic portion of evaporation (Boyd and Kasper, 2003). e_s^w is computed using Eqn B-4 (Chapra 2008; Raudkivi 1979).

$$e_s^w = 0.61275e^{\left(\frac{17.27T}{237.3+T}\right)} \tag{B-4}$$

The actual vapor pressure (e_a) is calculated as a function of relative humidity (RH) and saturation vapor pressure (e_s) using Eqn B-5.

$$e_a = \frac{RH}{100\%} e_s \tag{B-5}$$

where e_s is computed using Eqn B-6.

$$e_s = 0.61275 e^{\left(\frac{17.27 T_a}{237.3 + T_a}\right)} \tag{B-6}$$

where T_a is air temperature in $(°C)$.

Extensive observations have yielded Eqn B-7 as the general form of the wind function (Martin and McCutcheon 1998; Shanahan 1984).

$$f(\vec{w}) = a + b\vec{w} \tag{B-7}$$

where a and b are empirical coefficients with units $kPa^{-1}ms^{-1}$ and kPa^{-1} respectively and $\vec{w}$ is the wind speed measured approximately 2 meters above the water surface $\left(\frac{m}{s}\right)$. Several authors have proposed values for these coefficients including (Dunne and Loepold 1978), who proposed the values $1.505 \cdot 10^{-8}$ and $1.6 \cdot 10^{-8}$ for the coefficients a and b respectively.

Convective and Conductive Heat Fluxes

Estimating heat lost or gained through conduction/convection (J_c) with air in the atmosphere is typically performed using the Bowen ratio (B_r), which relates latent heat to sensible heat (Eqn B-8) (Bowen 1926; Evans et al. 1998; Glose et al. 2017; Webb and Zhang 1997b; Westhoff et al. 2007).

$$J_c = B_r \Phi_{evap} \tag{B-8}$$

The Bowen ratio is estimated as (Evans et al., 1998; Westhoff et al., 2007; Glose et al., 2017):

$$B_r = 6.1 \times 10^{-4} P_A \left(\frac{T_w - T_a}{e_s^w - e_a^w}\right) \tag{B-9}$$

where T_w and T_a are water and air temperature respectively and P_A is the adiabatic atmospheric pressure. P_A is computed as (Westhoff et al., 2007; Glose et al., 2017):

$$P_A = 101.3\left[\frac{293-0.0065z}{293}\right]^{5.256} \quad \text{(B-10)}$$

where z is the elevation above sea level (m).

Shortwave radiation

Shortwave radiation received at the water surface consists of direct shortwave radiation ($J_{sn,dir}$) originating from the sun and scaled by topographic shading factors (S_f) diffuse shortwave radiation ($J_{sn,diff}$) originating from any sky direction as the result of scattering by atmospheric gases and particles and scaled by the sky view factor (SV_f), and land-reflected longwave radiation ($J_{sn,refl}$) from nearby terrain (Eqn B-11).

$$J_{sn,net} = J_{sn,dir} + J_{sn,diff} + J_{sn,ref} \quad \text{(B-11)}$$

The individual components are estimated using nearby estimates of shortwave radiation, which is assumed to only be composed of the direct and diffuse components (Eqn B-12):

$$J_{sn,meas} = \hat{J}_{sn,dir} + \hat{J}_{sn,diff} \quad \text{(B-12)}$$

where $\hat{J}$ denotes estimates of shortwave radiation on a horizontal surface (e.g., above the canyon).

Direct and diffuse components of $J_{sn,meas}$ can be separated out through the application of empirical correlation equations (Dervishi and Mahdavi 2012) that predicts the fraction of diffuse radiation (k_d) as a function of the ratio between $J_{sn,meas}$ and modeled extraterrestrial radiation ($J_{sn,mod}$), known as the clearness index or clear sky index (k_t; Equation B-13):

$$k_t = J_{sn,meas}/J_{sn,mod} \times \cos\theta \quad \text{(B-13)}$$

where θ is the solar zenith angle and values of k_t range between 0 and 1 with a value of 1 indicating clear sky. Applying k_t to the correlation equation proposed by Erbs et al., (1982) results in an estimate of k_d, which represents the fraction of diffuse shortwave radiation (Equation B-14).

$$k_d = \begin{cases} 1 - 0.09k_t, & k_t \leq 0.22 \\ 0.9511 - 0.1604k_t + 4.39k_t^2 - 16.64k_t^3 + 12.34k_t^4, & 0.22 < k_t \leq 0.80 \\ 0.165, & k_t > 0.80 \end{cases} \quad \text{(B-14)}$$

The amount of diffuse radiation at the measurement location is then calculated as (Equation B-15):

$$\hat{J}_{sn,diff} = J_{sn,meas}(k_d) \quad \text{(B-15)}$$

The amount of direct shortwave radiation at the measurement location ($\hat{J}_{sn,dir}$) is then calculated from Equation B-12 via subtraction. The direct shortwave radiation at the water surface is then calculated by applying a topographic shading factors (S_f) estimated using the algorithm described by Mihalevich et al. (2020; Equation B-16).

$$J_{sn,dir} = (S_f)\hat{J}_{sn,dir} \quad \text{(B-16)}$$

Diffuse radiation incident at the water surface is reduced by the fraction of the overlying visible hemisphere, referred to as the sky view factor (SV_f) which is calculated using the formula from (Dozier and Frew 1990) (Equation B-17).

$$SV_f = \frac{1}{2}\sum_{\Phi_j=1}^{360} sin^2\,(90 - \Psi_{E,\Phi}) \quad \text{(B-17)}$$

where Φ is the azimuth angle and $\Psi_{E,\Phi}$ is the elevation angle in the Φ direction. The diffuse shortwave radiation reaching the water surface of each model cell over time is then calculated as (Equation B-18):

$$J_{sn,diff} = (SV_f)\hat{J}_{sn,diff} \quad \text{(B-18)}$$

Land-reflected radiation is the combination of both direct radiation and diffuse radiation incident on the water surface which has been reflected off the surrounding terrain (Chen et al. 2006), and is calculated following Gates, (1980) as (Equation B-19):

$$J_{sn,refl,c} = \alpha_{land}(1 - SV_{f,c}) \times (\hat{J}_{sn,dir} + \hat{J}_{sn,diff}) \quad \text{(B-19)}$$

where α_{land} is the albedo of the surrounding terrain.

Longwave radiation

Heat emitted from rock as longwave radiation (J_{rock}) was estimated following the Stefan-Boltzmann Law (Chapra 2008) and is reduced by the fraction of visible terrain as (Equation B-20):

$$J_{rock} = (1 - SV_f)(\varepsilon_{lc}\, \sigma\, T_{rock}^4) \quad \text{(B-20)}$$

where σ is the Stefan-Boltzmann constant ($W/m^2/K^4$) and $\mathcal{E}_{lc}$ is the emissivity of the land. T_{rock} is the rock temperature (K) and was assumed to be the same as the air temperature (T_{air}).

Heat emitted from the atmosphere as longwave radiation (J_{an}) is obstructed by surrounding topography, reducing the amount that is received at the water surface. To account for this, atmospheric longwave radiation was scaled by the sky view as (Equation B-21)

$$J_{an} = SV_f(\varepsilon_{atm}\, \sigma\, T_{air}^4)(1 - R_L) \quad \text{(B-21)}$$

where $\mathcal{E}_{atm}$ is the emissivity of the atmosphere and R_L is the reflection coefficient.

Text B-2: Green River temperature model information

Tributary Data

Inflows from several tributaries along the Green River were directly accounted for in the model. These include Jones Hole Creek, Duchesne River, White River, Price River, and San Rafael River (Figure 3-1). Flows for Jones Hole Creek are relatively stable year round and are assumed to be 1.03 m^3s^{-1} (Sumsion 1976; Thomas 1952) with a temperature of 13 °C (Sumsion, 1976; USFWS, 2020). Gages for the Duchesne, White, and Price are located 25 km, 95 km, and 43 km upstream, respectively, of their confluences with the Green River. Estimated travel times of 17, 57, and 6 hours for each tributary branch, respectively, was determined using simplistic hydraulic wave routing models in EPA SWMM (Storm Water Management Model; Rossman, 2006), and were applied to the input datasets as a constant time offset. The San Rafael River has a long-term gage located 59 km upstream and a relatively new gage located 6 km upstream of the confluence with the Green River. Hydrographs from these two gages were compared to estimate a travel time of 20 hours which was applied to the long-term dataset as a constant time offset. Temperature measurements at the Duchesne, Price and San Rafael river gages, were used to determine their inflow heat contributions. Temperature is not currently measured at the White River gage. In order to determine inflow heat contributions from the White River the monthly average temperatures from an inactive gage (*09306900 White River at Mouth near Ouray Utah*) were used with the upstream discharge measurements (near Watson, UT).

Distributed Flows

Differences in streamflow volume between upstream and downstream gages can arise due to ungaged tributary inflows, groundwater inflows or losses, and agricultural diversions and return flows. To close the flow balance for each river segment, which is

defined by the distance between locations where stream flow measurements are made, we computed a 10-day moving average of daily flow difference between gaging stations, accounting for gaged tributaries. This resulted in daily estimates (positive or negative) of distributed flows for each segment. Due to the uncertainty surrounding the location where inflows or outflows occur, these estimates were applied evenly over each model segment. Temperatures of these inflows also have great uncertainty since their source may be surface or subsurface flow or a combination of both. Acknowledging this uncertainty, we used the gridded meteorological data to estimate long-term average air temperatures and assigned these values to the corresponding model elements.

Sediment Heat Flux

A boundary condition sediment depth of 0.5 m and a sediment thermal diffusivity of 1.8×10^{-6} m^2/s were used to compute sediment conduction throughout the model domain. These values are based on measurements of active bed thickness and thermal diffusivity for the Green River in Brown's Park National Wildlife Refuge (approximately 55 km below FGD) by Carron (2000). The depth of the shallow sediment layer was assumed to be 0.25 m. We assumed the boundary condition temperature to be equal to the year-to-year average air temperatures estimated form the meteorological inputs and these values were assigned to the corresponding model elements.

Bedrock Longwave Radiation

Longwave radiation emitted from adjacent bedrock is estimated using the Stefan-Boltzmann Law as a function of rock temperature and emissivity. Following Mihalevich et al. (2020), we assumed the rock temperatures for each model element to be the same as

the corresponding air temperatures. Rock emissivity was assigned for each model element by determining the adjacent bedrock formation (Pederson and Tressler 2012) and corresponding emissivity value (Brewster 1992), which ranged between 0.7 and 0.9.

Topographic Shading Factors

Shading factors were calculated in the Green River using the algorithm described by Mihalevich et al. (2020). Here, factors were estimated using a 10 m resolution digital elevation model (DEM) in 15 minute increments at locations spaced every 100 m along the river centerline. Estimates were then averaged over space for each 1 km long model cell. This resulted in a timeseries of shade factors that represents the fraction of a cell being shaded at a given time.

Flow routing calibration

Hydraulic routing was calibrated in SWMM for each river segment, which is a section of river between two USGS gages. Calibration was carried out by sequentially incrementing Manning roughness values between 0.02 and 0.05 in 0.001 increments and simulating flows over the 2017 calendar year. Root mean squared error (RMSE) and Nash-Sutcliff efficiency (NSE) were used as performance metrics to determine roughness coefficients for each segment. Similar to Carron & Rajaram (2001), who simulated flows between FGD and the confluence of the Yampa River (105 km downstream), we found a Manning's n = 0.04 to minimize discharge RMSE for the segment between FGD and the Green River near Jensen, UT. Calibration of this segment was only evaluated during periods when the Yampa River had low and steady flows, since a gage near the confluence of the Green and Yampa does not exist. Similarly, roughness values for the

Yampa River were calibrated during times when FGD releases were relatively low and steady. Roughness values in other river segments ranged between 0.03 and 0.05.

Discharge and river temperatures were evaluated at several locations in the Green (Figure 3-1). Some discharge and temperature monitoring locations, particularly those farther downstream, are relatively new and have only existed since 2015. We calculated the RMSE for each temperature monitoring location to evaluate model performance.

Table B-1. Monthly estimates of air temperature lapse rates and dew point temperature lapse rates for the Northern Hemisphere (Kunkel 1989).

Month	Air Temperature Lapse Rate (°C km^{-1})	Dew Point Temperature Lapse Rate (°C km^{-1})
Jan	4.4	5.6
Feb	5.9	5.8
Mar	7.1	5.5
Apr	7.8	5.4
May	8.1	5.2
Jun	8.2	5.0
Jul	8.1	4.5
Aug	8.1	4.5
Sep	7.7	5.0
Oct	6.8	5.1
Nov	5.5	5.5
Dec	4.7	5.5

Table B-2. Mean error (ME) between remote automated weather stations (RAWS) and input weather data used in the river temperature models. CR-WS solar radiation is a median time series of all RAWS data. Error is calculated as the CR-WS or ERA-010 input weather dataset minus the RAWS data, resulting in positive errors equating to overestimates. The bottom two rows represent the mean error and standard deviation (σ) of all RAWS sites combined.

Solar Radiation ME [W/m^2]

	CR-WS	ERA5-010												
RAWS Name	Year	Year	Jan	Feb	Mar	Apr	May	Jun	Jul	Aug	Sep	Oct	Nov	Dec
DRY PARK	44.4	54.3	48.4	61.9	49.5	48.9	63.2	67.6	97.1	58.4	38.2	35.9	40.5	45.0
FOUR SPRINGS	-12.6	-0.2	-4.4	-0.1	10.9	-6.5	-6.2	-17.8	13.4	12.7	13.0	-3.4	-9.5	-4.1
FRAZIER WELLS	-1.5	11.8	2.5	7.8	12.3	11.7	11.2	9.7	37.4	23.5	14.7	4.5	0.6	4.4
GUNSIGHT	-11.8	-0.3	-0.8	2.2	9.4	-4.0	-2.3	-10.6	7.0	-0.4	-1.5	-0.4	-2.1	0.2
LINDBERGH HILL	17.3	28.3	15.7	45.2	39.0	33.3	27.6	18.5	64.3	44.2	23.9	17.1	5.1	12.0
MOUNT LOGAN	-5.4	6.7	13.8	10.0	7.1	3.9	4.1	-5.2	18.2	6.4	4.8	-4.5	8.3	13.8
MUSIC MOUNTAIN	-18.6	-1.6	-0.1	5.0	7.0	-3.3	-7.1	-9.5	4.1	-6.0	-0.8	-5.3	-3.0	0.7
NEVERSHINE	-6.6	4.5	5.7	8.5	11.1	8.5	7.7	0.1	-0.1	4.4	-0.9	3.6	2.6	3.5
NIXON FLATS	-1.0	10.5	11.6	9.5	7.4	-2.1	4.7	4.0	36.5	16.8	13.6	4.7	3.0	14.4
OLAF KNOLLS	-15.7	-3.2	-0.8	0.5	-3.0	4.4	-0.1	-7.7	0.9	-3.6	-10.9	-9.7	-6.9	-1.1
PARIA POINT	-11.1	2.0	-0.7	1.6	14.6	-0.9	-6.3	-15.1	10.6	11.4	19.1	-2.1	-5.9	-1.1
TUSAYAN	27.4	35.9	31.9	32.7	31.6	37.6	46.7	40.9	60.3	49.4	29.5	16.1	22.7	31.3
YELLOW JOHN MOUNTAIN	-3.9	9.7	5.9	9.1	19.1	10.2	9.1	-1.5	21.9	15.8	16.5	2.4	1.7	5.5
NAVAJO MONUMENT	8.0	20.1	13.2	16.6	16.2	23.7	30.3	11.4	42.2	42.0	21.4	5.6	8.1	10.6
HOPI	3.0	18.6	-0.3	8.6	16.3	31.4	37.4	33.5	47.1	33.8	16.4	4.1	-1.9	2.0
KANE GULCH	-5.4	7.1	4.7	9.3	8.0	5.8	11.6	3.3	19.9	7.9	5.9	2.7	-1.3	7.1
ME	-0.8	11.8	8.5	13.2	14.9	10.5	12.2	6.2	29.4	18.4	12.5	4.0	3.4	8.7
σ	93.9	105.9	72.5	89.1	102.4	113.7	121.1	119.6	149.0	133.3	109.2	82.3	69.1	67.6

Table B-3. Nash-Sutcliffe Efficiency (NSE) between GCMRC-WS data and input weather data used in the river temperature models before (Pre) and after (Post) elevation corrections were applied.

Grand Canyon Weather Stations (GCMRC-WS)	Air Temperature NSE					Relative Humidity NSE					Wind Speed NSE				
	CR-WS		ERA5-010		ERA-100	CR-WS		ERA5-010		ERA5-100	CR-WS		ERA5-010		ERA5-100
	Pre	Post	Pre	Post	Post	Pre	Post	Pre	Post	Post	Pre	Post	Pre	Post	Post
Mile -10	0.9	0.8	0.9	1.0	0.9	0.9	0.9	0.6	0.6	0.7	-1.3	-0.1	-0.6	-0.4	-0.2
Mile 0.5	1.0	0.8	0.9	0.9	0.9	0.8	0.8	0.7	0.7	0.7	-1.0	0.0	0.0	0.0	0.1
Mile 24.5 Upper	0.9	0.9	0.6	0.9	0.9	0.7	0.7	-0.1	0.0	0.3	-3.9	-0.3	-1.4	-0.1	0.0
Mile 24.5 Lower	0.7	0.9	0.6	0.9	0.9	0.7	0.7	-0.1	0.0	0.3	-4.9	-0.5	-2.3	-0.2	-0.1
Mile 58 Upper	0.8	0.9	0.5	0.9	0.9	0.3	0.3	0.3	0.3	0.5	-1.0	-0.5	0.3	-0.3	0.0
Mile 58 Lower	0.7	0.9	0.5	0.8	0.8	0.2	0.2	0.3	0.3	0.4	-4.8	-1.2	-0.4	-0.2	0.1
Mile 60	0.5	0.9	0.5	0.9	0.9	0.6	0.6	0.3	0.3	0.5	-3.0	-0.5	-0.4	-0.1	0.2
Mile 66	0.5	0.9	0.5	0.9	0.9	0.5	0.5	0.2	0.3	0.4	-0.9	-1.0	-0.1	-1.1	-0.5
Mile 70 Upper	0.7	0.8	0.7	0.9	0.9	0.7	0.6	0.5	0.5	0.6	-0.9	-0.2	0.4	-0.2	0.2
Mile 70 Lower	0.6	0.9	0.6	0.9	0.9	0.6	0.6	0.4	0.5	0.6	-0.7	-0.4	0.4	-0.2	0.2
Mile 88	0.8	0.9	0.6	0.8	0.9	0.7	0.7	0.6	0.6	0.6	-13.0	-1.2	-1.7	0.3	-0.5
Mile 125.5	0.8	0.9	0.6	0.9	0.9	0.7	0.7	0.5	0.6	0.6	-2.0	-0.5	-0.1	-0.6	-0.2
Mile 135	0.4	0.9	0.5	0.9	0.9	0.7	0.7	0.5	0.6	0.6	-1.5	-0.5	0.0	-0.2	0.1
Mile 203	0.1	0.8	0.4	0.9	0.9	0.4	0.5	0.5	0.5	0.5	-4.8	-0.7	-0.6	-0.4	-0.2
Mile 223	0.6	0.9	0.6	0.9	0.9	0.6	0.7	0.6	0.7	0.7	-2.2	-0.2	-0.5	-0.1	0.0

Table B-4. Root Mean Square Error (RMSE) between GCMRC-WS data and input weather data used in the river temperature models before (Pre) and after (Post) elevation corrections were applied.

Grand Canyon Weather Stations (GCMRC-WS)	Air Temperature RMSE [°C]					Relative Humidity RMSE [%]					Wind Speed RMSE [m/s]				
	CR-WS		ERA5-010		ERA-100	CR-WS		ERA5-010		ERA5-100	CR-WS		ERA5-010		ERA5-100
	Pre	Post	Pre	Post	Post	Pre	Post	Pre	Post	Post	Pre	Post	Pre	Post	Post
Mile -10	2.2	4.1	3.3	2.2	2.5	4.7	5.1	12.9	12.8	11.9	1.9	1.3	1.5	1.4	1.3
Mile 0.5	2.4	4.5	3.7	2.8	3.1	10.6	10.7	11.9	12.0	12.4	1.7	1.2	1.2	1.3	1.2
Mile 24.5 Upper	3.6	2.9	6.4	3.4	3.3	11.0	10.5	19.4	18.0	15.1	2.2	1.1	1.6	1.1	1.0
Mile 24.5 Lower	4.5	2.0	6.3	3.5	3.3	13.5	13.0	18.9	17.8	14.9	2.2	1.1	1.7	1.0	0.9
Mile 58 Upper	5.1	3.0	6.7	3.6	3.2	19.8	19.6	16.2	15.8	13.5	3.1	2.7	1.6	2.1	1.8
Mile 58 Lower	5.1	3.2	6.4	4.0	3.7	19.9	19.9	16.3	16.3	14.3	2.8	1.7	1.3	1.2	1.0
Mile 60	5.3	2.4	6.9	3.6	3.2	15.6	15.1	16.2	15.7	13.3	2.1	1.3	1.3	1.1	1.0
Mile 66	5.8	2.8	7.0	3.6	3.4	17.9	17.7	16.8	16.8	15.0	2.3	2.4	1.8	2.4	2.0
Mile 70 Upper	4.6	3.9	6.3	3.7	3.5	13.3	13.9	15.6	15.4	14.2	2.0	1.5	1.2	1.6	1.3
Mile 70 Lower	5.5	3.1	6.4	3.8	3.5	17.4	17.2	16.1	16.0	14.3	2.2	2.0	1.3	1.9	1.5
Mile 88	4.6	3.0	6.8	4.1	4.0	13.2	13.0	14.8	14.7	14.6	2.4	0.9	1.2	0.6	0.9
Mile 125.5	5.1	2.7	6.7	2.9	3.0	11.7	11.3	15.0	13.7	13.5	2.0	1.4	1.3	1.5	1.3
Mile 135	6.3	2.9	7.8	3.5	3.4	14.2	13.3	15.6	14.8	14.3	2.2	1.7	1.1	1.3	1.1
Mile 203	7.7	4.1	7.4	3.5	3.5	19.6	18.4	15.3	15.8	15.7	2.3	1.2	1.2	1.1	1.0
Mile 223	6.7	3.5	6.8	3.1	3.0	13.7	12.7	13.2	12.4	12.2	1.9	1.2	1.3	1.1	1.1

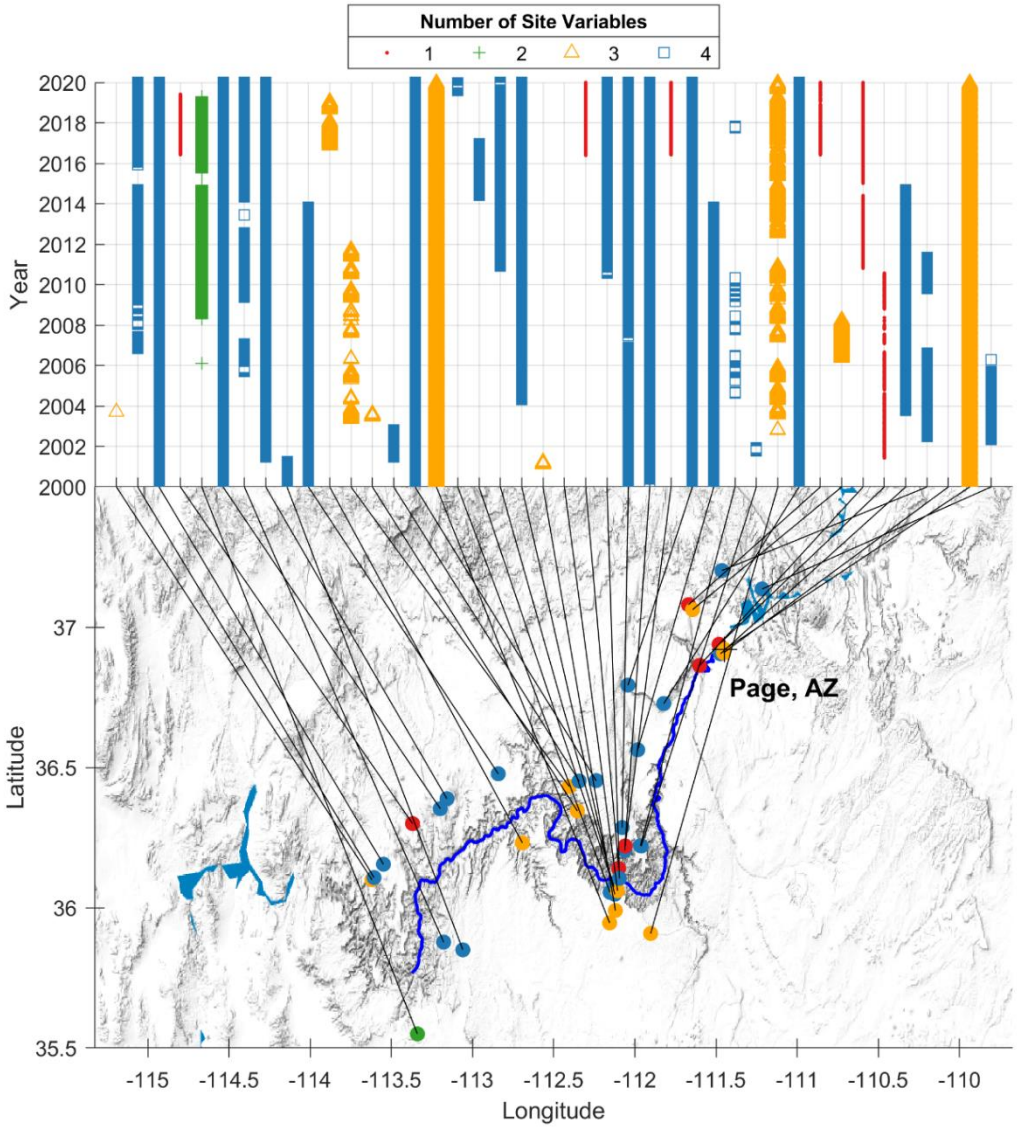

Figure B-1. Weather stations within 20 miles of the Colorado River in Grand Canyon available on the MesoWest database. The bar chart on top shows the temporal availability of data for each site. Sites are color coded by the number of variables available for river temperature modeling (i.e., air temperature, wind speed, solar radiation, and relative humidity or dew point temperature).

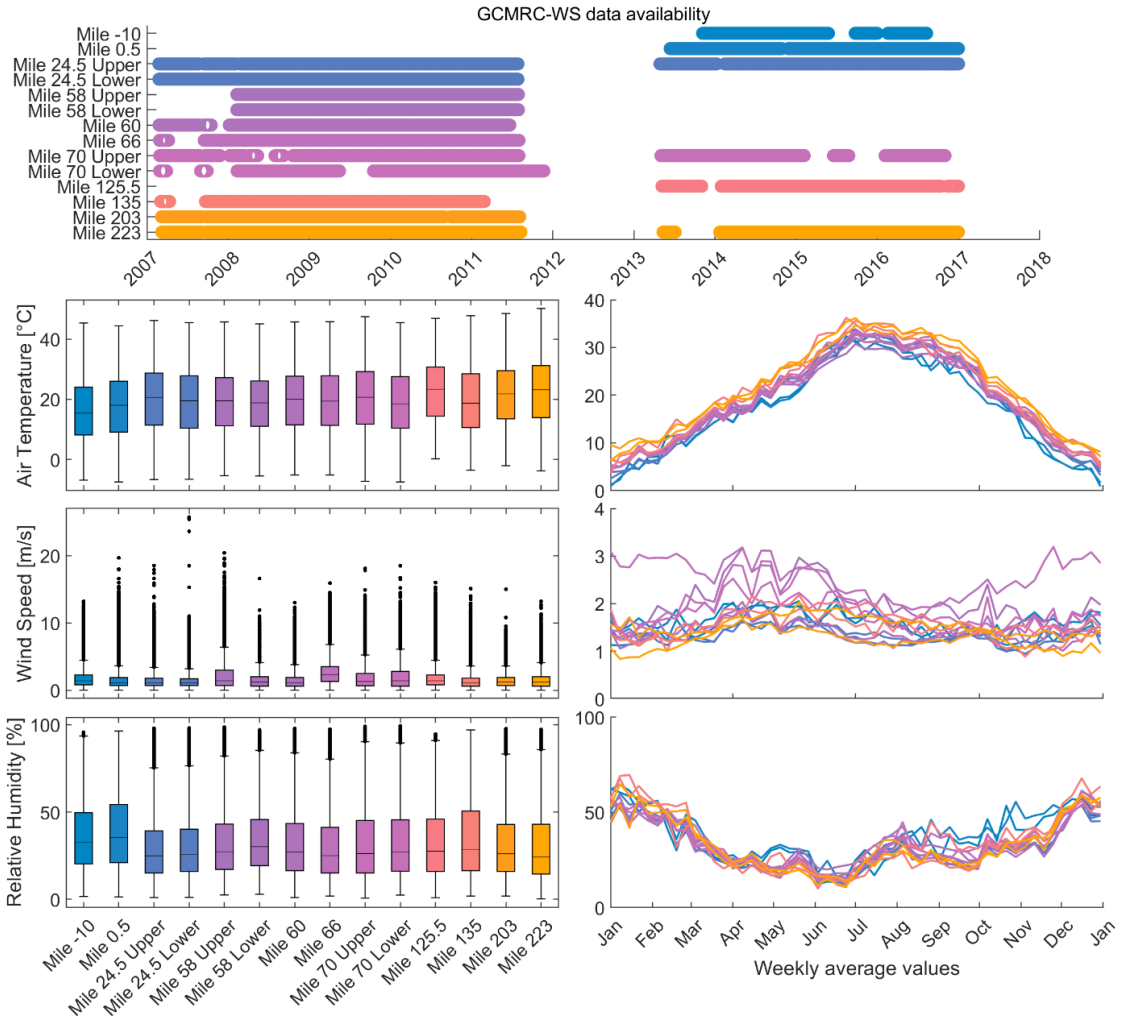

Figure B-2. Data availability for weather stations within Grand Canyon. Sites are listed top to bottom in order of distance downstream of Glen Canyon Dam. River mile zero is located at Lees Ferry (Table 2-2) and downstream river distances are positive and upstream river distances are negative. Spatial trends of each variable are shown in subsequent plots in the left column. Temporal trends of each variable are shown in subsequent plots in the right column. The color used for each location corresponds to the colors shown in Figure 1 of the manuscript.

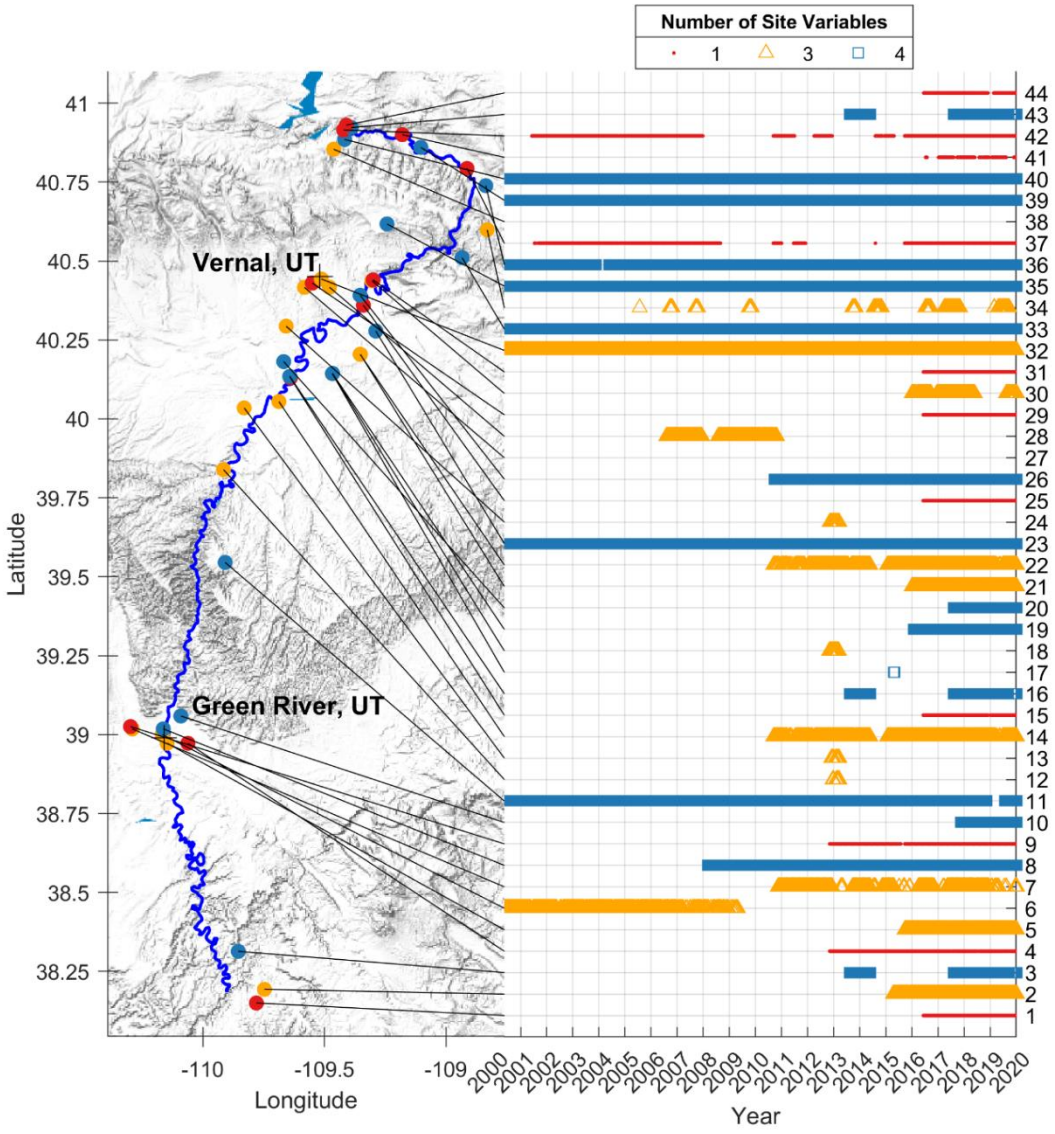

Figure B-3. Weather stations within 10 miles of the Green River available on the MesoWest database. The bar chart on right shows the temporal availability of data for each site. Sites are color coded by the number of variables available for river temperature modeling (i.e., air temperature, wind speed, solar radiation, and relative humidity or dew point temperature).

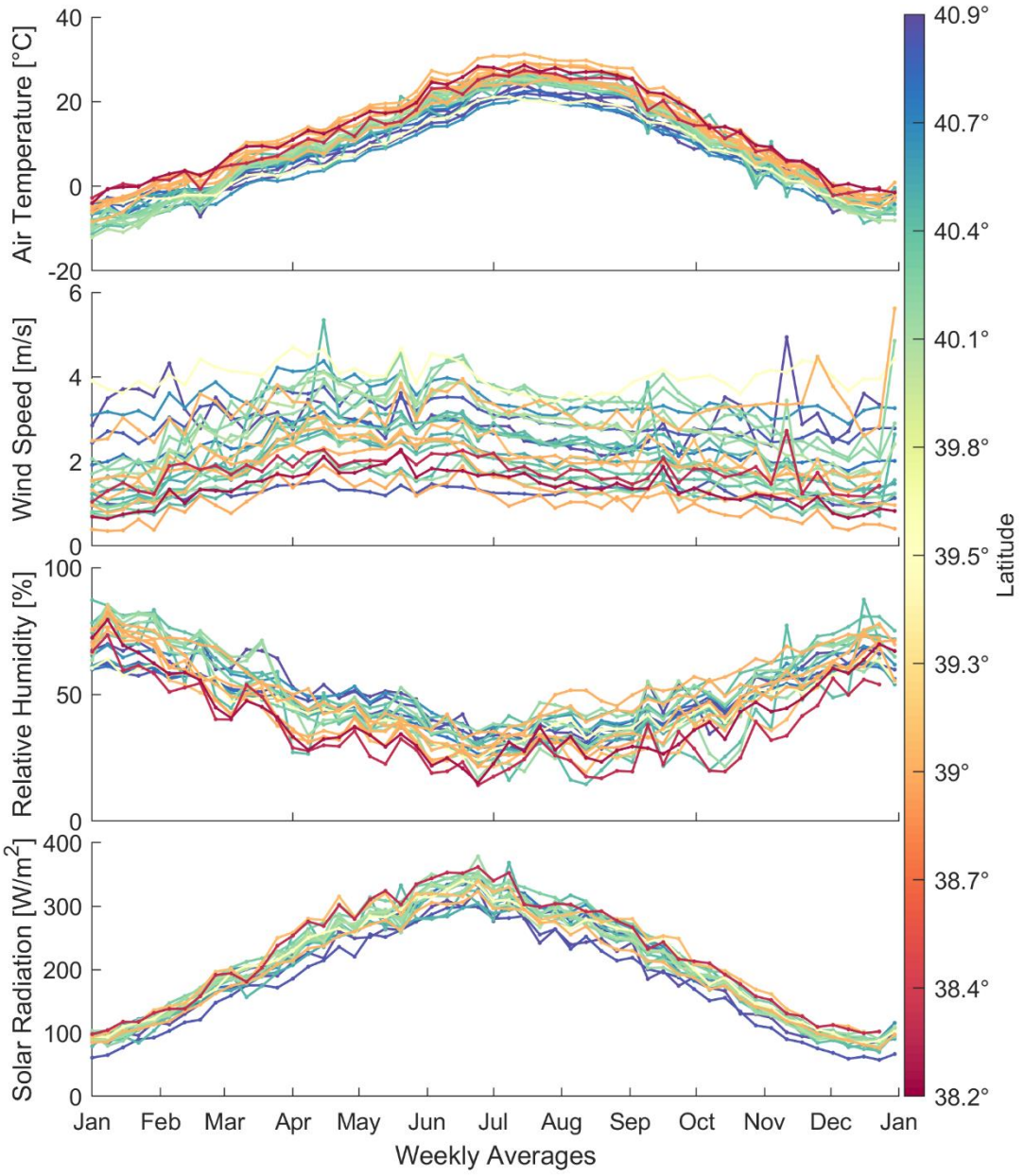

Figure B-4. Spatial and temporal tendencies of weather parameters for the stations shown in Figure B-3. Sites with limited information (n=16) were excluded.

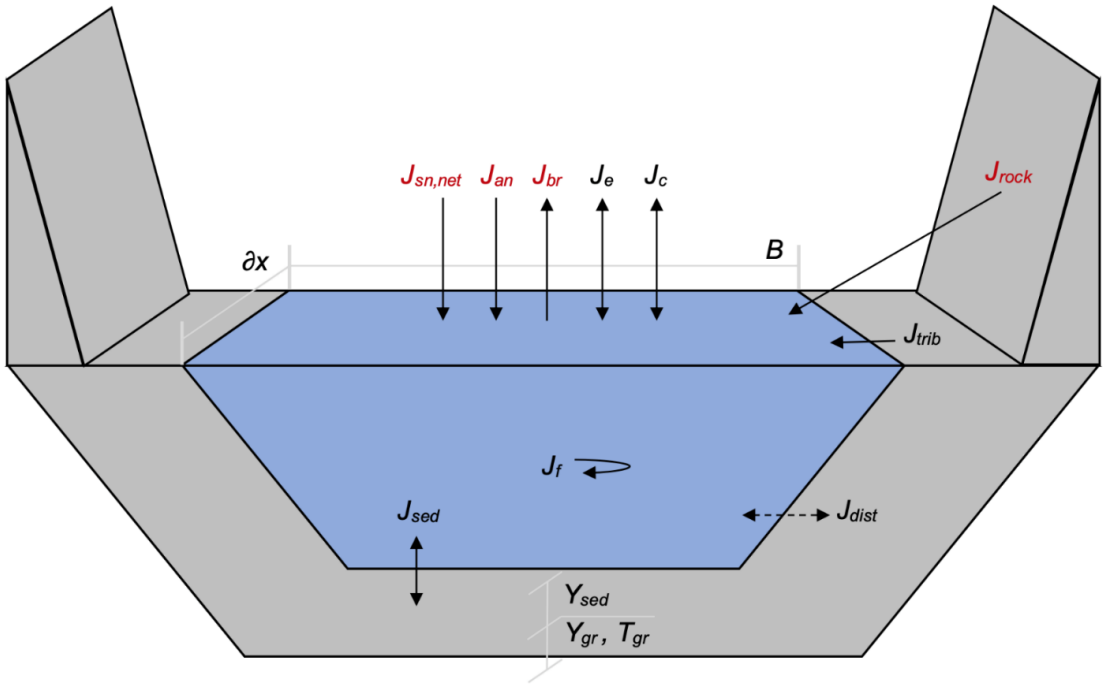

Figure B-5. Simple schematic of external heat fluxes and lateral inflows accounted for in the river temperature model. Included terms are net shortwave radiation ($J_{sn,net}$), atmospheric longwave radiation (J_{an}), water longwave radiation (J_{br}), bedrock longwave radiation (J_{rock}), sensible heat (conduction and convection; J_c), latent heat (evaporation and condensation; J_e), internal fluid shear friction (J_f), sediment conduction (J_{sed}), tributary flows (J_{trib}) and distributed flows (J_{dist}). Radiative terms are shown in red ($J_{sn,net}$, J_{an}, J_{br}, and J_{rock}) and are described and illustrated in greater detail in the manuscript. Y_{sed} is the depth of the shallow sediment layer, and Y_{gr} is the depth to the ground boundary layer. T_{sed} is the temperature of the shallow sediment layer and T_{gr} is the temperature of the ground boundary layer.

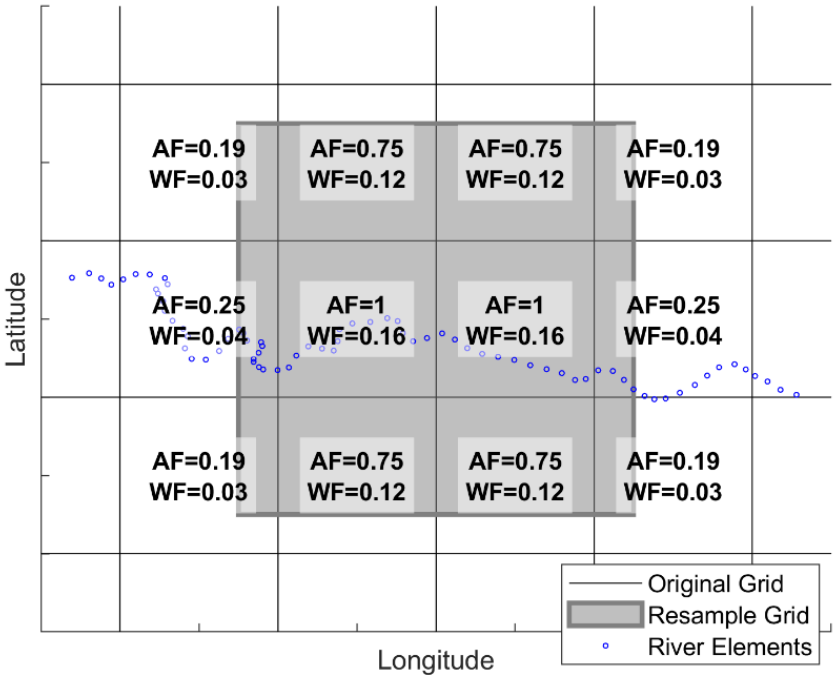

Figure B-6. Example ERA5-Land grid resampling technique. The areal fraction (AF) is the fraction of original grid overlapped by the resample grid. The weight fraction (WF) is calculated as the AF of a single grid divided by the sum of AF and sums to 1. Resampling is done after values have been elevation corrected.

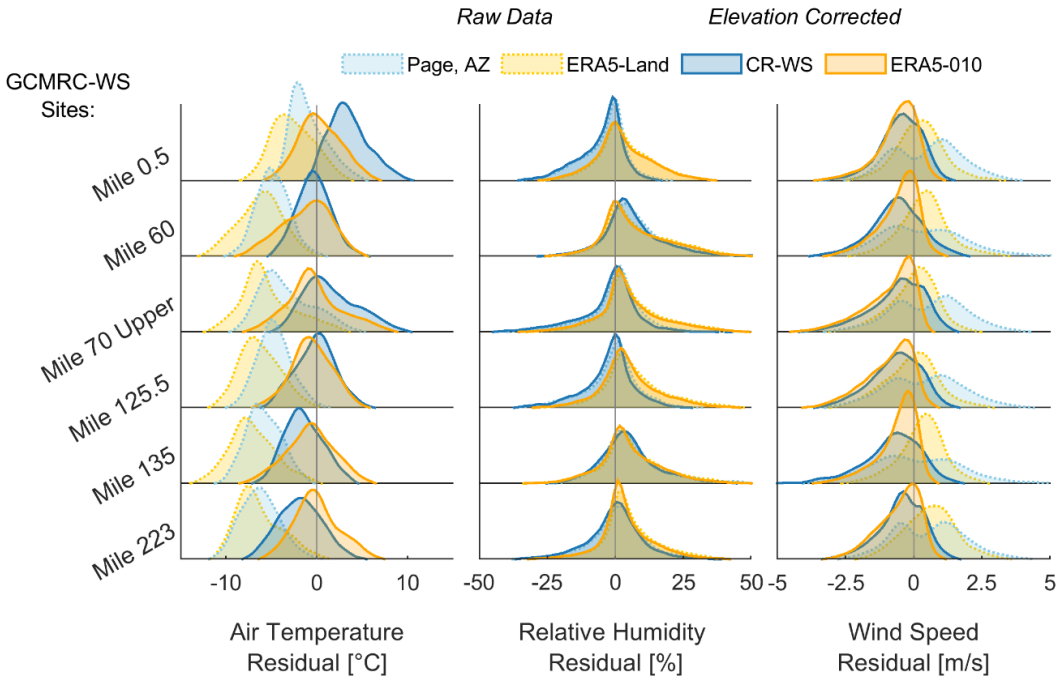

Figure B-7. Density ridgeline plots showing the distribution of residuals, calculated as Page, AZ or ERA5-Land data minus GCMRC-WS datasets, for each variable before and after elevation corrections were applied. Only a subset of GCMRC-WS is shown here, but before and after distributions were similar among all sites. Dashed ridgelines represent raw, uncorrected data, and solid ridgelines represent data after elevation corrections. Negative residuals represent underestimates and positive residuals represent overestimates.

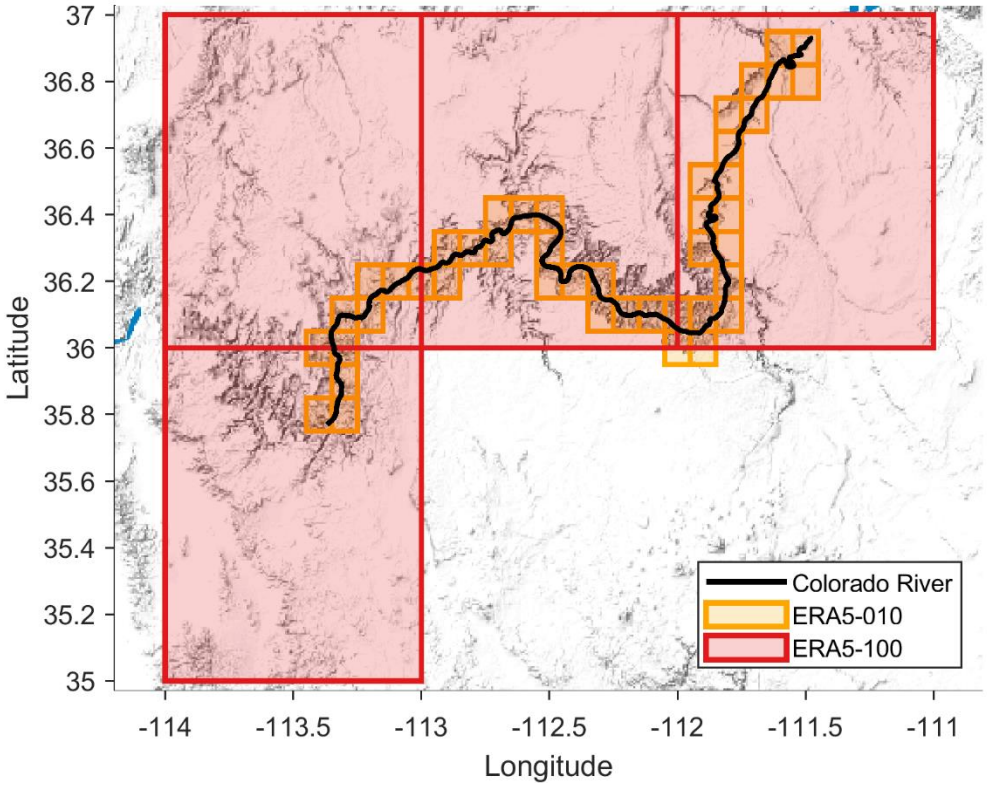

Figure B-8. Spatial coverage of ERA5-010 and ERA5-100 grids in the Colorado River Grand Canyon temperature model.

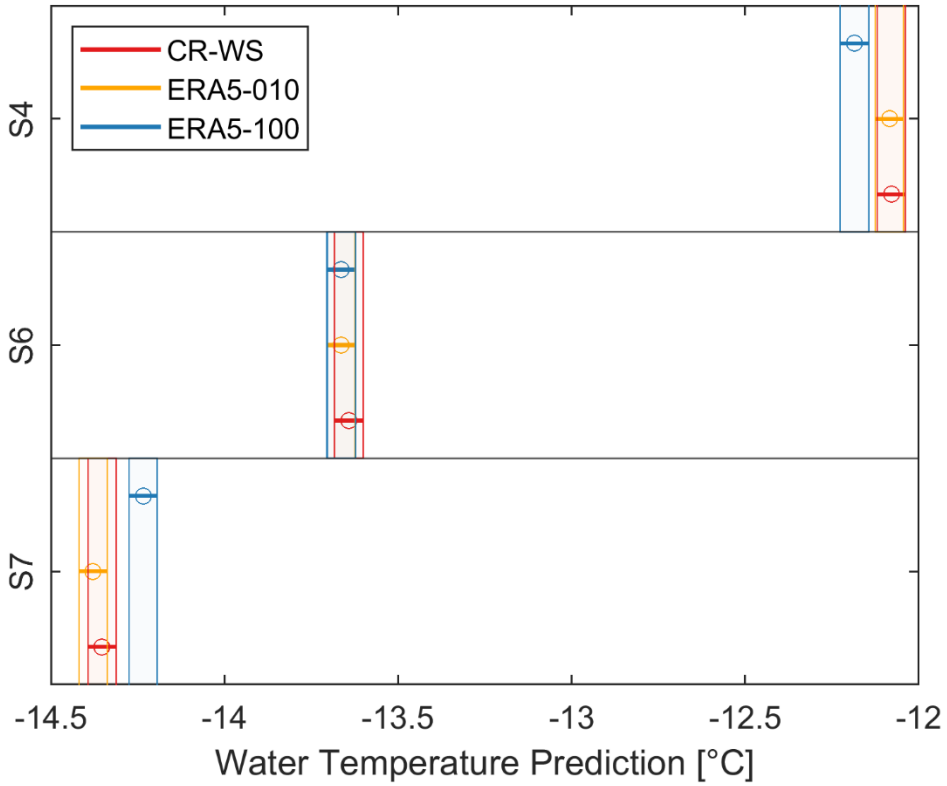

Figure B-9. Tukey's Honest Significant Difference test for each of the three input weather datasets at the three locations evaluated in the Colorado River in Grand Canyon. Vertical overlaps represent statistically similar means.

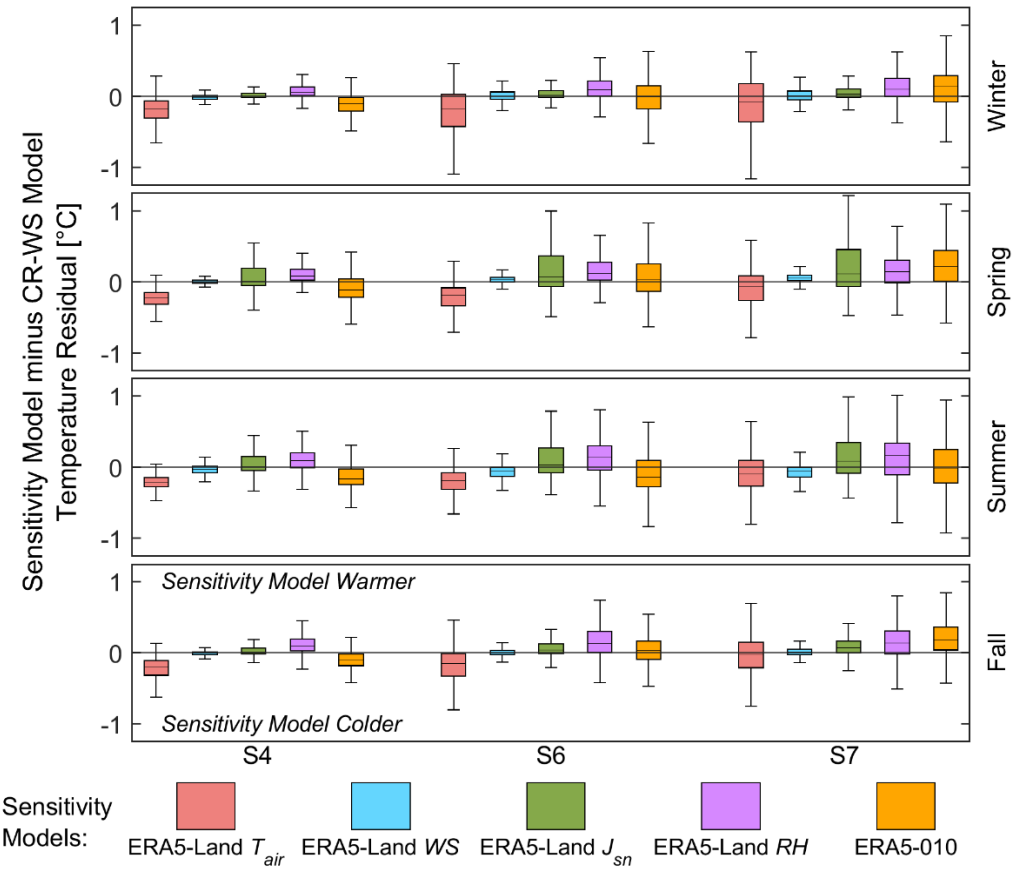

Figure B-10. Seasonal differences in water temperature predictions between the CR-WS model and different sensitivity runs that apply one spatially varying weather variable from ERA5-Land (elevation corrected) and the remaining three weather variables are from the CR-WS dataset. Each of the four weather inputs were tested independently. Comparison between CR-WS model and ERA5-010 model (which includes all four ERA5-Land variables) is also included for reference.

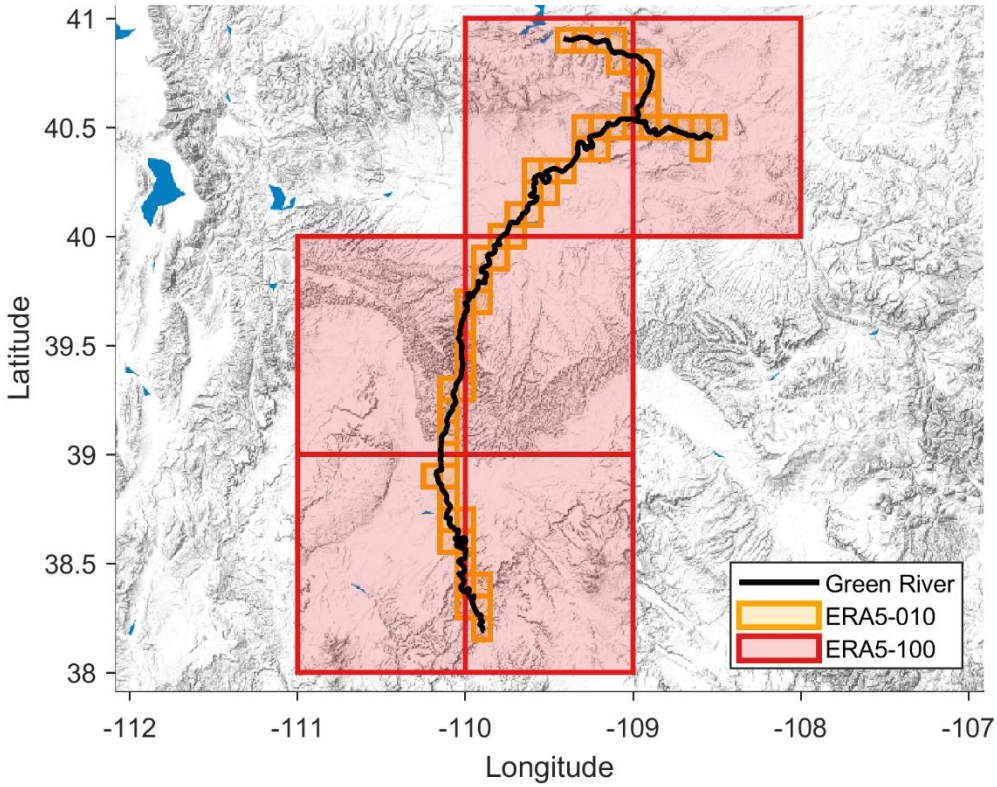

Figure B-11. Spatial coverage of ERA5-010 and ERA5-100 grids in the Green River temperature model.

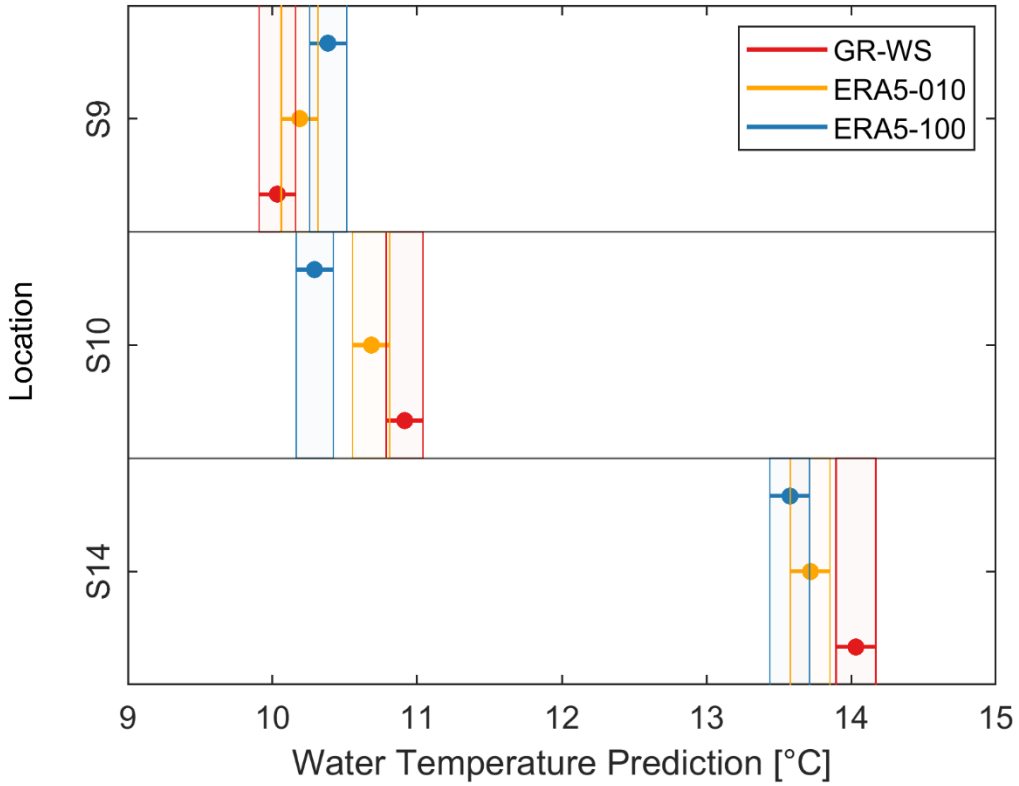

Figure B12. Tukey's Honest Significant Difference test for each of the three input weather datasets at the three locations evaluated in the Green River. Vertical overlaps represent statistically similar means.

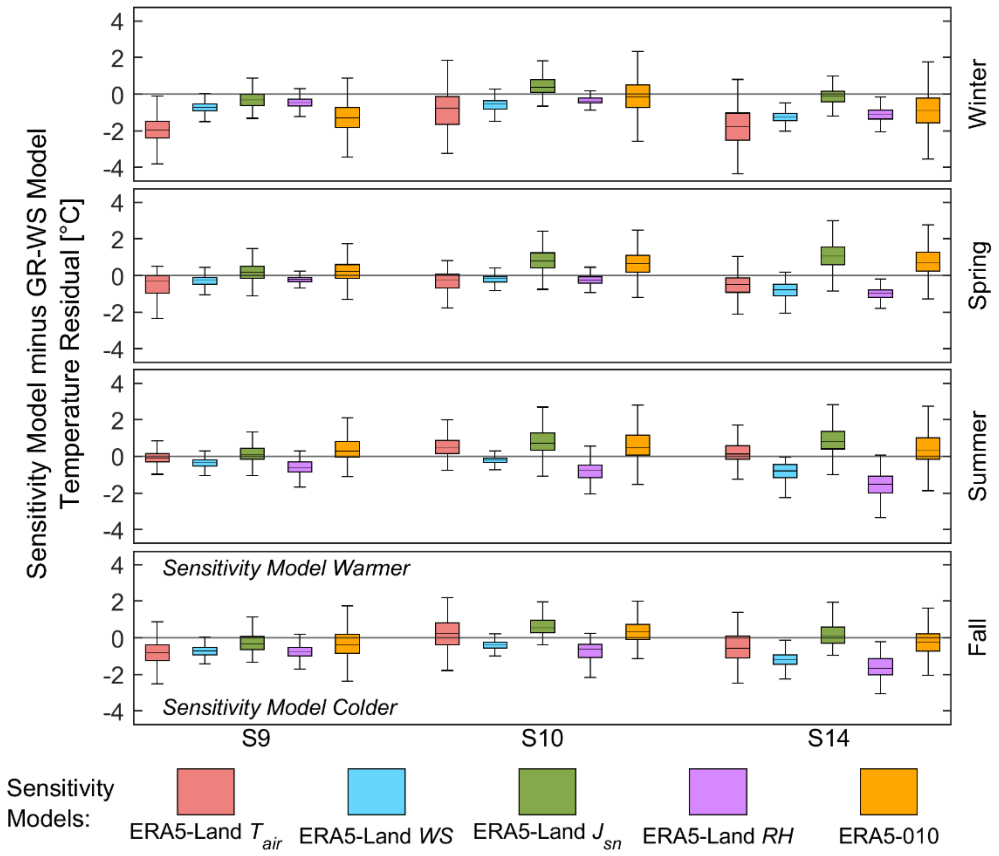

Figure B-13. Seasonal differences in water temperature predictions between the GR-WS model and different sensitivity runs that apply one spatially varying weather variable from ERA5-Land (elevation corrected) and the remaining three weather variables are from the GR-WS dataset. Each of the four weather inputs were tested independently. Comparison between GR-WS model and ERA5-010 model (which includes all four ERA5-Land variables) is also included for reference.

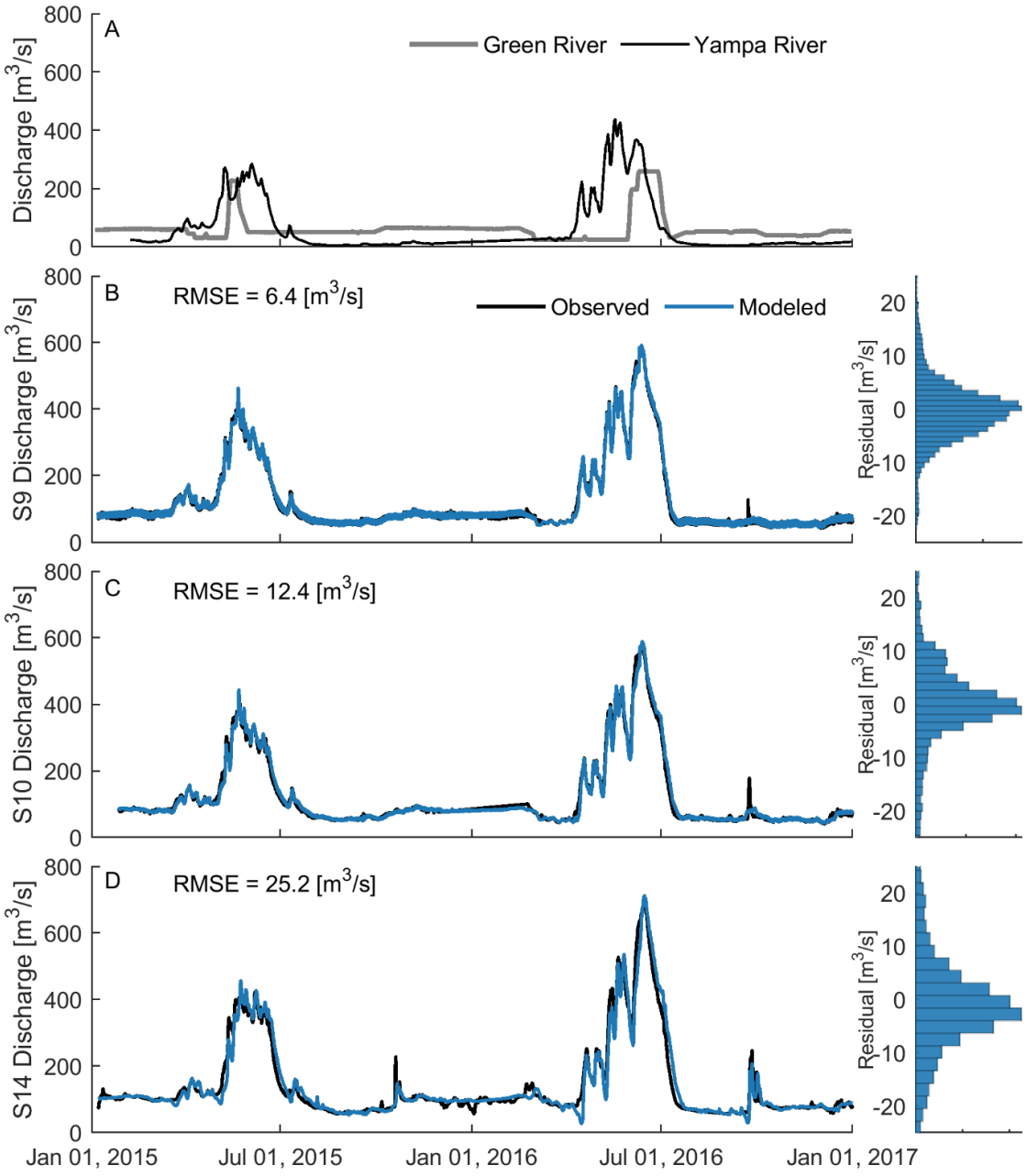

Figure B-14. Boundary condition flow for the Green River (A) with discharge predictions at downstream monitoring locations (B, C, and D) shown in Figure 1 and Table 2. Histograms on the right hand side show model residuals calculated as observed minus modeled. Time series data shown are hourly. Root mean square error (RMSE) values are for the data available over the two-year simulation period.

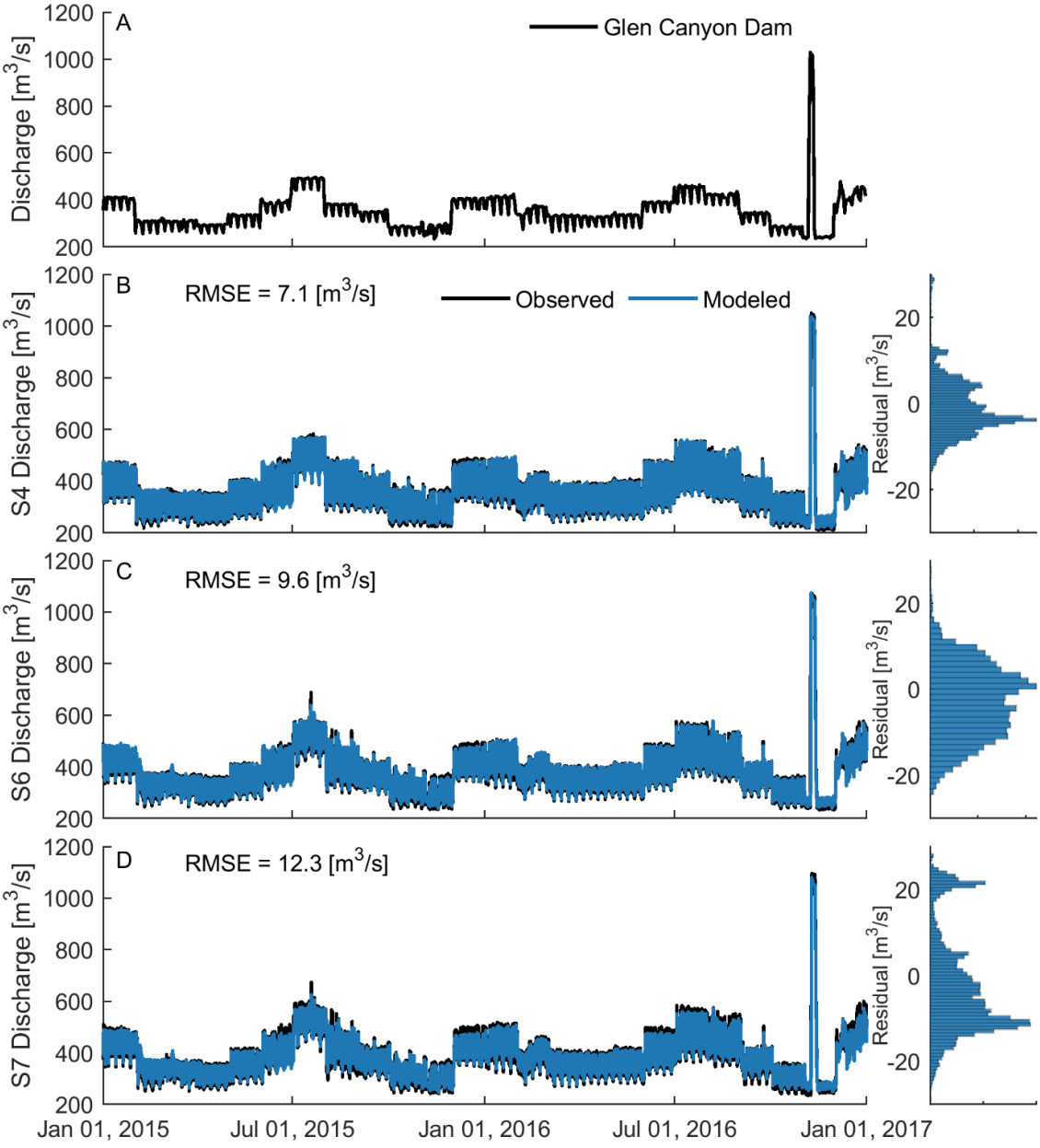

Figure B-15. Boundary condition flow for the Colorado River (A) with discharge predictions at downstream monitoring locations (B, C, and D) shown in Figure 1 and Table 2. Histograms on the right hand side show model residuals calculated as observed minus modeled. Time series data shown are hourly. Root mean square error (RMSE) values are for the data available over the two-year simulation period.

References

Bowen, I. S. (1926). The Ratio of Heat Losses by Conduction and by Evaporation from any Water Surface. Phys. Rev., 27, 779–787. https://doi.org/https://doi.org/10.1103/PhysRev.27.779.

Boyd, M., & Kasper, B. (2003). Analytical Methods for Dynamic Open Channel Heat and Mass Transfer: Methodology for the Heat Source Model Version 7.0. 204. http://www.deq.state.or.us/wq/TMDLs/tools.htm

Brewster, Q. M. (1992). Thermal radiative transfer and properties. John Wiley & Sons Ltd.

Buahin, C. A., Horsburgh, J. S., & Neilson, B. T. (2019). Parallel multi-objective calibration of a component-based river temperature model. Environmental Modelling & Software, 116(February), 57–71. https://doi.org/10.1016/j.envsoft.2019.02.012

Carron, J. C. (2000). Simulation and optimization of unsteady flow and water temperature in reservoir regulated rivers. Civil, Environmental and Architectual Engineering Ph.D. Thesis, University of Colorado, Boulder CO., 159.

Carron, J. C., & Rajaram, H. (2001). Impact of variable reservoir releases on management of downstream water temperatures. Water Resources Research, 37(6), 1733–1743. https://doi.org/10.1029/2000WR900390

Chapra, S. C. (2008). Surface water-quality modeling. In McGraw-Hill Series in Water Resources and Environmental Engineering.

Chen, Y., Hall, A., & Liou, K. N. (2006). Application of three-dimensional solar radiative transfer to mountains. Journal of Geophysical Research, 111(D21), D21111. https://doi.org/10.1029/2006JD007163

Dervishi, S., & Mahdavi, A. (2012). Computing diffuse fraction of global horizontal solar radiation: A model comparison. Solar Energy, 86(6), 1796–1802. https://doi.org/10.1016/j.solener.2012.03.008

Dingman, S. L. (2008). Physical Hydrology: Second Edition. Waveland Press Inc.

Dozier, J., & Frew, J. (1990). Rapid calculation of terrain parameters for radiation modeling from digital elevation data. IEEE Transactions on Geoscience and Remote Sensing, 28(5), 963–969. https://doi.org/10.1109/36.58986

Dunne, T., & Loepold, L. B. (1978). Water in Environmental Planning, first ed. W. H. Freeman.

Erbs, D. G., Klein, S. A., & Duffie, J. A. (1982). Estimation of the diffuse radiation fraction for hourly, daily and monthly-average global radiation. Solar Energy. https://doi.org/10.1016/0038-092X(82)90302-4

Evans, E. C., McGregor, G. R., & Petts, G. E. (1998). River energy budgets with special reference to river bed processes. Hydrological Processes, 12(4), 575–595. https://doi.org/10.1002/(sici)1099-1085(19980330)12:4<575::aid-hyp595>3.0.co;2-y

Gates, D. M. (1980). Biophysical ecology. Springer New York, 611p. https://doi.org/10.1007/978-1-4612-6024-0

Glose, A., Lautz, L. K., & Baker, E. A. (2017). Stream heat budget modeling with HFLUX: Model development, evaluation, and applications across contrasting sites and seasons. Environmental Modelling & Software, 92, 213–228. https://doi.org/10.1016/j.envsoft.2017.02.021

Kunkel, K. E. (1989). Simple Procedures for Extrapolation of Humidity Variables in the Mountainous Western United States. Journal of Climate, 2(7), 656–670. https://doi.org/10.1175/1520-0442(1989)002<0656:SPFEOH>2.0.CO;2

Martin, J. L., & McCutcheon, S. C. (1998). Hydrodynamics and Transport for Water Quality Modeling. CRC Press.

Mihalevich, B. A., Neilson, B. T., Buahin, C. A., Yackulic, C. B., & Schmidt, J. C. (2020). Water temperature controls for regulated canyon‐bound rivers. Water Resources Research, 1–24. https://doi.org/10.1029/2020wr027566

Pederson, J. L., & Tressler, C. (2012). Colorado River long-profile metrics, knickzones and their meaning. Earth and Planetary Science Letters, 345–348, 171–179. https://doi.org/10.1016/j.epsl.2012.06.047

Raudkivi, A. J. (1979). Hydrology: an advanced introduction to the hydrological processes and modeling.

Rossman, L. A. (2006). Storm water management model quality assurance report: Dynamic wave flow routing. Storm Water Management Model Quality Assurance Report, EPA/600/R-06/097, 1–115. http://www.epa.gov/water-research/storm-water-management-model-swmm

Shanahan, P. (1984). Water temperature modeling: a practical guide. In: Proceedings Stormwater and Water Quality Model Users Group Meeting.

Sumsion, C. T. (1976). Water Resources of Dinosaur National Monument. U.S. Geological Survey Open-File Report 76-580, Salt Lake.

Thomas, H. E. (1952). Hydrologci Reconnaissance of the Green River in Utah and Colorado. U.S. Geological Survey Circular 129.

U.S. Fish and Wildlife Service. Jones Hole National Fish Hatchery. https://www.fws.gov/mountain-prairie/fisheries/jonesHole.php. Accessed Aug 2020.

Webb, B. W., & Zhang, Y. (1997). Spatial and seasonal variability in the components of the river heat budget. Hydrological Processes, 11(1), 79–101. https://doi.org/10.1002/(SICI)1099-1085(199701)11:1<79::AID-HYP404>3.0.CO;2-N

Westhoff, M. C., Savenije, H. H. G., Luxemburg, W. M. J., Stelling, G. S., van de Giesen, N. C., Selker, J. S., Pfister, L., & Uhlenbrook, S. (2007). A distributed stream temperature model using high resolution temperature observations. Hydrology and Earth System Sciences Discussions, 4(1), 125–149. https://doi.org/10.5194/hessd-4-125-2007

APPENDIX C

Supporting Information for Chapter 4

Text C-1: Calculation of point and distributed flow sources from CRSS outputs.

The number of nodes and naming convention used in CRSS is subject to change with new versions developed by the Bureau of Reclamation. Therefore, we generally apply all "AggregateReach" nodes, which includes sub-branched nodes (e.g., "AggregateDiversionSite" and 'Confluence" nodes) as distributed inflows to the process-based models. We also include some "LevelPowerReservoir" Objects, such as *evaporation* and *change in bank storage,* when aggregating distributed flows for reservoirs. The equations below describe in detail the CRSS nodes used in this study (also shown in Table C-2 and Figure C-4).

Upper Basin Model

Linking CRSS outputs to the Upper Basin model requires flow information from 32 nodes. In general, the water balance in the Upper Basin model can be summarized using Eqn. C-1, where *Flaming Gorge Outflow*, *Yampa River Inflow*, *Duchesne River Inflow*, *White River Inflow*, *San Rafael River Inflow*, and *Colorado River Inflow* comes from the CRSS nodes FlamingGorge:Outflow, GreenYampa:Inflow2, GreenDuchesne:Inflow2, GreenWhite:Inflow2, SanRafaelGreen:Inflow2, and ColoradoNearCisco:GageOutflow, respectively. Each of these terms are *point* flows from CRSS and are applied to specific temperature model elements. For example, *Flaming Gorge Outflow* was applied as the upstream boundary condition in the Green River while *Yampa River Inflow* was applied as the upstream boundary condition in the Yampa River. Inflows from the Price River were not accounted for directly in this application because they are not represented by a specific CRSS node. The *Green River Distributed Flow* and *Colorado River Distributed Flow* terms represents all distributed sources in the Green

River and Colorado River sections, of Table 4-1, respectively. Distributed flows were disaggregated into three terms in the Green River, and two terms in the Colorado River so that they may be assigned to river segments based on their Object Name (Eqn. C-2; Eqn. C-3; Table C-2). For example, gains and losses associated with "GreenRWhiteToSanRafael" were evenly distributed in the Green River between the White River and San Rafael River confluences. Note that in Eqn C-2, *Flaming Gorge to Ouray Distributed Flow* represents distributed flow between Flaming Gorge Dam and the USGS gage near Ouray, UT, which is immediately upstream of the Duchesne and White River confluences. Distributed flows were not applied in the Yampa River segment because this stretch of river has no meaningful diversions or return flows. The individual terms used to calculate *Green River Distributed Flow* and *Colorado River Distributed Flow* are calculated below in Eqn. C4-C8.

Grand Canyon Model

In general, the water balance in the Grand Canyon model (Figure 4-3) can be summarized using Eqn. C-9, where the terms *Powell Outflow*, *Paria River Inflow*, and *Little Colorado River Inflow* represent point inflows to the model and are determined by the CRSS nodes Powell:Outflow, PariaColorado:Inflow2, and LittleCOColorado:Inflow2, respectively (Table C-2). The Grand Canyon Distributed Flow term is represented by the CRSS node CoRivLittleCOToVirgin:GainsAboveGC:LocalInflow and are only applied between Glen Canyon Dam and the USGS gage near Grand Canyon. Flows from tributaries downstream of the USGS gage near Grand Canyon (i.e., Bright Angel Creek, Kanab Creek, and Havasu Creek) are not represented by CRSS nodes but can be significant sources of intervening flow (Wang and Schmidt 2020). Since these inputs are beyond the

most downstream CRSS node in our modeling domain, and therefore do not affect the flow balance, we decided to include these inflows using their monthly average discharge determined from historical USGS gage data.

Lake Powell Model

The water balance in Lake Powell (Figure 4-3) can be checked using the monthly change in storage term shown in Eqn C-10, where the Δ*Powell Storage* term comes from the CRSS node Powell:Storage, *Colorado River Inflow to Powell* term comes from the simulated flow at the most downstream element in the Upper Basin HydroCouple model, which are a function of CRSS outputs, *San Juan River Inflow* comes from the CRSS node SanJuanColorado:Inflow2), and *Powell Outflows* comes from the CRSS node Powell:Outflow (Table C-2). All distributed sources associated with Lake Powell nodes were represented by the *Powell Distributed Flow* term and were aggregated together into a single time series and applied to the main Colorado River branch in the CE-QUAL-W2 model. *Powell Distributed Flow* was not applied to tributary branches (e.g., Escalante, Wahweap, etc., Figure C-6) to be consistent with BOR's current approach for handling distributed flows in the Lake Powell model. Note that there are several tributaries accounted for in the Lake Powell model as constant inflows. To maintain these flow sources which effect reservoir mixing, the volume of these inflows were subtracted from the *Powell Distributed Flow* term (Eqn C-11). Evaporative mass losses was turned off in CE-QUAL-W2 since it is included in the CRSS mass balance.

The individual terms used to calculate *Powell Distributed Flow* (Eqn. C-10) are calculated in Eqn. C-11. Note that there are several tributaries accounted for in the Lake

Powell model as constant inflows. These inflows are subtracted from the following equations.

Equations C-1 – C-11:

Colorado River Inflow to Powell =	*Flaming Gorge Outflow + Yampa River Inflow + Duchesne River Inflow + White River Inflow + San Rafael River Inflow + Colorado River Inflow ± Green River Distributed Flow ± Colorado River Distributed Flow*	(C-1)
Green River Distributed Flow =	*Flaming Gorge to Ouray Distributed Flow ± White To San Rafael Distributed Flow ± San Rafael to Green Confluence Distributed Flow*	(C-2)
Colorado River Distributed Flow =	*Cisco to Green Confluence Distributed Flow ± Green Confluence to Powell Distributed Flow*	(C-3)
Flaming Gorge to Ouray Distributed Flow =	*-GreenRYampaToDuchesne:RRAgUsePLBtwnGreendaleAndOuray:Diversion +GreenRYampaToDuchesne:RRAgUsePLBtwnGreendaleAndOuray:ReturnFlow -GreenRYampaToDuchesne:RRAgUseGrowthBtwnGreendaleAndOuray:Diversion +GreenRYampaToDuchesne:RRAgUseGrowthBtwnGreendaleAndOuray:ReturnFlow -GreenRYampaToDuchesne:RRMAndIUseBtwnGreendaleAndOuray:Diversion +GreenRYampaToDuchesne:RRMAndIUseBtwnGreendaleAndOuray:ReturnFlow -GreenRYampaToDuchesne:RREnergyUseBtwnGreendaleAndOuray:Diversion +GreenRYampaToDuchesne:RREnergyUseBtwnGreendaleAndOuray:ReturnFlow*	(C-4)

Ouray to San Rafael Distributed Flow =	*GreenRWhiteToSanRafael:GainsAboveGreenRiverUT:LocalInflow* *-GreenRWhiteToSanRafael:RRAgUsesPLAbvGreenRUT:Diversion* *+GreenRWhiteToSanRafael:RRAgUsesPLAbvGreenRUT:ReturnFlow* *-GreenRWhiteToSanRafael:RRAgUsesGrowthAbvGreenRUT:Diversion* *+GreenRWhiteToSanRafael:RRAgUsesGrowthAbvGreenRUT:ReturnFlow* *-GreenRWhiteToSanRafael:RRMiscUsesAbvGreenRUT:Diversion* *+GreenRWhiteToSanRafael:RRMiscUsesAbvGreenRUT:ReturnFlow* *-GreenRWhiteToSanRafael:RRExportUsesPriceRiver:Diversion* *+GreenRWhiteToSanRafael:RRExportUsesPriceRiver:ReturnFlow* *-GreenRWhiteToSanRafael:RRPriceRiverWQIP:Diversion* *+GreenRWhiteToSanRafael:RRPriceRiverWQIP:ReturnFlow* *-GreenRWhiteToSanRafael:RRMandIUsesPriceRiver:Diversion* *+GreenRWhiteToSanRafael:RRMandIUsesPriceRiver:ReturnFlow* *-GreenRWhiteToSanRafael:RREnergyUsesPriceRiver:Diversion* *+GreenRWhiteToSanRafael:RREnergyUsesPriceRiver:ReturnFlow* *-GreenRWhiteToSanRafael:GreenRiverUTWQIP:Diversion* *+GreenRWhiteToSanRafael:GreenRiverUTWQIP:ReturnFlow*	(C-5)
San Rafael to Green Confluence Distributed Flow =	*-SanRafaelToColorado:RRAgUsesPLSanRafaelToColorado:Diversion* *+SanRafaelToColorado:RRAgUsesPLSanRafaelToColorado:ReturnFlow* *-SanRafaelToColorado:RRAgUsesGrowthSanRafaelToColorado:Diversion* *+SanRafaelToColorado:RRAgUsesGrowthSanRafaelToColorado:ReturnFlow*	(C-6)
Cisco to Green Confluence Distributed Flow=	*GreenColorado:Inflow1- ColoradoNearCisco:GageOutflow*	(C-7)

Green Confluence to Powell Distributed Flow=	*-CoRiverAbovePowell:MuddyCreekWQIP:Diversion* *+CoRiverAbovePowell:MuddyCreekWQIP:ReturnFlow* *-CoRiverAbovePowell:AgUsesPLAbvPowell:Diversion* *+CoRiverAbovePowell:AgUsesPLAbvPowell:ReturnFlow* *-CoRiverAbovePowell:AgUsesGrowthAbvPowell:Diversion* *+CoRiverAbovePowell:AgUsesGrowthAbvPowell:ReturnFlow* *-CoRiverAbovePowell:MiscUsesAbvPowell:Diversion* *+CoRiverAbovePowell:MiscUsesAbvPowell:Return Flow* *-CoRiverAbovePowell:ExportUsesAbvPowell:Diversion* *+CoRiverAbovePowell:ExportUsesAbvPowell:Return Flow*	(C-8)
Colorado Near Grand Canyon =	*Powell Outflow + Paria River Inflow + Little Colorado River Inflow ± Grand Canyon Distributed Flow*	(C-9)
ΔPowell Storage =	*Colorado River Inflow to Powell + San Juan River Inflow ± Powell Distributed Flow – Powell Outflow*	(C-10)

$$
\begin{aligned}
\textit{Powell Distributed Flow} = {} & - \textit{SanRafaelToColorado:RRUtahUsesAboveLeesFerry:Diversion} \\
& + \textit{SanRafaelToColorado:RRUtahUsesAboveLeesFerry:Return Flow} \\
& - \textit{CoRiverAbovePowell:DirtyDevilWQIP:Diversion} \\
& + \textit{CoRiverAbovePowell:DirtyDevilWQIP:Return Flow} \\
& - \textit{CoRiverAbovePowell:UtahAnticipatedDepletions:Diversion} \\
& + \textit{CoRiverAbovePowell:UtahAnticipatedDepletions:Return Flow} \\
& - \textit{SanJuanPowell:ArizonaMiscUses:Diversion} \\
& + \textit{SanJuanPowell:ArizonaMiscUses:Return Flow} \\
& - \textit{SanJuanPowell:AddFutureWQIPs:Diversion} \\
& + \textit{SanJuanPowell:AddFutureWQIPs:Return Flow} \\
& - \textit{SanJuanPowell:USDATier2WQIP:Diversion} \\
& + \textit{SanJuanPowell:USDATier2WQIP:Return Flow} \\
& + \textit{SanJuanPowell:GainsAboveLeesFerry:Local Inflow} \\
& + \textit{SanJuanPowell:LeeFerryDeficitSupply:Local Inflow} \\
& - \textit{Powell:Evaporation} \\
& - \textit{Powell:Change in Bank Storage} \\
& - \textit{Constant Tributary Inflows}
\end{aligned}
\qquad \text{(C-11)}
$$

Text C-2: Estimating Cloud Cover from ERA5-Land

Cloud cover is a required variable in CE-QUAL-W2 and is used to compute atmospheric longwave radiation. Values of cloud cover range between 0 – 10, with a value of 0 meaning no clouds and 10 meaning fully cloudy. ERA5-Land does not have a cloud cover variable, which poses a challenge when using this dataset in CE-QUAL-W2.

While ERA5-Land does not include a cloud cover variable, the variable "Surface thermal radiation downwards" represents the amount of longwave radiation emitted by the atmosphere with clouds. Therefore, cloud cover can be estimated from the differences between ERA5-Land surface thermal radiation downwards ($J_{atm,ERA5}$) and calculated clear sky atmospheric longwave radiation ($J_{atm,clear}$). Clear sky atmospheric longwave radiation is estimated using the equation:

$$J_{atm,clear} = \varepsilon_{atm} \sigma T_{air}^4 \quad \text{(C-12)}$$

where σ is the Stefan-Boltzmann constant (W/m^2/K^4), $\mathcal{E}_{atm}$ is the emissivity of the atmosphere, and T_{air} is the ERA5-Land air temperature (K). Several models have been developed to estimate the emissivity during clear sky conditions (Choi et al., 2008). Choi et al. (2008) evaluated five models against measured observations at 11 locations in Florida, USA, and found that the Brunt (1932) formula produced the lowest average root mean square error (RMSE) among all monitoring sites. The Brunt (1932) formula is also used in CE-QUAL-W2 (Cole and Wells 2003) to estimate longwave radiation and takes the form of:

$$\varepsilon_{atm} = A + B\sqrt{e_{air}} \quad \text{(C-13)}$$

where A and B are locally calibrated coefficients, and e_{air} is the vapor pressure of air (Pa). The river temperature model developed by Buahin et al. (2019; HydroCouple),

which also uses the Brunt (1932) formula, uses values of 0.6 and 0.0027 for A and B, respectively. Using ERA5-Land values of dew point temperature (T_{dew}), the vapor pressure of air (e_{air}) can be estimated as:

$$e_{air} = 0.61275\, e^{\left(\frac{17.27T_{dew}}{237.3+T_{dew}}\right)}. \quad \text{(C-14)}$$

As with clear sky emissivity models, Choi et al. (2008) also evaluated seven models for estimating cloudy sky longwave radiation ($J_{atm,cloudy}$). Of these models, Choi et al. (2008) found that the $J_{atm,cloudy}$ model described by Crawford & Duchon (1999) produced the lowest average RMSE among the 11 monitoring sites. This model takes the form of:

$$J_{atm,cloudy} = J_{atm,clear}(1-c) + c\sigma\, T_{air}^4 \quad \text{(C-15)}$$

where c is the fractional cloud cover ranging between 0 and 1. Therefore, if we assume that $J_{atm,cloudy}$ equals $J_{atm,ERA5}$ we can solve for cloud cover by rearrange equation 4 to:

$$c = \frac{J_{atm,ERA5} - J_{atm,clear}}{\sigma\, T_{air}^4 - J_{atm,clear}}. \quad \text{(C-16)}$$

While *c* should only have values between 0 and 1, cloud cover values less than 0 and greater than 1 are possible using equation 5 because the simplified approach does not fully capture the complex calculation of $J_{atm,ERA5}$, which is based on 37 pressure levels of atmosphere between 1000 hPa to 1 hPa. Based on equation 4, cloud cover should always enhance the amount of longwave radiation. Therefore, $J_{atm,ERA5}$ should always be greater than or equal to $J_{atm,clear}$. For this reason, negative values of *c* were set to zero. To address cloud cover values greater than 1, *c* was normalized between 0 and 1. Lastly, cloud cover values were multiplied by 10 since CE-QUAL-W2 values range between 0 and 10.

Text C-3: Calculation of Thermally Suitable Days (TSD)

We estimated the number of thermally suitable days (TSD) in each year (y) from predicted hourly temperatures by modifying the equation presented by Dibble et al. (2021):

$$TSD_y = \frac{(\sum f(T_i)) * ts}{24} \quad \text{(C-17)}$$

where

$$f(T_i) = 0, \quad if\ T_i < T_{min} \mid T_i > T_{max} \quad \text{(C-18)}$$
$$f(T_i) = \frac{T_i - T_{min}}{T_{min.opt} - T_{min}}, \quad if\ T_{min} < T_i < T_{min.opt} \quad \text{(C-19)}$$
$$f(T_i) = 1, \quad if\ T_{min.opt} < T_i < T_{max.opt} \quad \text{(C-20)}$$
$$f(T_i) = \frac{T_{max} - T_i}{T_{max} - T_{max.opt}}, \quad if\ T_{max.opt} < T_i < T_{max} \quad \text{(C-21)}$$

Where *ts* is the model time step duration (in this case 3 hours) T_i is the water temperature at time step i, and T_{min}, $T_{min.opt}$, $T_{max.opt}$, and T_{max} are the minimum, minimum-optimal, maximum-optimal, and maximum temperatures needed for growth by a given species. For humpback chub these temperatures are 12 °C, 16 °C, 30 °C, and 37 °C, respectively (Dibble et al., 2020).

Table C-1. Example of two resampling methods used to generate plausible future hydrologic traces. For both examples historical flow information occurring between 2000 and 2018 (19 years) is resampled to produce traces that are used simulate flow between 2022 and 2040 in a water management model. The left Table illustrates a random resampling method that can generate N number of traces. The Table on the right illustrates the index-sequential method (ISM) for resampling that creates as many traces as there are years of information (i.e., 19 in this example).

Random Method

Historical Flow Year Resampled						
Trace 1	2010	2012	2003	…	2007
Trace 2	2009	2016	2011	…	2006
Trace 3	2011	2000	2000	…	2018
…	…	…	…	…	…
Trace N	2004	2006	2016	…	2015
Future Years	2022	2023	2024	…	2040

Index-Sequential Method

Historical Flow Year Resampled					
Trace 1	2000	2001	2002	…	2018
Trace 2	2001	2002	2003	…	2000
Trace 3	2002	2004	2004	…	2001
…	…	…	…	…	…
Trace 19	2018	2000	2001	…	2017
Future Years	2022	2023	2024	…	2040

Table C-2. Subset of CRSS nodes used to model river temperatures in the Colorado River basin.

Object Type	Object Name	Slot Name	Spatial Resolution
Green River			
LevelPowerReservoir	FlamingGorge	Outflow	Point
Confluence	GreenYampa	Inflow2	Point
Reach	GreenRYampaToDuchesne:RRUsesBetGreendaleAndOuray	Diversion	Distributed
Reach	GreenRYampaToDuchesne:RRUsesBetGreendaleAndOuray	Return Flow	Distributed
Reach	GreenRYampaToDuchesne:RRMAndIUseBtwnGreendaleAndOuray	Diversion	Distributed
Reach	GreenRYampaToDuchesne:RRMAndIUseBtwnGreendaleAndOuray	Return Flow	Distributed
Confluence	GreenDuchesne	Inflow2	Point
Confluence	GreenWhite	Inflow2	Point
Reach	GreenRWhiteToSanRafael:GainsAboveGreenRiverUT	Local Inflow	Distributed
Reach	GreenRWhiteToSanRafael:RRAgUsesAboveGreenRUt	Diversion	Distributed
Reach	GreenRWhiteToSanRafael:RRAgUsesAboveGreenRUt	Return Flow	Distributed
Reach	GreenRWhiteToSanRafael:RRPriceRiverExport	Diversion	Distributed
Reach	GreenRWhiteToSanRafael:RRPriceRiverExport	Return Flow	Distributed
Reach	GreenRWhiteToSanRafael:RRPriceRiverWQIP	Diversion	Distributed
Reach	GreenRWhiteToSanRafael:RRPriceRiverWQIP	Return Flow	Distributed
Reach	GreenRWhiteToSanRafael:RRPriceRMAndIAndEnergy	Diversion	Distributed
Reach	GreenRWhiteToSanRafael:RRPriceRMAndIAndEnergy	Return Flow	Distributed
Reach	GreenRWhiteToSanRafael:GreenRiverUTWQIP	Diversion	Distributed
Reach	GreenRWhiteToSanRafael:GreenRiverUTWQIP	Return Flow	Distributed
Confluence	SanRafaelGreen	Inflow2	Point
Reach	SanRafaelToColorado:RRUtahUsesAboveLeesFerry	Diversion	Distributed
Reach	SanRafaelToColorado:RRUtahUsesAboveLeesFerry	Return Flow	Distributed

Table C-2 continued. Subset of CRSS nodes used to model river temperatures in the Colorado River basin.

Colorado River			
StreamGage	ColoradoNearCisco	Gage Outflow	Point
Reach	UT_COStateLineToColorado:UtahUsesAboveGreenRiverConfluence	Diversion	Distributed
Reach	UT_COStateLineToColorado:UtahUsesAboveGreenRiverConfluence	Return Flow	Distributed
Reach	UT_COStateLineToColorado:BLMrangelandWQIP	Diversion	Distributed
Reach	UT_COStateLineToColorado:BLMrangelandWQIP	Return Flow	Distributed
Confluence	GreenColorado	Inflow1	Point
Reach	CoRiverAbovePowell:DirtyDevilWQIP	Diversion	Distributed
Reach	CoRiverAbovePowell:DirtyDevilWQIP	Return Flow	Distributed
Reach	CoRiverAbovePowell:UtahAnticipatedDepletions	Diversion	Distributed
Reach	CoRiverAbovePowell:UtahAnticipatedDepletions	Return Flow	Distributed

Table C-2 continued. Subset of CRSS nodes used to model river temperatures in the Colorado River basin.

Lake Powell and San Juan River Inflows			
Confluence	SanJuanColorado	Inflow2	Point
Reach	SanJuanPowell:ArizonaMiscUses	Diversion	Distributed
Reach	SanJuanPowell:ArizonaMiscUses	Return Flow	Distributed
Reach	SanJuanPowell:AddFutureWQIPs	Diversion	Distributed
Reach	SanJuanPowell:AddFutureWQIPs	Return Flow	Distributed
Reach	SanJuanPowell:USDATier2WQIP	Diversion	Distributed
Reach	SanJuanPowell:USDATier2WQIP	Return Flow	Distributed
Reach	SanJuanPowell:GainsAboveLeesFerry	Local Inflow	Distributed
Reach	SanJuanPowell:LeeFerryDeficitSupply	Local Inflow	Distributed
LevelPowerReservoir	Powell	Outflow	Point
LevelPowerReservoir	Powell	Evaporation	Distributed
LevelPowerReservoir	Powell	Change in Bank Storage	Distributed
Colorado River in Grand Canyon			
Confluence	PariaColorado	Inflow2	Point
Reach	CoRivLittleCOToVirgin:GainsAboveGC	Local Inflow	Distributed
Confluence	LittleCOColorado	Inflow2	Point
StreamGage	ColoradoNearGrandCanyon	Gage Outflow	Point

Table C-3 USGS gage sites used for boundary conditions and tributary inflow water temperature information. The temporal resolution column indicates how these data were resampled before being applied in the river temperature model.

Site Name	Site ID	Temporal Resolution
Upper Colorado River Basin Model		
Green River near Greendale UT (immediately below Flaming Gorge Dam)	09234500	Continuous
Yampa River at Deerlodge Park CO	09260050	Continuous
Colorado River near Cisco UT	09180500	Continuous
Duchesne River near Randlett, UT	09302000	Monthly Average
White River at mount near Ouray, UT	09306900	Monthly Average
San Rafael River near Green River, UT	09328500	Monthly Average
Lake Powell Model		
San Juan River near Bluff, UT	09379500	Continuous
Colorado River - Grand Canyon Model		
Paria River at Lees Ferry, AZ	09382000	Monthly Average
Little Colorado River above the mouth near Desert View, AZ	09402300	Monthly Average
Bright Angel Creek near Grand Canyon, AZ	09403000	Monthly Average
Kanab Creek above the mouth near Supai, AZ	09403850	Monthly Average
Havasu Creek above the mouth near Supai, AZ	09404115	Monthly Average

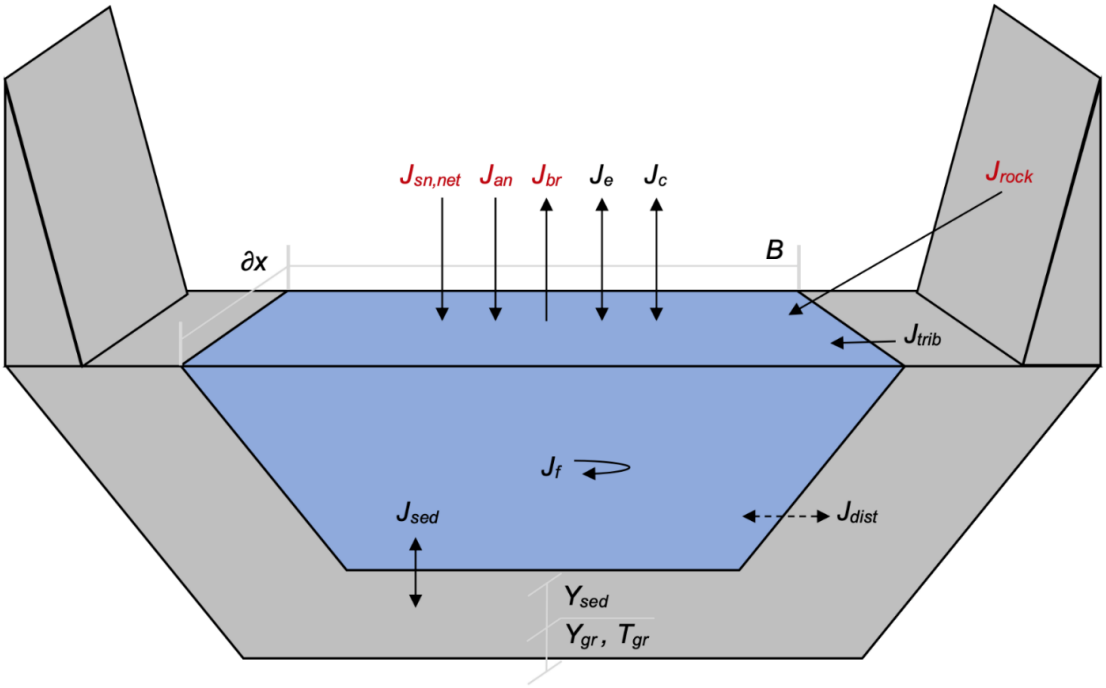

Figure C-1. Simple schematic of external heat fluxes and lateral inflows accounted for in the river temperature model. Included terms are net shortwave radiation (Jsn,net), atmospheric longwave radiation (Jan), water longwave radiation (Jbr), bedrock longwave radiation (Jrock), sensible heat (conduction and convection; Jc), latent heat (evaporation and condensation; Je), internal fluid shear friction (Jf), sediment conduction (Jsed), tributary flows (Jtrib) and distributed flows (Jdist). Radiative terms are shown in red (Jsn,net, Jan, Jbr, and Jrock) and are described and illustrated in greater detail in the manuscript. Ysed is the depth of the shallow sediment layer, and Ygr is the depth to the ground boundary layer. Tsed is the temperature of the shallow sediment layer and Tgr is the temperature of the ground boundary layer.

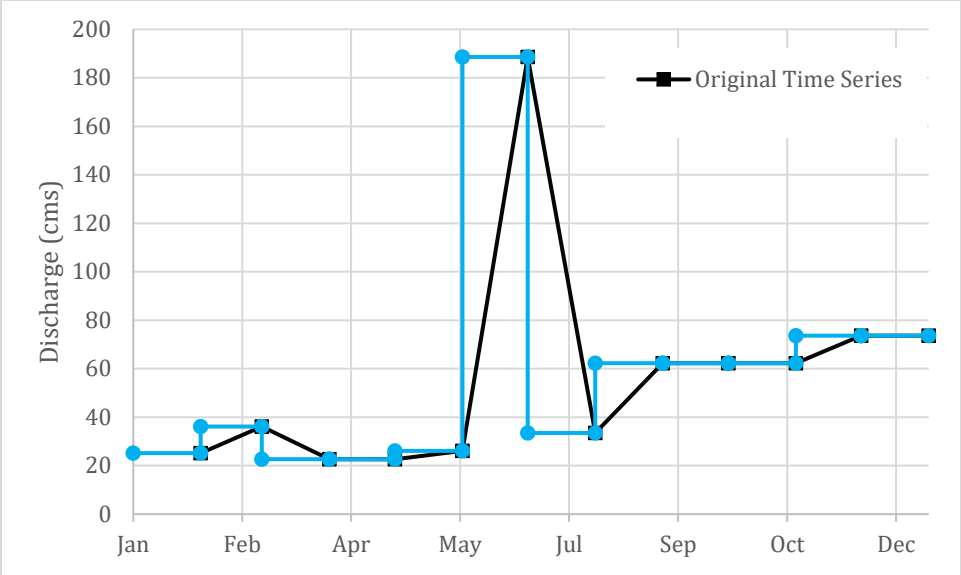

Figure C-2. Example of flow information from the water management model (black line) and flow information reformatted for the process-based river and reservoir models (blue line).

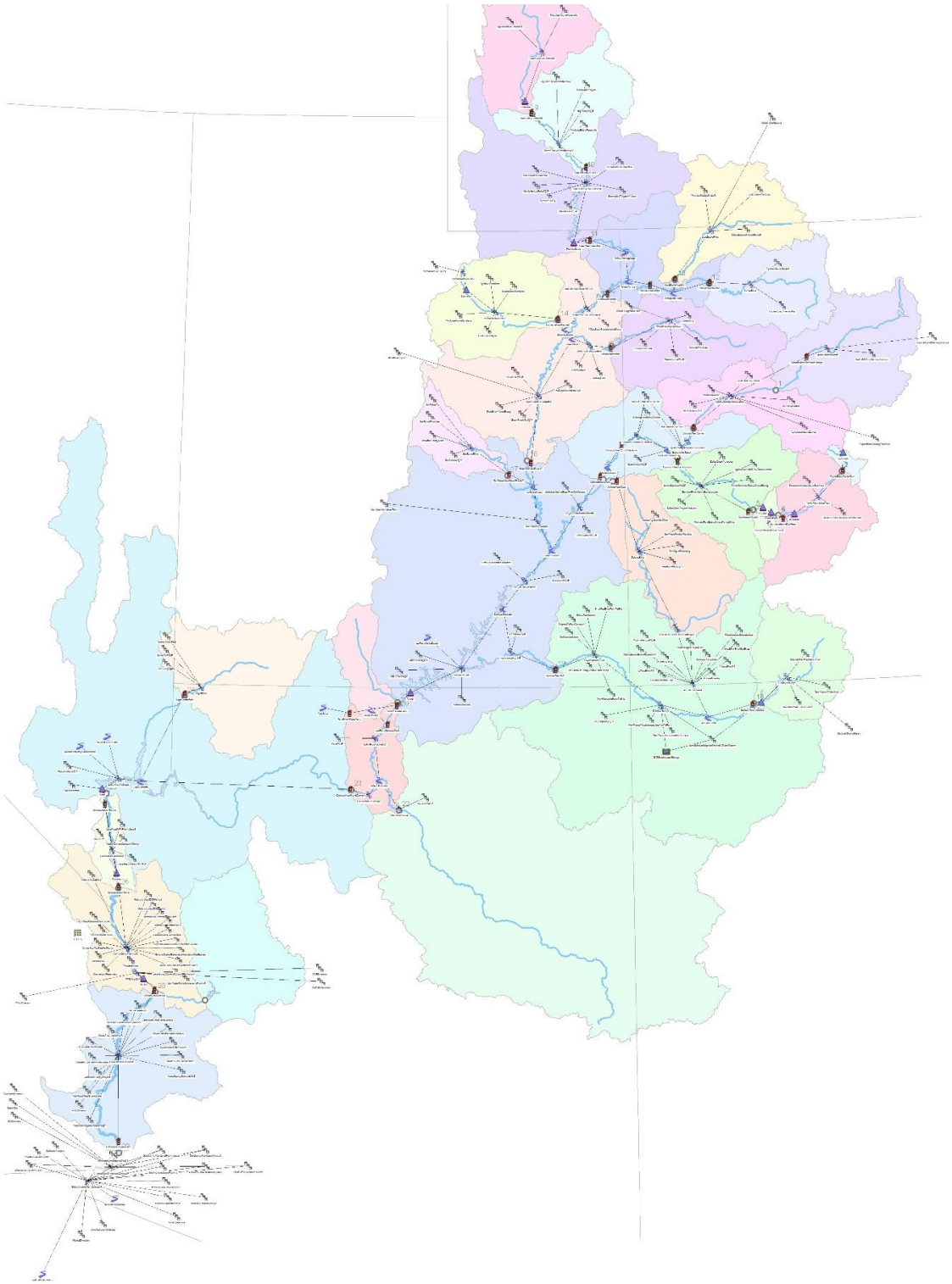

Figure C-3. Complete model schematic of the Colorado River Simulation System.

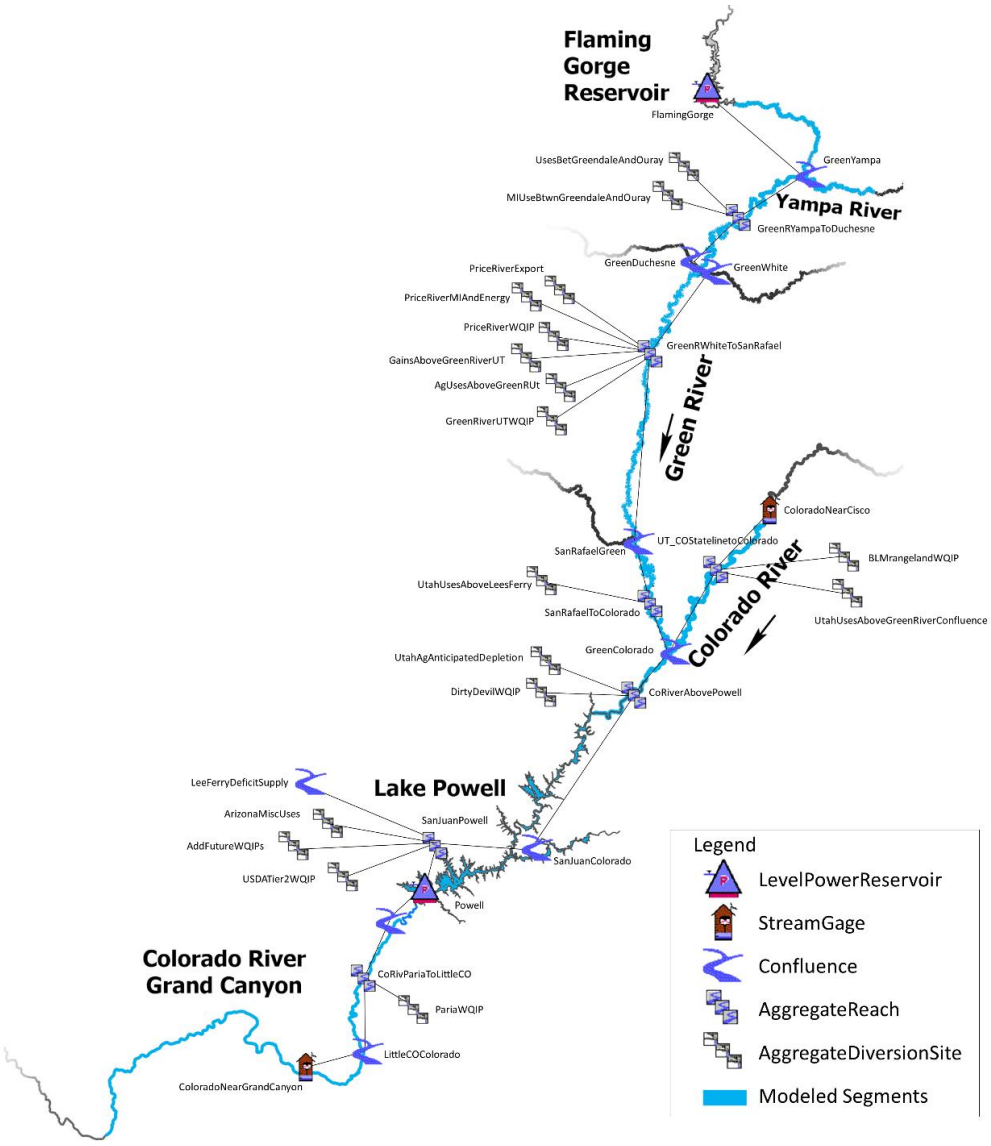

Figure C-4. Map of the Colorado River basin showing the subset of CRSS nodes (Table C-2) used to model river temperatures using process-based models. River segments highlighted in blue were simulated using HydroCouple and CE-QAUL-W2 models. Lake Powell evaporation and change in bank storage were applied as distributed flows to the main Colorado River branch in the CE-QUAL-W2 model.

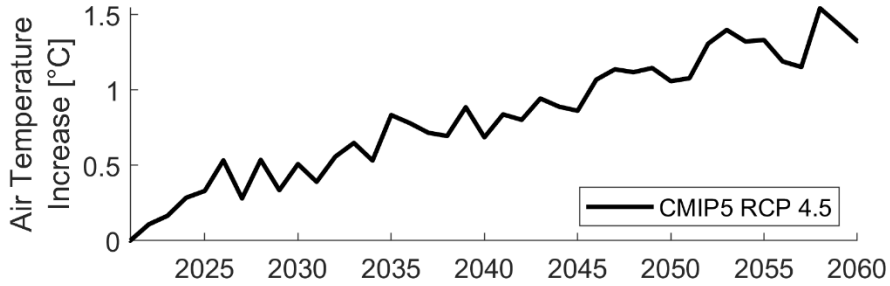

Figure C-5. Increases in air temperature relative to 2021 for a single 1.0° x 1.0° latitude and longitude grid located in the Colorado River basin based on the ensemble mean of BOR's Bias Corrected and Spatially Disaggregated (BCSD) CMIP5 projections with a RCP 4.5 emissions pathway.

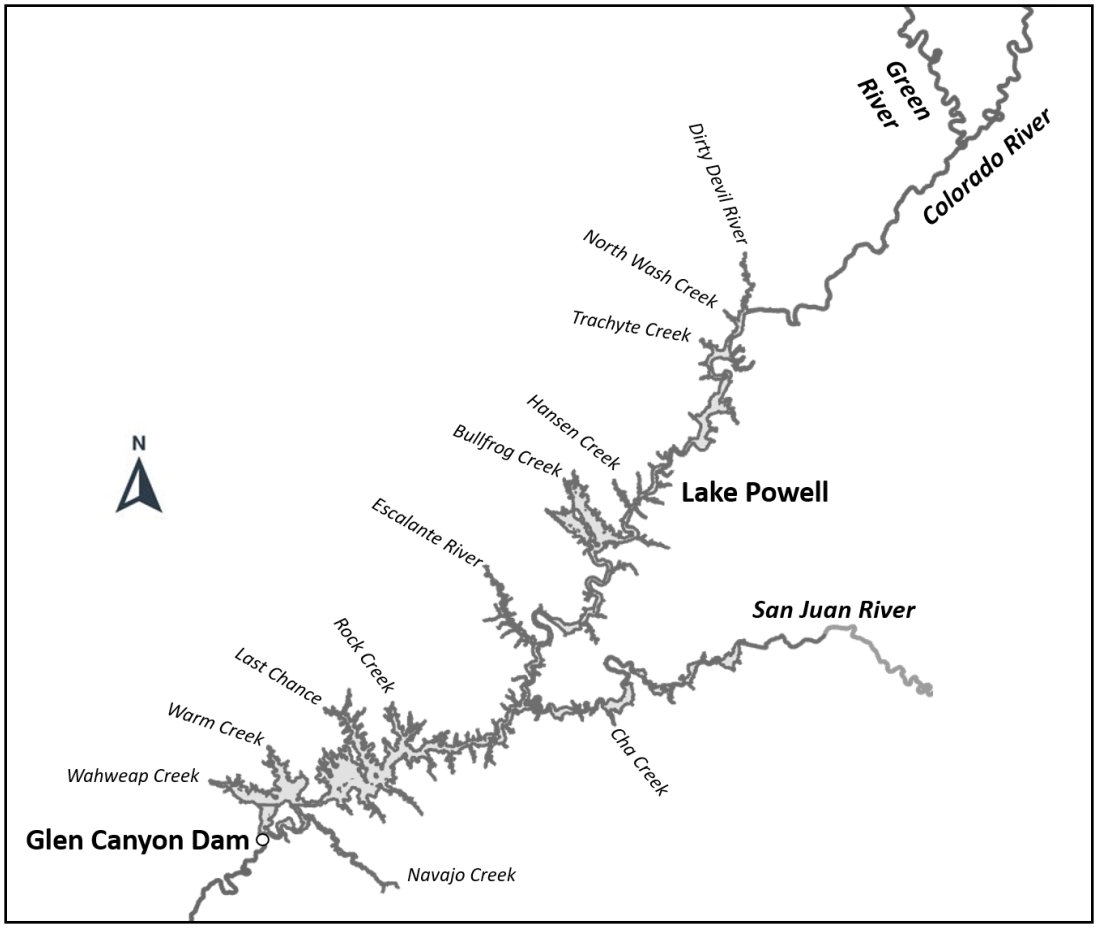

Figure C-6. Map of Lake Powell showing all inflow tributaries accounted for in the CE-QUAL-W2 model. Modeled branches include the main Lake Powell water body, Bullfrog Creek, Escalante River, San Juan River, Rock Creek, Last Chance Creek, Warm Creek, Navajo Creek, and Wahweap Creek.

References

Brunt, D. (1932). Notes on radiation in the atmosphere. I. Quarterly Journal of the Royal Meteorological Society, 58(247), 389–420. https://doi.org/10.1002/qj.49705824704

Buahin, C. A., Horsburgh, J. S., & Neilson, B. T. (2019). Parallel multi-objective calibration of a component-based river temperature model. Environmental Modelling & Software, 116(February), 57–71. https://doi.org/10.1016/j.envsoft.2019.02.012

Choi, M., Jacobs, J. M., & Kustas, W. P. (2008). Assessment of clear and cloudy sky parameterizations for daily downwelling longwave radiation over different land surfaces in Florida, USA. Geophysical Research Letters, 35(20). https://doi.org/10.1029/2008GL035731

Cole, T. M., & Wells, S. A. (2003). CE-QUAL-W2—A two- dimensional, laterally averaged, hydrodynamic and water quality model, version 3.2. U.S. Army Engineering and Research Development Center, Instruction Report EL-03-01.

Crawford, T. M., & Duchon, C. E. (1999). An improved parameterization for estimating effective atmospheric emissivity for use in calculating daytime downwelling longwave radiation. Journal of Applied Meteorology, 38(4), 474–480. https://doi.org/10.1175/1520-0450(1999)038<0474:AIPFEE>2.0.CO;2

Dibble, K. L., Yackulic, C. B., & Bestgen, K. R. (2020). Water temperature models, data and code for the Colorado, Green, San Juan, Yampa, and White rivers in the Colorado River basin. U.S. Geological Survey Data Release. https://doi.org/https://doi.org/10.5066/P9HFKV7Q

Dibble, K. L., Yackulic, C. B., Kennedy, T. A., Bestgen, K. R., & Schmidt, J. C. (2021). Water storage decisions will determine the distribution and persistence of imperiled river fishes. Ecological Applications, 31(2), 1–9. https://doi.org/10.1002/eap.2279

Wang, J., & Schmidt, J. C. (2020). Stream flow and Losses of the Colorado River in the Southern Colorado Plateau. Center for Colorado River Studies, white paper no. 5, 26.

APPENDIX D

License Agreement

JOHN WILEY AND SONS LICENSE TERMS AND CONDITIONS
Feb 09, 2022

This Agreement between Bryce Mihalevich ("You") and John Wiley and Sons ("John Wiley and Sons") consists of your license details and the terms and conditions provided by John Wiley and Sons and Copyright Clearance Center.

License Number	5244971015887
License date	9-Feb-22
Licensed Content Publisher	John Wiley and Sons
Licensed Content Publication	Water Resources Research
Licensed Content Title	Water Temperature Controls for Regulated Canyon-Bound Rivers
Licensed Content Author	Bryce A. Mihalevich, Bethany T. Neilson, Caleb A. Buahin, et al
Licensed Content Date	Dec 19, 2020
Licensed Content Volume	56
Licensed Content Issue	12
Licensed Content Pages	24
Type of use	Dissertation/Thesis
Requestor type	Author of this Wiley article
Format	Electronic
Portion	Full article
Will you be translating?	No
Title	Advances in Process Understanding and Methods to Support River Temperature Modeling in Large Regulated Systems
Institution name	Utah State University
Expected presentation date	Apr 2022
Requestor Location	Utah Water Research Laboratory 1600 Canyon Road LOGAN, UT 84321 United States Attn: Bryce Mihalevich
Publisher Tax ID	EU826007151
Total	0.00 USD

Terms and Conditions

TERMS AND CONDITIONS

This copyrighted material is owned by or exclusively licensed to John Wiley & Sons, Inc. or one of its group companies (each a "Wiley Company") or handled on behalf of a society with which a Wiley Company has exclusive publishing rights in relation to a

particular work (collectively "WILEY"). By clicking "accept" in connection with completing this licensing transaction, you agree that the following terms and conditions apply to this transaction (along with the billing and payment terms and conditions established by the Copyright Clearance Center Inc., ("CCC's Billing and Payment terms and conditions"), at the time that you opened your RightsLink account (these are available at any time at http://myaccount.copyright.com).

Terms and Conditions

- The materials you have requested permission to reproduce or reuse (the "Wiley Materials") are protected by copyright.
- You are hereby granted a personal, non-exclusive, non-sub licensable (on a standalone basis), non-transferable, worldwide, limited license to reproduce the Wiley Materials for the purpose specified in the licensing process. This license, and any CONTENT (PDF or image file) purchased as part of your order, is for a one-time use only and limited to any maximum distribution number specified in the license. The first instance of republication or reuse granted by this license must be completed within two years of the date of the grant of this license (although copies prepared before the end date may be distributed thereafter). The Wiley Materials shall not be used in any other manner or for any other purpose, beyond what is granted in the license. Permission is granted subject to an appropriate acknowledgement given to the author, title of the material/book/journal and the publisher. You shall also duplicate the copyright notice that appears in the Wiley publication in your use of the Wiley Material. Permission is also granted on the understanding that nowhere in the text is a previously published source acknowledged for all or part of this Wiley Material. Any third party content is expressly excluded from this permission.
- With respect to the Wiley Materials, all rights are reserved. Except as expressly granted by the terms of the license, no part of the Wiley Materials may be copied, modified, adapted (except for minor reformatting required by the new Publication), translated, reproduced, transferred or distributed, in any form or by any means, and no derivative works may be made based on the Wiley Materials without the prior permission of the respective copyright owner. For STM Signatory Publishers clearing permission under the terms of the STM Permissions Guidelines only, the terms of the license are extended to include subsequent editions and for editions in other languages, provided such editions are for the work as a whole in situ and does not involve the separate exploitation of the permitted figures or extracts, You may not alter, remove or suppress in any manner any copyright, trademark or other notices displayed by the Wiley Materials. You may not license, rent, sell, loan, lease, pledge, offer as security, transfer or assign the Wiley Materials on a stand-alone basis, or any of the rights granted to you hereunder to any other person.
- The Wiley Materials and all of the intellectual property rights therein shall at all times remain the exclusive property of John Wiley & Sons Inc, the Wiley Companies, or their respective licensors, and your interest therein is only that of having possession of and the right to reproduce the Wiley Materials pursuant to Section 2 herein during the continuance of this Agreement. You agree that you

own no right, title or interest in or to the Wiley Materials or any of the intellectual property rights therein. You shall have no rights hereunder other than the license as provided for above in Section 2. No right, license or interest to any trademark, trade name, service mark or other branding ("Marks") of WILEY or its licensors is granted hereunder, and you agree that you shall not assert any such right, license or interest with respect thereto

- NEITHER WILEY NOR ITS LICENSORS MAKES ANY WARRANTY OR REPRESENTATION OF ANY KIND TO YOU OR ANY THIRD PARTY, EXPRESS, IMPLIED OR STATUTORY, WITH RESPECT TO THE MATERIALS OR THE ACCURACY OF ANY INFORMATION CONTAINED IN THE MATERIALS, INCLUDING, WITHOUT LIMITATION, ANY IMPLIED WARRANTY OF MERCHANTABILITY, ACCURACY, SATISFACTORY QUALITY, FITNESS FOR A PARTICULAR PURPOSE, USABILITY, INTEGRATION OR NON-INFRINGEMENT AND ALL SUCH WARRANTIES ARE HEREBY EXCLUDED BY WILEY AND ITS LICENSORS AND WAIVED BY YOU.
- WILEY shall have the right to terminate this Agreement immediately upon breach of this Agreement by you.
- You shall indemnify, defend and hold harmless WILEY, its Licensors and their respective directors, officers, agents and employees, from and against any actual or threatened claims, demands, causes of action or proceedings arising from any breach of this Agreement by you.
- IN NO EVENT SHALL WILEY OR ITS LICENSORS BE LIABLE TO YOU OR ANY OTHER PARTY OR ANY OTHER PERSON OR ENTITY FOR ANYSPECIAL, CONSEQUENTIAL, INCIDENTAL, INDIRECT, EXEMPLARY OR PUNITIVE DAMAGES, HOWEVER CAUSED, ARISING OUT OF OR IN CONNECTION WITH THE DOWNLOADING, PROVISIONING, VIEWING OR USE OF THE MATERIALS REGARDLESS OF THE FORM OF ACTION, WHETHER FOR BREACH OF CONTRACT, BREACH OF WARRANTY, TORT, NEGLIGENCE, INFRINGEMENT OR OTHERWISE (INCLUDING, WITHOUT LIMITATION, DAMAGES BASED ON LOSS OF PROFITS, DATA, FILES, USE, BUSINESS OPPORTUNITY OR CLAIMS OF THIRD PARTIES), AND WHETHER OR NOT THE PARTY HAS BEEN ADVISED OF THE POSSIBILITY OF SUCH DAMAGES. THIS LIMITATION SHALL APPLY NOTWITHSTANDING ANY FAILURE OF ESSENTIAL PURPOSE OF ANY LIMITED REMEDY PROVIDED HEREIN.
- Should any provision of this Agreement be held by a court of competent jurisdiction to be illegal, invalid, or unenforceable, that provision shall be deemed amended to achieve as nearly as possible the same economic effect as the original provision, and the legality, validity and enforceability of the remaining provisions of this Agreement shall not be affected or impaired thereby.
- The failure of either party to enforce any term or condition of this Agreement shall not constitute a waiver of either party's right to enforce each and every term and condition of this Agreement. No breach under this agreement shall be deemed waived or excused by either party unless such waiver or consent is in writing signed by the party granting such waiver or consent. The waiver by or consent of

a party to a breach of any provision of this Agreement shall not operate or be construed as a waiver of or consent to any other or subsequent breach by such other party.

- This Agreement may not be assigned (including by operation of law or otherwise) by you without WILEY's prior written consent.
- Any fee required for this permission shall be non-refundable after thirty (30) days from receipt by the CCC.
- These terms and conditions together with CCC's Billing and Payment terms and conditions (which are incorporated herein) form the entire agreement between you and WILEY concerning this licensing transaction and (in the absence of fraud) supersedes all prior agreements and representations of the parties, oral or written. This Agreement may not be amended except in writing signed by both parties. This Agreement shall be binding upon and inure to the benefit of the parties' successors, legal representatives, and authorized assigns.
- In the event of any conflict between your obligations established by these terms and conditions and those established by CCC's Billing and Payment terms and conditions, these terms and conditions shall prevail.
- WILEY expressly reserves all rights not specifically granted in the combination of (i) the license details provided by you and accepted in the course of this licensing transaction, (ii) these terms and conditions and (iii) CCC's Billing and Payment terms and conditions.
- This Agreement will be void if the Type of Use, Format, Circulation, or Requestor Type was misrepresented during the licensing process.
- This Agreement shall be governed by and construed in accordance with the laws of the State of New York, USA, without regards to such state's conflict of law rules. Any legal action, suit or proceeding arising out of or relating to these Terms and Conditions or the breach thereof shall be instituted in a court of competent jurisdiction in New York County in the State of New York in the United States of America and each party hereby consents and submits to the personal jurisdiction of such court, waives any objection to venue in such court and consents to service of process by registered or certified mail, return receipt requested, at the last known address of such party.

WILEY OPEN ACCESS TERMS AND CONDITIONS

Wiley Publishes Open Access Articles in fully Open Access Journals and in Subscription journals offering Online Open. Although most of the fully Open Access journals publish open access articles under the terms of the Creative Commons Attribution (CC BY) License only, the subscription journals and a few of the Open Access Journals offer a choice of Creative Commons Licenses. The license type is clearly identified on the article.

The Creative Commons Attribution License

The Creative Commons Attribution License (CC-BY) allows users to copy, distribute and transmit an article, adapt the article and make commercial use of the article. The CC-BY license permits commercial and non-

VITA

Bryce A. Mihalevich
Graduate Research Assistant, PhD Candidate
Department of Civil and Environmental Engineering
Utah Water Research Laboratory, Utah State University
Email: bryce.mihalevich@gmail.com

EDUCATION

Ph.D. Civil and Environmental Engineering with Water Resources Emphasis
Utah State University – Logan, UT *Anticipated* March 2022
Graduate Research Assistant – Water Resources Engineering
Advisor: Dr. Bethany T. Neilson
Proposal defense passed Sep. 2020, Comprehensive defense passed Feb. 2019, GPA 3.85

M.S. Civil and Environmental Engineering with Water Resources Emphasis
Utah State University – Logan, UT June 2017
Graduate Research Assistant – Water Resources Engineering
Advisor: Dr. Jeffery S. Horsburgh

B.S. Biological Engineering with Environmental Emphasis
University of Missouri – Columbia, MO December 2013
Undergraduate Honors and Cum Laude
Advisor: Dr. Allen L. Thompson

EXPERTISE

My research and training are in watershed hydrology, surface water quality modeling, biogeochemistry, and environmental monitoring and data collection. I focus on the applications of new technology and methods to increase the understanding of environmental processes. This includes the use of process-based hydrologic models to identify temperature drivers in large regulated rivers subject to the effects of ongoing climate change and increasing water demand. My research interests include water quality modeling, water resources management, and remote sensing data products.

PROFESSIONAL EXPERIENCE

Graduate Teaching Assistant: *(10 hours/week)* Fall 2020, CEE 6740 - Surface Water Quality Modeling, Utah State University, Logan, UT.

- Developed and led Python coding labs and assisted students with programming help

Research Assistant: *(20 hours/week)* Fall 2017, Utah Water Research Laboratory, Utah State University, Logan, UT.

- Organization, management, and statistical analysis of groundwater and surface water quality data

Environmental Engineer I: *(40 hours/week)* Jan. 2014 – Dec. 2014, Air Pollution Control Program, Missouri Department of Natural Resources, Jefferson City, MO.

- Calculated potential criteria and hazardous air pollutants from facilities; wrote and issued permits

RESEARCH EXPERIENCE

Graduate Research Assistant (PhD) Jan. 2018 - Present
Utah Water Research Laboratory, Utah State University

- Researched mechanisms driving river temperature warming and cooling in large regulated systems
- Developed and calibrated hydraulic routing and river temperature models in the Colorado River Basin
- Downscaled gridded climate datasets to use in models as a surrogate for ground-based measurements
- Preformed installation and maintenance of 2 meteorological stations in remote area of Grand Canyon
- Conducted collection, verification, and database archival of hydro-meteorological data from 50+ sites
- Maintained working relationships with state and federal agencies to gain information and feedback
- Presented technical findings through peer reviewed publications and conference presentations

Graduate Research Assistant (MS) Jan. 2015 – Jun. 2017
Utah Water Research Laboratory, Utah State University

- Researched the sources and characteristics of dissolved organic matter contributions in stormwater
- Developed a mobile sensing platform to collect spatial and temporal measurements of water quality
- Preformed installation and maintenance of 6 water quality monitoring and data collection sites
- Programmed data loggers and installed radio communications to automate data archival from sites
- Conducted quality control and validation of collected data and applied corrections when needed
- Disseminated findings in a written thesis and through oral presentations at conferences

Undergraduate Research Assistant Jan. 2013 – Dec. 2013
University of Missouri – Columbia

- Designed experiments and analyzed performance of a proprietary subsurface irrigation product
- Research of irrigation systems and surface and subsurface water application efficiencies
- Gained written and verbal communication skills by presenting findings in a thesis and at conferences

PUBLICATIONS AND PRESENTATIONS

Journal Papers

1. Mihalevich, B. A., Neilson, B. T., Buahin, C. A. (in review). Evaluation of the ERA5-Land reanalysis as a meteorological dataset for process-based river temperature modeling over topographically complex regions.
2. Mihalevich, B. A., Neilson, B. T., Buahin, C. A., Yackulic, C. B., & Schmidt, J. C. (2020). Water temperature controls for regulated canyon-bound rivers. *Water Resources Research*, 1–24. https://doi.org/10.1029/2020wr027566.
3. Mihalevich, B. A., Horsburgh, J. S., Melcher, A. A. (2017). High-frequency measurements reveal spatial and temporal patterns of dissolved organic matter in an urban water

conveyance, *Environmental Monitoring and Assessment*, 189:593, doi: 10.1007/s10661-017-6310-y.

4. Bruckerhoff, L., Wheeler, K., Dibble, K., Mihalevich, B. A., Neilson, B. T., Wang, J., Yackulic, C., & Schmidt, J. C. (2022). Response of Colorado River Ecosystems to Alternative Water Storage Decisions during Severe Sustained Drought. *Journal of the American Water Resources Association.* (Accepted)

Technical Reports

5. Wheeler, K., Kuhn, E., Bruckerhoff, L., Udall, B., Wang, J., Gilbert, L., Goeking, S., Kasprak, A., Mihalevich, B. A., Neilson, B. T., Salehabadi, H., & Schmidt, J. C. (2020). Alternative Management Paradigms for the Future of the Colorado and Green Rivers. White Paper No. 6. The Future of the Colorado River Project, Center for Colorado River Studies, Quinney College of Natural Resources, Utah State University. https://qcnr.usu.edu/coloradoriver/files/WhitePaper6.pdf

Theses

1. Mihalevich, B. A. (2017). Resolving spatial and temporal variability in dissolved organic matter characteristics within combined agricultural and stormwater conveyances, M.S. Thesis, Utah State University, Logan, UT.
2. Mihalevich, B. A. (2013). Evaluation of alternative subsurface irrigation technology, Undergraduate Research Thesis, University of Missouri, Columbia, MO.

Invited Presentations

1. Mihalevich, B. A., Neilson, B. T., Buahin, C. A. (2020). Integrated Colorado River Basin Temperature Modeling Using a Component-Based Approach. Presented to Upper Colorado Region, U.S. Bureau of Reclamation, U.S. Department of Interior.
2. Mihalevich, B. A., Neilson, B. T. (2018). Stream Temperature Modeling in the Colorado River Basin Using a Component-Based Temperature Modeling Approach. Presented to Grand Canyon Monitoring and Research Center, U.S. Geological Survey, U.S. Department of Interior.

Conference Presentations and Posters

1. Mihalevich, B. A., Neilson, B. T., Buahin, C. A., Wheeler, K., Udall, B., Yackulic, C. B., Schmidt, J. C. (2021). Data Integration and coupled Modeling to Guide Water Management Decisions in the Colorado River Basin. AGU Fall Meeting, New Orleans, LA, 13-17 December, Abstract H22E-07.
2. Mihalevich, B. A., Neilson, B. T. (2020). Evaluation of a climate reanalysis model for process-based river temperature modeling in data-sparse regions. Utah State University Spring Runoff Conference, Logan, UT. Cancelled
3. Mihalevich, B. A., Neilson, B. T., Schmidt, J. C., Rosenberg, D., Tarboton, D., Buahin, C. A. (2019). A dynamic river temperature model for the Colorado River within Grand Canyon. Utah State University Spring Runoff Conference, Logan, UT, 26 March
4. Mihalevich, B. A., Neilson, B. T., Schmidt, J. C., Rosenberg, D., Tarboton, D., Buahin, C. A. (2018). A dynamic river temperature model for the Colorado River within Grand Canyon. AGU Fall Meeting, Washington, DC, 12-16 December. Abstract H43K-2643
5. Horsburgh, J. S., Melcher, A. A., Mihalevich, B. A. (2017). Stormwater Monitoring and Pollutant Load Estimation in Combined Agricultural and Urban Water Systems, Presented at: Rural Water Technology Conference, United States Bureau of Reclamation, Provo, UT, 8-9 March.

6. Mihalevich, B. A., Horsburgh, J. S. (2017). Resolving spatial and temporal variability in dissolved organic matter characteristics within combined agricultural and stormwater conveyances. Utah State University Spring Runoff Conference, Logan, UT, 28-29 March.
7. Mihalevich, B. A., Horsburgh, J. S., Melcher, A. A. (2016). Spatial and temporal variability of dissolved organic matter in a stormwater conveyance. Utah State University Spring Runoff Conference, Logan, UT, 5-6 April.
8. Melcher, A. A., Horsburgh, J. S., Mihalevich, B. A. (2016). Continuous surrogate monitoring for pollutant load estimation in urban water systems, Presented at: National Nonpoint Source Monitoring Workshop, Salt Lake City, UT, 23-25 August.
9. Melcher, A. A., Horsburgh, J. S., Mihalevich, B. A. (2016). Continuous monitoring for pollutant load estimation in combined conveyances, Presented at: Utah State University Spring Runoff Conference, Logan, UT, 5-6 April.
10. Mihalevich, B. A., Thompson A. L. (2013). Evaluation of alternative subsurface irrigation technology. Presented at: University of Missouri Undergraduate Research Symposium, Columbia, MO.

LEADERSHIP AND OUTREACH

- Advised and assisted three graduate students with hydrologic models — 2019 – 2021
- Mentored and advised an undergraduate technician — 2018
- Member and volunteer with Nordic United — 2015 – 2021
- Volunteer trail building and maintenance with Cache Trails Alliance — 2018 – 2020
- Earth Team volunteer with USDA NRCS in Columbia, Missouri — 2013

HONORS

- Dean's List (Honors) – University of Missouri — Fall 2009 – Fall 2013
- Joseph Mayer Academic Scholarship – University of Missouri — Fall 2009 – Spring 2013
- Robert Beasley Academic Scholarship– University of Missouri — Fall 2013